Electronic structure and bonding properties of hydrogen storage materials

Thesis submitted in partial fulfillment of the requirements

for the award of the degree of

Doctor of Philosophy

in

Physics

by

BHEEMA LINGAM CHITTARI

School of Physics,

University of Hyderabad,

Hyderabad-500 046

India

JULY 2012

DECLARATION

I hereby declare that the work embodied in this thesis entitled "**Electronic Structure and Bonding Properties of Hydrogen Storage Materials**" has been carried out by me, under the supervision of **Prof. Surya P. Tewari**, School of physics and Advanced Centre of Research in High Energy Materials (ACRHEM), University of Hyderabad and **Dr. G. S. Vaitheeswaran**, Advanced Centre of Research in High Energy Materials (ACRHEM), University of Hyderabad. I also declare that this is my own work and effort, and it has not been submitted at any other University or Institution for any degree. Wherever contributions of others are involved, every effort is made to indicate that clearly with due reference to literature, and acknowledgement of collaborative research and discussions.

Place: Hyderabad

Date: **Bheema Lingam Chittari**

CERTIFICATE

This is to certify that the work described in this dissertation entitled "**Electronic Structure and Bonding Properties of Hydrogen Storage Materials**" has been carried out by Mr. Bheema Lingam Chittari under our direct supervision for the full period prescribed under PhD ordinances of the University and the same has not been submitted for any other degree or diploma to this or any other University or Institution.

Prof. Surya P. Tewari
Supervisor
School of Physics and ACRHEM,
University of Hyderabad.

Dr. G. S. Vaitheeswaran
Co-Supervisor,
ACRHEM,
University of Hyderabad.

Dean
Prof. Surya P. Tewari,
School of Physics,
University of Hyderabad.

ACKNOWLEDGEMENTS

This thesis arose in part out of more than five years of research that has been done since August - 2006. During the time, I have worked with a great number of people whose contribution in assorted ways to the research and the making of the thesis deserved special mention. It is a pleasure to convey my gratitude to them all in my humble acknowledgment. It is really difficult for me to do the justice in this part since I do not have the record of many people who have contributed directly and indirectly over the years in various ways to the completion of this work. However, I tried my level best to acknowledge all of them but if your name is not included, I assure that my gratitude is not less than for those listed below.

First and foremost I offer my sincere gratitude to my supervisors, **Prof. Surya P. Tewari** and **Dr. G. S. Vaitheeswaran**, who has supported me throughout my thesis with their knowledge and insight whilst allowing me to work in my own way. Their encouragment and personal guidance have provided a good basis for the present thesis.

I gratefully acknowledge **Prof. K. P. N. Murthy**, **Prof. A. P. Pathak**, **Prof. V. S. S. Sastry**, **Prof. S. Chaturvedi** and **Prof. S. Dutta Gupta** for their valuable remarks of my research work during every six months, being in the doctoral committee.

I would like to express my sincere thanks to **Prof. C. S. Sunandana**, University of Hyderabad and **Dr. V. Kanchana**, Indian Institute of Technology, Hyderabad for critical reading of the thesis as well as all my research articles.

I am extremely grateful to **The Deans**, **Prof. Vipin Srivastava** and **Prof. C. Bansal**, School of Physics, **The Director**, Advanced Center of Research in High Energy Materials (ACRHEM) and **The Director**, Center for Modeling, Simulation and Design (CMSD) for providing excellent computing facilities and creating a nice atmosphere for doing my work.

I would like to thank **Prof. A. P. Pathak**, **Prof. S. N. Kaul**, **Prof. A. K. Kapoor**, **Prof. Vipin Srivastava**, **Prof. C. Bansal**, **Prof. Surya P. Tewari**, **Prof. S. Chaturvedi**, **Prof. C. S. Sunandana**, **Prof. R. Singh**, **Prof. S. Dutta Gupta**, **Prof. V. Seshubai**, **Prof. A. Chatterjee**, **Prof. G. Rajaram**, **Prof. K. P. N. Murthy**,

Prof. P. K. Suresh, **Dr. Suneel Singh**, **Dr. Rukmani Mohanta**, **Dr. Samrat L. Sabat**, **Prof. Natarajan**, **Prof. V. Srinivasan** and **Prof. Subodh R. Shenoy**. being my teachers during my MSc and PhD course work.

I am grateful to my groupmates **K. Ramesh Babu**, **S. Appalakondaiah** and **N. Yedukondalu**, who made my work to be finished and helped during critical situations, and gave a moral support in my entire research work. I would like to thank **Ghule Vikas**, **M. Maha Lakshmi**, **Sudha Nirmala**, **Srinivas**, **Sayed Hamad**, and **P. Ravi**.

I would like to thank all of my Ph.D batch mates [Rambabu, Venkaiah, Shankaraiah, Vasu, Sadik Ali, Arun Kumar, Deva Raju, Balaji, Sita, Vijayan, Sendil Kumar, Parthasarathy, Yugander, Anil Kumar and Deepak], my M.Sc classmates [Vamshidar, Santo, Anandam, Anji, Shankar, Nageswara Rao, Sanyasi Rao, Jagadeesh, Chandu, Suvarna, Madhumita, Sree Hari, Rajesh, Satya, Srinivas Reddy, Aswath, Tamang, Ghosh, Srikanth, Praveen and Subba Rao], Ph.D Scholars of School of Physics [Radhika, Srinivasa Rao, Suresh, Rajeswari, Shinto, Ravi, Lakshmi, Siva, Kalyan and Sanjeev Kumar] and ACRHEM [Sreedhar, Leela, Venkata Ramaiah, Debasis Swain, Ravi, Vikas, Nagendra, Ashwin, Gopala Krishna, Venkatesh, Prashanth, Sreeja and Anusha] for encouraging and making the whole research period worthful.

I thank my childhood friends Lavanya kumar, Laxman (vasu), Madhu (kusumanchi), Chandra Shekar, Krishna, Sarwar Pasha (Sarru), Anand, Eswar, Madhu, Satya, Sandhya and Shatrun for their interactions and good friendship.

I also want to thank Dr. D. Pamu, Kodanda Ram, Baby, Ashray, Anil Kumar, Kishore(KP), Kishore(HCU), Kiran(KP), Kiran(Tandur), Kiran(HCU), Kiran(Agra), Ratnakar, Henry, Calvin, Philip, Rajesh Babu, Rajesh Gudipalli, Yellaswamy, Prasad Anna, Joseph Anna, M. Raju, Benhur, Prakash Eliot, Ravi Kiran, Vijay, Ajay Kumar, Shyam, Ganesh, M.V.Suresh, Kesav, Manoj, Vara Lakshmi, Sujatha, Anitha, Sudheer staff anna, Sudheer(KP), Sudheer(BHEL), Paul Kiran Anna, Thomas Anna, Priya Akka, Hanah, Vijaya Prasad Anna, Neelima, Franky Anna and Family, Andrew Anna and Family, Karun, Sunil, Eswar, Nagar-

juna, Jhonson, Sumana Priya and Anil for their kind loving nature and spiritual support during my stay in the CAMPUS.

I thank office staff Mr. T. Abraham from School of Physics, Mr. Rajeswar, Mr. Nagaraju, Mr. Subhash, Mr. M. Mohan Rao, Mr. Y. H. Mohan Rao, Mr. Sadiq Hussain, Mr. Satyanarayana, Mr. Venkatasubbaiah, Mr. Mahesh, Mr. Prabhakar and Mr. Gopal from ACRHEM, Mrs. Shailaja from CAS, Mr. Davidraju from finance for their timely help in every occation and also in administrative matters. I would like to acknowledge the support from Mr. Vinod and Mr. Reddy and other CMSD staff for using softwares and high performance computing facility.

I am happy to express my gratitude for the financial support from University Grants Commission (UGC)-Centre for Advanced Studies (CAS)-Research Fellowships in Science for Meritorious Students (RFSMS) under Basic Scientific Research (BSR) Scheme as Junior Research Fellow (JRF), DRDO for Senior Research Fellow (SRF) in ACRHEM. The financial support received from ACRHEM (allowance for every month and for attending various national and international conferences), BBL (Boarding / BoardingCum-Lodging Allowance and Contingency) made me to reach the goal of success.

Finally I wish to express my sincere gratitude to my parents (Mr. Sambamurthy and Mrs. Chandrakala) who always encouraged and loved me without a second thought in everything I have done. They have supported me in all possible ways particularly in my studies in spite of many difficulties. I also thank my Brothers (Mr. Shankar Lingam and Mr. Sada Lingam), sisters (Miss. Sukanya and Miss. Mounika), cousins, uncles, aunties and all my relatives for their moral support and encouragement.

Last but not least, I thank God for HIS grace and mercy in my life. I praise and worship HIM for answering my prayers. Lord! You have made my life more bountiful. May your name be exalted, honored, and glorified.

BHEEMA LINGAM CHITTARI

To

My Parents, Brothers, Sisters & Friends

ABSTRACT

Hydrogen holds the promise to provide clean, safe, affordable and secure energy. The extensive use of hydrogen as energy source or fuel relies on the development of efficient hydrogen production and hydrogen storage. "Ammonia-based complexes" are found to be better choice for hydrogen storage applications. A detailed theoretical study on simple prototype metal hydride i.e., beryllium hydride and its oligomers to a complex hydride namely ammonia borane, along with its derivatives such as alkali, alkaline-earth metal amidoboranes and ploy-aminoboranes have been studied using density functional theory calculations. We have studied the electronic structure and bonding properties of hydrogen storage materials (NH_3BH_3, $LiNH_2BH_3$, $LiNH_3BH_4$, $NaNH_2BH_3$, $Mg(NH_2BH_3)_2$, $Ca(NH_2BH_3)_2$ and $Sr(NH_2BH_3)_2$) using density functional theory. Ammonia borane exhibits considerable vdW interactions and these interactions have negligible effect on the properties of alkali and alkaline-earth metal amidoboranes. From the band gaps we found that Ammonia borane has high band gap than other compounds. The mechanical stability of these compounds are assessed from the elastic constants. It is found that $Ca(NH_2BH_3)_2$ is mechanically stiffer than other compounds. The alkali metal amidoboranes are predicted to possess high thermal conductivity from their Debye temperature values. The bonding properties are explained from the Mulliken atomic and bond populations analysis and charge density distributions. From the bonding analysis, alkali metal amidoboranes shows the predominant covalency over ammonia borane and alkaline-earth metal amidoboranes. These systems contain simultaneously H^{+1} and H^{-1} and thus lead to dihydrogen bonding; the role of dihydrogen bonding on structural stability has been explored. Further, the structure dependent properties are addressed by considering the molecular level calculations of $(BeH_2)_n$; n=1-10 and $H(NH_2BH_2)_nH$ (n = 1 - 4). The barrier of the reaction between $[NH_2BH_3]^-$ ions found to be lower than that between two neutral NH_3BH_3 molecules, and it is concluded that alkali and alkaline-earth metal amidoboranes possess improved dehydrogenation properties over ammonia borane.

Table of Contents

Table of Contents **ix**

1 Introduction **2**

1.1 Hydrogen storage 4

1.2 Ammonia borane 8

1.2.1 Amidoboranes 10

1.2.2 Polyaminoborane 11

1.3 Scope of thesis 12

2 Theoretical and Computational details **14**

2.1 Density Functional Theory(DFT) 14

2.1.1 The Hohenberg-Kohn Theorems 16

2.1.2 The Kohn-Sham equations 17

2.2 Approximations for E_{xc} 20

2.3 Bloch's theorem and periodic boundary conditions 21

2.4 Pseudopotentials 23

2.4.1 A plane wave code: CASTEP 23

2.4.2 Dispersion correction for DFT 24
2.4.3 Gaussian03: A quantum chemical package 25

3 Beryllium Hydride and its Oligomers **27**

3.1 Introduction 27
3.2 Computational details 28
3.3 Results and discussion 29
3.3.1 Optimized structures 29
3.3.2 Electron affinity, ionization and chemical potentials 34
3.3.3 Hardness, softness and polarizability 36
3.3.4 Frontier molecular orbital energies 36
3.3.5 Mulliken atomic charges 39
3.3.6 Infrared and Raman spectra 42
3.4 Conclusions 43

4 Ammonia Borane (NH_3BH_3) **44**

4.1 Introduction 44
4.2 Computational details 46
4.2.1 The elastic constants 47
4.3 Results and discussion 48
4.3.1 Structural and electronic properties 48
4.3.2 High pressure studies on structural properties 54
4.3.3 The Mulliken atomic, bond population and the total charge density distributions 54
4.3.4 Elastic constants and mechanical properties 61

4.3.5 Vibrational properties at ambient and high pressures 67
4.4 Conclusions 69

5 Polyaminoboranes **71**
5.1 Introduction 71
5.2 Computational details 73
5.3 Results and discussion 74
5.3.1 Optimized structures 74
5.3.2 Dipole moment 76
5.3.3 Ionization and chemical potentials 80
5.3.4 Hardness and softness 85
5.3.5 Frontier molecular orbital energies 85
5.3.6 Electronegativity 87
5.3.7 Molecular electrostatic potential (MEP) surfaces 87
5.3.8 Infrared and Raman spectra 92
5.3.9 Bond Dissociation Energies (BDE) 93
5.4 Conclusions 95

6 Alkali Metal Amidoboranes **96**
6.1 Introduction 96
6.2 Computational details 98
6.3 Results and discussion 102
6.3.1 Structural properties 102
6.3.2 Electronic structure 103
6.3.3 Bonding properties 112

6.3.4 Mechanical properties 121
6.4 Conclusions 125

7 Alkaline-Earth Metal Amidoboranes **126**
7.1 Introduction 126
7.2 Computational details 128
7.3 Results and discussion 131
7.3.1 Structural properties 131
7.3.2 Electronic structure 133
7.3.3 Bonding properties 141
7.3.4 Mechanical properties 151
7.4 Conclusions 154

8 Conclusions and Future work **156**
8.1 Summary 156
8.2 Future work 161

Chapter 1

Introduction

The energy resources of the world are classified as fossil fuels (coal, oil and natural gas), nuclear fuel and renewable resources (solar, wind, tidal, geothermal, biomass, hydropower). Fossil fuels are non-renewable and nuclear fuels are limited. Renewable resources with low energy density are impractical for transportation applications. The demand on fossil fuels is growing day by day due to the high population growth rate and the increasing energy consumption. Combustion of fossil fuels releases carbon dioxide called greenhouse gas emissions. These are threat to the stability of Earth's climate due to global warming. Hence, a search for clean and alternative energy source that can replace the fossil fuels is in demand. A variety of suggested alternative fuels are methanol, ethanol, methane, synthetic liquids from natural gas or coal and also hydrogen. The hydrocarbon based energy sources are again produce green house gas (CO_2). If the energy generated from the hydrocarbons is divided into C and H contributions, it appears that only 32% of energy is originates from hydrogen combustion and 68% of energy from the CO_2. For past five decades hydrogen has been targeted as the ideal fuel for the transportation systems of the future due to its high natural abundance and environmental friendliness [1]. Hydrogen is the most attractive because its electron is accompanied by only one proton, and it has high energy gain per electron per proton. Hydrogen exhibits three common oxidation states: +1, 0 and -1 reflecting as $1s^0$, $1s^1$

or $1s^2$ electronic configuration respectively. The relative change in the number of electrons surrounding the nucleus associated with the transformations $H^0 \rightarrow H^{-1}$ and $H^0 \rightarrow H^{+1}$ ($\pm$1e, $\pm$100%) is thus the largest among the chemical elements of the periodic table. Hydrogen is most abundant element on Earth, but less than 1% is present as molecular hydrogen gas H_2 [1]. The overwhelming majority is in chemically bound H_2O as water and some others are bound as liquid or gaseous hydrocarbons. Hydrogen combines readily with almost all elements, and is also found in biomass, which includes all plants and animals. Hydrogen holds the promise to provide clean, safe, affordable energy from abundant domestic resources. Hydrogen can power cars, trucks, buses, and other vehicles, as well as homes, offices, factories, and also portable electronic equipment such as laptop computers. Fuel cells are the best choice to utilize the hydrogen for the future energy source. Hydrogen is the optimum choice for fuel cells, which are extremely efficient energy conversion devices that can be used for transportation and electricity generation. The use of hydrogen within H_2 fuel cell systems requires an adequate and readily accessible hydrogen storage medium.

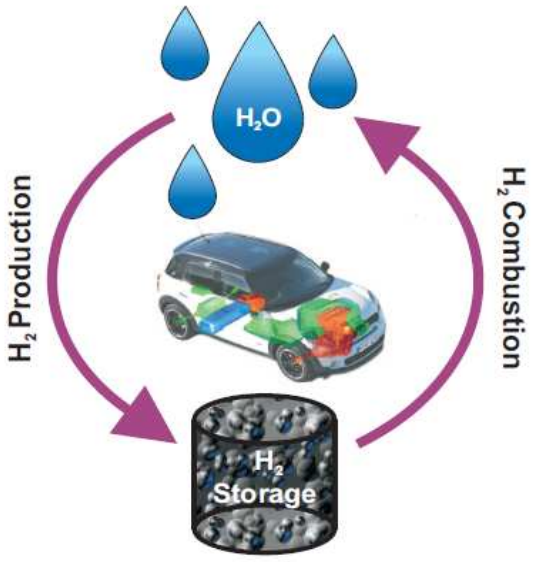

Figure 1.1: Conceptual diagram of the hydrogen cycle

1.1 Hydrogen storage

Interest in hydrogen experienced a revival in the late 1960s and in the 1970s and has grown even more dramatically since 1990 [3, 4] many advances in hydrogen production and utilization technologies have been made during the past decade. Although having many advantages as future fuel, hydrogen is not a primary energy source. Pure atomic hydrogen must be produced from other hydrogen compounds, such as fossil fuels, biomass, or water. Atomic hydrogen has the highest energy content per unit weight, but not per unit volume of any fuel. The relatively low volumetric energy content of hydrogen possesses significant challenge for storage. Therefore an extensive use of hydrogen as fuel relies on the development of efficient atomic hydrogen production and hydrogen storage systems [5]. Hydrogen storage is the greatest technical challenge to find the green solutions to the stages that complete the cycle shown in figure 1.1. One of the most critical elements in hydrogen economy is the development of safe, reliable, compact and cost-effective storage of the material. The drawback of utilizing hydrogen as alternative fuel is the problem in finding an appropriate storage medium. In principle hydrogen can be stored either in its elemental form, as gas or liquid or in chemical form. Depending on the temperature and the pressure, hydrogen can be found in various forms. Hydrogen exists in the H_2 gas phase at ambient pressure and temperature. The most traditional way of storing hydrogen is through compressed vessels. The energy density is increased by increasing the pressure of the storage vessel. The safety features and regulations that limit the allowable pressure of the container [6, 7]. The main advantages of storing hydrogen as compressed gas are simple, practically unlimited storage time, and the ease for refueling [8]. On the other hand, liquified hydrogen has been used as a fuel in space technology [9]. It is denser than gaseous hydrogen and therefore has higher energy content on a per-unit-volume basis. In order to convert gaseous hydrogen to a liquid, it must be cooled to -253^{o}C and must be in insulated pressure vessels [10]. The advantage of liquid hydrogen is that hydrogen stores approximately 2.6 times the energy per unit mass as gasoline. The disadvantage is that it needs about 4 times the volume for a given

amount of energy due to the very low density of liquid hydrogen. Moreover, the production of liquid or highly compressed hydrogen is energy intensive and may become dangerous in some circumstances.

An alternative way to liquefaction and compression is to store hydrogen in solids, either physically absorbed or chemically bound. The solid state hydrogen storage is found to be a better choice when compared to the gaseous and liquid states, being safe, less energy intensive and minimal in volume. Atomic hydrogen is a highly unstable species when contact with other atoms or molecules, it always be completely empty or a completely filled 1s shell to form the proton cation H^{+1} or the hydride anion H^{-1}, respectively. The first ionization potential energy, I_P= 1312 kJ/mol (13.60 eV), and the electron affinity, E_A=72.8 kJ/mol (0.75 eV) of a H atom indicates that H^{+1} is a hard electron density acceptor and H^{-1} is a soft electron density donor. The H has a fascinating duality in the physical and chemical properties as it behaves as hard cation as well as a soft anion. The H^{+1} or/and H^{-1} species are of necessity involved in the hydrogen storage materials as shown below:

$H^{-1} \rightarrow H^0 + e^-$ ($\triangle$ H^o= +0.75 eV)
$H^{+1} + e^- \rightarrow H^0$ ($\triangle$ H^o= -13.60 eV)
$2H^0 \rightarrow H_2$ ($\triangle$ H^o= -4.52 eV)
$H^{-1}+H^{+1} \rightarrow H_2$ ($\triangle$ H^o= -17.37 eV)

Hydrogen combines with many elements to form hydrides, MH_n. The hydrides of the most electropositive are best treated as solid ionic compounds with cations M^{n+} and anions H^-, and the hydrides of the most electronegative are best treated as ionic molecules, containing anions M^{n-} and protons H^+. The hydride anion H^{-1} is un questionably a better chemical source of hydrogen than the proton. However, one has to consider the systems which contain simultaneously H^{+1} and H^{-1}.

The hydrides are also found to be attractive for technological applications such as opti-

cal switchable mirrors because of the change in the physical properties of the host by the presence of hydrogen in it [11]. The uptake and release of hydrogen is typically controlled by temperature and pressure and is different for every hydride. The storage and release of hydrogen in any case should take place at temperatures and on a time scale suitable for applications in the transportation field. Total hydrogen capacity and reversible portion are usually presented as weight percentage of hydrogen, which is a key hydrogen storage property [8]. Basic research in hydrogen storage needs to focus on understanding the fundamental principles governing bond strength, kinetics, absorption and desorption processes, and degradation caused by cycling. It is further required to apply these principles to tailor the performance of known storage materials, and to identify or even design a new class of materials with properties modified so as to suit the transportation demands of hydrogen economy. A hydrogen storage system suitable for mobile applications must meet simultaneously the following six requirements based on economical and environmental considerations [12]:

- High gravimetric (>4.5 wt%) and volumetric (>36g H_2/L) densities.
- The operation temperature approximately in the range 60-120^{o}C.
- Reversibility of the thermal absorption/desorption cycle.
- Low cost.
- Low-toxicity.

It is important to stress at the outset that, at present no single material fulfills all of these requirements. The volumetric density of hydrogen in hydrides reaches approximately the double of the density of liquid hydrogen because the hydrogen intercalates in its atomic state in the host metal and acts like as metal atom in the host lattice. According to the Westlake criteria [13], the hydrogen atoms in hydrides have an interatomic distance of at

least 0.21 nm. This corresponds to an atomic volume of 0.00485 nm^3 and a maximum volumetric density of 187 kg m^{-3}. Therefore, the only way to increase the volumetric hydrogen density above the liquid hydrogen is the dissociation of hydrogen molecules in combination with tight binding (covalent) or an electron transfer to the host materials. In general, complex metal hydrides such as alanates have the potential for higher gravimetric hydrogen capacities in the operational window than conventional metal hydrides like lanthanum and magnesium hydrides or alloys with nickel ($LaNi_5H_7$ and Mg_2NiH_4) [14]. Besides alanates, mixed borohydrides offer good prospect as a chemical storage media, but they are still down on the energy density scale [12]. Metal-N-H systems have also been shown to be promising for reversible hydrogen storage [15, 16]. Currently, metal hydrides and complex hydrides do not reach the target for reversible hydrogen storage capacity [8]. Theoretical and experimental studies have shown that the most of first and second row elements of periodic table are having potential properties for chemical hydrogen storage [17, 18]. Among the required properties, research efforts have primarily been focused on finding materials that feature the highest storage capacity [2, 19]. In this context nitrogen attracted much attention as a suitable element for chemical hydrogen storage due to the possible high hydrogen contents [20, 21]. With its hyper-coordination, nitrogen can offer multiple valance within different compounds such as ammonia, hydrazine and metal amine systems. At the heart of the issue, ammonia (NH_3) derivatives become key-compounds for on-board hydrogen storage [18, 20–22]. Ammonia has several desirable characteristics that make it potentially attractive. First, it is non-flammable and non-explosive. Second, it can be liquified under mild conditions and has less complex processes compared to the reforming hydrocarbon fuels. Third, ammonia has a large weight fraction of hydrogen. Hydrogen constitutes 17.65% of the mass of ammonia [20–22]. In spite of many advantages ammonia still has problems need to be addressed. Liquid ammonia is toxic for both people and polymer electrolyte membrane fuel cells. One approach to mitigate ammonia's toxicity is to complex or combine it with other elements and molecules so that the resulting compound is stable and non-toxic. Substituting H atoms in

ammonia by light metal or metal hydrides is one way of having a new compound. This kind of compounds, being "nitrides, amides and imides", have been reviewed by many groups, and most of them focusing their attention on lithium like derivatives Li_3N, Li_2NH, $LiNH_2$ [23–25]. The other class of materials is complex amides with metal complex hydrides [26, 27]. This kind of materials are relatively cheap, easy to produce and they are considered as potential hydrogen storage media [26, 27]. Another class of compounds called "Ammonia-based complexes" are currently considered as a better alternative. These include the compounds containing only B and/or Al, N and H atoms [28–33]. As boron (B) and aluminium (Al) are lightweight elements capable of bearing multiple hydrogens, ammonia-based complexes meet the requirements of high gravimetric capacities. The critical point that leads the B/Al-N-H compounds to be the promising materials for chemical hydrogen storage is the polarity of the B/Al-H and N-H bonds. They tend to be hydridic and protic in the same compound and normally do facilitate hydrogen release [34–39]. Based on the light molecular weight and combined with ammonia in the form of complexes, B-N-H compounds have met these requirements, because both hydridic and protic centers ($H^{\delta-}$ and $H^{\delta+}$, respectively) facilitate hydrogen release. B-N-H compounds appear to satisfy the following conditions:

(i) They contain multiple hydrogen equivalents per main-group element.

(ii) They have a good match between the number of hydridic and protic hydrogens from B-H and N-H bonds.

(iii) They possess the necessary stability for safe storage [34, 36, 38].

1.2 Ammonia borane

Ammonia borane (NH_3BH_3) is one of the B-N-H compounds with highest hydrogen weight percentage (19.6%). It is the simplest compound, and has received much attention in recent years towards hydrogen storage applications [28, 31, 34, 36, 38, 40–42]. Isoelectronic

with ethane, ammonia borane is solid at room temperature, stable in air and water and commercially available. It contains both hydridic B-H and protic N-H bonds, three H atoms per main group element, and a relatively strong B-N bond. NH_3BH_3 is a donor-acceptor adduct formed as a result of the dative bond between a Lewis acid (BH_3) and Lewis base (NH_3). It is a colorless solid and stabilized primarily due to the di-hydrogen bonding and dipole-dipole interactions [43]. Ammonia borane has been analyzed by almost every possible spectroscopic technique, such as NMR, IR, Raman spectroscopy, and also by techniques involving diffraction or scattering, such as X-ray crystallography and inelastic neutron scattering. The material properties have been analyzed by inelastic spectroscopy and dipole measurements, thermogravimetric and calorimetric measurements. Figure 1.2 shows that the large portion of the hydrogen can only be liberated from ammonia borane, which has a higher gravimetric density than most other reported chemical systems. This capacity coupled with stability has resulted in renewed interest in studying ammonia borane as a potential hydrogen storage material [42].

Due to lower weight (30.7 g mol^{-1}) and high gravimetric hydrogen capacity (19.6%), NH_3BH_3 has attracted a flurry of recent investigations into hydrogen release. NH_3BH_3 can release more than 2 moles of H_2 on heating to modest temperature. The reactions are as follows:

$NH_3BH_3 \rightarrow NH_2BH_2 + H_2$

$NH_2BH_2 \rightarrow NHBH + H_2$

$NHBH \rightarrow BN + H_2$

Ammonia borane looks promising hydrogen storage material, but there are some technical challenges to be addressed like enhancing the rates of hydrogen release and economical chemical processing pathways to put hydrogen back onto the dehydrogenated material. NH_3BH_3 based materials have been further developed in combination with metal catalysts, acid catalysts, ionic liquids and nanoscafolds. New families of metal amidoboranes $M(NH_2BH_3)_2$ (M= K, Na, Li, Ca, Mg) have also been developed by replacing one H in NH_3BH_3 by an alkali

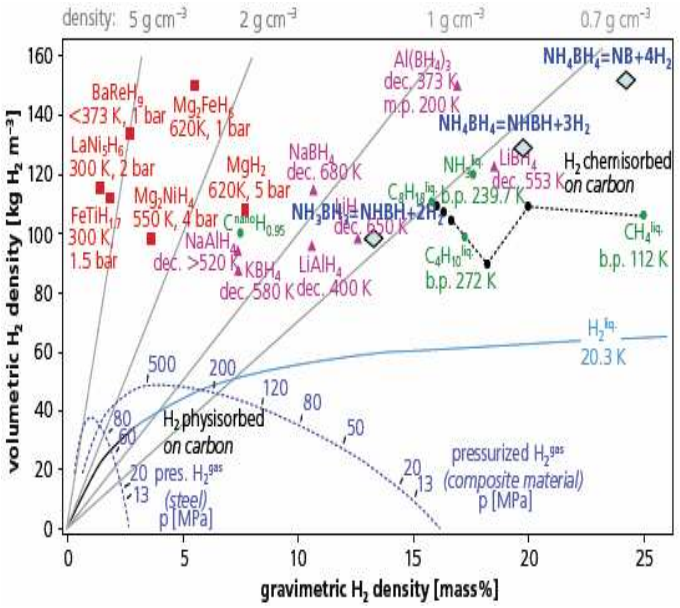

Figure 1.2: Comparison of gravimetric and volumetric densities of various hydrogen storage materials. NH_3BH_3 has high gravimetric and volumetric densities compared to complex hydrides, simple hydrides and carbohydrates. The curves related to H_2 gas and liquid showing the low volumetric density compared to all hydrides.

or alkaline earth element, which are believed to be promising materials for high hydrogen storage over NH_3BH_3

1.2.1 Amidoboranes

Metal amidoboranes with accelerating desorption kinetics and suppressed toxic borazine, are of great interest for their potential applications in hydrogen storage. These are stable under normal pressures, less exothermic than NH_3BH_3 and suitable for on-board H_2-storage application. Recently, $LiNH_2BH_3$, $NaNH_2BH_3$ and $Ca(NH_2BH_3)_2$ have been highlighted as potential materials for hydrogen storage applications, because they release H_2 at 363K. $LiNH_2BH_3$ and $Ca(NH_2BH_3)_2$ have been reported to show significantly enhanced dehydrogenation kinetics and suppressed borazine release.

The alkali and alkaline-earth metal amidoboranes not only provide high hydrogen storage

capacity but also exhibit dramatically improved dehydrogenation properties compared to pure solid ammonia borane (NH_3BH_3). The reduced dehydrogenation temperature is likely related to the different bonding nature and reactivity of the metal amidoboranes compared to NH_3BH_3. Similar to NH_3BH_3 in acid or ionic liquid, the dehydrogenation properties of amidoboranes in the solid state may also be significantly improved by tuning the reactivity of B-H and/or N-H through inducing polar species such as strong electropositive cations or highly active anions (e.g., NH_2^- and BH_4^-).

1.2.2 Polyaminoborane

While the mechanisms of catalytic and thermal decomposition of ammonia borane have been investigated in both the gas and the condensed phases, the mechanism for the formation and decomposition of the corresponding $H(NH_2BH_2)_nH$ oligomers has not been understood previously. The usefulness of BNH_x as hydrogen storage materials depends, among other things, on the kinetics and thermodynamics of dehydrogenation. Therefore, one of the key problems in investigating BNH_x as hydrogen storage materials is to understand the formation mechanisms, reactivities, reaction energetics, and dehydrogenation and reversed hydrogenation pathways in these materials. The $H(NH_2BH_2)_nH$ oligomers (or polyaminoborane, PAB), products of dehydrocoupling of NH_3BH_3, are thus a good starting point for understanding the thermodynamics and kinetics of the BNH_x materials at molecular level.

Eventhough there are numerous solid metal hydrides, none of them has been demonstrated yet to meet the above said requirements. The search for new potential compounds with desired properties for hydrogen storage is a challenge among researchers for past few decades. Development of new solid-state materials for hydrogen storage presents many scientific and technological challenges. A thorough understanding of hydrogen interaction in solid-state materials requires an efficient theoretical methods and modeling. Density functional theory is a robust theoretical approach for studying the hydrogen storage systems, which is a quantum mechanical approach to yield information about electronic structure

and chemical bonds. The main objective of our work is to gain fundamental insight into the chemical and physical properties of hydrogen rich compounds, which will provide thorough understanding of the systems and basis for developing new hydrogen storage systems.

Following are the important issues investigated in the present thesis:

- Structure dependent properties (effect of van der Waals interactions on basic ground state properties)
- Understanding the electronic properties of molecules and the corresponding crystalline solids
- The nature of bonding between hydrogen and metal atoms in simple and complex hydrides
- Dihydrogen bonding, which significantly affects the structure and dynamics of hydrogen rich molecular crystals
- Understanding the mechanical stability and related properties of the molecular solids.

1.3 Scope of thesis

The understanding of the various physical properties of the ammonia borane, amidoboranes and polyaminoboranes are important from fundamental point of view. In general the properties of a material are determined by its chemical composition and structure. All physical and chemical properties are linked by the electronic structure, the energy levels and dispersion of these levels of the electrons in the material. Hence, studying the properties of a material automatically means studying its electronic structure. The present thesis studies the above mentioned properties of hydrogen containing molecular materials ranging from simple prototype metal hydride (Beryllium hydride) to a complex hydride namely ammonia borane along with its derivatives such as Alkali and Alkaline-earth metal amidoboranes. We

also study the structural stability, electronic properties, ionization and chemical potentials, electron affinities, softness, hardness, polarizability, infrared and Raman spectra of various beryllium hydride oligomers and ammonia borane oligomers, called polyaminoboranes. All the calculations are carried out by means of density functional theory.

In the first chapter, based on the literature survey the importance of hydrogen storage materials, role of the electronic structure and bonding properties of materials in tailoring new class of hydrides, outstanding issues and approaches are elaborated. The motivation and objective of the present thesis is then discussed. The second chapter gives details of the theoretical methods used in the thesis to calculate the various properties of the studied materials. The computational details of the density functional theory (DFT) methods such as local density approximation (LDA), and generalized gradient approximation (GGA), semi-empirical dispersion corrections to density functional theory are described and discussed. In the third chapter, we present the electronic structure and bonding nature of known simple light metal hydride, Beryllium hydride (BeH_2) as solid and molecular polymer (upto decamer). The fourth chapter discusses complex hydride ammonia borane. Since ammonia borane is a molecular crystal, we consider van der Waals (vdW) correction to the total energy to attain the experimental volume at semi-empirical level. Further the mechanical stability of the complex hydride has been understood through the calculated elastic constants. We have also studied the hydrostatic pressure effects on structural and vibrational properties of solid NH_3BH_n upto 6 GPa.

In the fifth chapter, we describe the results of detailed calculations on structure, reaction stabilities, electrostatic potential surfaces and hydrogen dissociation energies of $H(NH_2BH_2)_nH$ (n = 1 - 4) oligomers by using density functional theory and in sixth and seventh chapters we consider the alkali and alkaline-earth metal amidoboranes to understand the changes brought in the electronic structure and bonding properties due to the presence of metal atom. Final chapter gives the overall conclusion of the thesis, comparison of the results and outlook for the future investigations in this exciting research area.

Chapter 2

Theoretical and Computational details

In this chapter we give the details of the theoretical techniques used in calculating various physical and chemical properties of the hydrogen storage materials. We also present the basic principles of density functional theory (DFT), local density approximation(LDA), and generalized gradient approximation(GGA) along with semi-empirical dispersion corrections to the density functional theory. The computational methods used in the DFT implementations are also described.

2.1 Density Functional Theory(DFT)

In order to describe an interacting electron-nucleus system one has to write the corresponding Hamiltonian as follows [44–46]:

$$H = -\sum_{I=1}^{P}\frac{\hbar^2}{2M_I}\nabla_I^2 - \sum_{i=1}^{N}\frac{\hbar^2}{2m_i}\nabla_i^2 + \frac{e^2}{2}\sum_{I=1}^{P}\sum_{J\neq I}^{P}\frac{Z_I Z_J}{|R_I - R_J|} + \frac{e^2}{2}\sum_{i=1}^{N}\sum_{i\neq j}^{N}\frac{1}{|r_i - r_j|} - \frac{e^2}{2}\sum_{I=1}^{P}\sum_{i=1}^{N}\frac{Z_I}{|R_I - r_i|} \tag{2.1}$$

where $R = \{R_I, I = 1, 2, ...P\}$ is a set of P nuclear coordinates, and $r = \{r_i, i = 1, 2, ...N\}$ is a set of N electronic coordinates. Z_I and M_I are the nuclear charges and masses, respectively. The first and second terms correspond to the kinetic energy operators for nuclei and electrons, whereas the third, fourth and fifth terms are the potential operators that describe the nucleus-nucleus, electron-electron and electron-nucleus interactions, respectively. In order to study the properties of an interacting electron-nucleus system, one has to solve the time-independent Schrödinger equation:

$$H\Psi_n(R, r) = \varepsilon_n \Psi_n(R, r) \tag{2.2}$$

where ε_n are the energy eigenvalues and $\Psi_n(R, r)$ are the corresponding eigenstates or wave functions. This problem is almost impossible to treat within quantum mechanical frame work, except for the hydrogen atom. There are several features that contribute to this difficulty, but the most important among them is the multi component many body nature of the system, and the two body nature of the Coulomb interaction which makes the above Schrödinger equation inseparable. The usual choice to solve the above complicated equation is to resort to a few reasonable and well-controlled approximations, which encompass a wide variety of problems of interest.

Born and Oppenheimer [47] proposed a scheme for separating the motion of nuclei from that of the electrons. The nuclei are much heavier than the electrons and consequently much slower, so the effects of nuclei are treated as an external potential applied to the electrons. Therefore, the wave function can now be written as the product of the electronic and ionic wave functions, with the electronic part being obtained by solving the following Schrödinger equation

$$H_e\psi_e(R, r) = \varepsilon_e \psi_e(R, r) \tag{2.3}$$

with the electronic Hamiltonian given by

$$H_e = -\sum_{i=1}^{N} \frac{\hbar^2}{2m_i}\nabla_i^2 + \frac{e^2}{2}\sum_{i=1}^{N}\sum_{i\neq j}^{N} \frac{1}{|r_i - r_j|} - \frac{e^2}{2}\sum_{I=1}^{P}\sum_{i=1}^{N} \frac{Z_I}{|R_I - r_i|} \tag{2.4}$$

$$H_e = T + U + V \tag{2.5}$$

where T represents the kinetic energy operator, V represents the external potential (i.e electron-nucleus interaction) and U represents the electron-electron interaction. Within the Born-Oppenheimer approximation the complexity of the system is significantly reduced. However, the problem is still too difficult to be solved due to the electron-electron interaction. The electrons cannot be treated as point like classical particles, as the main difficulty is that electrons interact among themselves via Coulomb two-body forces. For an atom with Z electrons, the probability of finding an electron in space depends on the location of the Z-1 electrons, so that they cannot be considered as individual entities. This phenomenon is known as *correlation*. Therefore, the image of one-electron wave functions can be some what crude in many cases. The wave function of many-electron system cannot be simply written as the product of the wave functions of individual electrons. Many approaches have been developed starting from Hartree-Fock method to density functional theory (DFT) to solve the above equation. In this thesis, we have used the DFT method, which is explained in the following sections.

2.1.1 The Hohenberg-Kohn Theorems

L.H. Thomas [48] and E. Fermi [49] proposed that the full electronic density is the fundamental variable of the many-body problem. Thomas and Fermi approach was developed in the hope that the energy can be written exclusively in terms of the electronic density. In 1964, Hohenberg and Kohn [50] formulated and proved a theorem that put on solid

mathematical ground the ideas of Thomas and Fermi. Based on these theorems Hohenberg and Kohn formulated *density functional theory* as an exact theory of many-body systems. It is applicable to any system of interacting particles. The theorems are as follows:

Theorem I: For any system of interacting particles in an external potential $V_{ext}(r)$, this potential is determined uniquely by the ground-state particle density $n(r)$.

There is a one-to-one correspondence between the potential and the ground state particle density $n(r)$. The ground state expectation value of any observable is a unique functional of the ground state particle density.

Theorem II: A universal functional for the energy $E[n(r)]$ can be defined, valid for any $V_{ext}(r)$.

For a particular $V_{ext}(r)$ the ground state energy of the system is the global minimum of $E[n(r)]$. The density $n(r)$ that minimizes $E[n(r)]$ is the ground state density.

2.1.2 The Kohn-Sham equations

Kohn and Sham have developed a frame work within which the Hohenberg and Kohn theorems can be applied for practical problems [51]. The main idea consists in replacing the interacting many-body problem by a corresponding non-interacting particle system in an appropriate external potential. It is useful to decompose the kinetic energy, $T[n]$ into two parts (non-interacting system + rest term)as $T[n] = T_s[n] + T_c[n]$, where $T_s[n]$ is the kinetic energy of the non-interacting system and $T_c[n]$ represents the remainder. $T_s[n]$ is not known as a functional of n, but it can be expressed in terms of the single-particle orbitals, $\phi_i(r)$, of a non-interacting system with density n via

$$T_s[n] = -\frac{1}{2}\sum_{\sigma}\sum_{I=1}^{N}\int dr\phi_i{}^*(r)\nabla^2\phi_i(r). \tag{2.6}$$

For a system containing an even number of spin-up and spin-down electrons the density of the original many-body system can be written in terms of the orbitals as

$$n(r) = \sum_{\sigma} n(r,\sigma) = \sum_{\sigma} \sum_{I=1}^{N} |\phi_i(r)|^2. \tag{2.7}$$

Thus, all $\phi_i(r)$ are functionals of n and since T_s is an explicit orbital functional it is also an implicit density functional, $T_s[n] = T_s[\phi_i[n]]$. Moreover the total number of electrons N is a simple functional of the density

$$N = \int n(r)dr \tag{2.8}$$

The classical Coulomb self-interaction energy of the electron density, i.e., Hartree energy is defined as

$$U_H[n] = \frac{1}{2} \int \int dr dr' \frac{n(r)n(r')}{|r-r'|} = \frac{1}{2} \int V_C(r)n(r)dr \tag{2.9}$$

where $V_C(r) = \int dr \frac{n(r)}{|r-r'|}$ and the energy of the external potential can be written as a functional of the density

$$\int n(r)V_{ext}(r)dr \tag{2.10}$$

The Kohn-Sham approach [51] is to rewrite the energy functional of the interacting system in the form

$$\begin{aligned} E_{KS}[n] &= T[n] + U[n] + V[n] \\ &= T_s[\phi_i[n]] + U_H[n] + E_{xc}[n] + V_{ext}[n] \\ &= T_s[n] + \int n(r)[V_{ext}(r) + \frac{1}{2}V_C(r)]dr + E_{xc}[n] \\ &= T_s[n] + V_{eff}. \end{aligned} \tag{2.11}$$

Where $V_{eff} = \int n(r)[V_{ext}(r) + \frac{1}{2}V_C(r)]dr + E_{xc}[n]$, The exchange-correlation energy $E_{xc}[n]$ contains the differences between $T - T_s$(i.e. T_C) and $U - U_H$. One has to find a good approximation to E_{xc} in order to get good results for real materials.

The effective Hamiltonian for a system of non-interacting particles moving in a potential called V_{KS}, constructed so that the total density of the system is the same as for the real system of interacting electrons, is

$$V_{KS}(r) = V_{ext}(r) + V_C(r) + V_{xc}(r) \tag{2.12}$$

with

$$V_{xc} = \frac{\delta E_{xc}}{\delta n} \tag{2.13}$$

is given as

$$H_{KS} = -\frac{1}{2}\nabla^2 + V_{KS}(r). \tag{2.14}$$

This gives rise to the Kohn-Sham Schrödinger-like equation

$$(H_{KS} - \varepsilon_i)\phi_i(r) = 0 \tag{2.15}$$

where ε_i are the eigenvalues of H_{KS}, and the orbitals satisfying above equation, ϕ_i, minimize the Kohn-Sham energy. This yields orbitals that reproduce the density of the original interacting system and the total energy, E_{KS}. These are independent particle equations with a potential that must be found self-consistently with the resulting density. In practice one starts with an initial guess for $n(r)$ and calculates the resulting $V_{KS}(r)$, and finally solves the Kohn-Sham Schrödinger-like equation for the ϕ_i. The orbitals yield a new density and the process is iteratively repeated until convergence.

2.2 Approximations for E_{xc}

Local Density Approximation (LDA)

In the Kohn-Sham approach [51], finding a good approximation for the exchange-correlation functional E_{xc} is the main challenge. Among many approaches, Local Density Approximation (LDA) has been the most commonly used. The LDA functional can be written as:

$$E_{xc}[n] = \int n(r)\epsilon_{xc}[n(r)]dr \tag{2.16}$$

where ϵ_{xc} is an energy per particle that depends only upon $n(r)$. Especially for a slowly varying $n(r)$ it is reasonable to assume that $\epsilon_{xc}[n(r)]$ is a functional of constant density $n(r) = n =$ constant. Then we need not find $\epsilon_{xc}[n(r)]$ for any shape of $n(r)$. Instead, it is enough to know $\epsilon_{xc}[n(r)]$ for a series of constant n. This is the idea behind the LDA.

Generalized Gradient Approximation (GGA)

An obvious way to improve on LDA is to take the gradients of the density into account. A first approach is systematic calculation of gradient corrections of the form $|\nabla n(r)|, |\nabla n(r)|^2, \nabla^2 n(r)$ etc. This is called the gradient expansion approximation (GEA), which gives worse results than LDA. It is realized that one could use more general functions of $n(r)$ and $\nabla n(r)$:

$${E_{xc}}^{GGA}[n] = \int f(n(r), \nabla n(r))dr \tag{2.17}$$

These are the GGA, different GGAs differ in the choice of the function $f(n(r), \nabla n(r))$. Some very popular functionals go beyond GGA, and may even contain parameters optimized for certain class of molecules. One example is Becke three parameter Lee Yang Parr (B3LYP), very common in quantum chemistry.

The LDA uses the exchange-correlation density of the uniform electron gas of the same

charge density at every point in the system regardless of the inhomogeneity of the real charge density. The GGA also uses the gradient of the charge density to correct for this deviation, and therefore thought to be more accurate.

Hybrid functionals

Hybrid functionals are a class of approximations to the exchange-correlation energy functional in density functional theory (DFT) that incorporate a portion of exact exchange from Hartree-Fock theory with exchange and correlation from ab initio or empirical. The hybrid approach to construct density functional approximations was introduced by Axel Becke in 1993 [52]. Hybridization with Hartree-Fock (exact) exchange provides a simple scheme for improving many molecular properties, such as atomization energies, bond lengths and vibration frequencies, which tend to be poorly described with simple "ab initio" functionals [53]. For example, the popular B3LYP (Becke, three-parameter, Lee-Yang-Parr) [54, 55] exchange-correlation functional is:

$$E_{xc}{}^{B3LYP} = E_{xc}{}^{LDA} + a_0(E_x{}^{HF} - E_x{}^{LDA}) + a_x(E_x{}^{GGA} - E_x{}^{LDA}) + a_c(E_c{}^{GGA} - E_c{}^{LDA}) \quad (2.18)$$

where a_0 =0.20, a_x =0.72 and a_c =0.81. B3P86 specifies the same functional with the non-local correlation provided by Perdew 86 [52].

2.3 Bloch's theorem and periodic boundary conditions

Condensed phases such as solids, liquids, amorphus materials, and systems of lower dimensionality such as surfaces or wires are macroscopic objects constituted by a huge number of atoms of the order of Avogadro's number (6x10^{23}/mol). In crystalline solids, a small number of atoms (a basis) is replicated periodically along one, two, or three directions in space. The unit or Wigner-Seitz cell, which is a minimal cell that contains the whole symmetry

of the system, together with the lattice vectors contains all the necessary information to reproduce the infinite crystalline structure. Bloch's theorem [56] connects the properties of the electrons in a periodic infinite system with those of the electrons in the unit cell. The wave function of an electron in external periodic potential $v(r) = v(r + a_i)$ can be written as the product of a function with the same periodicity of the potential and a purely imaginary phase factor arising from the translational symmetry, i.e

$$\psi_k(r) = e^{ik.r} u_k(r) \tag{2.19}$$

with $u_k(r) = u_k(r + a_i)$, a_i with $i = 1, 2, 3$ are primitive vectors of unit cell. The wave function at location displaced by the unit vector, $r + a_i$ assumes the form

$$\psi_k(r + a_i) = e^{ik.a_i} \psi_k(r) \tag{2.20}$$

so that the probability density $|\psi(r)|^2$ is exactly the same because the purely imaginary phase factor cancels out.

For each a_i, there will be set of k vectors which satisfies $e^{ik.a_i} = 1$. The set of the three smallest independent such vectors are called *reciprocal lattice vectors*. The primitive vectors in reciprocal space are defined by the relation $a_i.b_j = 2\pi\delta_{ij}$. We consider a system of non-interacting, free electrons in a one-dimensional periodic box of length a. The electronic wave functions are the solutions of the 1D Schrödinger equation

$$-\frac{\hbar^2}{2m}\frac{d^2\psi_k(x)}{dx^2} = \varepsilon(k)\psi_k(x) \tag{2.21}$$

The wave functions $\psi_k(x) = e^{ikx}$ are solutions of the above equation and the corresponding eigenvalues are

$$\varepsilon(k) = \frac{\hbar^2 k^2}{2m} \tag{2.22}$$

The relation between energy and wave vector is called *dispersion relation* and the allowed values of $\varepsilon(k)$-in this case all positive values-form the *energy bands*.

Bloch's theorem indicates that it is not necessary to determine the electronic wave functions everywhere in space. It is sufficient to know the solution in the unit cell. The wave function in the neighboring cell is exactly the same except for the phase factor $e^{ik.a}$.

2.4 Pseudopotentials

The wave functions for free electrons in a periodic crystal can be expanded in plane waves. However, a plane wave expansion of the wave functions in a real crystal requires number of plane wave components to represents the sphere type of core states. To calculate the electronic wave functions for a large system including all the electrons is an extremely hard task. In fact, the electronic states of an atom are classified into: (1) core states, which are highly localized and not involved in chemical bonding, (2) valance states, which are extended and responsible for chemical bonding, and (3) semi-core states, which are localized and polarizable, but do not contribute directly to chemical bonding. Based on these, the strong nuclear Coulomb potential of core levels can be replaced by an effective potential also called as pseudopotential, which is experienced by the valance states [57–59]. Therefore Pseudopotential plane wave method will only consider valance states for all calculations.

2.4.1 A plane wave code: CASTEP

CAmbridge Series of Total Energy Package (CASTEP) is a state-of-the-art quantum mechanics-based program designed specifically for solid-state materials science. CASTEP employs the density functional theory plane-wave pseudopotential method, which allows to perform first-principles quantum mechanics calculations that explore the properties of crystals and surfaces in materials such as semiconductors, ceramics, metals, minerals, and zeolites [60]. The wave functions are expanded out to a maximum G vector, which is equivalent to

an energy cutoff, as plane waves:

$$\psi_j = \sum_{C<G_{max}} {c_k}^j e^{j(k+Gr)} \tag{2.23}$$

where **k** is the k-point being considered in the Brillouin zone. This code uses non-local pseudopotentials of the Kerker type [61] in the Kleinman-Bylander form [62]. In all simulations performed herein, structures were considered relaxed when the force was less than 0.01 /eV, and the energy was changing by less than 1 meV.

2.4.2 Dispersion correction for DFT

Hydrogen bonding and van der Waals (vdW) interactions are crucial for the formation and stability of molecular type crystals. Hybrid semi-empirical solutions are used to introduce damped atom-pairwise dispersion corrections of the form $C_6 R^{-6}$ in the DFT formalism. The missing dispersion contribution to the interatomic interaction is approximated by a simple isotropic potential. At long range, this potential is given by the $C_{6,ij}{R_{ij}}^{-6}$ term, where $C_{6,ij}$ is a material-specific, so-called dispersion coefficient between any atom pair i and j at distance R_{ij}. At short range, the long-range expression is matched to the DFT potential by multiplication with a damping function $f({R_{ij}}^0, R_{ij})$, which reduces the additional dispersion contribution to zero, subject to a cutoff defined by some suitably calculated combination ${R_{ij}}^0$ of the vdW radii of the atom pair. As $C_{6,ij}$ coefficients are additive, the dispersion-corrected total energy E_{tot} may therefore be written as:

$$E_{tot} = E_{DFT} + S_i \sum_{i=1}^{N} \sum_{j>i}^{N} f(S_R {R_{ij}}^0, R_{ij}) C_{6,ij} {R_{ij}}^{-6} \tag{2.24}$$

where E_{DFT} is the standard DFT total energy. Differences between DFT exchange-correlation functionals in the description of short to medium-range dispersion interaction are taken into account by a suitable modification of the correction potential through the

parameters s_6 or S_R. The most well-known schemes were put forward by Grimme [63], Jurecka et al [64], Ortmann, Bechstedt, and Schmidt [65] and most recently by Tkatchenko and Scheffler [66].

2.4.3 Gaussian03: A quantum chemical package

Starting from the basic laws of quantum mechanics, Gaussian predicts the energies, molecular structures, and vibrational frequencies of molecular systems, along with numerous molecular properties derived from these basic computed quantities. It can be used to study molecules and reactions under a wide range of conditions, including both stable species and compounds which are difficult or impossible to observe experimentally such as short-lived intermediates and transition structures.

Ab initio molecular orbital calculations have been performed using the Gaussian 03 quantum chemical package [67]. The vibrational frequencies will be calculated for the optimized structures in order to characterize the nature of the stationary points, zero-point vibrational energy (ZPVE) and thermal correction (H_T). All the correction terms will be estimated by using the set of following equations [68]:

$$[H(T) - H(0)]_{trans} = \frac{5}{2}RT \tag{2.25}$$

$$[H(T) - H(0)]_{rot} = \frac{3}{2}RT \tag{2.26}$$

$$[H(T) - H(0)]_{vib} = RT \sum_{i=1}^{f} \frac{h\upsilon_i}{kT} \frac{\exp^{\frac{h\upsilon_i}{kT}}}{1 - \exp^{\frac{h\upsilon_i}{kT}}} \tag{2.27}$$

where k is the Boltzmann's constant, h is the Planck's constant, f is the number of vibrational degrees of freedom (3N-5 for linear and 3N-6 for nonlinear molecules with N being number

of atoms in the molecule), v_i is i^{th} vibrational frequency, R is the gas constant, H(0) and H(T) are the enthalpies at temperatures of 0 K and T K, respectively.

Chapter 3

Beryllium Hydride and its Oligomers

3.1 Introduction

The search for new potential compounds with desired properties for hydrogen storage has been a continuous challenge among researchers for past few decades [1, 69]. Hydrogen storage in the solid state is a better choice compared to the storage in gaseous or liquid state, because storage in solid state is safer, less sensitive to flammability and compact. The Alkali and Alkaline metal hydrides, amides, borates and alanates are hydrogen storage compounds with promising applications [5, 12, 70, 71]. In this chapter, we present the electronic structure and bonding nature of known simple light metal hydride, Beryllium hydride (BeH_2) as a solid and also as a molecular polymer (upto decamer). Beryllium hydride (BeH_2) is a simple light weight metal hydride well known for its hydrogen storage capability. The crystalline BeH_2 has been reported as a three dimensional array of tetrahedral BeH_4 molecules and not as BeH_2 chains [72–74]. The beryllium hydride oligomers are obtained from the excited beryllium (^1P_o) atom and hydrogen molecule [75]. These are very difficult to synthesize and are easily hydrolyzed by dilute acids. Because of its high hydrogen storage capacity (18.2 wt%), it is of considerable interest especially for use in nuclear reactor and also as a rocket fuel [12]. Therefore, a theoretical understanding of the geometry, stability and electronic

properties of beryllium hydride oligomers is essential for developing chemical methods of hydrogen release and recovery of oligomers. Several theoretical studies emphasizing the electron correlations [76], static dipole polarizabilities [77], and electronic structures [78] have been reported. Chen et al. [79] have reported the geometry and binding energies of possible beryllium hydride clusters $(BeH_2)_n$ (where, n = 1 to 4). However, the stability of these oligomers towards hydrogen storage applications is not clearly understood. Hence, an in-depth theoretical investigation is deemed necessary to explore the various properties such as stability, reactivity, electronic structure and spectroscopic parameters of molecules. In this chapter we describe, density functional theory calculations at HF/6-311++G**, B3LYP/6-31+G**, B3LYP/6-311++G**, B3P86/6-31+G** and B3P86/6-311++G** levels have been performed to investigate geometry, stability, reactivity, spectral parameters and electronic structure properties of model molecules. The stabilities of beryllium hydride oligomers are determined from the frontier molecular orbital energies and their gaps.

3.2 Computational details

Ab initio molecular orbital calculations have been performed for the molecules, BeH_2, Be_2H_4, Be_3H_6, Be_4H_8, Be_5H_10, Be_6H_{12}, Be_7H_{14}, Be_8H_{16}, Be_9H_{18} and $Be_{10}H_{20}$ using the Gaussian 03 quantum chemical package [67]. Their structure optimizations have been performed at the above mentioned levels. All the geometric parameters were allowed to be optimized and no constraints were imposed on the molecular structure during the optimization process. Vibrational frequencies were calculated for the optimized structures to enable us to characterize the nature of the stationary points, zero-point vibrational energy (ZPVE) and thermal correction (H_T). All stationary points have been positively identified as local minima with no imaginary frequencies [68]. Total energy has been used to evaluate reactive descriptors such as ionization potential (IP), electron affinity (EA), polarizability (α), chemical potential (μ), hardness (η), softness (S) and $\triangle E_{(LUMO-HOMO)}$ of model molecules. The chemical potential

(μ) and the hardness (η) of the molecules were calculated according to ref [80, 81].

Electronic structure calculations based on Kohn-Sham density functional theory are more efficient and accurate, therefore the DFT version of Koopman's theorem naturally becomes an interesting topic [82, 83]. Koopman's theorem has been used to calculate the ionization potential and electron affinity of the beryllium hydride oligomers. The ionization potential and electron affinity of the molecule are in general equal to the negative of the highest occupied molecular orbital (HOMO) and the lowest unoccupied molecular orbital (LUMO), respectively [84, 85]. The first principle calculations of crystalline BeH_2 were also carried out by using the plane wave pseudopotential density functional method using CAmbridge Series of Total Energy Package (CASTEP) [60, 86]. We have used ultra-soft pseudopotentials for electron-nuclei interactions with local density approximation (LDA) and generalized gradient approximation (GGA). A plane wave basis set with energy cut-off 480 eV has been applied. For the Brillouin zone sampling, the 5 x 8 x 5 Monkhorst-Pack [87] mesh has been used.

3.3 Results and discussion

This section presents and discusses the results on the geometry, electronic properties, ionization and chemical potentials, electron affinities, softness, hardness, polarizability infrared and Raman spectra of model compounds.

3.3.1 Optimized structures

At the outset, we have performed geometry optimizations of molecules, the optimized structures of model oligomers from the B3LYP/6-311++G** level are shown in figure 3.1. The terminal and bridge Be-H lengths in all molecules are in agreement with the experimental values of $\sim$1.33 and 1.44 $\pm$ 0.04 $\mathring{A}$, respectively [75, 76]. The calculated Be-H-Be angles vary from 84.54^o to 85.91^o with the method adopted and also with the size of basis set. The molecules are asymmetric and are tetragonal with four Be-H bonds i.e., there are two H-

Table 3.1: The total energy (E_0), thermal correction to enthalpy (H_T) and zero-point vibrational energy (ZPVE) of oligomers as computed from the various levels of theory arranged in different columns.(The total energy and thermal correction is in atomic units and zero point vibrational energy are in kcal/mol)

Compound	HF			B3LYP						B3P86					
	6-311++G**			6-31+G**			6-311++G**			6-31+G**			6-311++G**		
	E_0	H_T	ZPVE	E_0	H_T	ZPVE	E_0	H_T	ZPVE	E_0	H_T	ZPVE	E_0	ZPVE	H_T
BeH_2	-15.770	0.016	8.375	-15.919	0.016	8.250	-15.922	0.016	8.254	-16.014	0.016	8.188	-16.017	0.016	8.181
Be_2H_4	-31.580	0.037	20.794	-31.889	0.037	20.303	-31.896	0.037	20.393	-32.085	0.037	20.224	-32.091	0.037	20.298
Be_3H_5	-47.400	0.060	33.805	-47.873	0.059	33.250	-47.883	0.059	33.230	-48.170	0.059	33.126	-48.178	0.059	33.077
Be_4H_8	-63.219	0.082	46.607	-63.854	0.081	45.949	-63.867	0.081	45.874	-64.252	0.081	45.773	-64.263	0.080	45.663
Be_5H_{10}	-79.039	0.104	59.352	-79.835	0.102	58.563	-79.852	0.102	58.451	-80.334	0.102	58.359	-80.349	0.102	58.194
Be_6H_{12}	-94.858	0.126	72.024	-95.816	0.124	71.197	-95.836	0.124	70.994	-96.416	0.124	70.941	-96.434	0.124	70.517
Be_7H_{14}	-110.67	0.148	84.882	-111.79	0.146	83.647	-111.82	0.146	83.685	-112.49	0.146	83.545	-112.51	0.146	83.199
Be_8H_{16}	-126.49	0.170	97.590	-127.77	0.168	96.187	-127.80	0.168	96.191	-128.58	0.167	95.921	-128.60	0.167	95.803
Be_9H_{18}	-142.31	0.192	110.38	-143.75	0.189	108.56	-143.79	0.189	108.60	-144.66	0.189	108.29	-144.68	0.189	108.10
$Be_{10}H_{20}$	-158.09	0.212	121.74	-159.69	0.210	120.52	-159.77	0.211	121.21	-160.74	0.211	120.58	-160.77	0.211	120.73

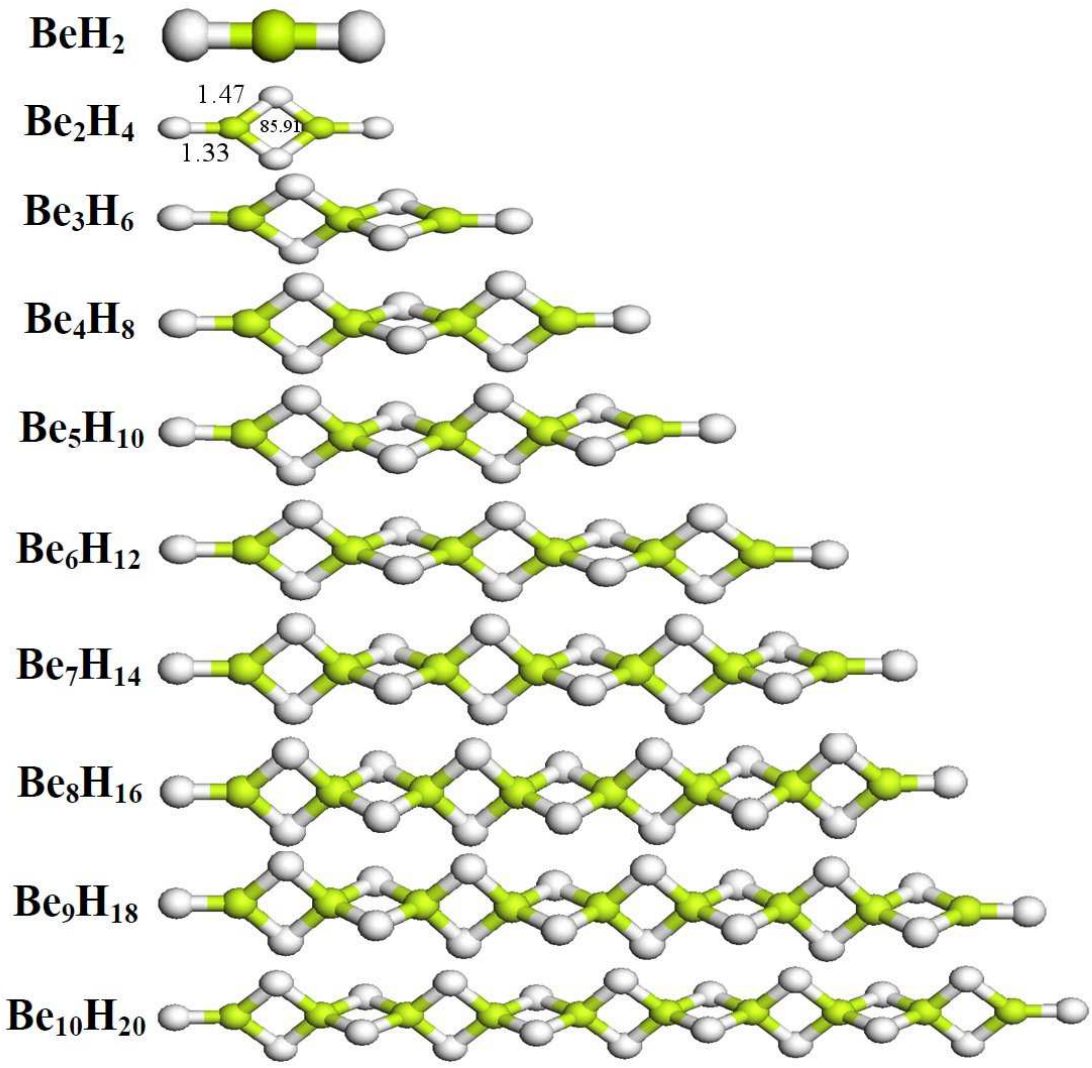

Figure 3.1: Optimized structures of model molecules computed at the B3LYP/6-311++ G** level. The bond lengths are in Angstrom and bond angles are in degree (Green spheres represents Beryllium atoms and white spheres represents Hydrogen atoms).

Be-H-Be-H planes that are perpendicular to each other in the Be_3H_6 to $B_{10}H_{20}$ molecules. With increase in the basis set as well as the size of the molecules the point group symmetries

change from $D_{\infty}h$ to Cl. The point groups of Be_2H_4, Be_4H_8, Be_6H_{12}, Be_8H_{16} and $Be_{10}H_{20}$ molecules at the three levels (HF, B3LYP and B3P86) of calculations are $D_{\infty h}$, C_2v, C_2, C_1 and C_1, respectively. The total energies (E_0) and zero point vibrational energies (ZPVE) of the oligomers computed from the HF, B3LYP and B3P86 methods with basis sets 6-31+G** and 6-311++G** are presented in table 3.1. The total energies of the molecules calculated from the basis set 6-311++G** with three methods are nearly same. The binding energies (BE) of oligomers are apparently higher, revealing that the stability of model molecules increases with increasing size. The binding energies calculated per unit and lowest harmonic frequencies of molecules are summarized in table 3.2.

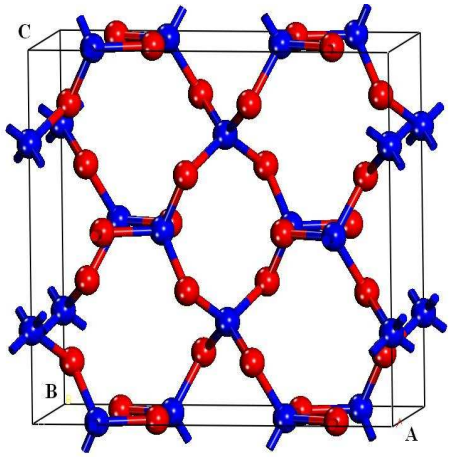

Figure 3.2: Optimized crystalline structure of BeH_2 with local density approximation (LDA). Blue spheres represents Beryllium atoms and red spheres represents Hydrogen atoms.

Furthermore, we have optimized the crystalline BeH_2 within LDA and GGA, the optimized crystalline structure of BeH_2 is shown in figure 3.2. The crystalline beryllium hydride contains twelve BeH_2 units with network of BeH_4 tetrahedral molecules in the unit cell. The structural parameters such as lattice constants, atomic positions and the band gap with experimental values are listed in table 3.3 except for band gap for which there is yet no experiment result. The calculated properties have been found to be in good agreement with the experimental values [73]. We have also calculated the electronic band structure as well

Table 3.2: The calculated binding energy (BE) and lowest harmonic frequencies (ω_L) of oligomers computed from the various levels of theory (The binding energies are in atomic units and lowest harmonic frequencies are in cm^{-1}).

Compound	HF		B3LYP				B3P86			
	6-311++G**		6-31+G**		6-311++G**		6-31+G**		6-311++G**	
	BE	ω_L	BE	ω_L	BE	ω_L	BE	ω_L	BE	ω_L
BeH_2	-15.770	750.427	-15.919	736.106	-15.922	739.186	-16.014	722.029	-16.017	723.669
Be_2H_4	-15.790	344.529	-15.944	325.674	-15.948	326.455	-16.042	317.452	-16.045	323.105
Be_3H_5	-15.800	159.258	-15.957	162.252	-15.961	147.876	-16.056	154.450	-16.059	141.750
Be_4H_8	-15.804	89.936	-15.963	97.993	-15.966	88.427	-16.063	93.771	-16.065	85.113
Be_5H_{10}	-15.807	64.528	-15.967	67.322	-15.970	61.670	-16.066	67.822	-16.069	58.648
Be_6H_{12}	-15.809	45.785	-15.969	48.427	-15.972	45.403	-16.069	45.953	-16.072	41.597
Be_7H_{14}	-15.811	34.355	-15.971	35.254	-15.974	34.792	-16.071	32.499	-16.074	33.276
Be_8H_{16}	-15.812	26.422	-15.972	26.734	-15.975	26.383	-16.072	24.389	-16.075	25.372
Be_9H_{18}	-15.812	21.135	-15.973	21.658	-15.976	20.230	-16.073	18.574	-16.076	18.481
$Be_{10}H_{20}$	-15.809	5.138	-15.969	15.748	-15.977	17.129	-16.074	15.036	-16.077	16.551

as the total and partial density of states of BeH_2. The density of states and band structure of the compound are shown in figure 3.3. The direct band gap along Γ- Γ direction of the crystalline BeH_2 has been calculated to be 5.51eV with LDA and 5.58 eV with GGA. The valence band consists of Be-2p states and H-1s states and the conduction band is dominated by the Be-2s states. The overlap of Be-2p states and H-1s states at Fermi level indicates the presence of *sp* hybridization in the molecule with covalent character.

Table 3.3: The Optimized lattice parameters, atomic positions and the calculated band gap of the crystalline BeH_2 along with experimental values.

Property	LDA	GGA	Expt[a]
a($\AA$)	8.700	8.964	9.082
b($\AA$)	3.939	4.147	4.160
c($\AA$)	7.477	7.633	7.707
	Atomic	Positions	
Be1(x)	0.000	0.000	0.000
Be1(y)	0.000	0.000	0.000
Be1(z)	0.250	0.250	0.250
Be2(x)	0.168	0.167	0.169
Be2(y)	0.121	0.118	0.125
Be2(z)	0.000	0.000	0.000
H1(x)	0.089	0.088	0.089
H1(y)	0.248	0.225	0.194
H1(z)	0.154	0.152	0.151
H2(x)	0.321	0.310	0.305
H2(y)	0.256	0.274	0.282
H2(z)	0.000	0.000	0.000
E_g(eV)	5.51	5.58	-

[a]Ref[74];

3.3.2 Electron affinity, ionization and chemical potentials

The ionization potential (IP) and electron affinities (EA) provide the information about the reactivity and stability of the compounds. The compounds with higher IP and lower EA

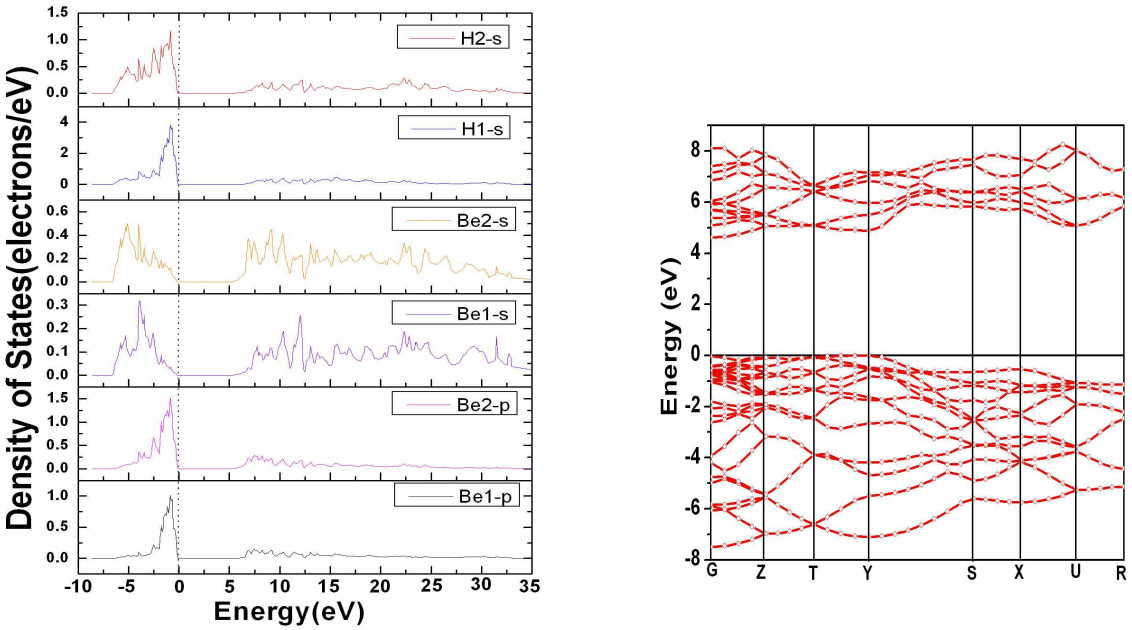

(a) (b)

Figure 3.3: (a) The density of states and (b) band structure of crystalline BeH_2 within local density approximation (LDA).

values are more stable compared to the compounds with lower IP and higher EA values. The chemical potential (μ) characterizes the tendency of electron to escape from the molecule in the equilibrium state. Koopman's theorem has been used to calculate IP, EA and μ of the molecules [84]. Electron affinity, ionization and chemical potentials of the model molecules are shown in figure 3.4. In our case, it has been observed that the IP and EA values of oligomers vary with the method and the basis set. The IP values decreased with the size of the oligomers. However, the IP of Be_2H_4 is less compared to that of Be_3H_6 molecule. A maximum EA value ($\sim$0.095 a.u) for the Be_2H_4 has been noticed. However, we have found that the EA values of Be_2H_4, Be_4H_8, Be_6H_{12}, Be_8H_{16} and $Be_{10}H_{20}$ molecules (even series) are higher compared to BeH_2, Be_3H_5, Be_5H_{10}, Be_7H_{14} and Be_9H_{18} molecules (odd series).

The higher EA values of even series indicate that these could be less stable or highly reactive compared to odd series. The variation in the EA values of the molecules is probably due to the charge transfer among the atoms within the molecule. The chemical potentials (μ) values of even series are also higher than those of the odd series.

3.3.3 Hardness, softness and polarizability

The hardness (η) and softness (S) are the important factors for the charge transfer resistance and these are inversely proportional to each other [88]. The calculated hardness and softness of the model oligomers in the present case are shown in figure 3.5. It is found that the hardness and softness values are independent of the method and choice of basis set. According to the principle of maximum hardness (PMH), it is expected that the molecule in the equilibrium state possess maximum hardness and in the transition state possess minimum hardness [89, 90]. It has been found that the odd series are more stable than the even series. The dipole polarizability (α) measures the distortion of electron density of molecules and the response of the molecule to external electric field. The polarizability, like for the other polymers, increases rapidly with size of the oligomers i.e., distortion of the electronic density of oligomer is linear with external electric field and it is in good agreement with the previous studies [78].

3.3.4 Frontier molecular orbital energies

The stability of the compounds is usually measured by the total energy (for isomers), bond length, bond dissociation energy, frontier orbital highest occupied molecular orbital (HOMO) and lowest unoccupied molecular orbital (LUMO) energy and their gaps. We have used frontier orbital energies to evaluate the stability of the BeH_2 oligomers. Fukui et al [91] noticed the prominent role played by HOMO and LUMO in governing chemical reactions. It has been revealed in several investigations that the band gap ($\triangle E_{(LUMO-HOMO)}$) in energy between the HOMO and LUMO is an important stability index of the molecules

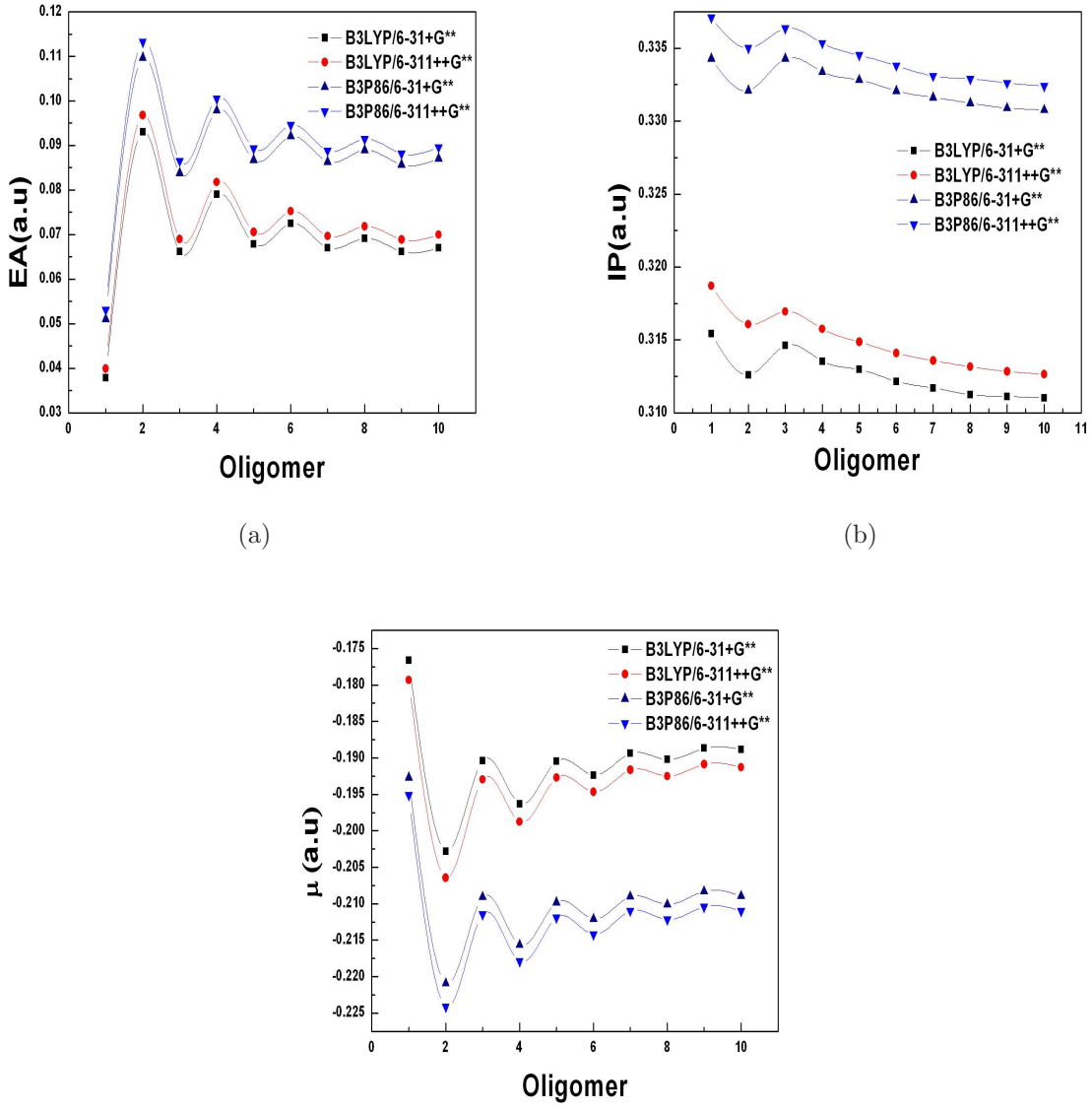

(a) (b)

(c)

Figure 3.4: (a) Electron affinity, (b) ionization and (c) chemical potential of the model molecules computed from various levels of the theory.

[92–95]. A large band gap implies high stability and small gap implies low stability. The high stability in turn indicates low chemical reactivity and small band gap indicates high chemical

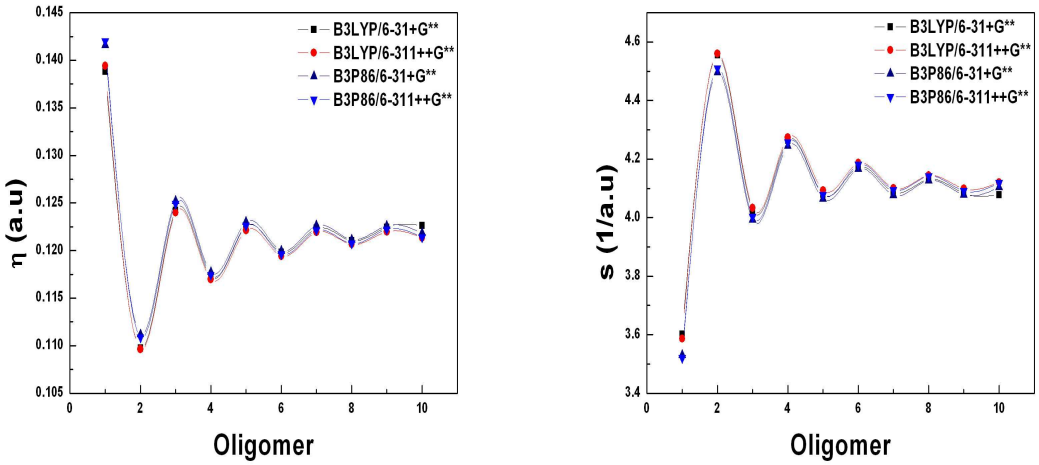

(a) (b)

Figure 3.5: (a) The calculated hardness and (b) softness of model oligomers computed from various levels of the theory.

reactivity. In other words, smaller the gap between HOMO and LUMO, the easier the electron transition and lesser the stability of the compound will be. The frontier molecular orbitals of model molecules obtained from the B3LYP/6-311++G** level are shown in figure 3.6. With increase of the monomer units of the BeH_2 oligomer, the HOMO has been observed to correspond to that of a finite-graphene-like-structure [96] and is prominent in the molecules Be_4H_8 to $Be_{10}H_{20}$. With increase of the basis set, the frontier molecular orbital energies and their gaps have increased. In the model compounds BeH_2 is found to be most stable and $Be_{10}H_{20}$ is found to be least stable, which is reflected in the band gap values. The frontier molecular orbital energies of odd series have higher values compared to even series. The frontier molecular orbital energies of the model molecules are shown in figure 3.7. BeH_2 oligomer structures are like the zig zag edge states of finite graphene [96]. The edge states in non metallic graphene ribbons are located on length confined zig zag edge have been discussed by Shemella et al [96]. We also observe a similar zig zag edge in the present oligomers. Therefore one can expect the similar HOMOs in BeH_2 oligomers like finite graphene or

nanotubes where they are located at the edges. In finite graphene ribbons this typical behavior is observed only for non metallic ribbons, which is not the case for metallic graphene ribbons. In the present case we observe the HOMO energy levels located at the length confined edge of the oligomers. Since HOMOs are localized at the edges, it may be possible to control the band gaps using different functionalized groups.

3.3.5 Mulliken atomic charges

One of the most important properties of a molecule is its charge or spin density distribution. Although there is no unique definition of how many electrons are attached to an atom in a molecule it has nevertheless proven useful in many cases to perform such population analysis. Due to its simplicity the Mulliken population analysis has become the most familiar method to count electrons to be associated with an atom. It has been found that the hydrogen and beryllium atoms have negative and positive Mulliken atomic charges, respectively. However, beryllium atoms in Be_4H_8, Be_5H_{10} and Be_6H_{12} molecule have negative charges of two, one and four, respectively. We have noticed only two negative charges in Be_7H_{14}, Be_8H_{16}, Be_9H_{18} and $Be_{10}H_{20}$ molecules. In general, if more electrons are shared by the hydrogen atom, higher is the negative charge. The higher negative charges have been observed for the beryllium atoms in Be_4H_8 to $Be_{10}H_{20}$ molecules and thus there is a possibility of covalent bonding among beryllium and hydrogen atoms.

The Mulliken population on the charge density distribution of crystalline BeH_2 is shown in figure 3.8. The charges of beryllium and hydrogen atoms of crystalline BeH_2 have been calculated to be -0.23, -0.24, +0.50 and +0.45 e for H(1), H(2), Be(1) and Be(2) atoms, respectively. The negative charge of hydrogen atoms implies the electronegative nature towards beryllium atoms. R. S. Mulliken [97] states that "If the total overlap population between two atoms is positive, they are bonded; if negative, they are anti-bonded". The high positive population indicates the possibility of having high degree of covalent character of bond [97, 98]. All Be-H bonds have bond population about 0.55 indicating the equal ionic

Oligomer	HOMO	LUMO
BeH_2	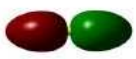	
Be_2H_4	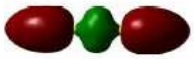	
Be_3H_6		
Be_4H_8	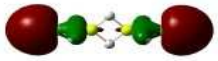	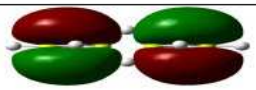
Be_5H_{10}		
Be_6H_{12}		
Be_7H_{14}	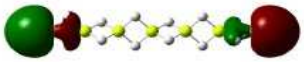	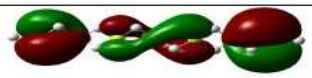
Be_8H_{16}	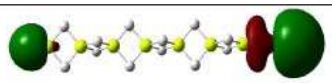	
Be_9H_{18}	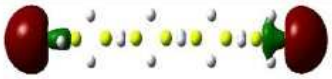	
$Be_{10}H_{20}$		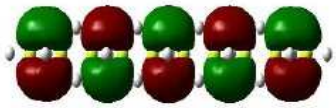

Figure 3.6: Frontier molecular orbitals of the model molecules computed at B3LYP/6-311++G** level. Green spheres represents Beryllium atoms and white spheres represents Hydrogen atoms.

and covalent character. Figure 3.8 shows the charge density distribution of crystalline BeH_2. The charge density around H atom has been found to be higher compared to beryllium atom.

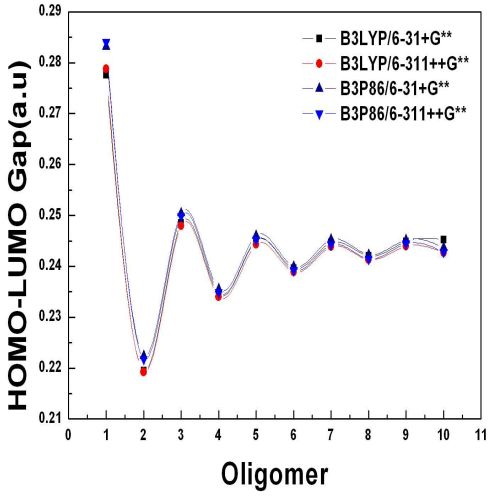

Figure 3.7: The HOMO-LUMO gap of the model molecules computed at B3LYP/6-311++G** level.

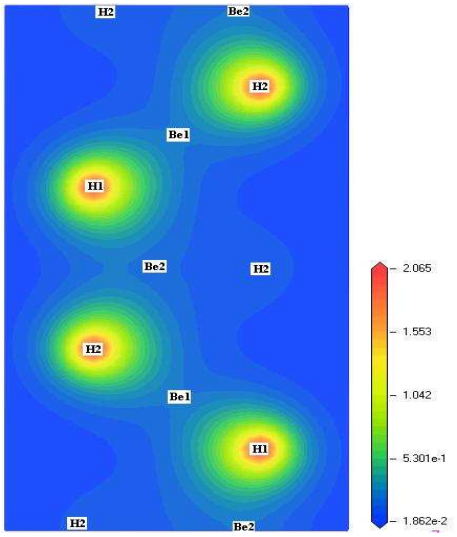

Figure 3.8: The charge density distribution of the crystalline BeH_2 within local density approximation (LDA)

The shape of charge density around hydrogen atoms is slightly deformed towards beryllium atoms. Therefore, there is possibility of equal covalent and ionic character of Be-H bonds in

BeH_2.

3.3.6 Infrared and Raman spectra

The infrared (IR) and Raman spectra of molecules are obtained from the computed structures at B3LYP/6-31++G** levels and are presented in figures 3.9 & 3.10. The calculated wave numbers of BeH_2 and Be_2H_4 molecules are in good agreement with experimental values [72–74]. It was observed that the stretching vibration (1510 cm^{-1}) of Be_3H_6 molecule is splitting and the same has been found sin all oligomers. The splitting of vibrational line of 1510 cm^{-1} has been observed in Be_3H_6 to $Be_{10}H_{20}$ molecules. However, the wave numbers corresponding to 1900, 1910, 1920 and 1930 cm^{-1} in Raman spectra of $Be_{10}H_{20}$ are probably due to the splitting of the line corresponding to 1810 cm^{-1}.

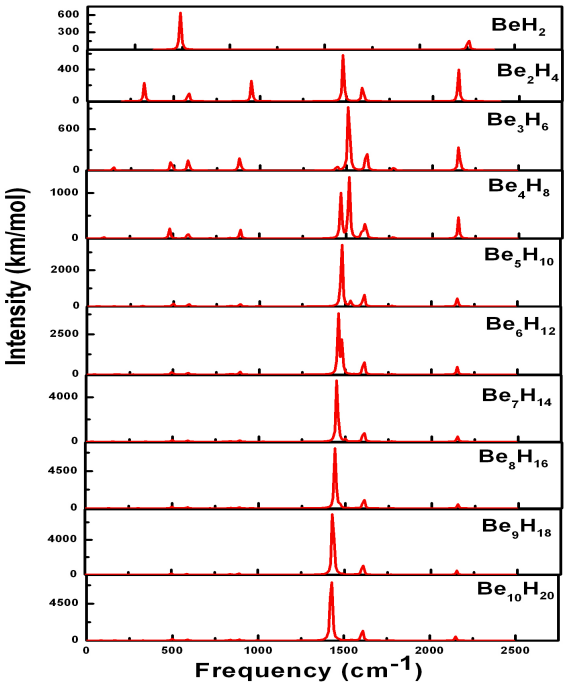

Figure 3.9: The infrared (IR) spectra of the molecule are obtained from the computed structures at B3LYP/6-31++G** level.

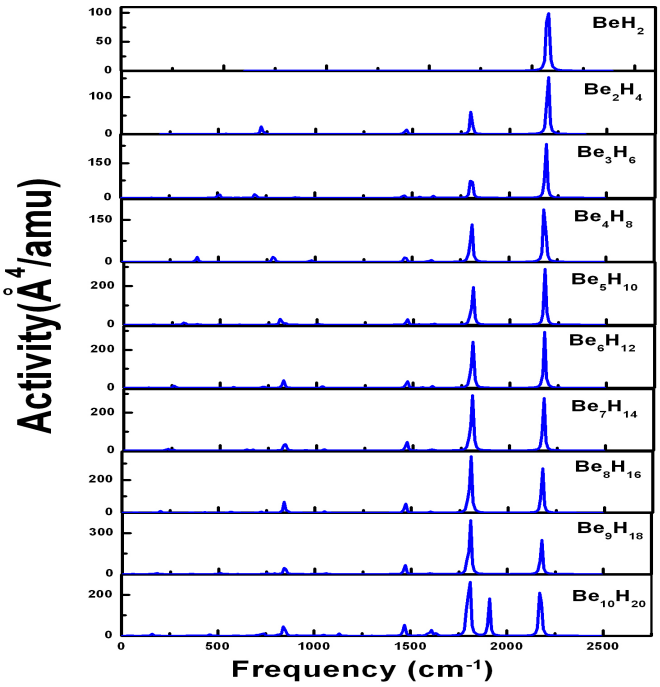

Figure 3.10: Raman spectra of the molecule are obtained from the computed structures at B3LYP/6-31++G** level.

3.4 Conclusions

The electronic structure properties of beryllium hydride oligomers have been carried out at HF, B3LYP and B3P86 methods with 6-31+G** and 6-311++G** basis sets. The band gap $\triangle E_{(LUMO-HOMO)}$, ionization potential (IP), electron affinity (EA), chemical potential (μ), hardness (η), softness (S) and polarizabilities (α) of beryllium hydride oligomers have been calculated. From the band gap, chemical potential, hardness and softness of molecules, BeH_2, Be_3H_5, Be_5H_{10}, Be_7H_{14} and Be_9H_{18} molecules have been found to be more stable compared to Be_2H_4, Be_4H_8, Be_6H_{12}, Be_8H_{16} and $Be_{10}H_{20}$ molecules. The IR spectra of BeH_2 and Be_2H_4 molecules were found to be in good agreement with the experimental values. The IR spectra of molecules have five fundamental bands (475 to 575, 840 to 890, 1410 to 1520, 1610 and 2150 cm^{-1}) that are prominent.

The next chapter discusses complex hydride ammonia borane (AB).

Chapter 4

Ammonia Borane (NH_3BH_3)

4.1 Introduction

Ammonia borane (NH_3BH_3) is a high hydrogen content (19.6 wt%), safe, non toxic and chemically stable compound [99–101]. Of late it has emerged as a potential candidate in H-based fuel cell applications [28, 38, 42, 102–104] being particularly attractive for the potential reversibility of hydrogen release reactions under mild conditions [105]. The kinetics and thermodynamics of hydrogen release of NH_3BH_3 can be improved by impregnating it with mesoporous materials which act as catalysts [103]. Ammonia borane has remarkably high gravimetric and volumetric hydrogen density and it releases H_2 at moderate temperatures [104]. The hydrogen can be released by thermolysis, starting at temperatures 80^oC, but at high temperatures the process tends to release volatile gases such as borazine ($B_3H_6N_3$) [104]. Recent experimental and theoretical works concentrated on the native defects [106] and substitution of Li or Na with hydrogen atoms connected to N in NH_3BH_3, which significantly enhances dehydrogenation kinetics and suppressed borazine release [107, 108]. Ammonia borane (NH_3BH_3) is a B-H-N compound, which is similar to simple hydrocarbon $_3HC\text{-}CH_3$. $_3HC\text{-}CH_3$ is a gas at room temperature whereas the $_3HB\text{-}NH_3$ is solid due to the difference in the electro-negativity between B and N resulting in multipolar molecules

[106–108]. NH_3BH_3 is a white crystalline solid, and is ether soluble. It slowly releases hydrogen at room temperature [109–119]. At low temperature (16 K) NH_3BH_3 crystallizes in an ordered orthorhombic structure. It has a transition around 225 K to a disordered tetragonal structure [109–119]. This transition is due to hydrogen atoms being exchanged between the -BH_3 and -NH_3 groups. The hydrogen atoms within -NH_3 are more mobile than that in -BH_3, at low temperatures [119–123]. In NH_3BH_3, the -NH_3 group has a tendency to attract electrons (protic nature) whereas -BH_3 group has a tendency to give up electrons (hydridic nature). This leads to a network N-$H^{\delta+}$...$^{-\delta}$H-B created due to dihydrogen bonding. These bonds have substantial interaction energy leading to unusually short H-H distances of 1.7-2.2 $\mathring{A}$ compared to the sum (2.4 $\mathring{A}$) of the van der Waals radii for two hydrogen atoms from neighboring molecules. This bonding between NH_3BH_3 molecules is thus by the "dihydrogen bonding". Similar dihydrogen bonding is observed in the 2-aminopyridine complex and also in $[ReH_5(PPh_3)_3]$.indole [109, 124–126]. The application of high pressure to materials may induce significant changes in molecular structures and associated properties, such as enhanced hydrogen storage capacities [127–131]. The high pressure behavior of NH_3BH_3 have been studied experimentally and theoretically [126, 132]. These studies are basically motivated by the anomalous lattice stability of NH_3BH_3. At room temperature, in contrast to the very similar compounds like diborane, B_2H_6 (liquid up to 4 GPa [129]) and ethane, C_2H_6 (gas), NH_3BH_3 forms a solid phase. The stability in NH_3BH_3 in this phase is due to the existence of dihydrogen bonds between NH_3BH_3 molecules [133]. At room temperature and above a pressure of 1.5 GPa, NH_3BH_3 crystallizes into a new ordered orthorhombic (Cmc21) structure with four molecules per unit cell. At high pressures it undergoes to triclinic (P1) phase around 8-13 GPa [134, 135]. Several experimental [28, 38, 42, 99–103, 105, 107–123, 125, 126, 136] and theoretical [99, 106–108, 111, 124, 136, 137] studies have been performed earlier to determine the phase transitions [106–110, 119, 120, 122, 123], structure [109–119], native defects [106], hydrogen release [38, 42, 99, 100, 103, 105, 137] and dihydrogen bonding [109, 124–126] in solid phase of NH_3BH_3. The mechanical properties

of NH_3BH_3, which are qualitatively different from that of other hydrides, have not been explored as yet.

This chapter is aimed in exploring the physical and chemical properties of the low temperature orthorhombic phase of NH_3BH_3. We have calculated the structural, electronic, bonding, vibrational properties and Debye temperature of the ordered orthorhombic phase. We also highlighted the role of van der Waals (vdW) interactions in NH_3BH_3. The rest of the chapter is organized as follows. In section 4.2 we discuss computational details including the calculation of elastic constants. Results are presented in section 4.3 and section 4.4 deals with the conclusions.

4.2 Computational details

The first principles calculations are carried out using the plane wave pseudopotential method based on density functional theory as implemented in CAmbridge Series of Total Energy Package (CASTEP) [60, 86]. The electron-ion interactions can be seen as the electrons are interacting with the rigid ions. Valence electrons experience the core as screened by the core electrons. The pseudopotential is an effective potential constructed to replace the atomic all-electron potential such that core states are eliminated and the valence electrons are described by pseudo-wave functions. For NH_3BH_3, the basis orbitals used as valence states are H: $1s^1$, B: $2s^2$,$2p^1$, and N: $2s^2$,$2p^3$. We use ultrasoft pseudopotentials (USP) introduced by Vanderbilt [59] together with local density approximation (LDA) of Ceperley and Alder [138] parameterized by Perdew and Zunger (CA-PZ) [139] and generalized gradient approximation (GGA) of Perdew-Burke-Ernzerhof (PBE) [140, 141]. A plane wave basis set with energy cut-off of 520 eV has been applied. The vdW forces were taken into account through the semiempirical methods proposed by the Grimme (G06) [63], Ortmann, Bechstedt, and Schmidt (OBS) [65], and most recently by Tkatchenko and Scheffler (TS) [66] using the ultrasoft pseudopotentials. For the Brillouin zone sampling, the 7 x 7 x 7

Monkhorst-Pack [87] mesh has been used, in which the forces on the atoms are converged to less than 0.0005 eV/$\mathring{A}$. The maximum ionic displacement is within 0.005$\mathring{A}$ and the total stress tensor is reduced to the order of 0.02 GPa.

4.2.1 The elastic constants

The response of a solid under external forces is a measure of the elastic constants. The strength of a solid material can be characterized by calculating the mechanical properties such as bulk, shear and Young's moduli and Poisson's ratio. A completely anisotropic materials elastic behavior is specified by 21 independent elastic constants. The materials with orthorhombic structure possess nine independent elastic constants namely C_{11}, C_{22}, C_{33}, C_{44}, C_{55}, C_{66}, C_{12}, C_{13} and C_{23}. These elastic constants can be obtained by applying small volume conserving elastic strains, and each time the strain changes, the coordinates of ions are fully relaxed to ensure the energy minimum rule. Here, we calculate these constants by applying a strain that transforms the lattice vectors as $R^{'} = \epsilon$ R, where R and $R^{'}$ are the old and new lattice vectors respectively and ϵ is the strain tensor [142, 143]. For small deformations, stress and strain tensors are related by $\sigma_i = \sum_j C_{ij} e_j$ where C_{ij} is elastic constant tensor, which can be represented by symmetric 6 X 6 matrix with compliance components c_{ij}. The mechanical stability criteria for orthorhombic crystalline structure [143] are as follows:

C_{11}, C_{22}, C_{33}, C_{44}, C_{55}, $C_{66} > 0$,
$[C_{11}+C_{22}+C_{33}+2(C_{12}+C_{13}+C_{23})] > 0$,
$(C_{11}+C_{22}-2C_{12}) > 0$,
$(C_{11}+C_{23}-2C_{13}) > 0$,
$(C_{22}+C_{33}-2C_{23}) > 0$.

After obtaining single crystal elastic constants one can calculate bulk and shear moduli of polycrystalline material from the Voigt-Ruess-Hill (VRH) approximation as discussed in

Ref [142–145]. The bulk modulus (B) and shear modulus (G), based on Hill approximation [145], are the arithmetic averages of Voigt and Reuss elastic modulus i.e., $B = \frac{1}{2}(B_R + B_V)$ and $G = \frac{1}{2}(G_R + G_V)$. The Young's modulus (E) and Poisson's ratio (σ) for isotropic materials are given by [146]

$$E = \frac{9BG}{3B+G}; \quad \sigma = \frac{3B-2G}{2(3B+G)}. \tag{4.1}$$

4.3 Results and discussion

4.3.1 Structural and electronic properties

The optimized crystal structure of low temperature orthorhombic phase of NH_3BH_3 obtained in our calculations is shown in figure 4.1, in which each formula unit contain pair of B and N atoms which are surrounded by three H atoms i.e., N is connected to one H1 and two H2, whereas B is connected to two H3 and one H4 as shown in figure 4.1.

The calculated structural parameters and fractional coordinates are given in tables 4.1 and 4.2 obtained using LDA and GGA along with OBS, G06 and TS, along with the experimental data for easy comparison. The unit cell volume obtained by LDA is underestimated by 12% and with GGA it is overestimated by 13.7%. NH_3BH_3 is a molecular crystal and the individual molecules in the crystal bind through van der Waals (vdW) interactions. The LDA has a spurious overbinding feature that bond vdW systems, but GGA does not have this overbinding effect for vdW crystals. In GGA, the molecules will drift apart so the lattice parameters become very large during geometry optimization. The geometry of vdW crystal is not well optimized in GGA [147, 148]. The lattice parameters obtained within GGA follow wrong tendency i.e, c > a > b, which is completely different from experimental trends a > c > b. Nevertheless, the sizable deviation of the GGA optimized structure from the experiment has to be corrected, suggesting the necessity of long-range vdW interactions [148]. The error remarkably reduced at various vdW methods, giving little difference of

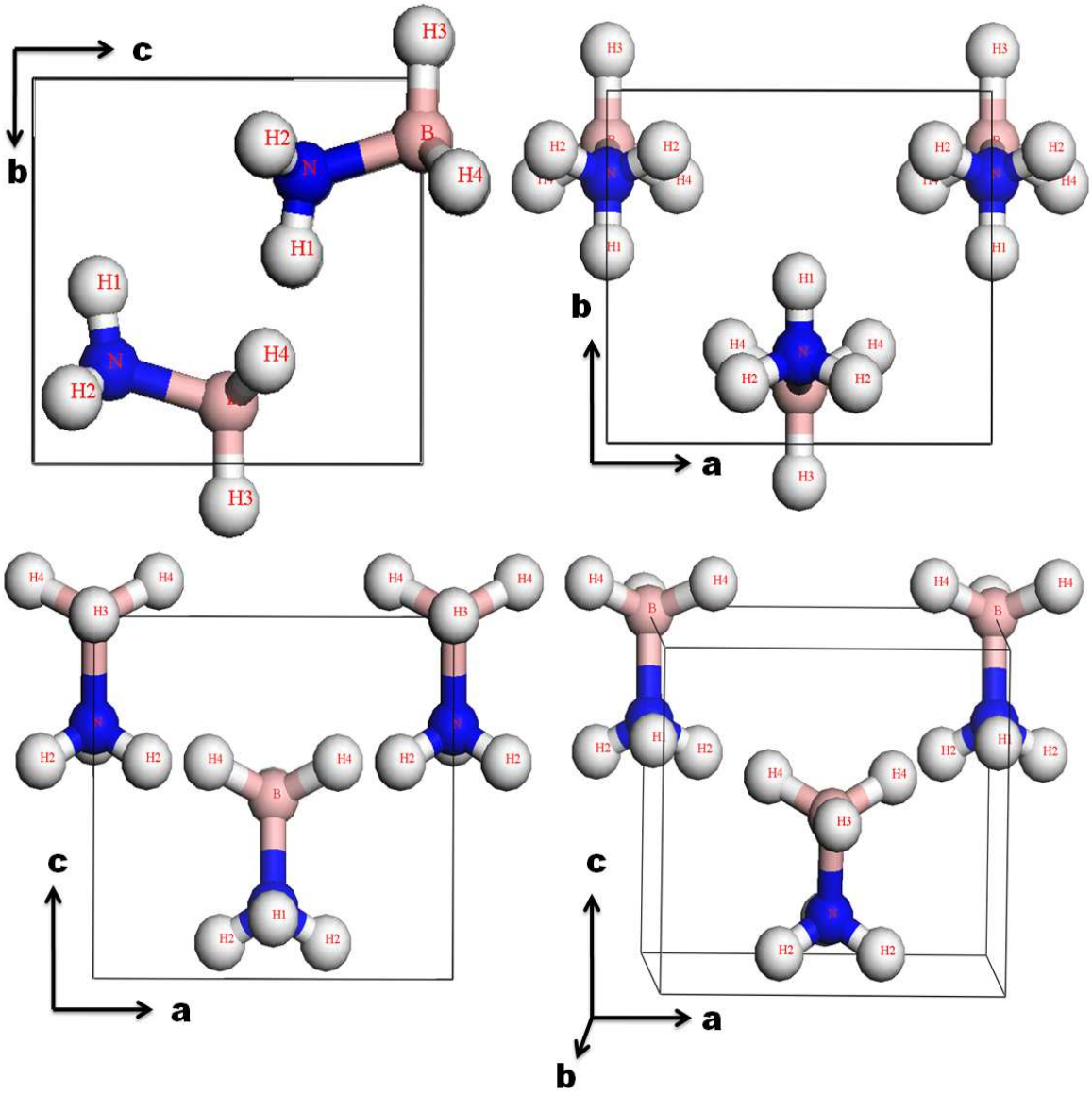

Figure 4.1: The optimized crystal structure of NH_3BH_3 at the theoretical equilibrium volume represented along different crystallographic directions (Blue spheres represents Nitrogen atoms, pink spheres represents Boron atoms, and white spheres represents Hydrogen atoms).

underestimation is 5% with TS from experimental volume. With the inclusion of long range vdW interactions, the ground state properties such as equilibrium lattice parameters, atomic

positions and bond lengths are in good agreement with the experiments. For comparison, we also tested other vdW methods, particularly OBS and G06. The OBS underestimated by 30% which is worse than regular LDA and GGA, whereas G06 a conventional dispersion correction method also underestimated by only 2% from experimental volume. G06 usually tends to overestimate lattice constants of molecular and layered crystals. G06 method imposes very small vdW radius [the vdW radius corresponds to half of the distance between the two atoms where Pauli repulsion balances the London dispersion interaction] (1.001$\mathring{A}$) for H atoms, which leads to overbinding of the dihydrogen bonds where the typical dihydrogen bond length in the NH_3BH_3 is 2.0$\simeq$2.2 $\mathring{A}$. Optimization of vdW radii for solids leads to significant improvement of lattice constants and binding energies. Therefore, the correction brought by the G06 scheme appears to be too strong, a fact that has been noticed in recent work [149] using the G06 method. In NH_3BH_3, the vdW radius of 1.301 $\mathring{A}$ for H atoms is the best choice to describe the correct structural properties of dihydrogen bonded molecular NH_3BH_3 system in general, where the vdW correction effectively works to bind molecules only over a long range while keeping short range covalent bonds unchanged [150]. Further calculations are compared using vdW method TS along with LDA.

The band structure and density of states (DOS) of NH_3BH_3 are shown in figures 4.2a and 4.2b, respectively. The band structure is plotted along the high symmetry directions in Brillouin zone given as follows: Γ (0.0 0.0 0.0)$\rightarrow$ Z (0.0, 0.0, 0.5)$\rightarrow$ T (-0.5, 0.0, 0.5)$\rightarrow$ Y (-0.5, 0.0, 0.0)$\rightarrow$ S (-0.5, 0.5, 0.0)$\rightarrow$ X (0.0, 0.5, 0.0)$\rightarrow$ U (0.0, 0.5, 0.5)$\rightarrow$ R (-0.5, 0.5, 0.5). From the band structure, it is found that NH_3BH_3 has an indirect band gap of 5.644 eV (5.959 eV) with LDA(GGA) along the Γ- Z direction indicating that the compound is an insulator. Whereas the band gap obtained with vdW correction by OBS is 5.767, 6.021 eV with G06 and with TS, it is 6.041 eV. The effect of vdW interaction on the calculated band gap is very less. This band gap is comparable with Alkaline earth dihydrides i.e close to the BeH_2 [151] and larger than that of MgH_2 [152]. The calculated band gap value is consistent with other theoretical studies i.e., with VASP-GGA [106] it is 6.0 eV, with Dmol3-LDA [111]

Table 4.1: The optimized structural parameters of NH_3BH_3 along with experimental values.

Property	LDA	OBS	GGA	G06	TS	Other	Expt
a($\mathring{A}$)	5.189	5.130	5.370	5.367	5.410	$5.366^a 5.302^b 5.29^c$	$5.55395(29)^f$
b($\mathring{A}$)	4.473	3.879	4.975	4.585	4.549	$4.614^a 4.939^b 4.89^c$	$4.61048(21)^f$
c($\mathring{A}$)	4.826	4.451	5.418	5.077	4.909	$5.100^a 5.172^b 5.13^c$	$5.00004(21)^f$
V($\mathring{A}^3$)	112.03	88.61	144.77	124.97	120.83		128.033
B-N($\mathring{A}$)	1.551	1.525	1.596	1.587	1.586	$1.59^{b-d} 1.57^e$	$1.58(2)^g$
N-H1($\mathring{A}$)	1.040	1.042	1.032	1.034	1.033	$1.03^{b,c} 1.028^d 1.042^e$	$1.07(4)^g$
N-H2($\mathring{A}$)	1.049	1.049	1.040	1.039	1.039	1.03^{a-e}	$0.96(3)^g$
B-H3($\mathring{A}$)	1.233	1.220	1.228	1.228	1.228	$1.22^{b,d} 1.23^{c,e}$	$1.15(3)^g$
B-H4($\mathring{A}$)	1.224	1.205	1.221	1.221	1.218	$1.22^{b-d} 1.23^e$	$1.18(3)^g$
H1...H2($\mathring{A}$)	1.681	1.692	1.669	1.667	1.666		
H1...H3($\mathring{A}$)	2.584	1.829	3.038	2.663	2.771		
H1...H4($\mathring{A}$)	1.989	1.804	2.380	2.101	2.112	$2.27^a 2.19^c 2.29^e$	$2.21(4)^g$
H2...H3($\mathring{A}$)	1.785	1.739	1.946	1.909	1.899	$1.90^a 1.89^{c,e}$	$2.02(3)^g$
H2...H4($\mathring{A}$)	2.027	1.831	2.121	2.115	2.108	$2.17^a 2.22^c 2.09^e$	$2.23(4)^g$
H3...H4($\mathring{A}$)	2.007	1.965	2.015	2.011	2.008		
H2...H2($\mathring{A}$)	1.694	1.699	1.672	1.676	1.675		
H4...H4($\mathring{A}$)	2.000	1.964	2.004	2.006	1.993		

[a]Ref[124]; [b]Ref[137]; [c]Ref[106]; [d]Ref[136]; [e]Ref[111]; [f]Ref[110]; [g]Ref[109];

it is 5.85 eV and with PWscf [136] it is 6.0 eV. The discrepancy is because the band gaps obtained from similar calculations are always equal or smaller than the true gaps, due to the well known DFT band gap underestimation. However one has to use GW approximation for exact band gap calculations, which is better than LDA and GGA [153]. From, recent study the band gap of NH_3BH_3 using GW approximation is found to be 9.60 eV [154].

In the band structure, the valence band has essentially three regions, -1.5eV to 0 eV (higher), -4eV to -2.5 eV (middle) and -7.5eV to -5.5eV (lower). The lower regions are mainly due to the *p* states of N, *s* states of B and with minor contribution from *s* states of all hydrogens. The middle region is because of the *p* states of B, N and with migrant contribution from *s* states of H3 & H4. The *p* states of B and *s* states of H3 & H4 are governing the higher energy region with minor contribution from *p* states of N. The conduction band

Table 4.2: The optimized fractional atomic coordinates of NH_3BH_3 along with experimental values.

Atom		LDA	OBS	GGA	G06	TS	Other[a]	Expt[b]
	x	0.0	0.0	0.0	0.0	0.0	0.0	0.0
B	y	0.162	0.141	0.153	0.166	0.163	0.160	0.169
	z	0.003	0.0005	0.014	0.005	0.001	-0.005	0.002
	x	0.0	0.0	0.0	0.0	0.0	0.0	0.0
N	y	0.242	0.274	0.220	0.236	0.242	0.216	0.245
	z	0.316	0.322	0.302	0.311	0.316	0.304	0.312
	x	0.0	0.0	0.0	0.0	0.0	0.0	0.0
H1	y	0.472	0.543	0.424	0.457	0.466	0.422	0.414
	z	0.351	0.330	0.336	0.351	0.350	0.351	0.333
	x	0.163	0.165	0.155	0.156	0.154	0.155	0.141
H2	y	0.155	0.187	0.139	0.148	0.157	0.422	0.167
	z	0.415	0.438	0.389	0.403	0.413	0.351	0.395
	x	0.0	0.0	0.0	0.0	0.0	0.0	0.0
H3	y	-0.111	-0.173	-0.092	-0.099	-0.105	-0.090	-0.070
	z	-0.020	0.001	-0.006	-0.020	-0.019	-0.037	-0.006
	x	0.192	0.191	0.186	0.185	0.185	0.186	0.155
H4	y	0.265	0.237	0.249	0.271	0.267	0.261	0.275
	z	-0.107	-0.132	-0.079	-0.094	-0.103	-0.107	-0.082

[a]Ref[136]; [b]Ref[110];

consists almost equal contributions from p states of B, N, and s states of all hydrogens. Figure 4.2b shows the total and partial DOS of NH_3BH_3, with the states between -7.5eV to -5.5eV including the interaction of B-s and N-p and all hydrogens s states. The states between -4eV to -2eV basically arise from interaction of N-p, B-p and the s states of H3 & H4 with minor interaction of B-s states, whereas the interaction of hydrogens connected to N (i.e) H1 & H2 is zero. Close to the Fermi level, only B-p states and s states of H3 & H4 are available. The conduction states essentially arises from B-p and the s states of hydrogens connected to N (i.e) H1 & H2 with minor contributions from N-p, s states of hydrogens connected to B (i.e) H3 & H4. The decomposed partial density of states (PDOS) of NH_3BH_3 is consistent with earlier theoretical studies [106, 136]

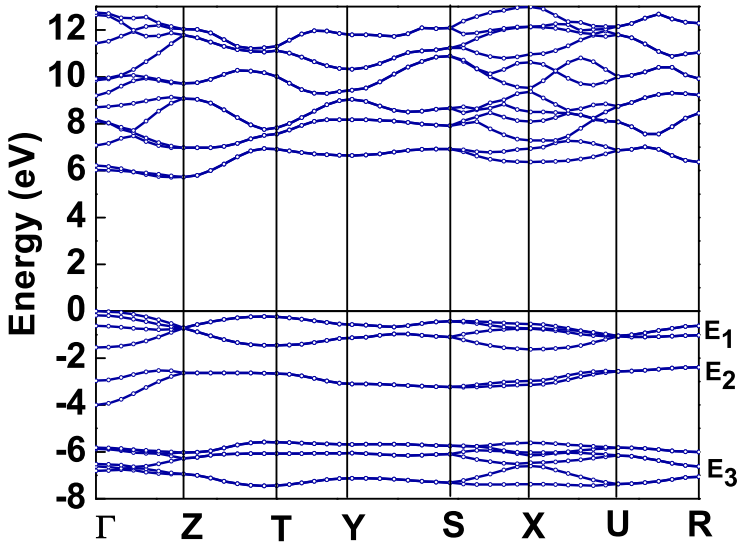

(a)

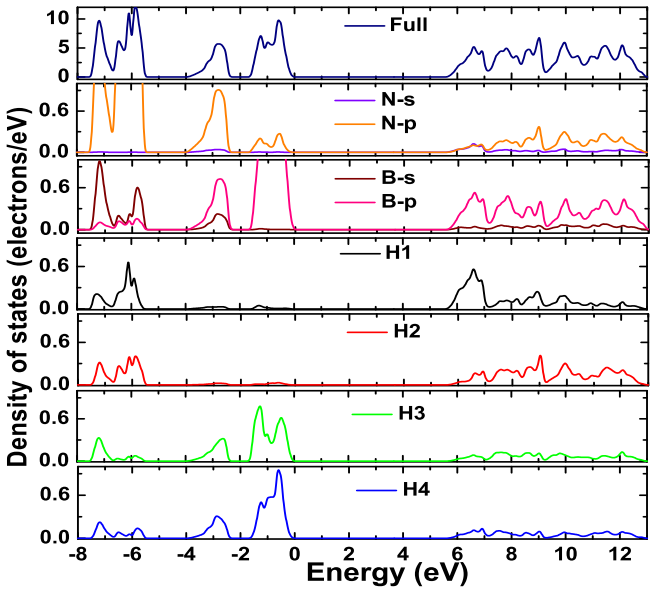

(b)

Figure 4.2: (a) Band structure and (b) density of states of NH_3BH_3 calculated at the theoretical equilibrium volume. The zero represents the Fermi level.

4.3.2 High pressure studies on structural properties

The high pressure behavior and properties of NH_3BH_3 have been studied earlier [125, 126]. These studies are basically motivated by the anomalous lattice stability of NH_3BH_3.The crystalline phases of NH_3BH_3 are found to be orthorhombic (Pmn21) at 16K and tetragonal (I4mm) at 225K [119]. Upon application of pressure, NH_3BH_3 undergoes transition to orthorhombic (Cmc21) phase at 1.22 GPa and at further increased pressures it transforms to triclinic (P1) phase at 8 GPa [134]. Recent studies suggest that the Cmc21 phase can be obtained from low temperature Pmn21 phase upon application of pressure [155]. We report the pressure studies of structural properties of low temperature orthorhombic (Pmn21) phase of NH_3BH_3 up to 10 GPa. The hydrostatic pressures upto 10 GPa has been applied to the theoretical equilibrated volume. The external pressure was gradually increased by an increment of 1 GPa in each step. From the hydrostatic compression simulations, the isothermal equation of state (EOS) was obtained and is shown in figure 4.3a as a function of the volume compression ratio, V/Vo, where V and Vo are the compressed and uncompressed volumes, respectively. The volume compression of NH_3BH_3 is found to be linear with pressure. This result indicates that no structural transitions occur up to 10 GPa pressures, although there could be a transition beyond this pressure. The crystallographic a-, b-, and c-axis lengths are reported in figure 4.3b as a function of pressure. The crystallographic b- and c-axes exhibit a relatively smooth monotonic decrease with pressure, but the crystallographic direction a, is almost constant. This is an indication of anisotropic compressibility. It is understood that the compression of NH_3BH_3 along the crystallographic a-axis is very hard.

4.3.3 The Mulliken atomic, bond population and the total charge density distributions

Mulliken atomic and bond population analysis:

The Mulliken atomic and bond population analysis is carried out for the orthorhombic

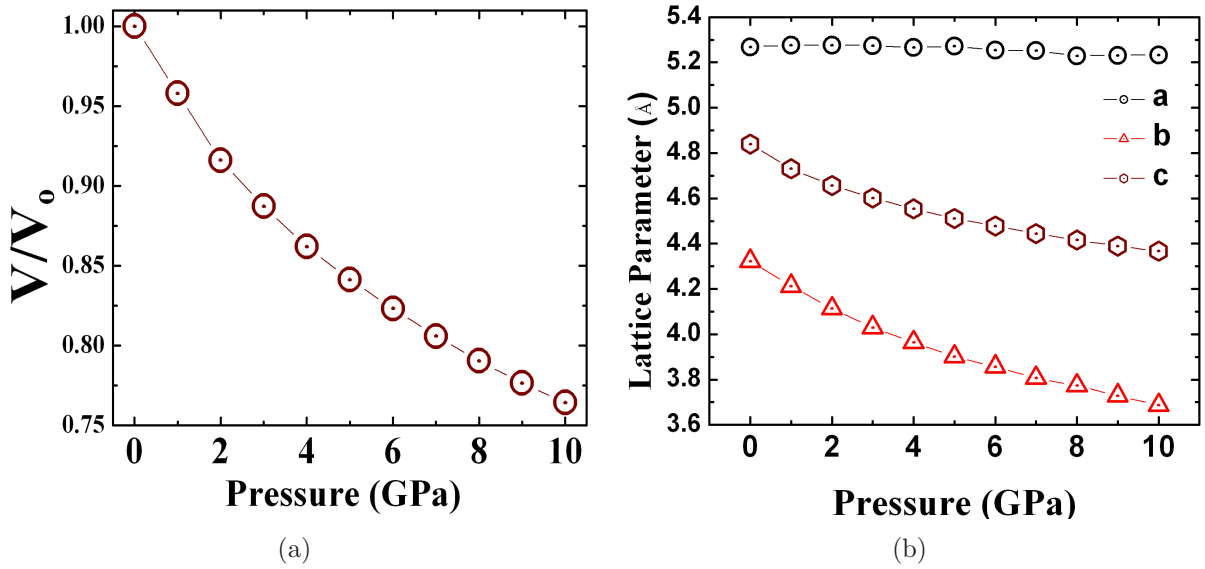

Figure 4.3: (a)Isothermal equation of states (EOS) and (b) Lattice constants as a function of pressure of NH_3BH_3.

NH_3BH_3. Here, we calculate the electronic populations of atomic orbitals and net populations of N, B, and H atoms. The total overlap (bond) population for any pair of atoms in a molecule is in general made up of positive and negative contributions. If the total overlap population between two atoms is positive, they are bonded; if negative, they are antibonded [97]. The Mulliken charges (see tables 4.3 and 4.4) are determined to be -0.29 e for B atoms, -0.85 e for N atoms, +0.43 e for H1 atoms, +0.43 e for H2 atoms, -0.04 e for H3 atoms and -0.04 e for H4 atoms with LDA, these values are found negligible variation with TS. The negative charges of the H3 and H4 imply the electronegative behavior towards the B atoms. Tables 4.3 and 4.4 list the atomic, bond (overlap) populations (P) and population ionicity (P_i) of B-N, B-H and N-H bonds of the orthorhombic NH_3BH_3. A high positive bond population indicates a high degree of covalence. The bond populations of B-H and N-H bonds are more than + 0.5 indicating a strong covalence. One can then scale the percentage of the covalence by calculating the population ionicity. The population ionicity can be calculated

from the following equation [97, 98, 156, 157]

$$P_i = 1 - exp(-\frac{P_c - P}{P}) \tag{4.2}$$

where P is the overlap population of the bond and P_c is the bond population for a purely covalent bond. The lower limit i.e. $P_i = 0$ indicates a pure covalent bond while the upper limit (i.e) $P_i = 1$ indicates a purely ionic bond [97, 98, 156, 157]. In order to find the population ionicity we assume the value of P_c is equal to 1. From the Eq 4.2, the population ionicity of B-H bonds is almost zero, whereas the population ionicity of N-H bond is 0.3, i.e the B-H bonds are more covalent than the N-H bonds. The population ionicity of B-N bond is 0.68 showing a fair ionic behavior i.e it is a dative or coordination bond. From the above discussions, we conclude that NH_3BH_3 has a overall covalent bonding. Due to the ionic nature of N-H bonds, it attracts electrons leading to protic nature and due to the covalent nature of B-H bonds, it gives up the electrons leading to hydridic nature.

Table 4.3: The calculated Mulliken atomic charges and atomic populations of NH_3BH_3.

Atoms	Method	s	p	Total	Charge
H1	LDA	0.57	0.0	0.57	0.43
	TS	0.57	0.0	0.57	0.43
H2	LDA	0.57	0.0	0.57	0.43
	TS	0.57	0.0	0.57	0.43
H3	LDA	1.04	0.0	1.04	-0.04
	TS	1.06	0.0	1.06	-0.06
H4	LDA	1.04	0.0	0.58	-0.04
	TS	1.05	0.0	1.05	-0.05
B	LDA	0.89	2.40	3.29	-0.29
	TS	0.92	2.35	3.27	-0.27
N	LDA	1.62	4.23	5.85	-0.85
	TS	1.64	4.23	5.87	-0.87

The electron density iso surfaces and charge density distributions:

The electron density iso surface and charge density distributions of NH_3BH_3 are studied in

Table 4.4: The calculated bond population (P), population ionicity(P_i) and bond lengths of NH_3BH_3.

Bonds	Method	P	P_i
B-N	LDA	0.46	0.69
	TS	0.43	0.73
N-H1	LDA	0.73	0.30
	TS	0.72	0.32
N-H2	LDA	0.76	0.27
	TS	0.79	0.21
B-H3	LDA	0.96	0.04
	TS	0.95	0.05
B-H4	LDA	0.99	0.01
	TS	0.97	0.03

order to visualize the nature of the bonds and to explain the charge transfer and bonding properties. From figure 4.4, the distorted spherical shape of total electron density iso surfaces indicate the distribution/sharing of the charge in the individual NH_3BH_3 molecule, which is an indication of dominating covalent nature in the NH_3BH_3 molecule within the crystal. In order to clearly analyze the various atom's contribution, the corresponding charge density distributions along (100), (010) and (001) planes and corresponding partial density of states (PDOS) at different energy ranges in the valence band are plotted in figure 4.5, for which the energy ranges are defined as E1=-1.5 to 0 eV (the Fermi level), E2=-4 to -2.5 eV and E3=-7.5 to -5.5 eV. From the plot, in the E1 energy region, the main contribution is from B-2p states and H3 and H4 s sates are also found in this region. It has been replicated in the charge density plots in all three planes, which indicates that the Fermi level is composed from the hybridized states of B-2p and H3 and H4 s states. In the E2 energy region, the main contribution is from 2p states of B and N atoms along with hybridization of B-2s and N-2p states, which we can see from the charge density plots along (100) and (010) planes. In the E3 energy region, from PDOS and charge density plots it is clear that all states are from the hybridization of N-2p states and H1 and H2 s states. Overall, we can clearly observe

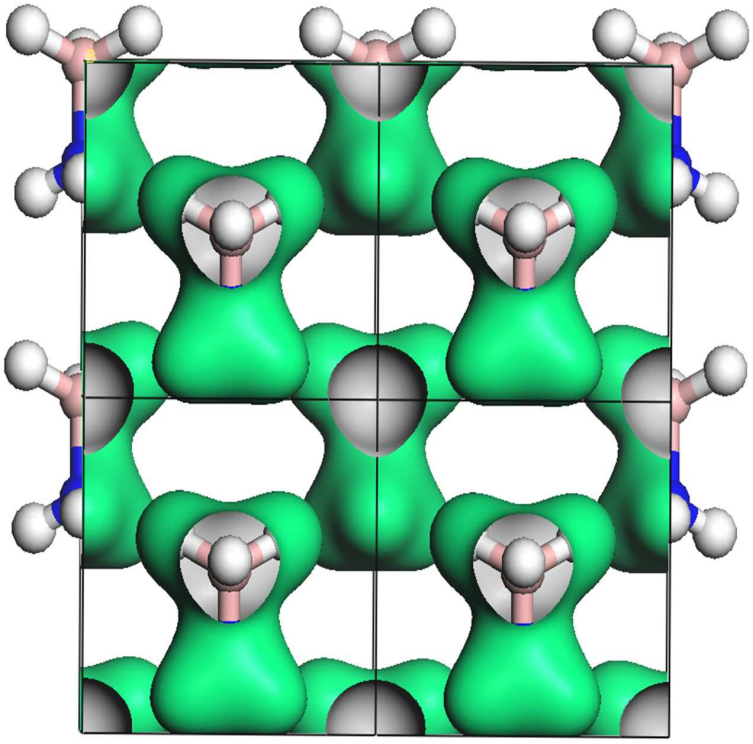

Figure 4.4: The electron density iso surface of NH_3BH_3 calculated at the theoretical equilibrium volume along b axis (Blue spheres represents Nitrogen atoms, pink spheres represents Boron atoms, and white spheres represents Hydrogen atoms).

that the high negative charge distribution is found around BH_3 group rather than around the NH_3 group which also implies a dominating covalent bonding in BH_3. From the charge density distribution plots once again we conclude that, a strong covalent bonding observed between the B-H bonds which is less pronounced in the case of N-H bonds.

Dihydrogen bonding:

Dihydrogen bond is a kind of hydrogen bond, which indicates an interaction between a metal bond and an OH or NH group or any proton donor group. This dihydrogen bond can exist in one molecule or between two molecules and affects molecular structure, physical and chemical properties of solids. This also plays an important role in crystal assembly and in super molecular systems. So the investigation of dihydrogen bonds is of great importance

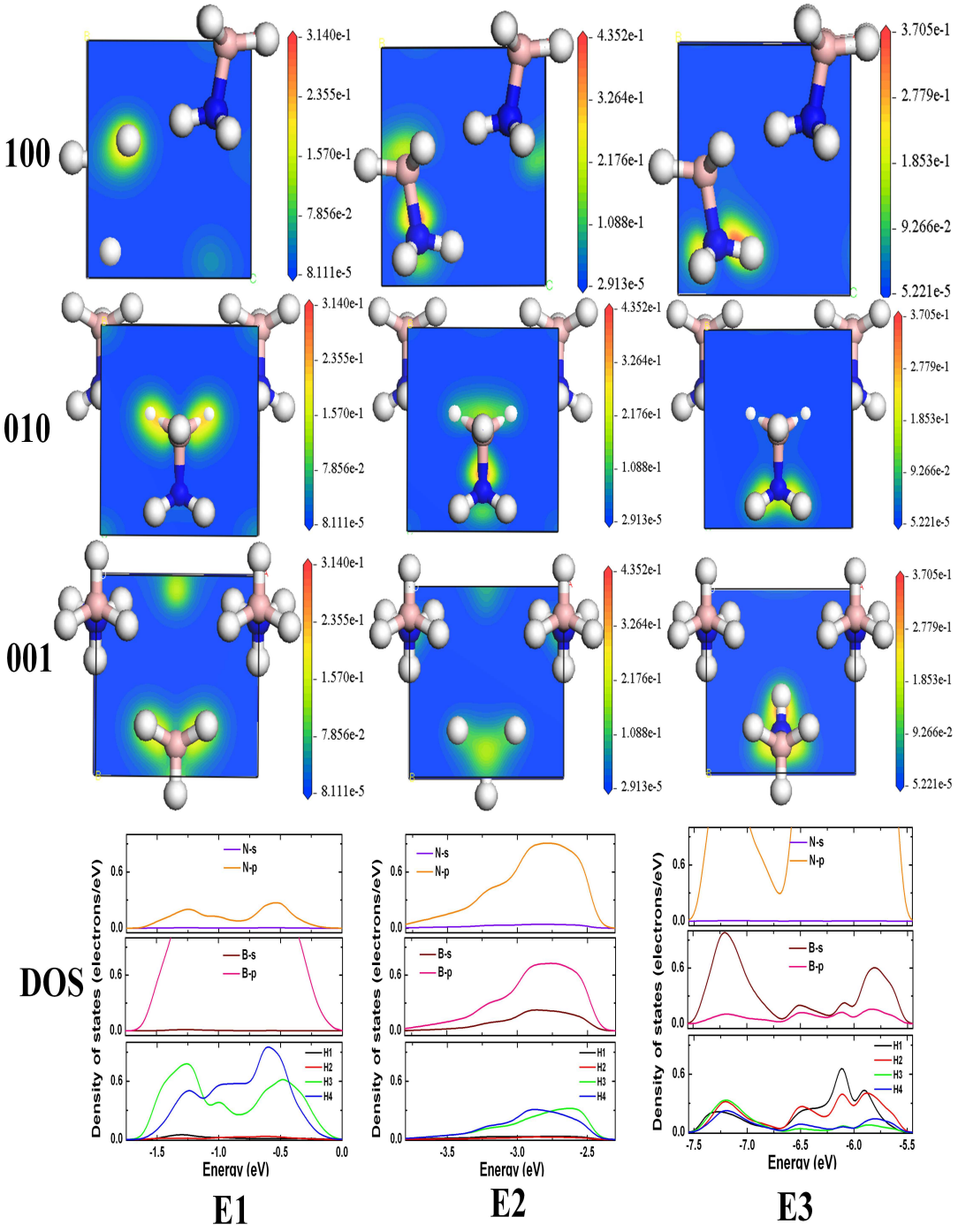

Figure 4.5: The charge density distributions along (100), (010) and (001) planes and corresponding partial density of states (PDOS) at different energy ranges E1=-1.5 to 0 eV (the Fermi level), E2=-4 to -2.5 eV and E3=-7.5 to -5.5 eV in the valence band of NH_3BH_3 (Blue spheres represents Nitrogen atoms, pink spheres represents Boron atoms, and white spheres represents Hydrogen atoms).

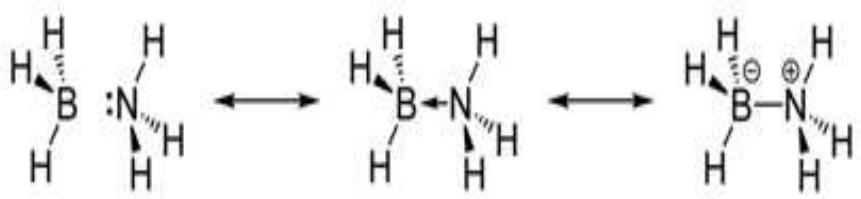

Figure 4.6: The schematic diagram of formation of NH_3BH_3.

[133, 158].

BH_3 unit needs two more electrons (i.e. pair of electrons) to form stable octet configuration, whereas NH_3 unit has a lone pair of electrons. When they combine as NH_3BH_3, the BH_3 has positive charge and the NH_3 has negative charge then the lone pair electrons of NH_3 unit are shared by them, which leads to formation of donor-acceptor (coordination) bond (see figure 4.6). This coordination bond indicates the transfer of electric charge from one unit to another [159]. Due to this we have a partial negative charge on hydrogen atoms of B-H group and a partial positive charge on hydrogen atoms of N-H group. Usually, these bonds (B-N) are covalent in character and have also a partial ionic nature, which is evident from Mulliken bond population analysis as discussed earlier. When the partial positive charged hydrogen atoms of NH_3 and the partial negative charged hydrogen atoms of BH_3 group of different molecules come closer (see figure 4.7) they lead to substantial interaction energies and unusual short H-H distances. The resulting B-H...H-N attractions stabilize the molecules in a solid. The H...H distances in the NH_3BH_3 solid compound are tabulated in table 4.1. These values are found almost equal to the values obtained in the experiments.

For any metal hydride, the H-H separation should obey "the 2-$\mathring{A}$ rule" i.e., the minimum H-H separation in ordered metal hydrides is greater than $2\mathring{A}$ [160, 161]. In the present case the H-H minimum separation in inter molecules i.e H1...H3, H1...H4, H2..H3 and H2...H4 are found to be 2.771 $\mathring{A}$, 2.112 $\mathring{A}$, 1.899 $\mathring{A}$ and 2.108 $\mathring{A}$, respectively within TS. Among them, H2..H3 is found to be less than $2\mathring{A}$. Within the molecules (intra molecules) the H-H minimum

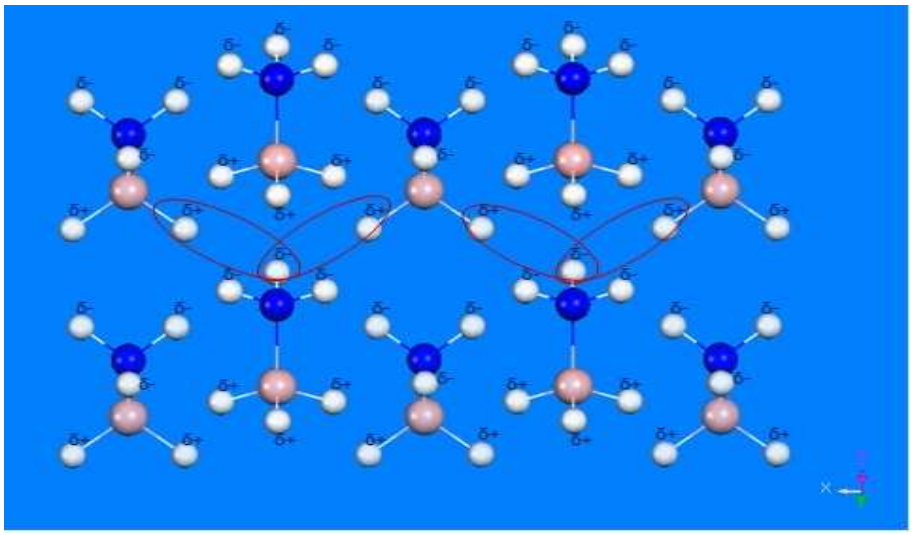

Figure 4.7: The schematic diagram of dihydrogen bonding in NH_3BH_3 (Blue spheres represents Nitrogen atoms, pink spheres represents Boron atoms, and white spheres represents Hydrogen atoms).

separation i.e H1...H2, H3..H4, H2..H2 and H4...H4 are found to be 1.666 $\mathring{A}$, 2.008 $\mathring{A}$, 1.675 $\mathring{A}$ and 2.993 $\mathring{A}$, respectively within TS. The H1..H2 and H2...H2 distances found to be less than $2\mathring{A}$. The H-H minimum separation rule is violated within the molecules. This violation is due to the polarization of negative charges on H atoms towards the electropositive N and B atoms.

4.3.4 Elastic constants and mechanical properties

The elastic constants are fundamental and indispensable for describing the mechanical properties of materials. These elastic constants of solids provide information about the mechanical, dynamical behavior of crystals and the nature of forces operating in solids, in addition to the stability and stiffness of materials. The pressure effect on these elastic constants will help in understanding the inter-atomic interactions, mechanical stability and phase-transition mechanisms. NH_3BH_3 is a molecular crystal and the individual molecules in the crystal bind through van der Waals (vdW) interactions. The geometry of vdW crystal is

not well optimized in GGA, i.e crystal is unstable and one can gets negative elastic constants. Within the LDA, vdW crystals are stable [147], hence in this work we further proceeded with LDA and TS to calculate the elastic constants of NH_3BH_3 molecular crystal. The complete set of elastic constants and the related properties are tabulated in table 4.5. NH_3BH_3 shows anisotropy in structural parameters with respect to the vdW interaction. The calculated structural parameters a, b, c are close to experimental values using vdW interactions than the usual LDA procedure. The percentage of deviation from experimental data is different along three crystallographic directions. In addition, the effect of vdW interactions is more in NH_3BH_3 because the volume obtained with the vdW interactions is in close agreement with experiment using TS. Since the calculated volume is improved significantly, we have also calculated the elastic constants through TS for NH_3BH_3 system (see table 4.5). The magnitude of the calculated elastic constants (C_{11}, C_{22} and C_{33}) with vdW interaction decreased when compared to the LDA values along the three crystallographic directions in NH_3BH_3. But this can be validated only when the experimental elastic constants are known. Hence we conclude that the elastic constants obtained through LDA give improved results along certain crystal directions where vdW interaction play an important role. Further, we have used LDA based values in explaining all the mechanical properties. The elastic constants of NH_3BH_3 satisfy all the stability criteria thereby revealing that NH_3BH_3 crystal is mechanically stable at ambient pressures. We have also considered the external pressure effect on the elastic constants; for this we have optimized NH_3BH_3 crystal for 0-6 GPa pressures and thereby evaluated the complete set of elastic constants. The elastic constants of NH_3BH_3 satisfy all the stability criteria hence revealing that NH_3BH_3 crystal is mechanically stable under external pressures up to 6 GPa. As shown in figure 4.8 all the elastic constants (C_{11}, C_{22}, C_{33}, C_{44}, C_{55}, C_{66}, C_{12}, C_{13} and C_{23}) increase with pressure except the elastic constant, C_{55}, which decreases with pressure. In the orthorhombic lattice, C_{11}, C_{22} and C_{33} denote the elastic properties along the X, Y and Z directions. From figure 4.8, we can see that C_{33} is larger than C_{11} and C_{22} under higher pressure, indicating high elasticity in the Z axis than

that in the X and Y directions. On the other hand, C_{44}, C_{55} and C_{66} in the orthorhombic structure indicate the shear elasticity applied to the two-dimensional rectangle lattice, such as in the (100), (010) and (001) planes. According to our calculations, C_{66} increases with increasing pressure and C_{55} decreases under high pressures, but C_{44} does not increase under high pressures. It implies shear transformations in the NH_3BH_3 are easy along (010) plane. Considering that single crystal samples are not available for orthorhombic NH_3BH_3, it is not possible to measure the individual elastic constants C_{ij}. Therefore, by treating polycrystalline materials as aggregates of single crystals with random orientations, the isotropic polycrystalline elastic modulus can be computed as averages of anisotropic single-crystal elastic constants. From the obtained elastic constants, such as averaged values of the bulk (B), shear (G), Young's moduli (E), and Poisson's ratio (σ) are calculated using the Voigt-Reuss-Hill (VRH) approximation [142–145, 162] for ambient pressures, and tabulated in table 4.6.

Table 4.5: The calculated elastic constants, in GPa, of NH_3BH_3 within LDA and TS.

Method	C_{11}	C_{22}	C_{33}	C_{44}	C_{55}	C_{66}	C_{12}	C_{13}	C_{23}
LDA	40.24	28.34	29.75	5.02	13.02	18.34	23.78	14.40	4.65
TS	29.58	13.79	22.86	14.07	6.44	8.94	15.79	14.16	7.18

From the knowledge of elastic constants, one can explain the mechanical behavior of the NH_3BH_3. The bulk modulus (B) represents the resistance to the volume change against external forces which indicate the average bond strength. For the case of NH_3BH_3 it is found to be 18.46 (13.55) GPa within LDA (TS) and the compressibility is 0.0541 $(GPa)^{-1}$, which reveals that the NH_3BH_3 is soft and easily compressible. The shear modulus (G) represents the resistance to the shear deformation against external forces which indicates the resistance to the change in the bond angle. The Young's modulus (E) of a material is defined as the ratio of the linear stress and linear strain, which tells about the stiffness of the materials. The Young's modulus of the NH_3BH_3 is found to be 24.36 (16.29) GPa within

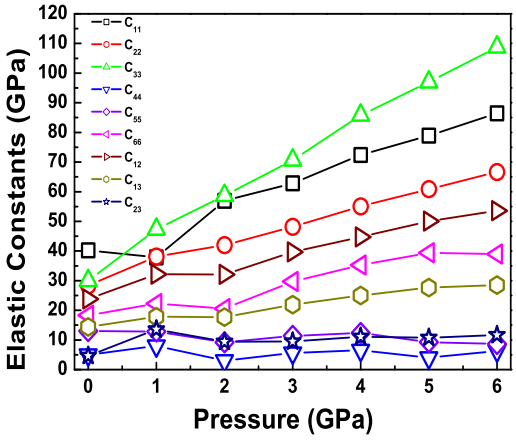

Figure 4.8: Variation of elastic constants as function of pressure up to 6 GPa.

LDA (TS), which renders the material to be less stiff. When compared to Alkaline earth metal hydrides (BeH_2, MgH_2, CaH_2, SrH_2 and BaH_2) [163], NH_3BH_3 found to be a soft material . Generally the Poisson's ratio of a material quantifies the stability of the crystal against shear. The Poisson's ratio has a value of -1 for the materials which does not change its shape and the value 0.5 for the materials which does not change its volume. These values are lower and upper bounds of the Poisson's ratio. For NH_3BH_3 the value of σ is around 0.28, which is closer towards the upper bound indicating the stability towards the volume and instability towards shape change. The bulk modulus of the crystals always decrease with the increase of temperature, hence the low temperature phases have high bulk modulus values compare to high temperature phases [164, 165]. In general low temperature phases are less plastic than the high temperature ones [166]. It is known that NH_3BH_3 is a plastic solid at room temperature because of the orientational disorder present in this material [117]. As the temperature decreases from room temperature, NH_3BH_3 under goes a phase transition to disorder tetragonal (225 K) and to orthorhombic (16 K) structure, so one could expect low temperature phase to be less plastic. This feature was established by the recent

inelastic spectroscopy experiments [123] and our calculation also confirms this behavior as the calculated bulk modulus of low temperature phase is 18.46 (13.55) GPa within LDA (TS), which is larger than the room temperature phase value of 9.9 (8) GPa [167].

Table 4.6: The calculated bulk (B), shear (G), Young's moduli (E) in GPa, G/B ratio, Poisson's ratio(σ) and Cauchy's pressure (C_{12} - C_{44}) in GPa of NH_3BH_3 within LDA and TS.

Method	B_V	G_V	B_R	G_R	B	G	G/B	E	σ	C_{12}-C_{44}
LDA	20.44	10.97	16.49	8.06	18.46	9.51	0.51	24.36	0.28	18.76
TS	15.61	7.97	10.70	5.11	13.55	6.54	0.61	16.29	0.24	1.02

The knowledge of elastic constants can also give information about the ductile and brittle nature of materials in terms of Cauchy's pressure and G/B ratio. The difference between the two elastic constants C_{12} and C_{44} (i.e., C_{12} - C_{44}) is called as Cauchy's pressure. The negative and positive values of Cauchy's pressure indicate the brittle nature and ductile nature of the material [168]. The Cauchy's pressure for NH_3BH_3 is positive, indicating that the material is expected to be ductile in nature. We can also index the ductility of the material by the G/B ratio. The G/B ratio higher than 0.57 is associated with the brittle nature and the G/B ratio lower than 0.57 indicates ductile nature [162, 169]. The G/B ratio for NH_3BH_3 is found to be 0.51 (0.61) within LDA (TS) which categorizes the material to be ductile in nature. The elastic anisotropy correlates with the possibility of inducing micro cracks in the crystals [170]. The anisotropy A takes value unity for a perfect isotropic material and the deviations from unity gives the degree of elastic anisotropy. As the shear anisotropy is a measure of the degree of anisotropy in bonding between the atoms in different planes, the shear anisotropic factor for the (100) shear planes between $< 011 >$ and $< 010 >$ directions can be written as follows:

$$A_1 = \frac{4C_{44}}{(C_{11} + C_{33} - 2C_{13})} \tag{4.3}$$

for the (010) shear planes between $< 101 >$ and $< 001 >$ directions it is

$$A_2 = \frac{4C_{55}}{(C_{22} + C_{33} - 2C_{23})} \tag{4.4}$$

and for the (001) shear planes between $< 101 >$ and $< 001 >$ directions it is

$$A_3 = \frac{4C_{66}}{(C_{11} + C_{22} - 2C_{12})} \tag{4.5}$$

For an isotropic crystal the factors A_1, A_2 and A_3 must be one, while any value smaller or greater than unity is a measure of the degree of elastic anisotropy possessed by the crystal. The shear anisotropic factors are obtained and tabulated in the table 4.7. The values of A_1 and A_3 are smaller and greater than unity, indicates the elastic anisotropic behavior of NH_3BH_3 along planes (100) and (001) respectively. Chung and Buessem introduced a concept of percent elastic anisotropy which is also a measure of the elastic anisotropy and can be obtained using B and G [142, 169]. The percentage of the anisotropy in compressibility (B) and shear (G) are defined as follows:

$$A_B = (\frac{B_v - B_R}{B_v + B_R}); \quad A_G = (\frac{G_v - G_R}{G_v + G_R}) \tag{4.6}$$

The percentage of the anisotropy in the compressibility (A_B) and shear modulii (A_G) of NH_3BH_3 are calculated at ambient pressure, presented in table 4.7. The percentage bulk modulus anisotropy A_B is lower than the percentage shear modulus anisotropy A_G, implying that NH_3BH_3 is more anisotropic in shear than in compressibility. As an extension, we also estimated the Debye temperature (Θ_D), a fundamental quantity which correlates many physical properties such as specific heat and melting point of the solids, from elastic constants. It also determines the thermal characteristics of the material, a high value of Θ_D implies a higher thermal conductivity. At low temperature, Θ_D can be estimated from the average wave velocity v_m which is the average of velocities of all longitudinal(v_l) and transverse (v_t)modes [142, 171]. The calculated values of v_l, v_t and v_m are 6.31 km/s, 3.49 km/s and 3.88 km/s, respectively, thereby the obtained Θ_D value is 573.92 K. This is the

first qualitative prediction of mechanical properties which awaits experimental confirmation

Table 4.7: The calculated shear anisotropy factors for (100) plane (A_1), for (010) plane (A_2), for (001) plane (A_3), the percentage of the anisotropy in the compressibility (A_B) and shear modulii (A_G) of NH_3BH_3 within LDA and TS at ambient pressure.

Method	A_1	A_2	A_3	A_B	A_G
LDA	0.487	1.067	3.490	0.106	0.152
TS	2.449	1.155	3.033	0.186	0.218

4.3.5 Vibrational properties at ambient and high pressures

We have also performed the density functional perturbation calculations to find the zone center vibrational frequencies of NH_3BH_3 for ambient and 10 GPa pressures. The harmonic vibrational frequencies of the compound were computed from the matrix of Cartesian second derivatives (i.e. Hessian matrix). The Hessian elements were computed by displacing each atom, and finding a gradient vector thus building up a complete second derivative matrix. The infrared intensities are obtained from the atomic polar tensor, which is a second derivative of the total energy with respect to the Cartesian coordinates and dipole moments. The intensity of each mode can be evaluated as a square of all transition moments of the mode and expressed in terms of the atomic polar tensor matrix and eigenvectors of the mass-weighted Hessian. Figure 4.9 shows the infrared absorbance as a function of frequency. The zone center vibrational frequencies are shown in table 4.8.

The group symmetry decomposition into irreducible representations of the Pmn21 space group of NH_3BH_3 yields sums A1 + B1 + B2 for three acoustic modes and 13A1 + 10A2 + 9B1 + 13B2 for 45 optical modes for ambient and 10 GPa pressures. Except A2 symmetry modes, all other modes are found to be Raman active. At ambient pressure, the lowest frequencies of A1, A2, B1 and B2 are found to be 98.9 cm^{-1}, 95 cm^{-1}, 245.6 cm^{-1} and 155.4 cm^{-1}, respectively. At 10 GPa, the lowest frequencies of A1, A2, B1 and B2 are found to be 169.5 cm^{-1}, 95.8 cm^{-1}, 279.8 cm^{-1} and 97.4 cm^{-1}, respectively. The A2 and B1

Table 4.8: The calculated vibrational frequencies (ν) of NH_3BH_3 at ambient and 10 GPa pressures.

0 GPA		10 GPa		0 GPa		10GPa	
ν (cm^{-1})	Symmetry	ν (cm^{-1})	Symmetry	ν (cm^{-1})	Symmetry	ν (cm^{-1})	Symmetry
15.65	B2	5.81	A1	1104.17	A1	1145.02	B2
19.06	A1	20.72	B2	1109.87	B2	1147.05	A1
27.20	B1	30.46	B1	1132.84	A1	1164.24	A1
95.00	A2	95.84	A2	1138.20	B2	1168.71	B2
98.99	A1	97.48	B2	1179.19	B1	1200.03	B1
155.48	B2	169.52	A1	1182.97	A2	1210.12	A2
218.84	A2	248.70	A2	1331.17	A1	1296.07	A1
227.67	A1	279.84	B1	1360.90	B2	1344.39	B2
245.68	B1	300.91	A1	1484.00	B1	1445.30	B1
248.56	B2	349.27	B2	1497.57	A2	1462.97	A2
274.05	A2	406.26	A2	1543.71	A1	1508.76	A1
296.74	B1	416.86	B1	1562.54	B2	1547.18	B2
395.90	B1	483.46	B1	2303.59	A1	2413.67	A1
416.79	A2	491.79	A2	2314.47	B2	2420.44	B2
720.84	B2	705.38	B2	2386.85	A1	2530.95	A1
729.09	A2	722.13	A1	2398.08	B2	2538.89	B2
736.00	A1	779.78	A2	2413.92	B1	2566.35	B1
739.71	B1	806.55	B1	2417.36	A2	2567.85	A2
877.13	B2	960.98	A1	3194.66	A1	3218.32	A1
877.15	A1	973.54	B2	3210.94	B2	3235.68	B2
1032.49	A1	1037.60	A1	3236.21	A2	3254.24	A2
1050.23	B1	1047.11	B1	3236.56	B1	3255.12	B1
1061.39	A2	1059.89	A2	3349.13	A1	3372.10	A1
1066.96	B2	1083.77	B2	3353.12	B2	3376.25	B2

symmetry modes are independent of pressure, whereas the A1 symmetry modes increases and B2 symmetry modes decreases with pressure. Higher bond orders result in higher frequencies i.e., higher the frequency, stronger are the bonds. The frequencies around 2300-2400 cm^{-1} are shifted to 2400-2500 cm^{-1} at 10 GPa pressures, the lower frequencies upto 877 cm^{-1} are shifted to 973 cm^{-1} at 10 GPa pressures. A blue shift represents decrease in wavelength (increase in frequency); the opposite effect is referred to as red shift [172]. The frequencies around 2300-2400 cm^{-1} are increased (shifted) to 2400-2500 cm^{-1} at 10 GPa pressures, the

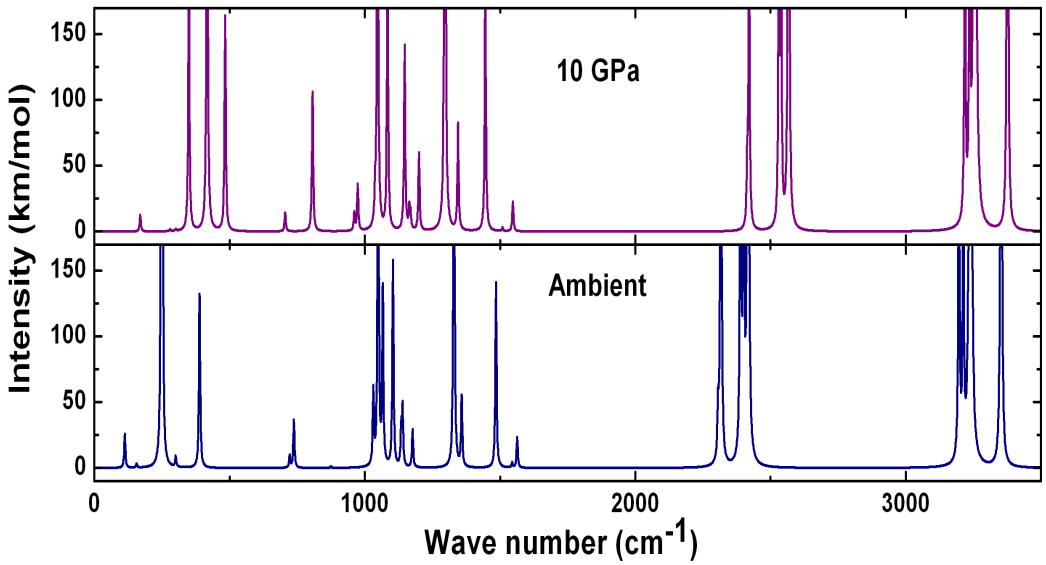

Figure 4.9: IR spectrum of NH_3BH_3 at ambient and 10 GPa pressures

lower frequencies upto 877 cm^{-1} are increased (shifted) to 973 cm^{-1} at 10 GPa pressures. This is an indication of blue shift. The blue shift indicates the contraction of bonds under pressure [172]. The rest of the frequencies are unchanged. This is a clear indication that, NH_3BH_3 under pressure becomes a relatively hard material.

4.4 Conclusions

The low temperature phase of NH_3BH_3 was fully optimized using LDA and GGA functional, and it was found that both the functionals are not efficient to reproduce the experimental volume, where the vdW interactions are playing an important role in crystallizing NH_3BH_3. Hence, vdW forces were taken into account through semiempirical methods such as OBS, G06 and TS. We found that, the TS is the better choice in reproducing the experimental volume with a difference of 5% error. The optimized structural parameters are in good agreement with the experimental data. From the band structure and density of states

calculations, it is found that NH_3BH_3 has an indirect band gap of 5.65eV (5.90eV) with LDA (GGA) along the Γ-Z direction indicating that the compound is an insulator. The effect of vdW interactions is found to be very less in calculating the electronic properties. From the charge density distribution and bond population analysis we conclude that there exists a strong covalent bond between B-H atoms. From the calculated elastic constants the material is found to be mechanically stable at ambient and external pressures up to 6 GPa. Upon increase of pressure, NH_3BH_3 becomes stiffer and hard to compress. Low temperature phase of NH_3BH_3 is found to be less plastic than the high temperature phase. The orthorhombic NH_3BH_3 has lower shear anisotropy along (100) shear plane and higher anisotropy along (001) shear plane. The structural, mechanical and vibrational properties of NH_3BH_3 under hydrostatic compression up to 10 GPa reveals that the NH_3BH_3 is soft towards the compression and becomes hard upon pressure. Finally we hope our calculation will stimulate experiments to validate our predictions.

We next examine that the dehydrogenated NH_3BH_3 which are nothing but polyaminoboranes $(NH_2BH_2)_n$.

Chapter 5

Polyaminoboranes

5.1 Introduction

Ammonia borane (NH_3BH_3) and ammonium borohydride (NH_4BH_4) are fascinating hydrogen storage materials with 19.6 wt% and 24.5 wt% of hydrogen content, respectively [12, 36, 71, 103, 104, 113, 173–176]. The dehydrogenation by catalytic and thermal decomposition of NH_3BH_3 and NH_4BH_4 results polyaminoboranes $(NH_2BH_2)_n$, which again come under the BNH_x compounds and are promising materials for chemical hydrogen storage [177–181]. The geometries and electronic structure of zigzag, square wave and coiled structured oligomers i.e., isomers and conformers of $H(NH_2BH_2)_nH$ (n = 1 - 6) oligomers have been investigated recently [182]. It is found that coiled structured oligomers are most stable whereas zigzag oligomers are unstable with respect to the other structured oligomers. The coiled structure oligomers are stabilized because of the protic $H\delta^+$(N) hydrogens interact with hydridic $H\delta^-$(B) hydrogens [182]. The formation and dehydrogenation reaction pathways of $H(NH_2BH_2)_nH$ (n = 1 - 4) oligomers [183] have been investigated and found that the oligomers are likely formed through reactions of the $H(NH_2BH_2)_nH$ oligomers first with BH_3, followed by the NH_3 and eventual release of H_2. The dehydrogenation of the $H(NH_2BH_2)_nH$ oligomers encounters significant barriers. It has been concluded that the de-

hydrogenation of $H(NH_2BH_2)_nH$ oligomers lead to formation of cyclic or ring type structures [183]. On the other hand there is a theoretical evidence of existence of infinite aminoboranes $(NH_2BH_2)_\infty$ polymers [184, 185]. However, the stability of these oligomers towards hydrogen storage applications is not clearly established. Hence, an in-depth theoretical investigation is deemed necessary and is taken up below to explore stability, reactivity, electronic structure and spectroscopic parameters of molecules. A unit molecule BH_3 needs two more electrons i.e pair of electrons to form stable octet configuration, whereas a unit NH_3 molecule, has a lone pair of electrons. Here, the BH_3 has positive charge and the NH_3 has negative charge; when they combine as NH_3BH_3, the lone pair electrons are shared by them, which lead to the formation of donor-acceptor (coordination) bond. This coordination bond indicates the transfer of electric charge from one atom to another. Because of this, there is a partial negative charge on hydrogen atoms of B-H group and a partial positive charge on hydrogen atoms of N-H group. When the partial positively charged hydrogen atoms of NH_3 and the partial negatively charged hydrogen atoms of BH_3 group come closer it leads to substantial interaction energies and unusually short H-H distances [186]. Therefore $H(NH_2BH_2)_nH$ oligomers are found to have large dipole moments if they adopt linear chain structures. These structures would become less stable as the oligomer chains grow longer because the dipole moment increases with the size of the oligomers. These linear oligomers transform to more stable species with smaller dipole moments [183]. Many theoretical studies on the gas-phase geometry and electronic structure of the NH_3BH_3 monomer suggest that ammonia borane has staggered structures as the most stable conformations [187–190]. But there are no studies available in explaining the structural stability of staggered structures of ammonia borane oligomers. In this study we aim to understand the structural stabilities and the electronic structure of various possible staggered structures of ammonia borane like “coil”, “ring”, “square wave (SW)” and “zigzag (zig)” structures.

5.2 Computational details

Ab initio molecular orbital calculations have been performed for the "coil", "ring", "square wave (SW)" and "zigzag (zig)" structured aminoborane oligomers using the Gaussian 03 quantum chemical package [67]. Structure optimizations have been performed. All the geometric parameters were allowed to be optimized and no constraints were imposed on the molecular structure during the optimization process. Vibrational frequencies were calculated for the optimized structures to enable us to characterize the nature of the stationary points, zero-point vibrational energy (ZPVE) and thermal correction (H_T). All stationary points have been positively identified as local minima with no imaginary frequencies [68]. Total energy has been used to evaluate reactive descriptors such as ionization potential (IP), chemical potential (μ), hardness (η), softness (S) and $\triangle$E(HOMO-LUMO) of "coil", "ring", "square wave (SW)" and "zigzag (zig)" aminoborane oligomers. The chemical potential (μ) and the hardness (η) of the molecules were calculated according to ref [80, 81]. Koopman's theorem has been used to calculate the ionization potential and electron affinity of the aminoborane oligomers. The ionization potential and electron affinity of the molecule are estimated as equal to the negative of the highest occupied molecular orbital (HOMO) and the lowest unoccupied molecular orbital (LUMO), respectively [84, 85]. In the present study, density functional theory calculations at HF/6-311++G**, B3LYP/6-31G**, B3LYP/6-311++G**, B3P86/6-31G** and B3P86/6-311++G** besides semi-empirical method MP2 levels have been performed to investigate geometry, stability, reactivity, spectral parameters and electronic structure properties of "coil", "ring", "square wave (SW)" and "zigzag (zig)" aminoborane oligomers. The stabilities of aminoborane oligomers are determined from the frontier molecular orbital energies and their gaps.

5.3 Results and discussion

This section presents and discusses the results including the geometry, electronic properties, ionization and chemical potentials, softness, hardness, electronegativity, molecular electrostatic potential surfaces, infrared and Raman spectra of aminoborane oligomers.

5.3.1 Optimized structures

At the outset, we have performed geometry optimizations of molecules. The optimized structures of oligomers from the B3LYP/6-311++G** level are shown in figure 5.1. NH_3BH_3 monomer has C3 symmetry, having a total energy of -83.250 au, with B3LYP/6-311++G** level calculations. The "zigzag" linear chain structure is a trans-trans conformation of $H(NH_2BH_2)_nH$ where have C_S symmetry, in which both the $(NH_2BH_2)_n$ unit is the interconnect. The "square wave" linear chain structure is a trans-cis confirmation with C_1 symmetry, staggered within the - (NH_2-BH_2) - unit but an eclipsed conformation between the (NH_2-BH_2) units. The "coil" chain structures are as similar structure as square wave linear chain structures where the hydrogen atoms of the two ends of the oligomer are connect through dihydrogen bonding. The "ring" structures are cyclic compounds, in which BH units and NH units connect alternately. The n = 2, 3 and 4 ring structure oligomers have C_S, C_3V and C_4V symmetries respectively. The B-N, N-H and B-H lengths in the monomer are found to be 1.580 $\mathring{A}$, 1.0 $\mathring{A}$ and 1.180 $\mathring{A}$ respectively. The B-N bond length 1.580 $\mathring{A}$ is in close agreement with gas-phase experimental distance 1.672 $\mathring{A}$ [191]. The B-N, N-H and B-H lengths remain unchanged in zigzag, square wave and coiled structured aminoborane oligomers. Whereas in the case of ring structured aminoborane oligomers these lengths are found to be slightly distorted. For dimer ring structure, $(NH_2BH_2)_2$, the B-N, N-H and B-H lengths are found to be 1.611 $\mathring{A}$, 1.011 $\mathring{A}$ and 1.209 $\mathring{A}$ respectively. For trimer ring structure, $(NH_2BH_2)_3$, the B-N length is 1.594 $\mathring{A}$, the B-H lengths are 1.210 $\mathring{A}$ for out of plane and 1.219 $\mathring{A}$ for in plane, similarly in plane and out of plane the N-H lengths are

1.021 $\mathring{A}$ and 1.019 $\mathring{A}$. For tetramer ring structure, $(NH_2BH_2)_4$, the B-N length is 1.596 $\mathring{A}$, the B-H lengths are 1.206 $\mathring{A}$ for out of plane and 1.224 $\mathring{A}$ for in plane, similarly the N-H lengths are 1.023 $\mathring{A}$ for out of plane and 1.021 $\mathring{A}$ for in plane. The calculated dihydrogen bond distances in n = 2, 3 and 4 of coiled structured aminoborane oligomers are found to be 1.967 $\mathring{A}$, 2.340 $\mathring{A}$ and 1.505 $\mathring{A}$ respectively. The total energy (E_0), thermal correction to en-

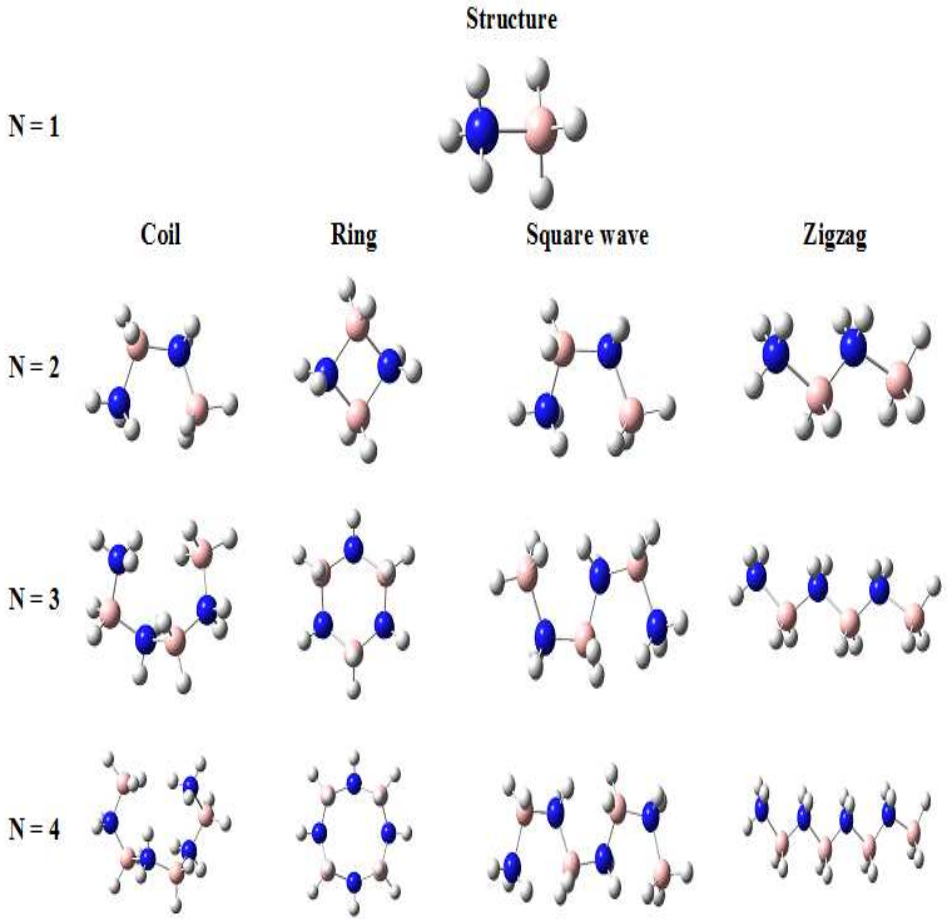

Figure 5.1: Optimized structures of model molecules computed at the B3LYP/6-311++ G** level (Blue spheres represents Nitrogen atoms, pink spheres represents Boron atoms, and white spheres represents Hydrogen atoms).

thalpy (H_T), zero-point vibrational energy (ZPVE) and lowest harmonic frequencies (ω_L) of

the aminoborane oligomers computed from the MP2, HF, B3LYP and B3P86 methods with basis sets 6-31G and 6-311++G** are presented in tables 5.1, 5.2 and 5.3. The total energies of the molecules calculated from the basis set 6-311++G** with three methods is found to be nearly the same. The total energies of "coil" structured aminoborane oligomers are apparently higher compared to "ring", "square wave" and "zigzag" structured aminoborane oligomers, and reveals the stability of "coil" structured aminoborane oligomers. The relative energies ($\triangle$E) of oligomers from the MP2, HF, B3LYP and B3P86 methods with basis sets 6-31G and 6-311++G** are presented in tables 5.4, 5.5 and 5.6. The relative energies for the "square wave" and zigzag structured aminoborane oligomers compared to "coil" structured aminoborane oligomers are found to be almost $\sim$0.003 a.u. whereas for the "ring" structured aminoborane oligomers, the relative energies are found to be almost $\sim$1.2 a.u. higher than "coil" structured aminoborane oligomers. Therefore, the coil structure aminoborane oligomers are found to be stable compounds compared to the square wave, zigzag and ring structure aminoborane oligomers. We have also calculated the average binding energies per unit molecule (BE), to be $\sim$82.4 a.u.

5.3.2 Dipole moment

Molecules having two equal and opposite charges separated by a certain distance are said to possess an electric dipole moment. In the case of polar molecules, the center of negative charge does not coincide with the center of positive charge. The extent of polarity in such covalent molecules characterized by the Dipole moment (D) [192]. Dipole moment can be defined as the product of the magnitude of the charge and the distance of separation between the charges measured in Debye. In polyatomic molecules the dipole moment not only depends upon the individual dipole moments of the bonds but also on the spatial arrangement of the various bonds in the molecule [192]. In such molecules the dipole moment of the molecule is the vector sum of the dipole moments. It is a measure of the asymmetry in the molecular charge distribution. It also can be defines as the first derivative of the energy with respect to

Table 5.1: The total energy (E_0), thermal correction to enthalpy (HT), zero-point vibrational energy (ZPVE) and relative energies ($\triangle$E) of H-$(NH_2BH_2)_n$-H, n = 2, aminoborane oligomers computed from the various levels of theory. (All values are in atomic units except zero point vibrational energy which is in kcal/mol and lowest harmonic frequencies are in cm^{-1}.)

Compound	Coil			Ring			SW			Zigzag		
	E_0	H_T	ZPVE	$\triangle$ E	H_T	ZPVE	$\triangle$ E	H_T	ZPVE	$\triangle$ E	H_T	ZPVE
MP2	-162.11	0.149	89.393	-1.092	0.124	74.758	0.0	0.149	89.393	-0.020	0.148	88.729
HF/6-311++G**	-164.17	0.137	81.899	-1.127	0.114	68.553	0.0	0.132	81.900	-0.017	0.136	80.913
B3LYP/6-31G	-165.23	0.132	78.510	-1.169	0.110	65.750	0.0	0.132	78.508	-0.021	0.131	77.616
B3LYP/6-311++G**	-165.34	0.130	77.505	-1.176	0.109	64.876	0.0	0.130	77.502	-0.019	0.129	76.622
B3P86/6-31G	-165.85	0.132	78.865	-1.207	0.110	66.082	0.0	0.132	78.864	-0.023	0.131	78.034
B3P86/6-311++G**	-165.95	0.130	77.720	-1.213	0.109	65.089	0.0	0.130	77.728	-0.021	0.130	76.946

Table 5.2: The total energy (E_0), thermal correction to enthalpy (HT), zero-point vibrational energy (ZPVE) and relative energies ($\triangle$E) of H-$(NH_2BH_2)_n$-H, n = 3, aminoborane oligomers computed from the various levels of theory. (All values are in atomic units except zero point vibrational energy which is in kcal/mol and lowest harmonic frequencies are in cm^{-1}.)

Compound	Coil			Ring			SW			Zigzag		
	E_0	H_T	ZPVE	$\triangle$ E	H_T	ZPVE	$\triangle$ E	H_T	ZPVE	$\triangle$ E	H_T	ZPVE
MP2	-242.63	0.213	128.32	-0.780	0.189	114.66	-0.009	0.213	127.93	-0.038	0.212	126.90
HF/6-311++G**	-245.70	0.196	117.58	-1.120	0.175	105.17	-0.010	0.196	117.26	-0.036	0.195	115.93
B3LYP/6-31G	-247.28	0.188	112.53	-1.162	0.167	100.53	-0.009	0.189	112.37	-0.041	0.187	110.96
B3LYP/6-311++G**	-247.43	0.186	111.13	-1.166	0.166	99.419	-0.008	0.186	110.85	-0.036	0.185	109.74
B3P86/6-31G	-248.18	0.189	112.91	-1.199	0.168	101.00	-0.008	0.186	112.85	-0.040	0.188	111.23
B3P86/6-311++G**	-248.33	0.187	111.42	-1.203	0.166	99.708	-0.009	0.187	111.17	-0.039	0.186	110.03

Table 5.3: The total energy (E_0), thermal correction to enthalpy (HT), zero-point vibrational energy (ZPVE) and relative energies ($\triangle$E) of H-$(NH_2BH_2)_n$-H, n = 4, aminoborane oligomers computed from the various levels of theory. (All values are in atomic units except zero point vibrational energies are in kcal/mol).

Compound	Coil			Ring			SW			Zigzag		
	E_0	H_T	ZPVE	$\triangle$ E	H_T	ZPVE	$\triangle$ E	H_T	ZPVE	$\triangle$ E	H_T	ZPVE
MP2	-323.15	0.277	167.14	-0.709	0.252	152.90	-0.009	0.277	166.50	-0.346	0.275	165.03
HF/6-311++G**	-327.23	0.256	153.13	-1.141	0.191	140.18	-0.007	0.255	152.69	-0.042	0.253	150.97
B3LYP/6-31G	-329.32	0.245	146.79	-1.192	0.224	133.99	-0.011	0.245	146.24	-0.054	0.243	144.43
B3LYP/6-311++G**	-329.52	0.243	144.87	-1.191	0.222	132.57	-0.010	0.243	144.30	-0.048	0.241	142.92
B3P86/6-31G	-330.52	0.246	147.35	-1.231	0.225	134.61	-0.011	0.246	146.93	-0.058	0.244	145.20
B3P86/6-311++G**	-330.71	0.240	144.82	-1.230	0.222	132.95	-0.011	0.243	144.76	-0.053	0.242	143.35

an applied electric filed. The measurement of dipole moment helps in distinguishing between polar and non-polar molecules. Non-polar molecules have zero dipole moment while polar molecules have finite value of dipole moment. The greater the dipole moment the greater is the polarity in a molecule [192]. The calculated dipole moment of the NH_3BH_3 is found to be 5.438 Debye which is close to the experimentally measured gas-phase value 5.216 Debye [193]. The calculated dipole moments (D) for the (n = 2, 3 and 4) aminoborane oligomers are summarized in tables 5.4, 5.5 and 5.6. It is found that the dipole moment decreases from monomer to dimer aminoborane oligomers. The dipole moment of the coiled structured aminoborane oligomers decreases with the size, i.e., for n = 2, 3 and 4, the dipole moment values are found to be 4.224 Debye, 1.911 Debye and 1.487 Debye respectively, with B3LYP/6-311++G** level calculations. Whereas the dipole moment of the "square wave" and "zigzag" structured aminoborane oligomers increase with the size. The polarity of the coiled structured aminoborane oligomers decreases with the size, whereas for ring, square wave and zigzag increases with the size. The dipole moment of dimer ring structure has almost zero value (∼0.0003 Debye), which indicates symmetric charge distribution. The dipole moments of trimer and tetramer ring structure has the 3.601 Debye and 6.081 Debye respectively, with B3LYP/6-311++G** level calculations, which are lower than the "square wave" and "zigzag" structured aminoborane oligomers. The dipole moment exhibits the following trends for dimers: ring < square wave < coil < zigzag, for trimer and tetramer: coil < ring < square wave < zigzag.

5.3.3 Ionization and chemical potentials

The ionization potential (IP) provides the information about the reactivity and stability of the compounds. It is well known that the compounds with higher IP values are more stable compared to the compounds with lower IP values. The chemical potential (μ) characterizes the tendency of an electron to escape from the molecule in the equilibrium state. Koopman's theorem has been used to calculate IP and μ of the molecules [84]. Ionization and chemical

Table 5.4: The lowest harmonic frequencies (ω_L), average binding energies per unit molecule (BE) and dipole moment (D) of H-$(NH_2BH_2)_n$-H, n = 2, aminoborane oligomers computed from the various levels of theory. (The binding energies are in atomic units, lowest harmonic frequencies are in cm^{-1} and dipole moment in Debye.)

Compound	Coil			Ring			SW			Zigzag		
	ω_L	BE	D	ω_L	BE	D	ω_L	BE	D	ω_L	BE	D
MP2	94.752	-81.057	4.968	131.85	-80.511	0.0003	94.835	-81.057	4.969	93.080	-81.047	11.941
HF/6-311++G**	107.42	-82.086	4.706	97.503	-81.523	0.0014	107.75	-82.086	4.708	72.606	-82.078	10.816
B3LYP/6-31G	97.139	-82.619	4.130	94.640	-82.034	0.0003	96.664	-82.619	4.128	74.212	-82.608	11.084
B3LYP/6-311++G**	107.99	-82.670	4.226	90.197	-82.082	0.0003	107.80	-82.670	4.220	74.849	-82.661	10.749
B3P86/6-31G	106.55	-82.926	4.058	85.900	-82.323	0.0004	105.99	-82.926	4.056	71.526	-82.915	11.193
B3P86/6-311++G**	113.52	-82.975	4.086	74.410	-82.369	0.0004	113.83	-82.975	4.086	72.238	-82.965	10.844

Table 5.5: The lowest harmonic frequencies (ω_L), average binding energies per unit molecule (BE) and dipole moment (D) of H-$(NH_2BH_2)_n$-H, n = 3, aminoborane oligomers computed from the various levels of theory. (The binding energies in atomic units, lowest harmonic frequencies in cm^{-1} and dipole moment in Debye.)

Compound	Coil			Ring			SW			Zigzag		
	ω_L	BE	D	ω_L	BE	D	ω_L	BE	D	ω_L	BE	D
MP2	95.415	-80.879	2.482	176.177	-80.619	4.002	30.011	-80.876	10.13	50.54	-80.866	18.399
HF/6-311++G**	113.07	-81.902	2.409	172.516	-81.529	3.745	52.097	-81.899	9.188	20.33	-81.890	16.778
B3LYP/6-31G	78.048	-82.428	1.959	158.568	-82.041	3.783	44.435	-82.425	8.615	6.754	-82.414	17.129
B3LYP/6-311++G**	72.802	-82.478	1.911	161.660	-82.089	3.601	48.546	-82.475	8.606	28.64	-82.466	16.665
B3P86/6-31G	75.995	-82.729	1.741	160.071	-82.330	3.844	51.602	-82.727	8.527	9.013	-82.716	16.989
B3P86/6-311++G**	83.318	-82.777	1.662	161.976	-82.376	3.660	52.973	-82.774	8.402	9.064	-82.764	16.762

Table 5.6: The lowest harmonic frequencies (ω_L), average binding energies per unit molecule (BE) and dipole moment (D) of H-$(NH_2BH_2)_n$-H, n = 4, aminoborane oligomers computed from the various levels of theory. (The binding energies in atomic units, lowest harmonic frequencies in cm^{-1} and dipole moment in Debye.)

Compound	Coil			Ring			SW			Zigzag		
	ω_L	BE	D	ω_L	BE	D	ω_L	BE	D	ω_L	BE	D
MP2	62.314	-80.789	1.667	-38.81	-80.612	6.999	33.344	-80.787	11.58	29.544	-80.876	24.948
HF/6-311++G**	33.099	-81.808	2.250	-32.06	-81.523	6.296	39.356	-81.806	10.86	-17.87	-81.797	23.014
B3LYP/6-31G	61.948	-82.332	1.522	18.140	-82.034	6.550	34.431	-82.329	9.559	-8.804	-82.369	23.506
B3LYP/6-311++G**	62.237	-82.381	1.487	28.296	-82.084	6.081	39.398	-82.379	9.814	23.766	-82.369	22.881
B3P86/6-31G	56.195	-82.630	1.592	16.824	-82.323	6.629	44.923	-82.628	9.319	-19.00	-82.616	23.615
B3P86/6-311++G**	62.372	-82.678	1.532	31.076	-82.370	6.150	42.806	-82.675	9.360	23.665	-82.665	22.978

potentials of the model molecules are shown in figure 5.2. It has been observed that the IP values of oligomers vary with the method and the basis set. The IP values of dimer and trimer of the ring type structured aminoborane oligomers are found to be higher compared to the other structured aminoborane oligomers. For tetramer, coil structure has higher value than other structured aminoborane oligomers. The zigzag structured aminoborane oligomers have lowest IP values. The IP values remain almost unchanged with the size of the oligomers. The higher IP values of dimer and trimer of the ring type structured aminoborane oligomers indicate that these could be stable or hard to react compared to the other structured aminoborane oligomers. For tetramer, coil structured aminoborane oligomers could be stable or hard to react compared to the other structured aminoborane oligomers. The stability of the dimer and trimer ring structured aminoborane oligomers probably due to the symmetric distribution of the charge among the atoms within the molecule. The chemical potential (μ) values of oligomers are found to be constant with the size of the molecules.

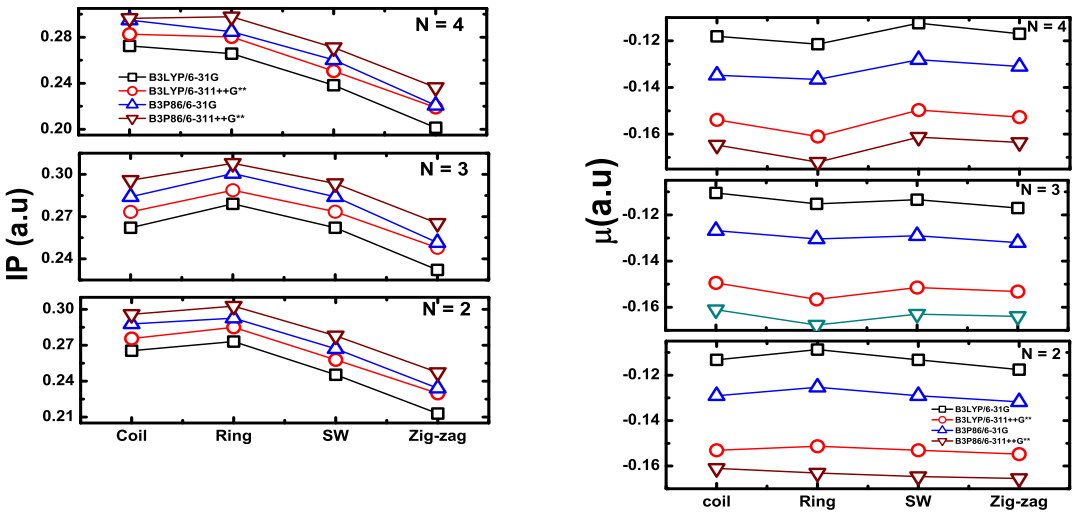

(a) (b)

Figure 5.2: Ionization (IP) and chemical potentials (μ) of the model molecules computed from the various levels of theory.

5.3.4 Hardness and softness

The hardness (η) and softness (S) of a compound are the important factors of the charge transfer resistance and these are inversely proportional to each other [88]. The calculated hardness and softness of model oligomers are presented in figure 5.3. It is found that the hardness and softness values vary with the method and choice of basis set. According to the principle of maximum hardness (PMH), the molecule in the equilibrium state possess maximum hardness and in the transition state possess minimum hardness [89, 90]. It has been found that the coil structured oligomers have maximum hardness and zigzag structured oligomers have minimum hardness. The hardness of the ring structured aminoborane oligomers decreases with the size. Whereas, the hardness of the coil structure aminoborane oligomers increases with the size. In the case of square wave and zigzag structured aminoborane oligomers, the values of the hardness remain unchanged with the size. The hardness of the dimer ring type structured aminoborane oligomer has highest maximum. The softness has the exact converse behavior to the hardness. From the hardness and softness of the aminoborane oligomers it is concluded that, dimer ring type structured aminoborane oligomer has more resistance to charge transfer. The coiled structured aminoborane oligomers are found to have more resistance to charge transfer than other aminoborane oligomers. The charge transfer resistance indicates the reactive nature of a molecule.

5.3.5 Frontier molecular orbital energies

The stability of the compounds is usually measured by the total energy (for isomers), bond length, bond dissociation energy, frontier orbital energy and their gaps. We have used frontier orbital energies to evaluate stability. However, the band gap between highest occupied molecular orbital (HOMO) and lowest unoccupied molecular orbital (LUMO) has been suggested to be related to the stability or sensitivity of materials. The principle of easiest transition (PET) states that the smaller the band gap ($\triangle$E(LUMO- HOMO)) be-

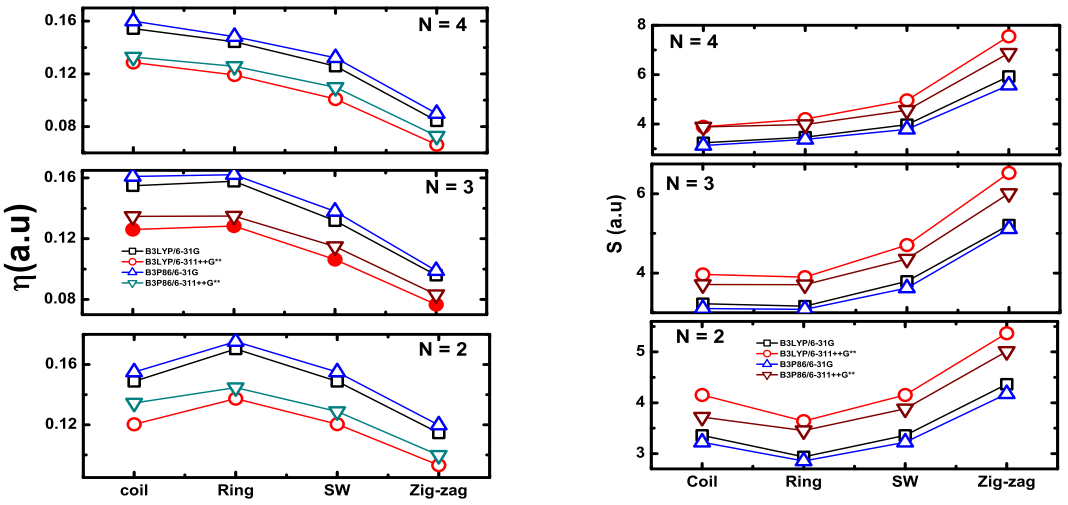

(a) (b)

Figure 5.3: The calculated hardness (η) and softness (S) of model oligomers computed from the various levels of theory.

tween HOMO and LUMO, easier the electron transition and lesser the stability [92, 93]. The frontier molecular orbitals of model molecules obtained from the B3LYP/6-311++G** level are shown in figures 5.4 and 5.5. The frontier molecular orbital energies of aminoborane oligomers vary with the size. The dimer and trimer ring structure oligomers have high $\triangle$E(LUMO- HOMO), band gaps values 7.4557 eV and 6.9838 eV respectively, with B3LYP/6-311++G** level calculations. For tetramer, coil structure has high $\triangle$E(LUMO-HOMO), band gap values, 6.99 eV, with B3LYP/6-311++G** level calculations. The band gap increase with the size in coil structure oligomers, whereas the band gap decrease with the size in ring, square wave and zigzag structures. For dimer, the relative band gap of coil, square wave and zigzag with respect to ring structure are found to be 0.9254, 0.9235 and 2.4046 eV respectively. For trimer, the relative band gap of coil, square wave and zigzag with respect to ring structure are found to be 0.1213, 1.1992 and 2.6903 eV respectively. For tetramer, the relative band gap of coil, square wave and zigzag with respect to ring structure are found to be -0.5137, 0.9978 and 2.8822 eV respectively. Here, we also examine the

orbitals contribution for the HOMO and LUMO levels. For the monomer, the B-H orbitals dominate with the admixture of N-H orbitals in the HOMO levels, whereas the N-H orbitals dominate with the admixture of B-H orbitals for LUMO levels. This trend is followed in the case of coil structure aminoborane oligomers. For square wave and zigzag structures, the B-H orbitals present in the HOMO levels and the N-H orbitals present in the LUMO levels. In the case of ring structures, the contribution from N-H and B-H orbitals for HOMO and LUMO levels found to be equal.

5.3.6 Electronegativity

Electronegativity (χ) is a measure of the tendency of an atom to attract a bonding pair of electrons. If the atoms are equally electronegative, both have the same tendency to attract the bonding pair of electrons, and so it will be found on average half way between the two atoms. Zero electronegativity difference between two atoms leads to a pure non-polar covalent bond. A small electronegativity difference leads to a polar covalent bond. A large electronegativity difference leads to an ionic bond [194, 195]. The calculated hardness and softness of model oligomers are presented in figure 5.6. The electronegativity of Boron, Nitrogen and Hydrogen are 2.04, 3.04 and 2.20 respectively. From the electronegativity difference, the N-H bonds are found to be more polar compared to the B-H bonds. So, all these aminoborane oligomers have polar bonds. The electronegativity value of the aminoborane oligomers does not show a significant change with the structure as well as size of the oligomers. It has been observed that the χ values of oligomers vary with the method and the basis set. The tendency of attracting pair of electrons to these oligomers is found to be insensitive to the size and structure.

5.3.7 Molecular electrostatic potential (MEP) surfaces

Molecular electrostatic potential surfaces illustrate the three dimensional charge distributions within the molecule. These surfaces visualize variably charged regions of a molecule

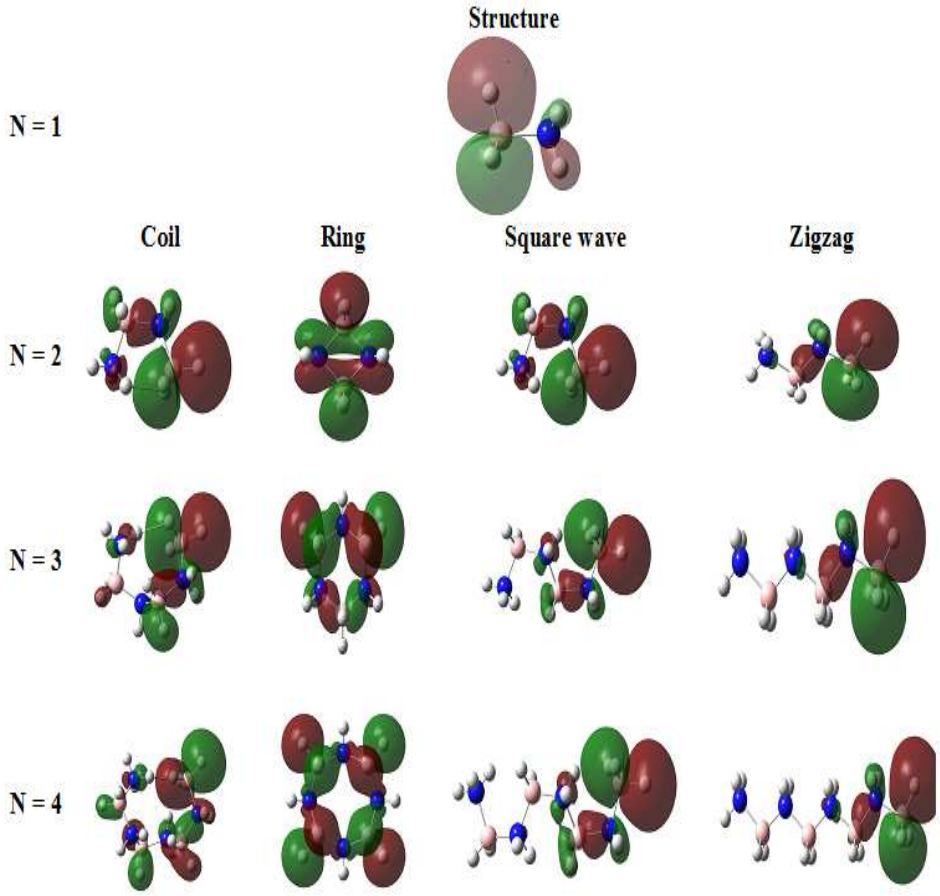

Figure 5.4: Highest Occupied Molecular Orbitals (HOMO) computed at the B3LYP/6-311++ G** level (Blue spheres represents Nitrogen atoms, pink spheres represents Boron atoms, and white spheres represents Hydrogen atoms).

[196]. The charge distributions determine how molecules interact with one another. For simplicity, consider moving a positively charged test charge along the spherical isosurface of an atom. The positively charged nucleus emits a constant electric field. A region of higher electrostatic potential indicates the presence of a stronger positive charge or a weaker negative charger or the absence of negative charges, which would mean that there are fewer electrons in this region. Thus, a high electrostatic potential indicates the relative absence of electrons

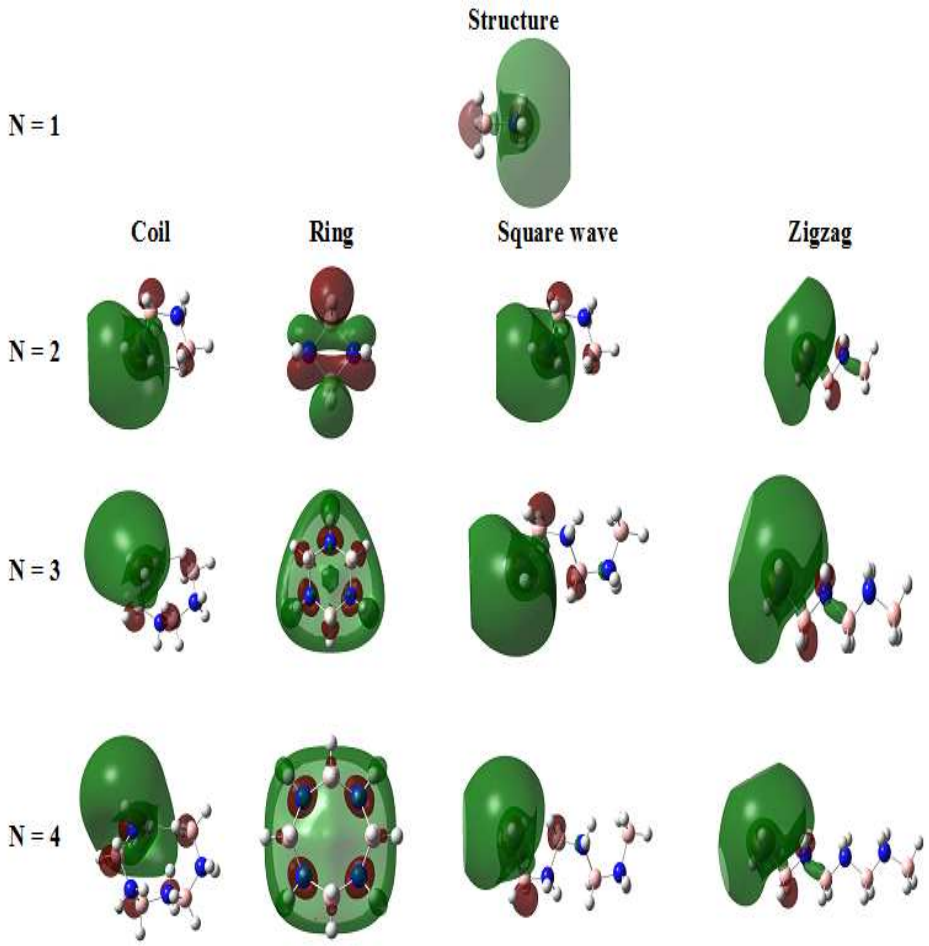

Figure 5.5: Lowest Un-occupied Molecular Orbitals (LUMO) computed at the B3LYP/6-311++ G** level (Blue spheres represents Nitrogen atoms, pink spheres represents Boron atoms, and white spheres represents Hydrogen atoms).

and a low electrostatic potential indicates an abundance of electrons [196]. The calculated molecular electrostatic potential surfaces of model oligomers are presented in figure 5.7. The red color indicates the lowest electrostatic potential energy, and blue indicates the highest electrostatic potential energy. Intermediate colors represent intermediate electrostatic potentials. Areas of low potential, red are characterized by an abundance of electrons. Areas of high potential, blue are characterized by a relative absence of electrons. The electronega-

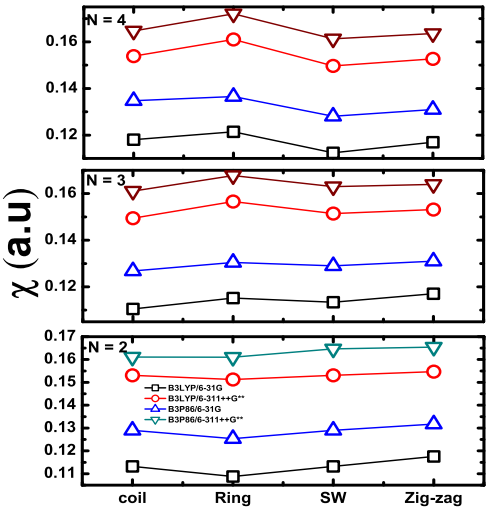

Figure 5.6: The calculated electronegativity (χ) of model oligomers computed at various levels of theory.

tivity difference of the N-H bonds is higher compared to the B-H bonds. N-H bonds would consequently have a higher electron density around them than B-H bonds. From MEP of the monomer, it is clear that NH_3BH_3 has high electrostatic potential from the B-H bonds and N-H bonds have low electrostatic potential, i.e., B-H bonds are characterized by an abundance of electrons, so these bonds behaves like donors and N-H bonds are characterized by a relative absence of electrons, so these bonds behaves like acceptors. It is well known that, the end hydrogens with acceptor and donor behavior always lead to "dihydrogen bonding" [197, 198], that is why a substantial dihydrogen bonding is observed in the NH_3BH_3 compounds. This could lead to either end-to-end or side-by-side interactions. These results are consistent with previous studies [196]. This has been observed in all structured aminoborane oligomers. This led us to conclude that, these aminoborane oligomers form considerable "dihydrogen bonding" and will have end-to-end or side-by-side interactions. We also note that the electrostatic potential surface area of the B-H bonds found to be higher surface area compared to the electrostatic potential surface area of the N-H bonds, which is an indication of the unbalanced charge distribution, resulting a dipolemoment of 5.438 D. The unbalanced

area of MEP surfaces are found to be increased with the size for the ring, square wave and zigzag structures, whereas it decreased with size for coil structure. This has been reflected in the dipole moment values.

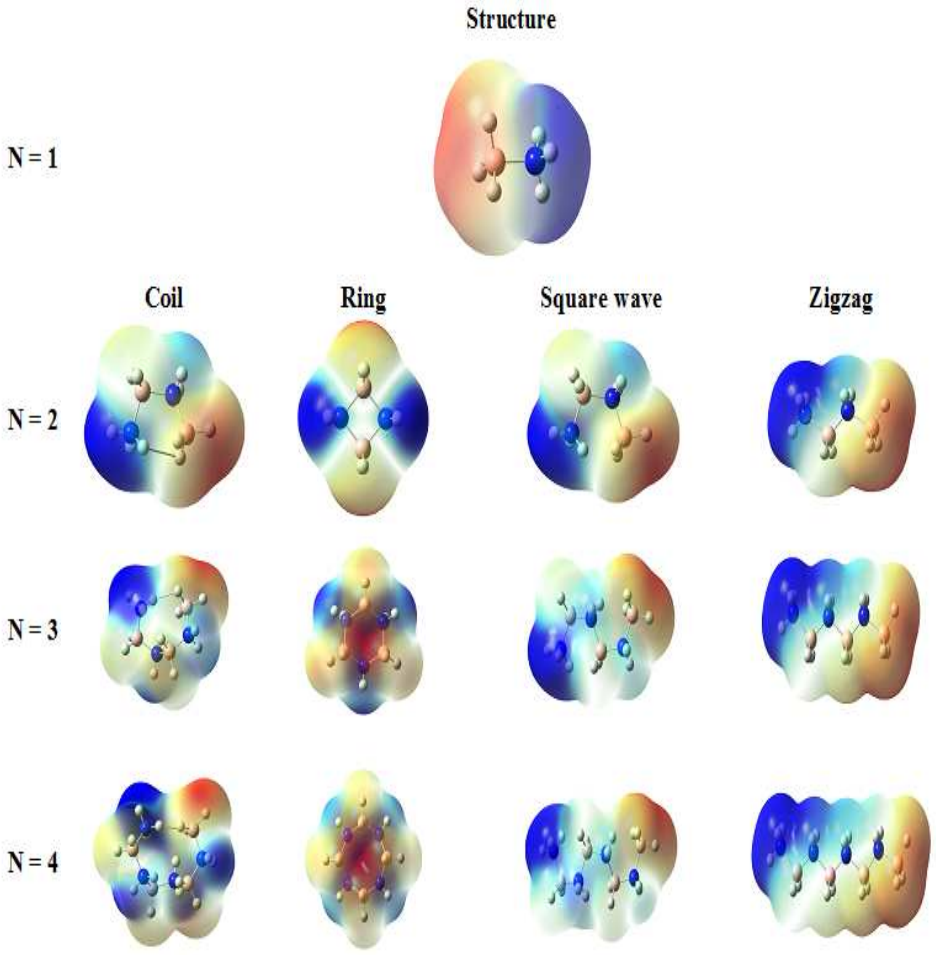

Figure 5.7: Molecular Electrostatic Potential (MEP) surfaces computed at the B3LYP/6-311++ G** level (Blue spheres represents Nitrogen atoms, pink spheres represents Boron atoms, and white spheres represents Hydrogen atoms).

5.3.8 Infrared and Raman spectra

The infrared (IR) and Raman spectra of molecules are obtained from the computed structures at HF/6-31++G** levels, these are presented in figures 5.8 and 5.9. For the monomer, we note that the spectra range from 607 cm^{-1} to 684 cm^{-1}, from 1125 cm^{-1} to 1446 cm^{-1}, 1797 cm^{-1}, from 2494 cm^{-1} to 2526 cm^{-1}, from 3688 cm^{-1} to 3799 cm^{-1} in both IR and Raman. There are four fundamental bands starting from 100 cm^{-1} to 1400 cm^{-1}, from 1500 cm^{-1} to 1800 cm^{-1}, from 2300 cm^{-1} to 2700 cm^{-1} and from 3600 cm^{-1} to 3800 cm^{-1} for n = 2 - 4 of aminoborane oligomers in IR and Raman spectra. The particular mode at ∼1500 cm^{-1} is observed only in the coil and square wave structure. The modes of vibrations starting from 1500 cm^{-1} to 1800 cm^{-1} are due to the N-H bond wagging, from 2300 cm^{-1} to 2700 cm^{-1} and 3600 cm^{-1} to 3800 cm^{-1} are due to N-H and B-H bond stretching respectively.

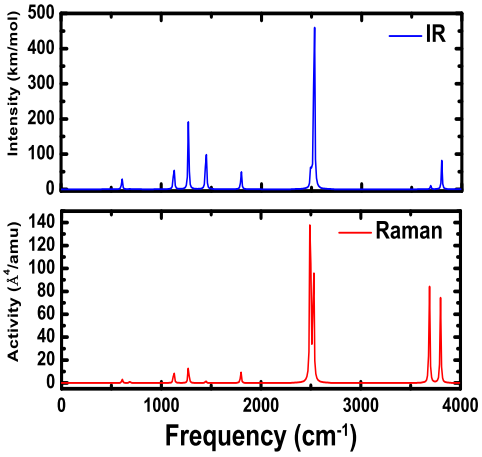

Figure 5.8: The infrared (IR) and Raman spectra of the monomer are obtained from the computed structures at HF/6-31++G** level.

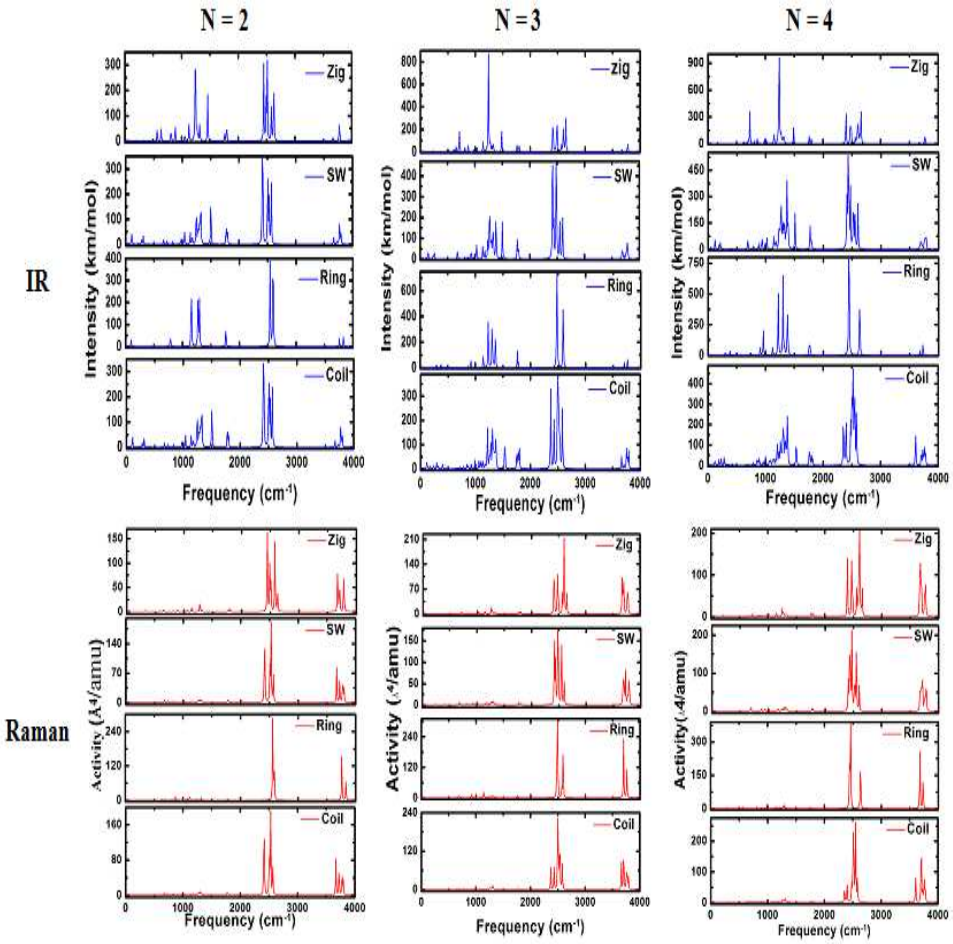

Figure 5.9: The calculated hardness (η) and softness (S) of model oligomers computed at various levels of theory.

5.3.9 Bond Dissociation Energies (BDE)

The making and breaking of bonds is the basis of all chemical transformations. A sound knowledge of the energies required to break bonds and the energies released upon their formation is fundamental to understanding chemical processes [199]. Bond dissociation energy (BDE) is a measure of the bond strength in a chemical bond. It is defined as the standard enthalpy change when a bond is broken by a reaction, with reactants and products of the reaction. For instance, the bond-dissociation energy for one of the A-B bond in A_2B_2 is

defined as follows:

$A_2B_2 \rightarrow A_2B^- + B^-$

The BDE of A-B bond will be calculated as follows:

$BDE_{(A-B)} = [\triangle H(A_2B^-) + \triangle H(B^-)]$ - $\triangle H(A_2B_2)$

Here, we have calculated the BDE of N-H and B-H bonds of the aminoborane oligomers at B3LYP/6-311++G** levels which are tabulated in the table 5.7. The N-H and B-H bond dissociation energies of single NH_3BH_3 molecules are found to be 96.61 and 105.66 kcal/mol, respectively. The N-H bond dissociation energies of coil, square wave and zigzag structured dimer oligomers are found to be lower compared to the monomer, whereas in the ring structured dimer oligomer has higher value. The B-H bond dissociation energies of coil, ring, square wave and zigzag structured dimer oligomers are found to be higher compared to the monomer. The BDE values of N-H and B-H bonds in zigzag and square wave oligomers are found to be almost equal. But in the case of ring and coil structured oligomers, the N-H bonds BDE values decrease with the size. Overall, the BDE values of N-H bonds are found to be lower compared to the BDE values of B-H bonds.

Table 5.7: The bond dissociation energies of N-H and B-H bonds of H-$(NH_2BH_2)_n$-H, aminoborane oligomers computed from the B3LYP/6-311++ G** level of theory. (All values are in kcal/mol.)

Bond	N-H				B-H			
	Coil	Ring	SW	Zigzag	Coil	Ring	SW	Zigzag
Dimer(n=2)	95.156	101.81	95.156	83.296	107.40	107.55	107.40	108.17
Trimer(n=3)	94.119	94.901	96.588	82.450	106.03	101.34	105.58	108.46
Tetramer(n=4)	94.106	84.371	96.314	81.796	105.65	97.473	103.98	108.78

5.4 Conclusions

The electronic structure properties of aminoborane oligomers have been carried out at MP2, HF, B3LYP and B3P86 methods with 6-31+G** and 6-311++G** basis sets. The band gap $\triangle$E(LUMO-HOMO), ionization potential (IP), chemical potential (μ), hardness (η), softness (S) and electronegativity (χ) of aminoborane oligomers have been calculated. From the total and relative energies, the coil structure aminoborane oligomers found to be more stable compared to other structured oligomers. For dimer and trimer, the ring structure oligomers are found to have high band gap whereas for tetramer coil structure has higher band gap. The band gap increase with the size in coil structure oligomers, whereas the band gap decrease with the size in ring, square wave and zigzag structures. The B-H orbitals participate in the HOMO levels, whereas for the LUMO levels, only the N-H orbitals are present. From MEP, it is clear that aminoborane oligomers have high electrostatic potential from the B-H bonds and N-H bonds have low electrostatic potential, i.e., B-H bonds behave like donors and N-H bonds behave like acceptors, which led to form considerable "dihydrogen bonding" and end-to-end or side-by-side interactions. The IR and Raman spectra of molecules have four fundamental bands (from 100 cm^{-1} to 1400 cm^{-1}, from 1500 cm^{-1} to 1800 cm^{-1}, from 2300 cm^{-1} to 2700 cm^{-1} and 3600 cm^{-1} to 3800 cm^{-1}). The modes from 2300 cm^{-1} to 2700 cm^{-1} and 3600 cm^{-1} to 3800 cm^{-1} are due to N-H and B-H bonds stretching modes respectively. The N-H and B-H bond dissociation energies reveal that, N-H bonds are easily dissociated compared to the B-H bonds.

In the next chapters we discuss the role of the metal atom on the physical and chemical properties of NH_3BH_3

Chapter 6

Alkali Metal Amidoboranes

6.1 Introduction

Ammonia borane (NH_3BH_3) with its high hydrogen content and low releasing temperatures of H_2, has been extensively explored for the fuel cell applications [99–101]. Solid NH_3BH_3 releases one molar equivalent of H_2 at temperatures of $\sim$ 380K, and a second equivalent at $\sim$ 420K [28, 38, 42, 102, 103, 105]. Thus, NH_3BH_3 based materials have been further developed in combination with metal catalysts, acid catalysts, ionic liquids and nanoscaffolds [41, 104]. Although, these exhibit some promising properties for hydrogen storage, they still have drawbacks such as low H_2 density, high H_2 release kinetics, irreversibility and impurities [41, 104]. As a remedy to this problem, new families of metal amidoboranes have been developed by replacing one H in NH_3BH_3 by an alkali or alkaline earth metal [136, 200, 201]. These metal amidoboranes have high desorption kinetics and suppressed toxic borazine and thus have great potential for hydrogen storage applications [136, 200]. These are stable under normal pressures, less exothermic than NH_3BH_3 and suitable for on-board H_2-storage application [136, 200]. Recently, $LiNH_2BH_3$, $NaNH_2BH_3$ and $Ca(NH_2BH_3)_2$ have been highlighted as potential materials [107] for hydrogen storage applications as they release H_2 at $\sim$363K [136, 200]. $LiNH_2BH_3$ and $Ca(NH_2BH_3)_2$ have been reported to show significantly enhanced

dehydrogenation kinetics and suppressed borazine release over parent NH_3BH_3 [136, 200]. Alkali metal amidoboranes such as sodium or lithium are even considered as efficient hydrogen sources for low temperature proton exchange membranes (PEM) fuel cells. Lithium amidoboranes possess a hydrogen content of 13.7% and are excellent hydrogen source for PEM fuel cells since the waste heat generated by the fuel cell can be utilized to free almost all of the material's hydrogen content in one step at ∼363K. Although, the hydrogen content of sodium amidoborane is some what lower (9.5%), it is still much higher than that of conventional hydrogen sources such as magnesium hydride (7.7%) or sodium aluminium hydride (7.5%). Even though, Lithium amidoborane ($LiNH_2BH_3$) and Sodium amidoboranes ($NaNH_2BH_3$) are reported earlier in twentieth century [202, 203], no valid structural information was presented. In early twenty first century [204, 205], the complete crystal structures and solid state synthesis of $LiNH_2BH_3$ and $NaNH_2BH_3$ were reported and their dehydrogenation properties were also investigated [136, 201, 206–210]. More recently, solid state synthesis of potassium amidoborane (KNH_2BH_3) was reported [211].

Metal amidoboranes (MAB) can be synthesized by stoichiometric amounts of metal hydrides (or organic hydrides) and ammonia borane through the following reaction:
$MH_n + nNH_3BH_3 \rightarrow M(NH_2BH_3)_n + nH_2$
where n is the valance state of metal atom M (Li or Na). In this reaction one equivalent of H_2 per NH_3BH_3 is released. The above reaction is an acid-base reaction in which NH_3BH_3 is a combination of $H^{\delta+}$ Lewis acid and $[NH_2BH_3]^-$ Lewis base. In metal hydrides $H^{\delta-}$ acts as a Lewis base that competes with $[NH_2BH_3]^-$ to bind with $H^{\delta+}$. Therefore, the formation of MAB is strongly dependent on the basicity of metal hydride. Metal hydrides with strong Lewis basicity would combine with $H^{\delta+}$ in NH_3BH_3 to form H_2 and MAB; whereas hydrides of weak Lewis basicity may be difficult to react with NH_3BH_3 [136]. $LiNH_2BH_3$ has been synthesized using several methods such as interaction of NH_3BH_3 with LiH (Metal hydride) or $LiNH_2$ (Amide) or Li_2NH (Imide) or Li_3N (Nitride). $LiNH_2BH_3$ crystallizes in two phases α and β and a lithiated subsidiary phase also available. The α and β phases have

orthorhombic structures with space group *Pbca*, the lattice parameters for α-$LiNH_2BH_3$ are a = 13.94682(7) $\mathring{A}$, b = 5.14883(3) $\mathring{A}$ and c = 7.11254(3) $\mathring{A}$, whereas for β-$LiNH_2BH_3$, a = 15.146(6) $\mathring{A}$, b = 7.721(3) $\mathring{A}$ and c = 9.268(4) $\mathring{A}$, respectively. The lithiated phase has tetragonal structure with a space group of *P-42c*, the lattice parameters are as a = 4.0288(3) $\mathring{A}$ and c = 16.984(4) $\mathring{A}$ [212, 213]. $LiNH_2BH_3$ also reported with another set of lattice parameters a = 7.11274(6) $\mathring{A}$, b = 13.94877(14) $\mathring{A}$ and c = 5.15018(6) $\mathring{A}$ having orthorhombic structure with the same space group [206, 213]. This phase has been confirmed by other experiments [136] and supported well by theoretical calculations [107, 213]. There is a similar compound named monoammoniate borohydride ($LiNH_3BH_4$), which is formed when LiH interacts with and NH_4BH_4. $LiNH_3BH_4$ crystallizes into orthorhombic structure with the space group *Pnma* and the lattice parameters are a = 5.96910(3)$\mathring{A}$, b = 4.462632(2)$\mathring{A}$ and c = 14.34199(8)$\mathring{A}$, respectively [214–216]. The $NaNH_2BH_3$ has a structure similar to $LiNH_2BH_3$ and crystallizes in orthorhombic structure with space group of *Pbca* and the lattice parameters are a = 7.46931(7)$\mathring{A}$, b = 14.65483(16)$\mathring{A}$ and c = 5.65280(8)$\mathring{A}$. Since the molecular structure and the crystal geometries of $LiNH_2BH_3$, $LiNH_3BH_4$ and $NaNH_2BH_3$ are entirely different with that of parent NH_3BH_3, there would be significant changes in intermolecular forces and thereby in the physical and chemical properties. In this chapter, we will discuss about the structural, electronic, bonding and mechanical properties of alkali metal amidoboranes ($LiNH_2BH_3$, $LiNH_3BH_4$ and $NaNH_2BH_3$). The rest of the chapter is organized as follows. In section 6.2 we discuss computational details including the calculation of elastic constants. Results are presented in section 6.3 and section 6.4 deals with the conclusions.

6.2 Computational details

The first principles calculations were carried out by using plane wave pseudopotential method based on density functional theory as implemented in the CAmbridge Series of Total Energy Package (CASTEP) [60, 86]. For $LiNH_2BH_3$, $LiNH_3BH_4$ and $NaNH_2BH_3$, the basis

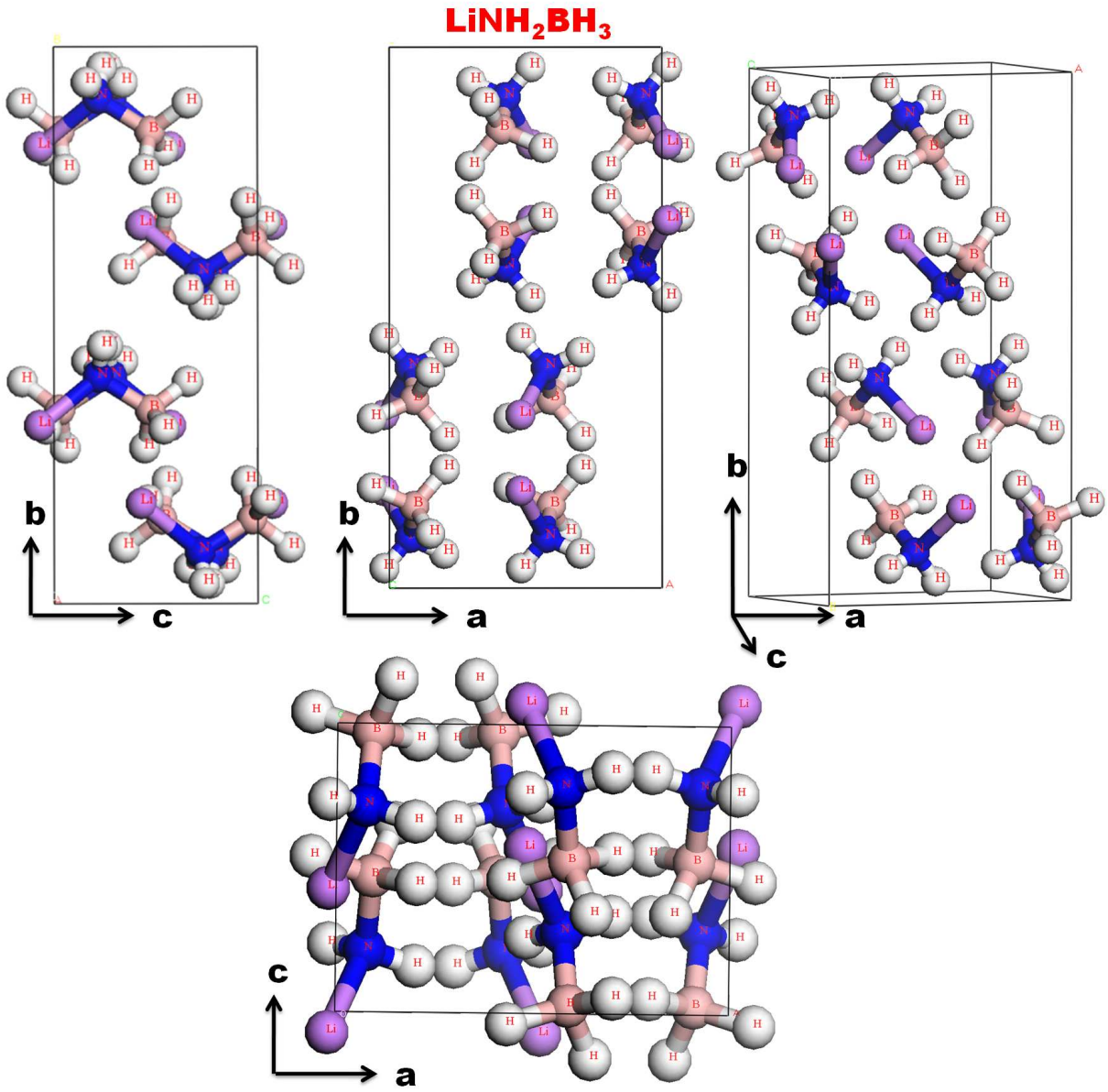

Figure 6.1: The optimized crystal structure of $LiNH_2BH_3$ within GGA represented along different crystallographic directions (Blue spheres represents Nitrogen atoms, pink spheres represents Boron atoms, purple spheres represents Lithium atoms and white spheres represents Hydrogen atoms).

orbitals used as valence states are Li: $2s^1$, Na: $2s^2\ 2p^6\ 3s^1$, H: $1s^1$, B: $2s^2\ 2p^1$, and N: $2s^2\ 2p^3$. We have used ultrasoft pseudopotentials introduced by Vanderbilt [59] together with local

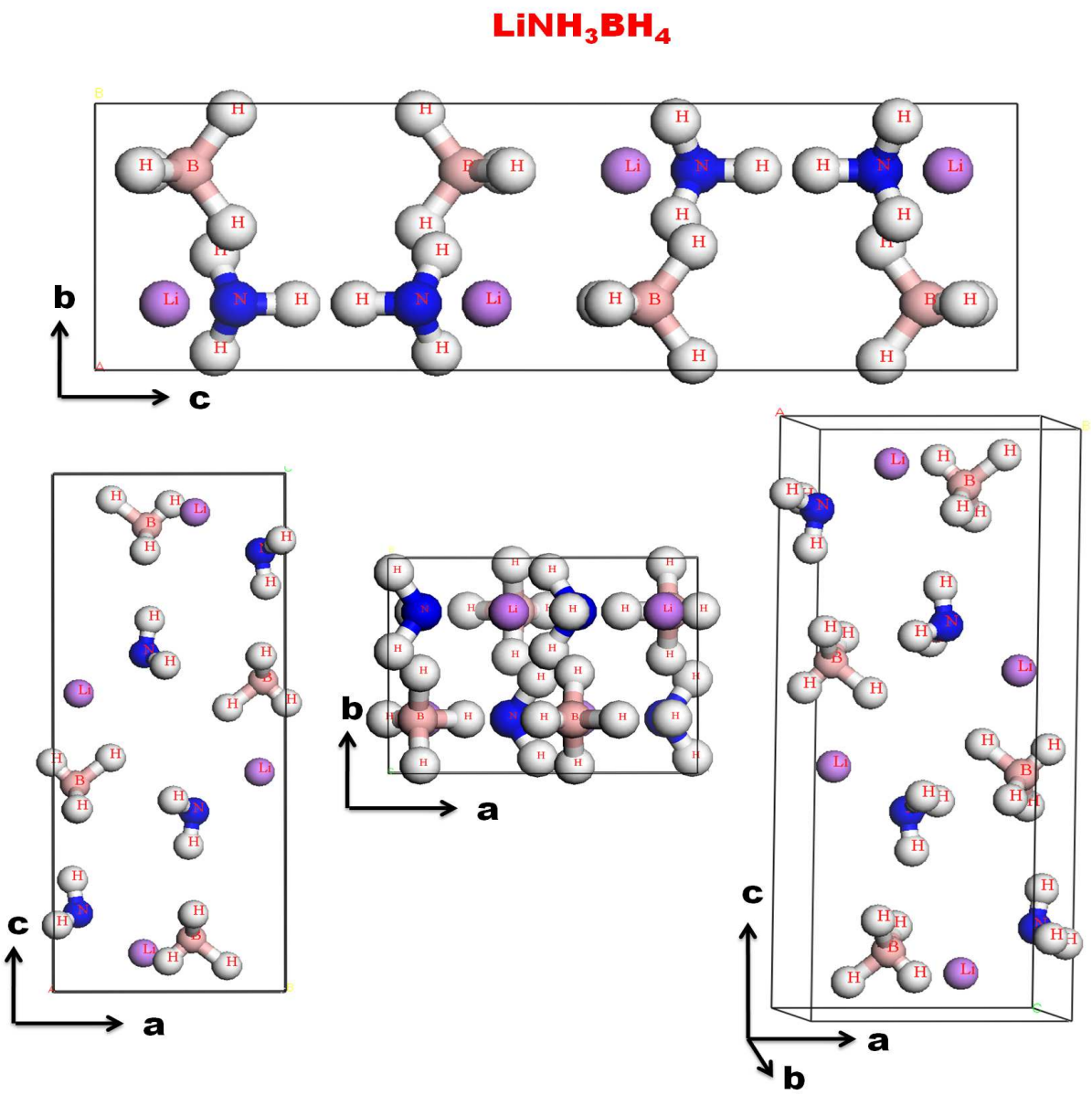

Figure 6.2: The optimized crystal structure of $LiNH_3BH_4$ within GGA represented along different crystallographic directions (Blue spheres represents Nitrogen atoms, pink spheres represents Boron atoms, purple spheres represents Lithium atoms and white spheres represents Hydrogen atoms).

density approximation (LDA) of Ceperley and Alder [138] parameterized by Perdew and Zunger (CA-PZ) [139] and also with generalized gradient approximation (GGA) of Perdew-

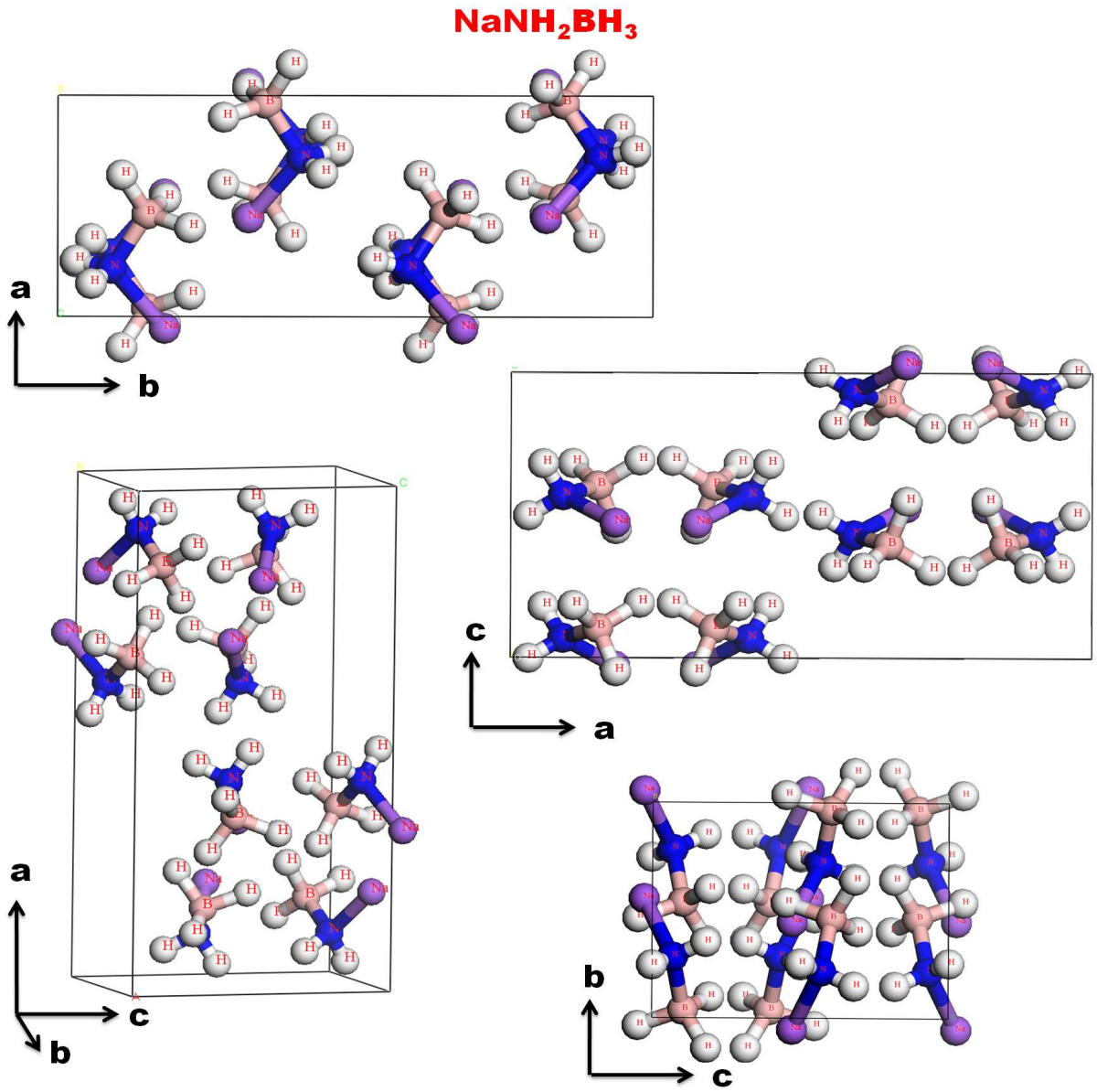

Figure 6.3: The optimized crystal structure of $NaNH_2BH_3$ within GGA represented along different crystallographic directions (Blue spheres represents Nitrogen atoms, pink spheres represents Boron atoms, purple spheres represents Sodium atoms and white spheres represents Hydrogen atoms).

Burke-Ernzerhof (PBE) [140, 141]. A plane wave basis set with energy cut-off of 460, 430 and 490 eV has been applied for $LiNH_2BH_3$, $LiNH_3BH_4$ and $NaNH_2BH_3$, respectively. The

vdW forces were taken into account through the semiempirical methods proposed by the Grimme (G06) [63], Ortmann, Bechstedt, and Schmidt (OBS) [65], and by Tkatchenko and Scheffler (TS) [66]. For the Brillouin zone sampling, the 5 x 4 x 6, 5 x 7 x 3 and 4 x 5 x 5 Monkhorst-Pack [87] mesh has been used for $LiNH_2BH_3$, $LiNH_3BH_4$ and $NaNH_2BH_3$ respectively, in which the forces on the atoms are converged to less than 0.0005 eV/$\AA$. The maximum ionic displacement is within 0.005$\AA$ and the total stress tensor is reduced to the order of 0.02 GPa.

6.3 Results and discussion

6.3.1 Structural properties

The optimized crystal structures of $LiNH_2BH_3$, $LiNH_3BH_4$ and $NaNH_2BH_3$ are shown in figures 6.1, 6.2 and 6.3 respectively, in which each formula unit contain pair of B and N atoms. In the molecular units of $LiNH_2BH_3$ and $NaNH_2BH_3$, B is connected to H1, H2 and H3 atoms, N is connected to H3 and H4 atoms as shown in figures 6.1 & 6.3 and the metal atoms are connected to N atoms respectively. Whereas in the case of $LiNH_3BH_4$, each B is surrounded by four H atoms i.e., to H1, H2 and two H3 atoms as shown in figure 6.2. Each N is surrounded by three H atoms i.e., to one H4 and two H5 atoms. The optimized structural parameters and fractional coordinates using LDA and GGA functionals along with OBS, G06 and TS corrections are given in tables 6.1, 6.2, 6.3 and 6.4, along compared with experimental data. From the tables it is inferred that the unit cell volume obtained by LDA is underestimated by 17% for both $LiNH_2BH_3$ and $LiNH_3BH_4$, and 15% for $NaNH_2BH_3$ whereas the same is overestimated by 1.1% for $LiNH_2BH_3$, 0.7% for $LiNH_3BH_4$ and 3% for $NaNH_2BH_3$ using GGA. In order to study the role of vdW interactions in $LiNH_2BH_3$, $LiNH_3BH_4$ and $NaNH_2BH_3$ we have also carried out the calculations including vdW forces. Interestingly, alkali metal amidoboranes does not show the effect of vdW interactions on the structural properties. This is may be due to the change in the bonding nature of B-H and

N-H bonds when the alkali atom is replaced with one of the H atoms of N. From the present calculations we came to a conclusion that GGA is better choice to reproduce the experimental structural parameters of alkali metal amidoboranes. Hence all further calculations of alkali metal amidoboranes are carried out using the GGA functionals.

Table 6.1: The optimized structural parameters of $LiNH_2BH_3$, $LiNH_3BH_4$ and $NaNH_2BH_3$ along with experimental data.

Property	LDA	OBS	GGA	G06	TS	Other	Expt
				$LiNH_2BH_3$			
a($\AA$)	6.624	6.062	7.102	6.604	6.719	7.108[a]	7.1127(6)[b]
b($\AA$)	12.938	12.133	14.037	13.129	13.092	13.945[a]	13.94877(14)[b]
c($\AA$)	4.940	4.524	5.183	4.936	5.029	5.150[a]	5.15018(6)[b]
V($\AA^3$)	423.49	332.78	516.82	428.08	442.49	510.47[a]	510.970(15)[b]
				$LiNH_3BH_4$			
a($\AA$)	5.506	5.256	5.918	5.713	5.641	5.926[c]	5.96910(3)[d]
b($\AA$)	4.234	3.876	4.464	4.259	4.294	4.462[c]	4.46355(2)[d]
c($\AA$)	13.491	12.490	14.571	14.022	13.688	14.541[c]	14.34199(8)[d]
V($\AA^3$)	314.58	254.47	384.98	341.22	331.65	384.59[c]	382.119[d]
				$NaNH_2BH_3$			
a($\AA$)	13.729	12.789	14.750	13.881	13.845	-	14.6474(32)[e]
b($\AA$)	5.415	5.278	5.722	5.405	5.518	-	5.6548(09)[e]
c($\AA$)	7.015	6.341	7.540	7.116	6.843	-	7.4680(16)[e]
V($\AA^3$)	521.58	428.12	636.44	533.97	522.84	-	618.56[e]

[a]Ref[107]; [b]Ref[206]; [c]Ref[215]; [d]Ref[214]; [e]Ref[213];

6.3.2 Electronic structure

The electronic structure of $LiNH_2BH_3$, $LiNH_3BH_4$ and $NaNH_2BH_3$ is studied through the calculated band structure and density of states (DOS). In figures 6.4a, 6.4b and 6.4c, the calculated band structures of $LiNH_2BH_3$, $LiNH_3BH_4$ and $NaNH_2BH_3$ are presented, respectively. From the band structure, is found that $LiNH_2BH_3$, $LiNH_3BH_4$ and $NaNH_2BH_3$ are wide band gap insulators with the band gaps of 4.081 eV, 5.618 eV and 3.963 eV,

Table 6.2: The optimized atomic fractional coordinates of $LiNH_2BH_3$ along with experimental values.

Atom		LDA	OBS	GGA	G06	TS	other[a]	Expt[a]
	x	0.095	0.110	0.100	0.096	0.103	0.09080	0.091(4)
B	y	0.148	0.144	0.153	0.150	0.148	0.14998	0.152(4)
	z	0.959	0.964	0.968	0.960	0.974	0.96163	0.972(5)
	x	0.068	0.087	0.064	0.072	0.072	0.05593	0.074(1)
N	y	0.083	0.068	0.093	0.081	0.082	0.09003	0.093(3)
	z	0.707	0.708	0.722	0.711	0.725	0.71334	0.716(5)
	x	0.181	0.198	0.181	0.178	0.188	0.17223	0.149
H1	y	0.106	0.108	0.110	0.112	0.105	0.10732	0.101
	z	0.155	0.189	0.148	0.163	0.164	0.14269	0.155
	x	0.192	0.211	0.194	0.195	0.201	0.18394	0.204
H2	y	0.227	0.227	0.224	0.226	0.224	0.22233	0.220
	z	0.905	0.892	0.915	0.901	0.919	0.90818	0.945
	x	-0.072	-0.074	-0.052	-0.072	-0.058	0.93720	-0.064
H3	y	0.177	0.173	0.182	0.180	0.178	0.17870	0.186
	z	0.042	0.039	0.055	0.032	0.057	0.04822	0.038
	x	0.205	0.232	0.189	0.209	0.206	0.18118	0.200
H4	y	0.061	0.045	0.070	0.060	0.059	0.06777	0.064
	z	0.624	0.606	0.644	0.631	0.645	0.63478	0.661
	x	-0.010	-0.003	-0.010	-0.005	-0.004	0.98416	-0.018
H5	y	0.015	-0.002	0.032	0.015	0.016	0.02771	0.037
	z	0.739	0.746	0.759	0.745	0.761	0.75213	0.736
	x	-0.050	-0.030	-0.046	-0.044	-0.042	0.93217	-0.020(1)
Li	y	0.173	0.174	0.176	0.173	0.169	0.17465	0.180(2)
	z	0.428	0.434	0.438	0.418	0.439	0.43217	0.428(3)

[a]Ref[136];

respectively. The valence band maximum and the conduction band minimum of $LiNH_2BH_3$ are found to be along Γ-Z direction and the counter part for $NaNH_2BH_3$ are found along Y-S direction indicates that these two compounds are indirect band gap insulators. On the other hand $LiNH_3BH_4$ is found to be an indirect band gap insulator as its valence band maximum and conduction band minimum are found to be along the same direction Γ. The band gap value of these compounds follows the trend: $LiNH_3BH_4 > LiNH_2BH_3 > NaNH_2BH_3$.

Table 6.3: The optimized atomic fractional coordinates of $LiNH_3BH_4$ along with experimental values.

Atom		LDA	OBS	GGA	G06	TS	other[a]	Expt[b]
	x	0.914	0.882	0.916	0.906	0.962	0.9191	0.9059(4)
B	y	0.750	0.750	0.750	0.750	0.750	0.75	0.75
	z	0.398	0.395	0.402	0.403	0.396	0.4024	0.3993(1)
	x	0.573	0.596	0.582	0.595	0.523	0.5802	0.6081(4)
N	y	0.750	0.750	0.750	0.750	0.750	0.75	0.75
	z	0.649	0.649	0.643	0.651	0.647	0.6430	0.6514(1)
	x	0.724	0.702	0.738	0.730	0.764	0.7411	0.754(2)
H1	y	0.750	0.750	0.750	0.750	0.750	0.75	0.75
	z	0.446	0.457	0.446	0.453	0.434	0.4459	0.451(1)
	x	0.092	0.087	0.080	0.083	0.116	0.0819	0.073(2)
H2	y	0.750	0.750	0.750	0.750	0.750	0.75	0.75
	z	0.454	0.442	0.455	0.453	0.460	0.4553	0.442(1)
	x	0.921	0.865	0.924	0.906	0.981	0.9266	0.898(1)
H3	y	0.517	0.501	0.528	0.520	0.521	0.5285	0.536(2)
	z	0.344	0.339	0.353	0.351	0.344	0.3528	0.352(1)
	x	0.609	0.576	0.610	0.626	0.567	0.6071	0.585(3)
H4	y	0.750	0.750	0.750	0.750	0.750	0.75	0.75
	z	0.725	0.732	0.713	0.723	0.721	0.7132	0.717(1)
	x	0.463	0.490	0.481	0.492	0.414	0.4789	0.519(2)
H5	y	0.555	0.540	0.566	0.557	0.559	0.5668	0.584(1)
	z	0.635	0.624	0.630	0.636	0.637	0.6296	0.632(2)
	x	0.876	0.912	0.881	0.902	0.821	0.8800	0.8903(8)
Li	y	0.750	0.750	0.750	0.750	0.750	0.75	0.75
	z	0.575	0.580	0.572	0.574	0.571	0.5728	0.5752(3)

[c]Ref[215]; [d]Ref[214];

Total and partial density of states :

The calculated total and partial density of states (DOS) of $LiNH_2BH_3$, $LiNH_3BH_4$ and $NaNH_2BH_3$ are presented in figures 6.5, 6.6 and 6.7, respectively. The detailed discussion for each compound is as follows:

$LiNH_2BH_3$: The total DOS is made of five well-separated regions in energy (see figure 6.5): first region corresponds to states between -1.5 eV and 0 eV i.e., near to fermi level. It is made

Table 6.4: The optimized atomic fractional coordinates of $NaNH_2BH_3$ along with experimental values.

Atom		LDA	OBS	GGA	G06	TS	Expt[a]
	x	0.139	0.135	0.146	0.141	0.139	0.1500300
B	y	0.050	0.045	0.039	0.050	0.068	0.036470
	z	0.087	0.102	0.092	0.090	0.091	0.103510
	x	0.067	0.046	0.081	0.068	0.074	0.0899679
N	y	0.260	0.231	0.250	0.261	0.291	0.283161
	z	0.073	0.108	0.072	0.079	0.081	0.068662
	x	0.108	0.117	0.111	0.111	0.101	0.1073566
H1	y	-0.144	-0.158	-0.137	-0.145	-0.118	-0.13982
	z	0.164	0.190	0.163	0.165	0.161	0.182589
	x	0.212	0.211	0.212	0.212	0.211	0.2216664
H2	y	0.115	0.139	0.095	0.117	0.113	0.0982673
	y	0.181	0.192	0.182	0.182	0.191	0.192206
	x	0.168	0.160	0.174	0.169	0.166	0.1811787
H3	y	-0.009	-0.011	-0.022	-0.006	0.015	-0.035689
	z	-0.074	-0.078	-0.055	-0.069	-0.075	-0.048619
	x	0.006	-0.021	0.024	0.007	0.013	0.0303835
H4	y	0.219	0.162	0.209	0.218	0.262	0.245799
	z	-0.005	0.042	-0.000	0.002	-0.001	-0.002018
	x	0.043	0.027	0.057	0.044	0.049	0.0559582
H5	y	0.323	0.284	0.306	0.319	0.344	0.351845
	z	0.204	0.261	0.193	0.208	0.216	0.180261
	x	0.167	0.159	0.168	0.167	0.172	0.1795554
Na	y	0.571	0.535	0.572	0.580	0.613	0.553818
	z	-0.040	-0.001	-0.040	-0.040	-0.043	-0.027695

[a]Ref[213];

of peaks coming from B-p and N-p states, together with s states of hydrogens connected to B atom. An important point is that a small contribution appears in the PDOS of Li-s states at the same energy, which indicates that the bonding is not totally ionic but contains also a small amount of covalency. The second region is between -4 eV to -1.5 eV, and it corresponds to N-p, B-p and s states of hydrogens connected to B atom. The states between -5.5 eV to -4 eV corresponds to third region. It is made of several peaks coming from N-p, B-p states

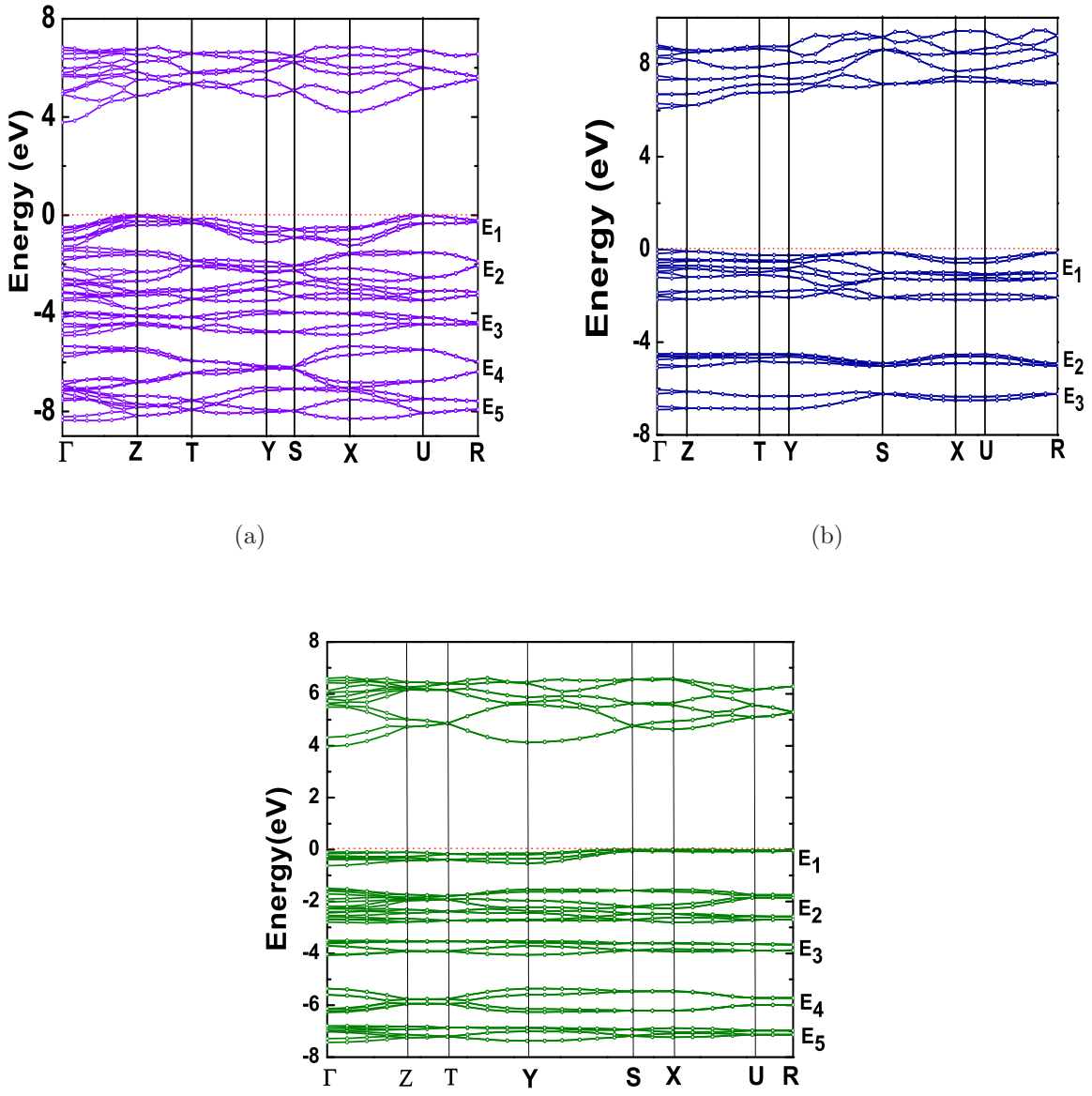

Figure 6.4: The band structure of alkali metal amidoboranes (a) $LiNH_2BH_3$ (b) $LiNH_3BH_4$ and (c) $NaNH_2BH_3$ calculated within GGA. The zero represents the Fermi level.

with an admixture of all H-s states. The fourth region is the states between -6.5 eV to -5.5 and is from the peaks of N-p, s states of H's connected to N together with small contribution from B-p states. Then, from -8 eV to -6.5 eV states are corresponding to fifth region and it is from N-p and B-s along with the s states all H's.

In the conduction band, it has s states of Li and p states of B, with minor contribution from all H-s states. The B-p, N-p and H-s states are hybridized in all the energy regions implying a sp hybridization between B-H and N-H bonds. Overall the present study concludes that both B-H, N-H bonds are covalent in nature whereas a strong ionic bonding exist between Li and N with a small covalency.

$LiNH_3BH_4$: The total DOS is made of three well-separated regions in energy (see figure 6.6): the first region corresponds to the states between -2.5 eV to 0 eV i.e., near to fermi level. It has mainly B-p states together with N-p and Li-s states along with small contribution from s states from H's connected to B. The second region corresponds to states between -5 eV to -4 eV and it is dominated by N-p and s states of H's connected to N. A small contribution from B-s *&* p states appears at the same energy. Finally, the third region is from the states between -7 eV to -5.5 eV. It is made of peaks coming from B-s and s states of H's connected to B, together with N-p states.

The conduction band has s states of Li and p states of B, together with smaller contribution from all H-s states. The B-p, N-p and H-s states are hybridized in all the energy regions implying a sp hybridization between B-H and N-H bonds. Overall the study concludes that both B-H, N-H bonds are covalent.

$NaNH_2BH_3$: The total DOS is made of five well-separated regions in energy (see figure 6.7): the first region corresponds to states between -1 eV and 0 eV i.e., near to fermi level. It is dominated by B-p and N-p states, together with H1-s states. An important point is that a small contribution appears in the PDOS of Na-s *&* p at the same energy, which indicates

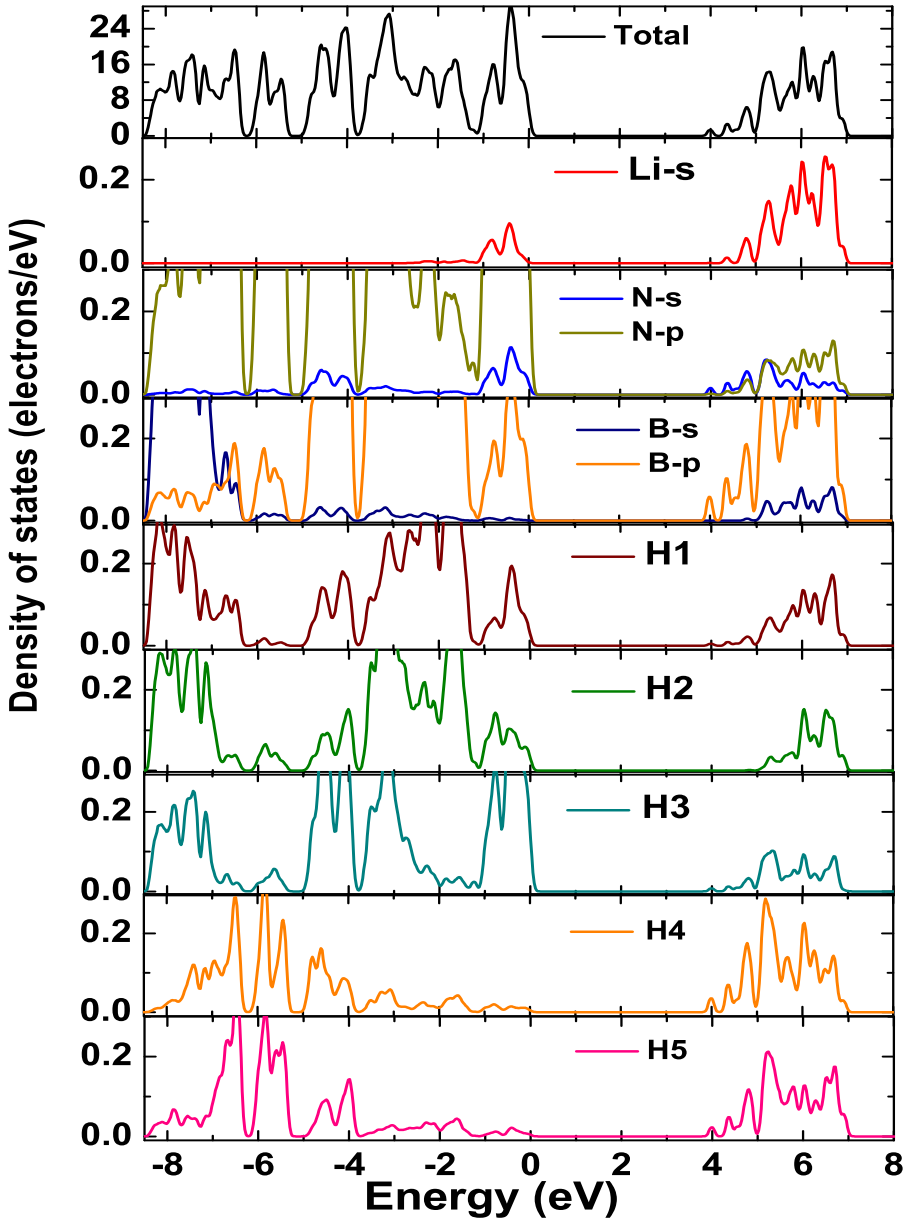

Figure 6.5: The total, partial and local density of states of $LiNH_2BH_3$ calculated within GGA. The zero represents the Fermi level.

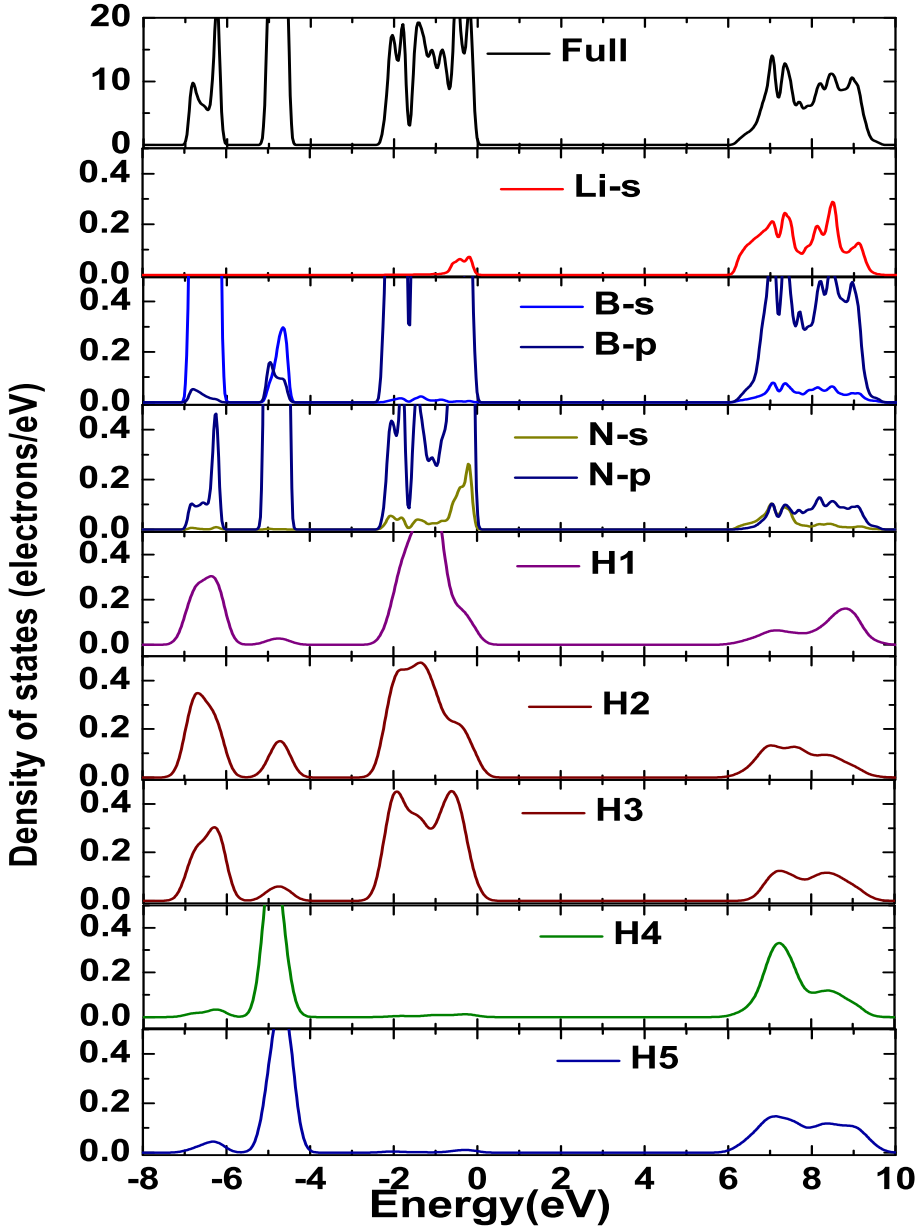

Figure 6.6: The total, partial and local density of states of $LiNH_3BH_4$ calculated within GGA. The zero represents the Fermi level.

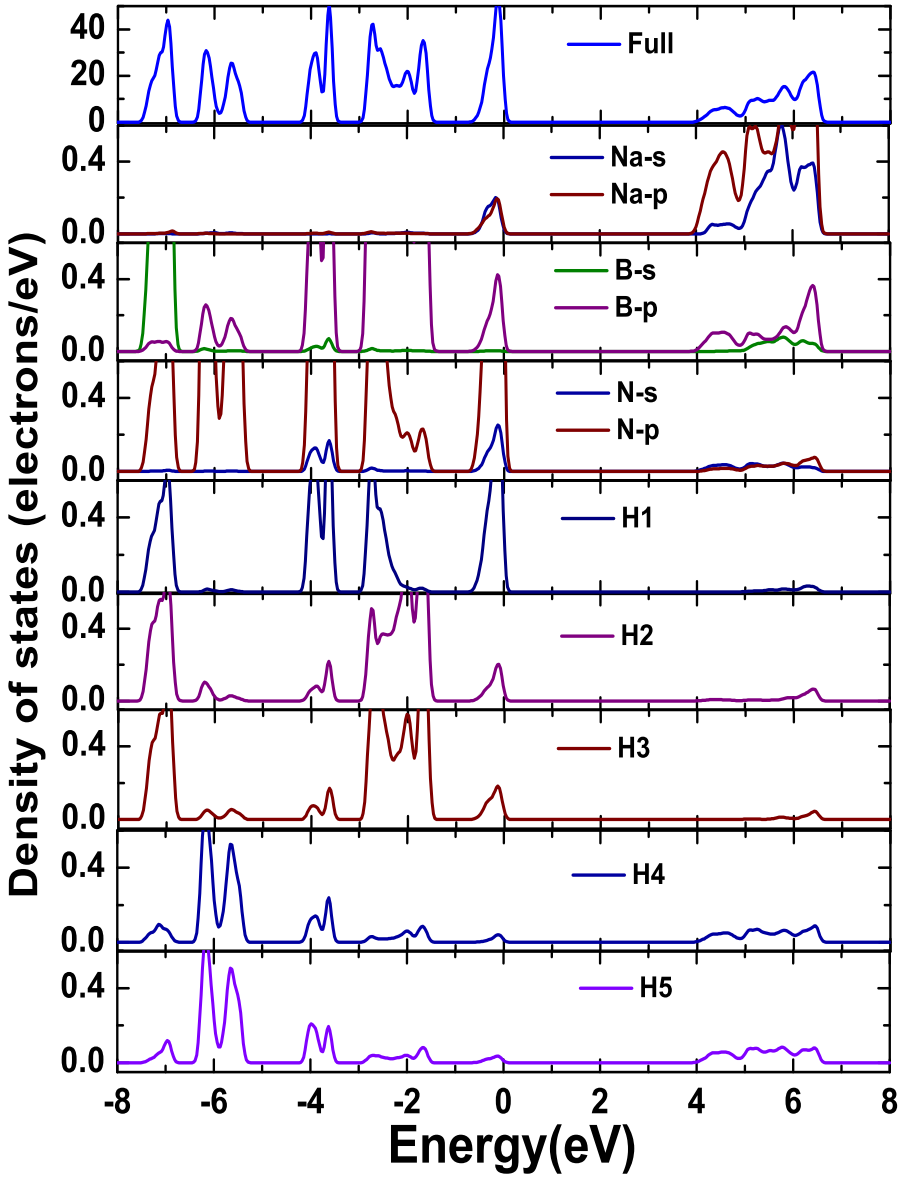

Figure 6.7: The total, partial and local density of states of $NaNH_2BH_3$ calculated within GGA. The zero represents the Fermi level.

that the bonding is not totally ionic but contains also a small amount of covalency. The second region is between -3 eV to -1.5 eV, and it corresponds to N-p, B-p and s states of hydrogens connected to B atom. The states between -4 eV to -3 eV corresponds to third region. It is made of several peaks coming from N-p, B-p states with an admixture of H1-s states. The fourth region consists of states between -6.5 eV to -5 and is from the peaks of N-p, s states of H's connected to N together with small contribution from B-p states. Finally the states from -7.5 eV to -6.5 eV correspond to fifth region, comprised of N-p and B-s along with the s states H's connected to B.

The conduction band has Na-s & p states. The B-p, N-p and H-s states are hybradizing in all the energy regions implies a sp hybridization between B-H and N-H bonds. Overall the study concludes that both B-H, N-H bonds are covalent in nature whereas a strong ionic bonding exist between Na and N with a small covalency.

6.3.3 Bonding properties

Mulliken atomic and bond population analysis:

To quantify the charge distribution in $LiNH_2BH_3$, $LiNH_3BH_4$ and $NaNH_2BH_3$, we have calculated Mulliken atomic charges, orbital contributions are presented in table 6.5. The Mulliken atomic charges for Li and Na are found to be positive and it is negative for the B and N atoms. The hydrogens connected to B and N atoms are found to have negative and positive charges, respectively. This scenario clearly indicates the protic and hydridic nature of B-H and N-H bonds in alkali metal amidoboranes. To understand the bonding nature we have calculated the Mulliken bond populations for each bond and presented in table 6.6. The total overlap (bond) population for any pair of atoms in a molecule is in general made up of positive and negative contributions. If the total overlap population between two atoms is positive, they are bonded; if negative, they are antibonded [97]. A high positive bond population indicates a high degree of covalence. From the calculated bond populations it is

found that all the bonds are covalent in nature. The B-H bonds with high bond population, shows their dominating covalent nature relative to N-H bonds in these compounds.

Table 6.5: The calculated Mulliken atomic charges and atomic populations of $LiNH_2BH_3$, $LiNH_3BH_4$ and $NaNH_2BH_3$.

Atom	Compound	s	p	Total	Charge
H1	$LiNH_2BH_3$	1.16	0.0	1.16	-0.16
	$LiNH_3BH_4$	1.14	0.0	1.14	-0.14
	$NaNH_2BH_3$	1.23	0.0	1.23	-0.23
H2	$LiNH_2BH_3$	1.17	0.0	1.17	-0.17
	$LiNH_3BH_4$	1.17	0.0	1.17	-0.17
	$NaNH_2BH_3$	1.21	0.0	1.21	-0.21
H3	$LiNH_2BH_3$	1.22	0.0	1.22	-0.22
	$LiNH_3BH_4$	1.13	0.0	1.13	-0.13
	$NaNH_2BH_3$	1.22	0.0	1.22	-0.22
H4	$LiNH_2BH_3$	0.66	0.0	0.66	0.34
	$LiNH_3BH_4$	0.62	0.0	0.62	0.38
	$NaNH_2BH_3$	0.74	0.0	0.74	0.26
H5	$LiNH_2BH_3$	0.61	0.0	0.61	0.39
	$LiNH_3BH_4$	0.62	0.0	0.62	0.38
	$NaNH_2BH_3$	0.74	0.0	0.74	0.26
B	$LiNH_2BH_3$	0.89	2.48	3.37	-0.37
	$LiNH_3BH_4$	0.99	2.78	3.77	-0.77
	$NaNH_2BH_3$	0.91	2.52	3.43	-0.43
N	$LiNH_2BH_3$	1.66	4.40	6.05	-1.05
	$LiNH_3BH_4$	1.71	4.44	6.15	-1.15
	$NaNH_2BH_3$	1.62	4.31	5.93	-0.93
Li	$LiNH_2BH_3$	1.70	0.0	1.70	1.30
	$LiNH_3BH_4$	1.68	0.0	1.68	1.32
Na	$NaNH_2BH_3$	2.02	5.48	7.49	1.51

To know the percentage of the covalence, we have calculated the population ionicity of each of the bonds of these compounds as discussed earlier in chapter 4. The lower limit i.e. $P_i = 0$ indicates a pure covalent bond while the upper limit (i.e) $P_i = 1$ indicates a purely ionic bond [97, 98, 156, 157]. As expected, B-H bonds show zero population ionicity and N-H

Table 6.6: The calculated bond populations (P), population ionicity(P_i) and bond lengths of $LiNH_2BH_3$, $LiNH_3BH_4$ and $NaNH_2BH_3$.

Bond	Compound	P	P_i	Bond Length($\mathring{A}$)
B-H1	$LiNH_2BH_3$	0.90	0.10	1.23368
	$LiNH_3BH_4$	0.96	0.04	1.22976
	$NaNH_2BH_3$	1.03	-0.02	1.23832
B-H2	$LiNH_2BH_3$	0.93	0.07	1.24234
	$LiNH_3BH_4$	0.99	0.10	1.23406
	$NaNH_2BH_3$	1.03	-0.02	1.24170
B-H3	$LiNH_2BH_3$	0.89	0.11	1.24603
	$LiNH_3BH_4$	0.98	0.02	1.22431
	$NaNH_2BH_3$	1.00	0.0	1.25579
N-H4	$LiNH_2BH_3$	0.74	0.29	1.03103
	$LiNH_3BH_4$	0.71	0.33	1.03234
	$NaNH_2BH_3$	0.80	0.22	1.03094
N-H5	$LiNH_2BH_3$	0.74	0.29	1.03176
	$LiNH_3BH_4$	0.71	0.33	1.03304
	$NaNH_2BH_3$	0.80	0.22	1.03106
B-N	$LiNH_2BH_3$	0.65	0.41	1.54765
	$LiNH_3BH_4$	-0.08	-	3.76516
	$NaNH_2BH_3$	0.71	0.33	1.54496
N-Li	$LiNH_2BH_3$	0.12	0.99	2.03114
	$LiNH_3BH_4$	0.11	0.99	2.05089
N-Na	$NaNH_2BH_3$	0.12	0.99	2.39139

bond show very low value (0.3) of population ionicity. The B-N bond with 0.41 population ionicity shows a dominating covalent character. So, B-N bond is no more a dative or coordinative bond in alkali metal amidoboranes. Which results in the reduction of hydridic nature of H1, H2 and H3 atoms and the protic nature of H3 and H4 atoms. Moreover, the average ionicity value of B-N, N-H and B-H bonds in $LiNH_2BH_3$, $LiNH_3BH_4$ and $NaNH_2BH_3$ are found to be 0.23, 0.19 and 0.18, respectively and these are relatively lower when compared to the average ionicity value of NH_3BH_3. From the above discussions, we conclude that alkali metal amidoboranes exhibit relatively a high covalency compared to NH_3BH_3.

The electron density iso surface and charge density distributions:

Another meaningful way to understand the electron distribution is to look at iso surface of electron density and the electron density in (100), (010) and (001) planes. In figures 6.8a, 6.8b and 6.8c we present our calculated electron density iso surfaces of $LiNH_2BH_3$, $LiNH_3BH_4$ and $NaNH_2BH_3$, respectively. The electron density around NH_2BH_3 ligand has a distorted spherical shape but it is spherical in shape around Li and Na atoms. The aspherical shape indicates the distribution/sharing of the charge in entire NH_2BH_3 ligand and spherical in shape indicates the localization of charge, which confirms the bonding in these compound is mainly covalent.

The calculated charge density distributions in (100), (010) and (001) planes and corresponding partial density of states (PDOS) in different energy ranges in the valence band as defined in the band structures of the $LiNH_2BH_3$, $LiNH_3BH_4$ and $NaNH_2BH_3$ are presented in figures 6.9, 6.10 and 6.11, respectively. For $LiNH_2BH_3$, from the plot (see figure 6.9), in the E1 & E2 energy region, the main states are from N 2p states along with weak hybridization between B 2p states and H1, H2 & H3 s states. In the energy region E3 one finds equal contribution of 2p states of B & N atoms. States of strong hybridization between N 2p states and H3 & H4 s states are found in E4 energy region, while E5 energy region displays the hybridization between the B 2s and N 2p states along with a small contribution from s states of all hydrogens.

For $LiNH_3BH_4$, from the plot (see figure 6.10), in the E1 energy region, the main states are the B 2p states. At the same time, a weak hybridization between B 2p states and H1, H2 & H3 s states is also found in this energy region. In the E2 energy region, there is a strong hybridization between H4 & H5 s states and 2p states of N atoms. The next region E3 displays the hybridization between the B 2s and N 2p states along with a small contribution from H1, H2 & H3 s states.

For $NaNH_2BH_3$, from the plot (see figure 6.11), in the E1 energy region, a strong N 2p

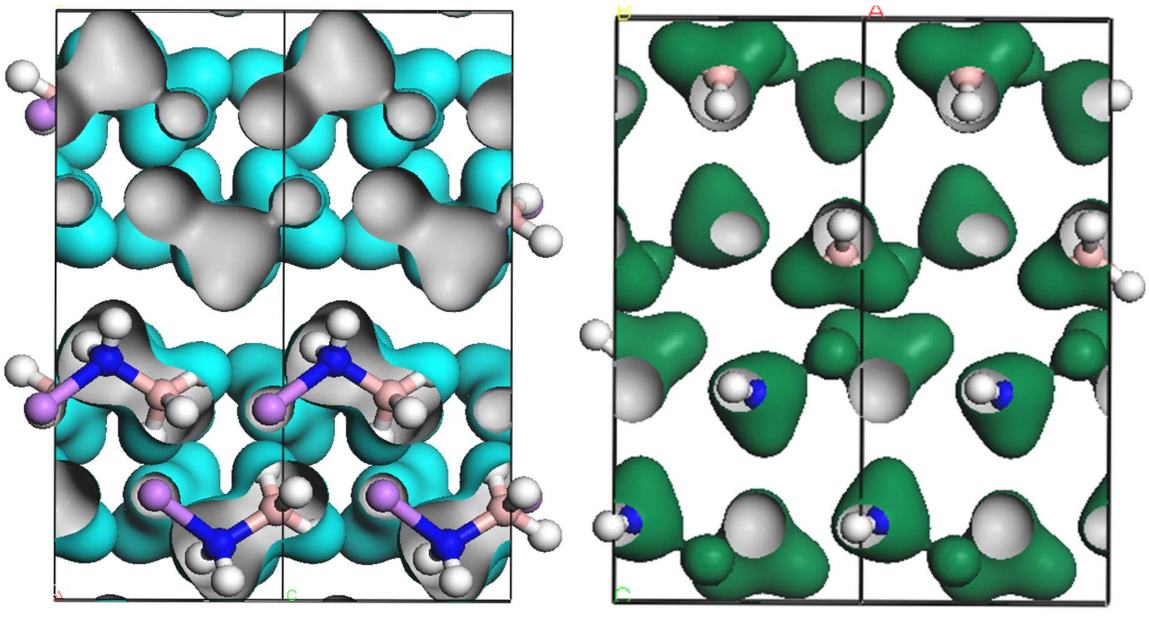

(a) (b)

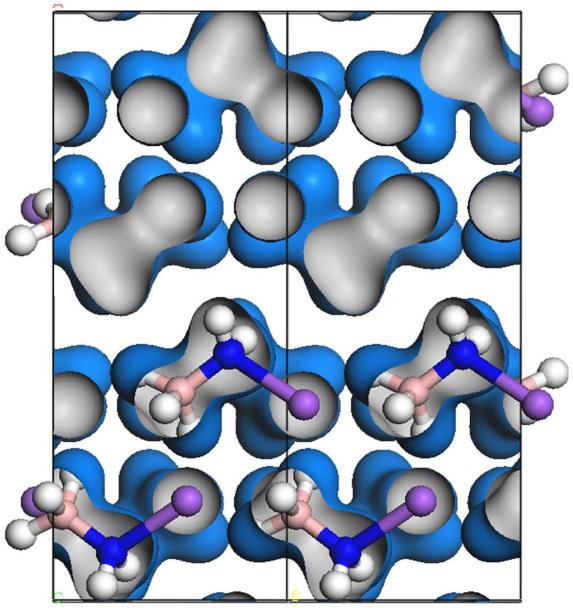

(c)

Figure 6.8: The total electron density iso-surfaces of alkali metal amidoboranes (a) $LiNH_2BH_3$ along a axis (b) $LiNH_3BH_4$ along b axis and (c) $NaNH_2BH_3$ along b axis calculated within GGA. (Blue spheres represents Nitrogen atoms, pink spheres represents Boron atoms, purple spheres represents metal (Lithium or Sodium) atoms and white spheres represents Hydrogen atoms).

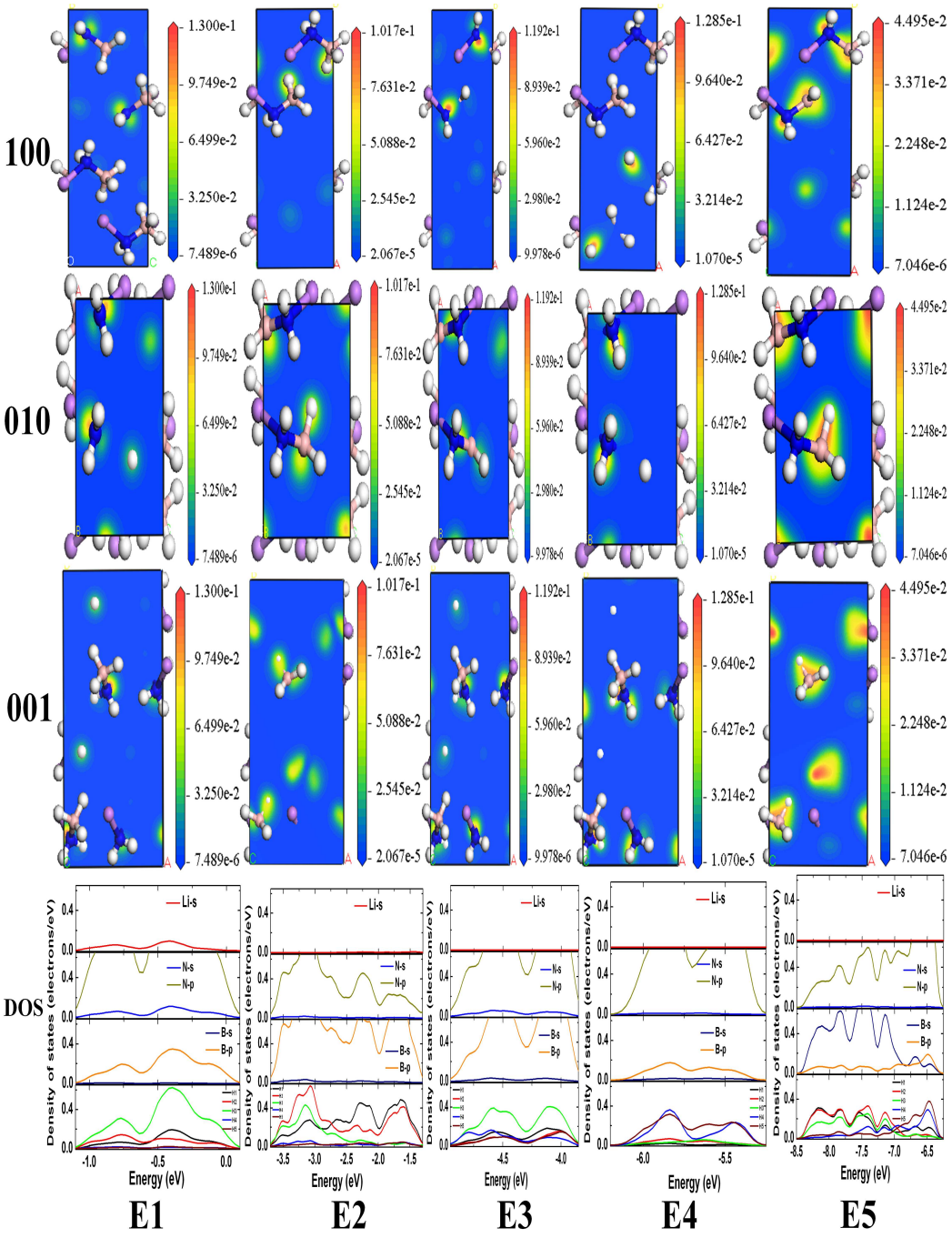

Figure 6.9: The charge density distributions of $LiNH_2BH_3$ along (100), (010) and (001) planes, and the corresponding partial density of states (PDOS) are shown for different energy ranges in the valance band defined as E1=-1.5 to 0 eV (at Fermi level), E2=-4 to -1.5 eV, E3=-5.5 to -4 eV, E4=-5.5 to -6.5 eV and E5=-6.5 to -8.5 eV (Blue spheres represents Nitrogen atoms, pink spheres represents Boron atoms, purple spheres represents Lithium atoms and white spheres represents Hydrogen atoms).

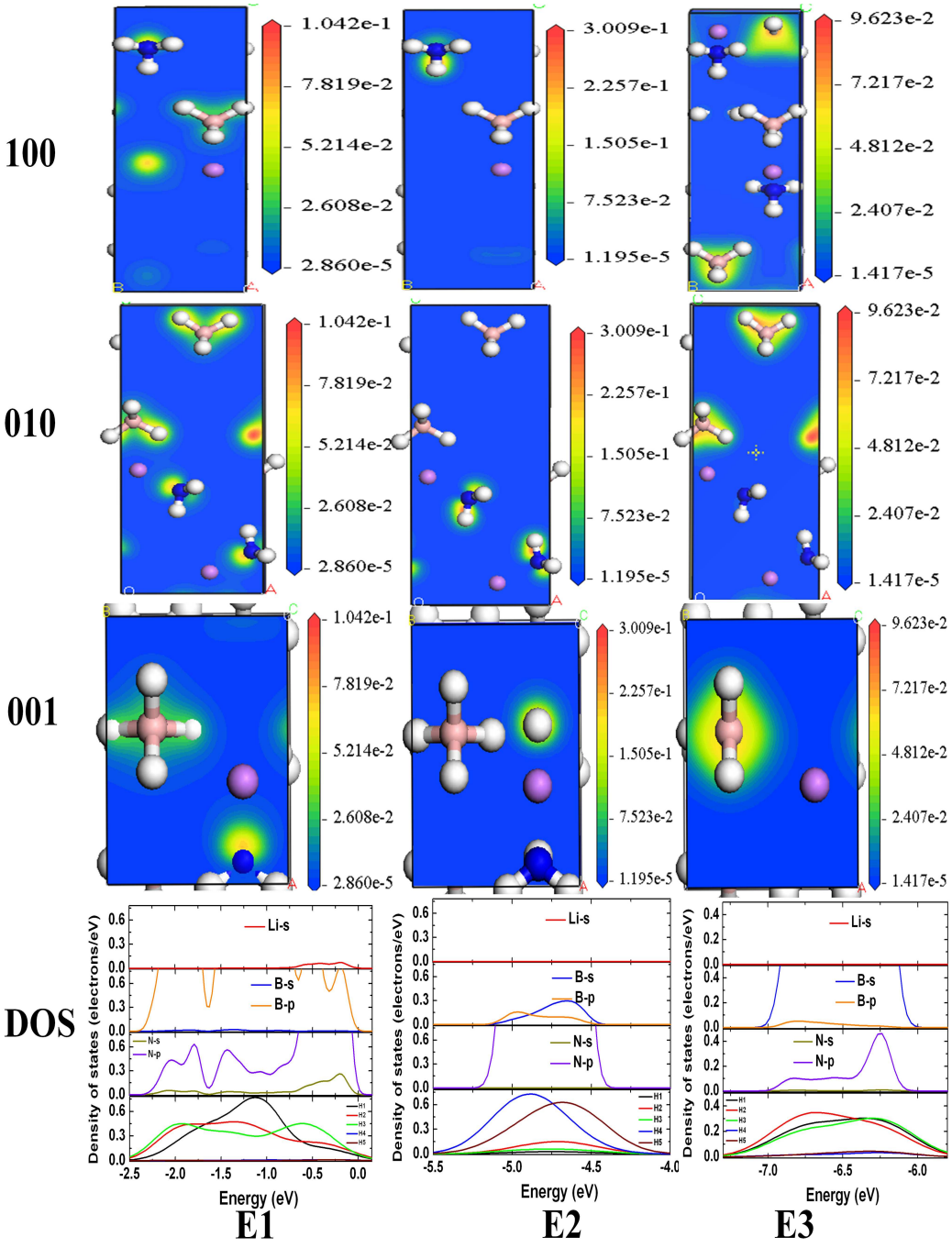

Figure 6.10: The charge density distributions of $LiNH_3BH_4$ along (100), (010) and (001) planes, and the corresponding partial density of states (PDOS) are shown for different energy ranges in the valance band defined as E1=-2.5 to 0 eV (at Fermi level), E2=-5 to -4 eV and E3=-5 to -7.5 eV (Blue spheres represents Nitrogen atoms, pink spheres represents Boron atoms, purple spheres represents Lithium atoms and white spheres represents Hydrogen atoms).

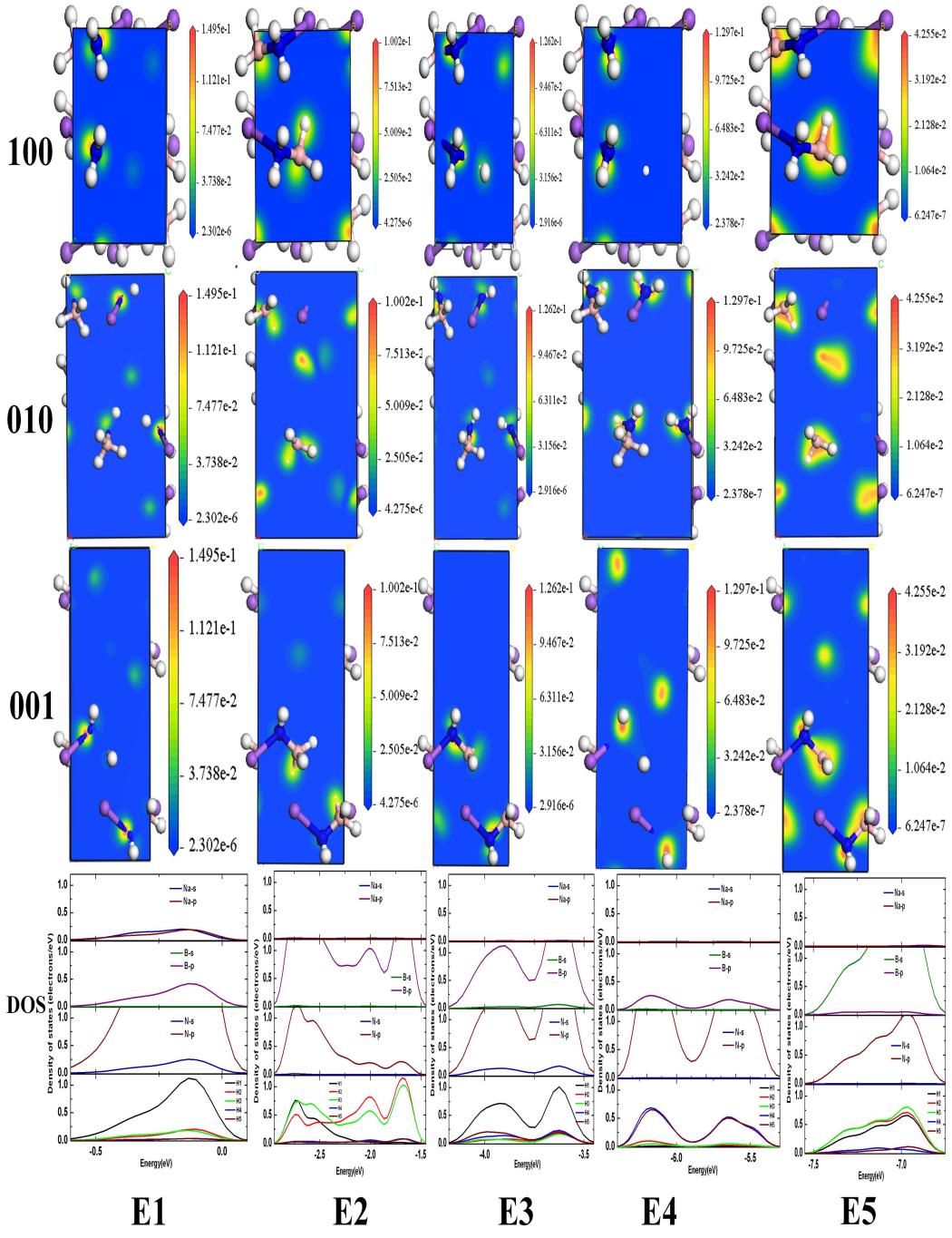

Figure 6.11: The charge density distributions of $NaNH_2BH_3$ along (100), (010) and (001) planes, and the corresponding partial density of states (PDOS) are shown for different energy ranges in the valance band defined as E1=-1 to 0 eV (at Fermi level), E2=-3 to -1.5 eV, E3=-4 to -3 eV, E4=-5 to -6.5 eV and E5=-7 to -7.5 eV (Blue spheres represents Nitrogen atoms, pink spheres represents Boron atoms, purple spheres represents Sodium atoms and white spheres represents Hydrogen atoms).

states and a considerable contribution from H1 s states is found. The E2 energy region consists of hybridization between B 2p states and H1, H2 & H3 s states. At the same time a weak N 2p states also found. Equal contribution from 2p states of B & N atoms are found in E3 energy region with almost equal contribution from H1 s sates. A strong hybridization between N 2p states and H4 & H5 s states is seen in E4 energy region, while E5 energy region displays the hybridization between the B 2s and N 2p states along with a small contribution from H1, H2 & H3 s states.

The electron distribution between Li or Na atoms and the neighboring atoms is very low, which confirms the bonding between Li or Na and NH_2BH_3 ligand is ionic in nature. A high negative charge distribution around BH_3 group implies predominantly covalent bonding. From the charge density distribution plots once again we conclude that, a strong covalent bonding observed between the B-H bonds which is less pronounced in the case of N-H bonds.

Dihydrogen bonding:

Dihydrogen bond is a kind of hydrogen bond, which indicates an interaction between a metal bond and a OH or NH group or any proton donor group. This dihydrogen bond can exist in one molecule or between two molecules and affects molecular structure, physical and chemical properties of solids. This also plays an important role in crystal assembly and in super molecular systems. So the investigation of dihydrogen bonds is of great importance [133, 158]. To understand the dihydrogen bonding in the alkali metal amidoboranes, we have calculated the H-H separation for the inter and intra molecules. The calculated shortest distances between inter and intra hydrogen atoms for $LiNH_2BH_3$, $LiNH_3BH_4$ and $NaNH_2BH_3$ are listed in table 6.7. All the possible shortest distances between inter hydrogen atoms are found to be greater than 2.5 $\mathring{A}$. The intra hydrogens atoms (H4 & H5) of N are having a shortest distance around 1.63 $\mathring{A}$ and for hydrogen atoms (H1, H2 & H3) of B is around 2 $\mathring{A}$ in all $LiNH_2BH_3$, $LiNH_3BH_4$ and $NaNH_2BH_3$. It may be because of the predominant of short range interactions over long range interactions in alkali metal amidoboranes. The inter

Table 6.7: The calculated shortest distances between inter and intra hydrogen atom of $LiNH_2BH_3$, $LiNH_3BH_4$ and $NaNH_2BH_3$ within GGA.

Bond	$LiNH_2BH_3$	$LiNH_3BH_4$	$NaNH_2BH_3$
H1...H2	2.00092	2.02588	2.00587
H1...H3	1.99891	2.00537	2.00636
H1...H4	2.63374	3.97001	2.39685
H1...H5	2.39705	2.22202	2.67329
H2...H3	1.98955	2.00933	2.00268
H2...H4	2.57297	3.79222	3.16862
H2...H5	3.16759	3.20812	2.58800
H3...H4	2.62369	2.39209	2.60870
H3...H5	2.62142	2.44803	2.83939
H4...H5	1.63059	1.64969	1.63601

molecular H-H separations are beyond the typical dihydrogen bond separation implying the absence of the vdW interactions in alkali metal amidoboranes.

6.3.4 Mechanical properties

The elastic constants provide information about the mechanical and dynamical behavior, in addition to the stability and stiffness of solids. As alkali metal amidoboranes are molecular crystals, LDA is the best choice in calculating the elastic constants as discussed earlier in chapter 4. Alkali metal amidoboranes crystallize in primitive orthorhombic structure similar to NH_3BH_3. From the calculated elastic constants, $LiNH_2BH_3$, $LiNH_3BH_4$ and $NaNH_2BH_3$ satisfy the Born's stability criteria thereby revealing the mechanical stability of these compounds (see table 6.8). In general C_{11}, C_{22} and C_{33} denote the mechanical stiffness along X, Y and Z directions. The trends of the mechanical stiffness along three directions in $LiNH_2BH_3$, $LiNH_3BH_4$ and $NaNH_2BH_3$ are as follows: For $LiNH_2BH_3$ we find C_{33} (62.80 GPa) > C_{11} (51.32 GPa) > C_{22} (45.18 GPa) and for $LiNH_3BH_4$, C_{22} (33.13 GPa) > C_{11} (29.13 GPa) > C_{33} (19.38 GPa) whereas C_{11} (38.86 GPa) > C_{33} (30.43 GPa) > C_{22} (27.80

GPa) for $NaNH_2BH_3$. From this analysis we conclude that $LiNH_2BH_3$ is mechanically stiffer along Z direction whereas $LiNH_3BH_4$ and $NaNH_2BH_3$ have higher mechanical stiffness along Y and X directions, respectively. The magnitude of the elastic constants decrease in the order $LiNH_2BH_3 > NaNH_2BH_3 > LiNH_3BH_4$, which indicates that $LiNH_2BH_3$ is mechanical stiffer system among three alkali metal amidoboranes.

The shear elasticity applied to the two-dimensional rectangular lattice such as in the (100), (010) and (001) planes in $LiNH_2BH_3$, $LiNH_3BH_4$ and $NaNH_2BH_3$ can be estimated from the C_{44}, C_{55} and C_{66} elastic constants. The trends in the shear elasticity is as follows: For $LiNH_2BH_3$ we find C_{44} (16.31 GPa) > C_{66} (13.09 GPa) > C_{55} (7.13 GPa) and for $LiNH_3BH_4$, C_{66} (9.89 GPa) > C_{44} (6.87 GPa) > C_{55} (2.69 GPa) whereas C_{66} (7.83 GPa) > C_{55} (4.18 GPa) > C_{44} (1.43 GPa) for $NaNH_2BH_3$. From the above, the strong shear elasticity is found along (100) plane for $LiNH_2BH_3$ and for $LiNH_3BH_4$ and $NaNH_2BH_3$ it is along (001) plane. The shear elasticity follows the trend $LiNH_2BH_3 > LiNH_3BH_4 > NaNH_2BH_3$ confirming the higher shear elasticity of $LiNH_2BH_3$.

Table 6.8: The calculated elastic constants, in GPa, of $LiNH_2BH_3$, $LiNH_3BH_4$ and $NaNH_2BH_3$.

Compound	C_{11}	C_{22}	C_{33}	C_{44}	C_{55}	C_{66}	C_{12}	C_{13}	C_{23}
$LiNH_2BH_3$	51.32	45.18	62.80	16.31	7.13	13.09	16.84	4.62	15.35
$LiNH_3BH_4$	29.13	33.13	19.38	6.87	2.69	9.89	15.37	7.66	14.75
$NaNH_2BH_3$	38.86	27.80	30.43	1.43	4.18	7.83	11.78	13.35	7.41

Table 6.9: The calculated bulk (B), shear (G), Young's moduli (E) in GPa, G/B ratio, Poisson's ratio (σ) and Cauchy's pressure (C_{12} - C_{44}), in GPa, of $LiNH_2BH_3$, $LiNH_3BH_4$ and $NaNH_2BH_3$.

Compound	B_V	G_V	B_R	G_R	B	G	G/B	E	σ	C_{12}-C_{44}
$LiNH_2BH_3$	25.88	15.47	25.77	12.96	20.67	14.21	0.51	36.41	0.28	0.53
$LiNH_3BH_4$	17.47	6.81	15.24	5.37	16.35	6.09	0.39	16.12	0.32	8.50
$NaNH_2BH_3$	18.02	6.99	17.20	3.98	17.61	5.48	0.31	14.89	0.39	10.35

Further, we also calculated the polycrystalline elastic modulii from single-crystal elastic

constants. The calculated bulk (B), shear (G), Young's modulus (E), and Poisson's ratio (σ) using the Voigt-Reuss-Hill (VRH) approximation [142–145, 162] are given in table 6.9. The bulk modulus (B) for the $LiNH_2BH_3$, $LiNH_3BH_4$ and $NaNH_2BH_3$ are calculated to be 20.67 GPa, 16.35 GPa and 17.61 GPa, respectively (see table 6.9). The Young's modulus (E) of the $LiNH_2BH_3$, $LiNH_3BH_4$ and $NaNH_2BH_3$ are calculated to be 36.41 GPa, 16.12 GPa and 14.89 GPa. The calculated bulk and Young's modulii values once again confirms that $LiNH_2BH_3$ is the stiffest compound among the three alkali metal amidoboranes. The stability of these crystals against shear has been scaled by calculating the Poisson's ratio (σ) value. From the σ values we concluded that $LiNH_2BH_3$ is soft towards volume change whereas $LiNH_3BH_4$ and $NaNH_2BH_3$ are soft towards the shape change.

Table 6.10: The calculated shear anisotropy factors for (100) plane (A_1), for (010) plane (A_2), for (001) plane (A_3), the percentage of the anisotropy in the compressibility (A_B) and shear modulii (A_G) of $LiNH_2BH_3$, $LiNH_3BH_4$ and $NaNH_2BH_3$ at the theoretical equilibrium volume.

Compound	A_1	A_2	A_3	A_B	A_G
$LiNH_2BH_3$	0.622	0.369	0.833	0.002	0.068
$LiNH_3BH_4$	0.827	0.467	1.255	0.218	0.118
$NaNH_2BH_3$	0.134	0.385	0.726	0.002	0.088

The ductile and brittle nature of the materials can be known from the elastic constants in terms of Cauchy's pressure (C_{12} - C_{44}) and G/B ratio. If Cauchy's pressure is positive, it indicates the ductile nature other wise the material is brittle [168]. The critical value of G/B ratio that separates ductile or brittle nature of the materials is 0.57. If G/B $>$ 0.57 indicates brittle nature and G/B $<$ 0.57 indicates ductile nature [162, 169]. The positive values of the Cauchy's pressure of $LiNH_2BH_3$, $LiNH_3BH_4$ and $NaNH_2BH_3$ indicates their ductility behavior, and this has been confirmed from the calculated G/B ratios. The value of Cauchy's pressure of $LiNH_2BH_3$ found to be very low compared to the $LiNH_3BH_4$ and $NaNH_2BH_3$, which is an indication of the highest ductility of $LiNH_3BH_4$ and $NaNH_2BH_3$ over $LiNH_2BH_3$.

The shear anisotropy is a measure of the degree of anisotropy in bonding between the atoms in different planes. Here, we have calculated the shear anisotropy of $LiNH_2BH_3$, $LiNH_3BH_4$ and $NaNH_2BH_3$ along (100), (010) and (001) shear planes (see table 6.10). The values of A_1, A_2 and A_3 are found to be differ from unity, indicating the shear anisotropic behavior of alkali metal amidoboranes. The percentage of the anisotropy in compressibility (A_B) and shear (A_G) are calculated as discussed earlier in chapter 4. From the percentage bulk modulus anisotropy A_B is found to be lower than the percentage shear modulus anisotropy A_G of $LiNH_2BH_3$ and $NaNH_2BH_3$, implying that $LiNH_2BH_3$ and $NaNH_2BH_3$ are more anisotropic in shear than in compressibility. Whereas, $LiNH_3BH_4$ is more anisotropic in compressibility than in shear.

Table 6.11: The calculated average wave velocity (v_m), longitudinal (v_l) and transverse (v_t) wave velocities and the Debye temperature (Θ_D) of $LiNH_2BH_3$, $LiNH_3BH_4$ and $NaNH_2BH_3$.

Compound	v_m(km/s)	v_l(km/s)	v_t(km/s)	Θ_D (K)
$LiNH_2BH_3$	4.288	6.471	3.875	636.60
$LiNH_3BH_4$	3.383	6.045	3.015	473.75
$NaNH_2BH_3$	2.509	4.752	2.228	347.48

The Debye temperature (Θ_D), a fundamental quantity which correlates many physical properties such as specific heat and melting point of the solids, is an important thermodynamic parameter can be calculated from elastic constants. Θ_D determines the thermal characteristics of the material, a high value of Θ_D implying a higher thermal conductivity. In the present study we have calculated the Debye temperatures (Θ_D) of $LiNH_2BH_3$, $LiNH_3BH_4$ and $NaNH_2BH_3$ from the average wave velocity (v_m) which is the average of velocities of all longitudinal (v_l) and transverse (v_t) waves as discussed in the Chapter 4, and are listed in the table 6.11. From the calculated Θ_D values, we found that $\Theta_D(LiNH_2BH_3) > \Theta_D(LiNH_3BH_4) > \Theta_D(NaNH_2BH_3)$. Therefore, $LiNH_2BH_3$ can possess high thermal conductivity than those of $LiNH_3BH_4$ and $NaNH_2BH_3$. This is the first qualitative prediction

of mechanical properties of the alkali metal amidoboranes which still awaits experimental confirmation

6.4 Conclusions

The crystal structures of alkali metal amidoboranes ($LiNH_2BH_3$, $LiNH_3BH_4$ and $NaNH_2BH_3$) are fully optimized using LDA and GGA functionals, GGA functionals are found to reproduce the experimental better volume. Interestingly, alkali metal amidoboranes not showing any effect of vdW interactions. The optimized structural parameters are in good agreement with the experimental data. From the band structure and density of states calculations, it is found that alkali metal amidoboranes are wide band gap insulators. The band gap values for $LiNH_2BH_3$, $LiNH_3BH_4$ and $NaNH_2BH_3$ are 4.081 eV, 5.618 eV and 3.963 eV, respectively with GGA which are lower than that of ammonia borane. From the charge density distribution and bond population analysis we conclude that there exists a strong covalent bond between B-H and N-H atoms. From the calculated elastic constants the alkali metal amidoboranes are found to be mechanically stable and $LiNH_2BH_3$ found to be less plastic than $LiNH_3BH_4$ and $NaNH_2BH_3$.

In the next chapter we discuss the computational studies on alkaline earth metal amidoboranes

Chapter 7

Alkaline-Earth Metal Amidoboranes

7.1 Introduction

Chemical compositional modifications are found to be an effective way in the alteration of dehydrogenation thermodynamics of NH_3BH_3. In particular, replacing one of the hydrogen atoms of N in NH_3BH_3 with metal element leads to the formation of new class of materials, named metal amidoboranes (MAB) [201, 217]. Due to the relatively high hydrogen content and attractive dehydrogenation properties, these newly developed class of materials have received increasing attention as one of the promising candidates for hydrogen storage [136, 206, 207, 211]. In the previous chapter, we discussed the alkali metal amidoboranes, in the present chapter we deal with the alkaline-earth metal amidoboranes ($Mg(NH_2BH_3)_2$, $Ca(NH_2BH_3)_2$ and $Sr(NH_2BH_3)_2$)). Alkaline-earth metal amidoboranes have shown improved dehydrogenation properties over NH_3BH_3 [136, 211, 218, 219] but poorer than alkali metal amidobranes. In the case of $Ca(NH_2BH_3)_2$, hydrogen desorption starts at $\sim 80^0$C and vigorous hydrogen release takes place at $\sim$100 and 140^0C [136], whereas in the case of $Sr(NH_2BH_3)_2$ it starts at even lower temperatures $\sim 60^0$C. In the alkaline-earth metal amidoboranes, calcium amidoborane ($Ca(NH_2BH_3)_2$) has been identified in both liquid [202, 203] and solid form [206, 211]. CaH_2 and NH_3BH_3 react to form $Ca(NH_2BH_3)_2$ with

release of one equivalent of H_2 [211, 220]. Recently, the crystal structure of $Ca(NH_2BH_3)_2$ has been reported [136, 221] as monoclinic with space group *C2* with two formula units per cell. In $Ca(NH_2BH_3)_2$, the Ca^{2+} ions are octahedrally coordinated by $[NH_2BH_3]^-$ groups, in which two Ca-N bonds have an average distance of 2.466 $\AA$. The next compound in the alkaline-earth metal amidoboranes, is Magnesium amidoborane ($Mg(NH_2BH_3)_2$). It is an attractive candidate for hydrogen storage with 11.8% hydrogen content [136, 221, 222], but unfortunately the synthesis of $Mg(NH_2BH_3)_2$ is unsuccessful [223]. This is due to the condensed charge by Mg cation and an incomplete dihydrogen bonding which lead to an unstable in crystal of $Mg(NH_2BH_3)_2$ under ambient conditions. A theoretical model [223] for $Mg(NH_2BH_3)_2$ has been proposed with a similar crystal structure as $Ca(NH_2BH_3)_2$, in which $[NH_2BH_3]^-$ groups coordinate tetrahedrally to Mg^{2+} and establish two Mg-N bonds and two Mg...BH_3 coordinates. Recently, Strontium amidoborane ($Sr(NH_2BH_3)_2$)) has been synthesized [218]. It crystallizes into a similar structure as $Ca(NH_2BH_3)_2$, in which each Sr^{2+} is octahedrally coordinated by the surrounding $[NH_2BH_3]^-$ groups, forming two Sr-N bonds and four Sr...BH_3 coordinations.

The molecular structure and the crystal geometries of alkaline-earth metal amidoboranes are very different from that of alkali metal amidoboranes and amino borane. So it is interesting to investigate the changes in the bonding which involves on the intermolecular forces and thereby the physical and chemical properties. This chapter is aimed at understanding the structural, electronic, bonding and mechanical properties of $Ca(NH_2BH_3)_2$ and $Sr(NH_2BH_3)_2$ which are different from that of alkali metal amidoboranes. We have also considered $Mg(NH_2BH_3)_2$ model structure for comparison. The rest of the chapter is organized as follows, in section 7.2 we discuss computational details. Results are presented in section 7.3 and section 7.4 deals with the conclusions.

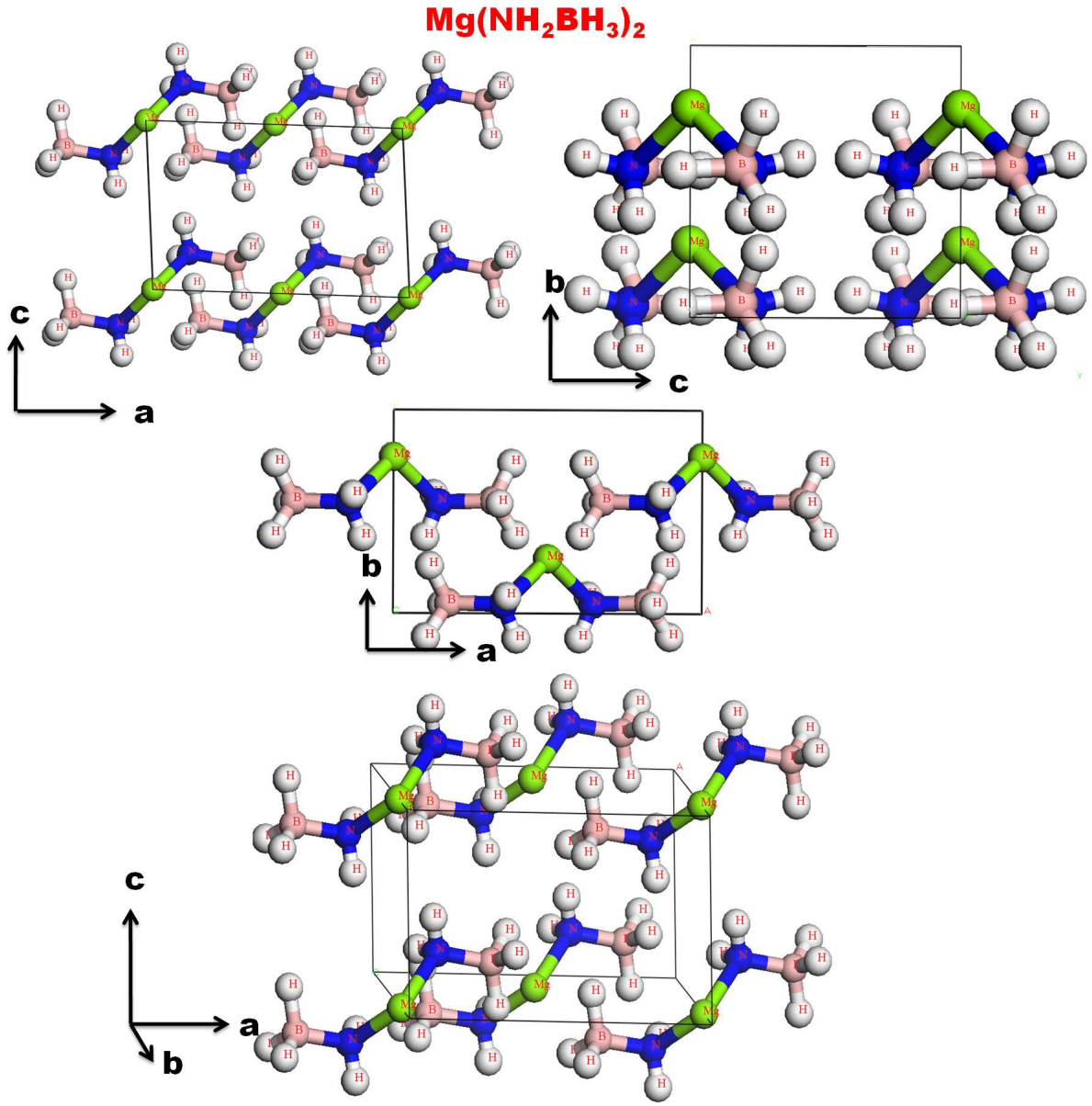

Figure 7.1: The optimized crystal structure of $Mg(NH_2BH_3)_2$ within GGA represented along different crystallographic directions (Blue spheres represents Nitrogen atoms, pink spheres represents Boron atoms, green spheres represents Magnesium atoms and white spheres represents Hydrogen atoms).

7.2 Computational details

The first principles calculations were carried out by using the plane wave pseudopotential method based on density functional theory as implemented in the CAmbridge Series of Total

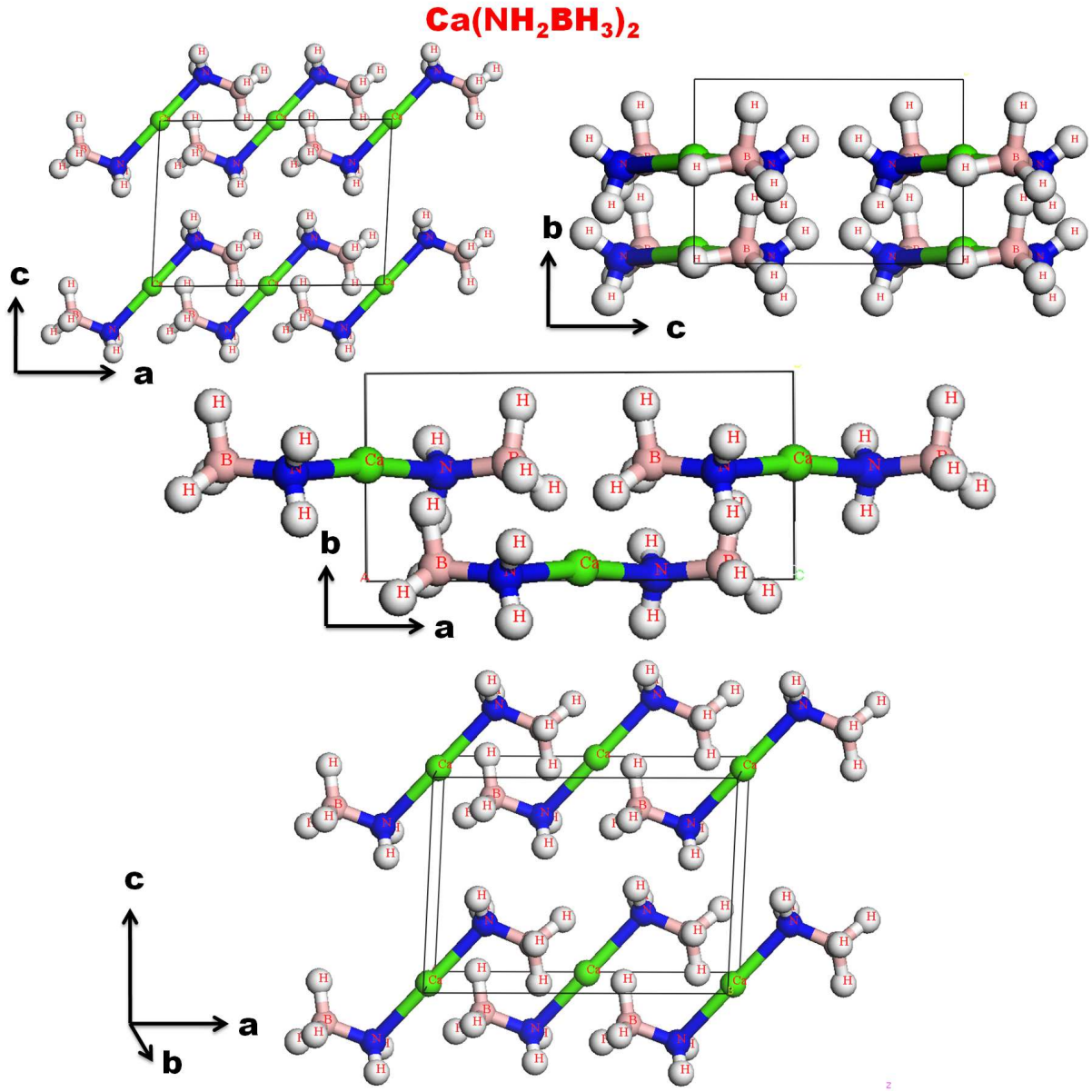

Figure 7.2: The optimized crystal structure of $Ca(NH_2BH_3)_2$ within GGA represented along different crystallographic directions (Blue spheres represents Nitrogen atoms, pink spheres represents Boron atoms, green spheres represents Calcium atoms and white spheres represents Hydrogen atoms).

Energy Package (CASTEP) [60, 86]. For $Mg(NH_2BH_3)_2$, $Ca(NH_2BH_3)_2$ and $Sr(NH_2BH_3)_2$, the basis orbitals used are valence states for Mg: $2p^6$, $3s^2$, Ca: $3s^2$ $3p^6$ $4s^2$, Sr: $4s^2$ $4p^6$

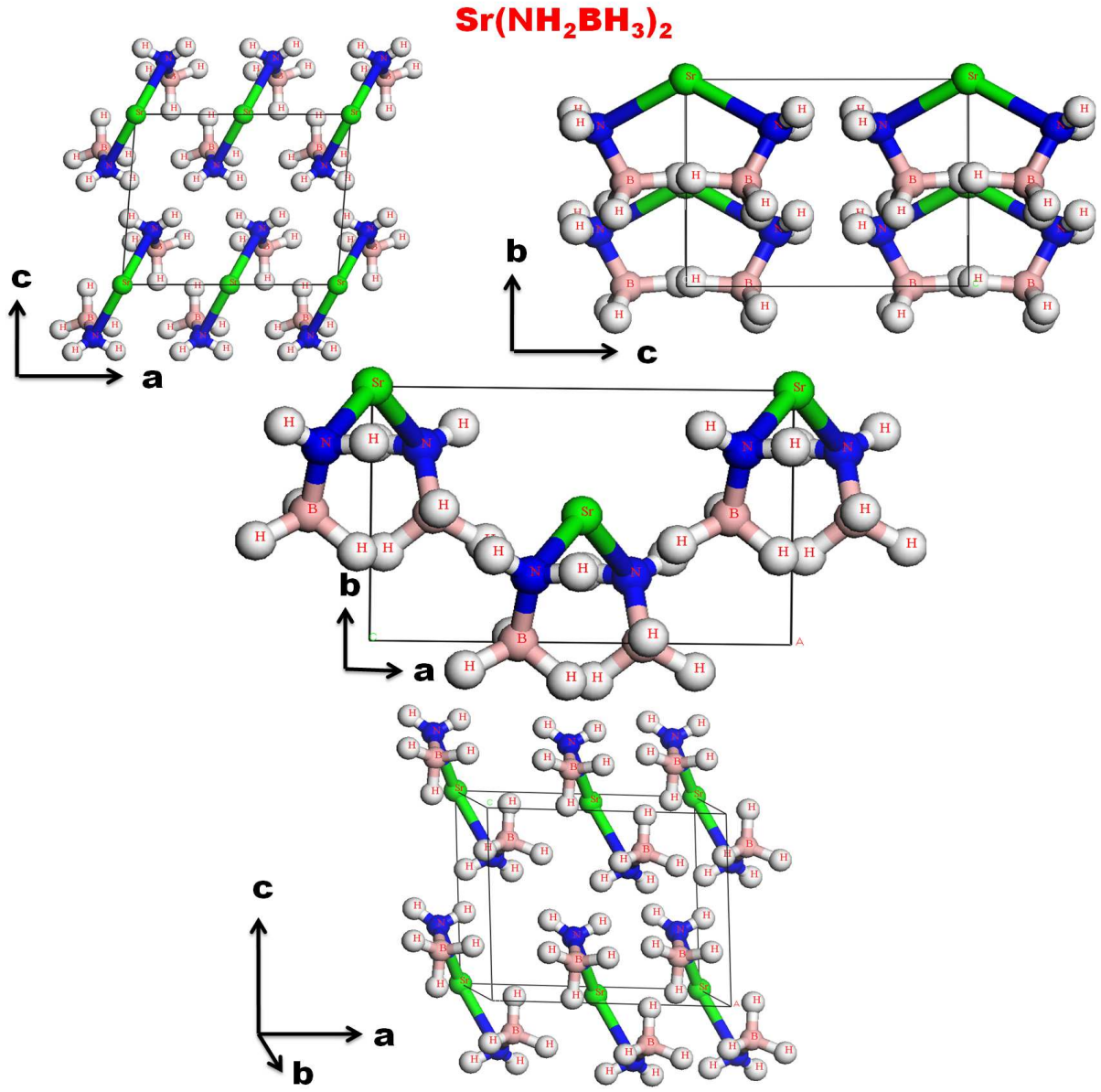

Figure 7.3: The optimized crystal structure of $Sr(NH_2BH_3)_2$ within TS represented along different crystallographic directions (Blue spheres represents Nitrogen atoms, pink spheres represents Boron atoms, green spheres represents Strontium atoms and white spheres represents Hydrogen atoms).

$5s^2$ H: $1s^1$, B: $2s^2$,$2p^1$, and N: $2s^2$,$2p^3$. We have used ultrasoft pseudopotentials introduced by Vanderbilt [59] together with local density approximation (LDA) of Ceperley and Alder

[138] parameterized by Perdew and Zunger (CA-PZ) [139] and also generalized gradient approximation (GGA) of Perdew-Burke-Ernzerhof (PBE) [140, 141]. A plane wave basis set with energy cut-off of 500 eV has been applied for $Mg(NH_2BH_3)_2$, $Ca(NH_2BH_3)_2$ and $Sr(NH_2BH_3)_2$. The vdW forces were taken into account through the semiempirical methods proposed by the Grimme (G06) [63], Ortmann, Bechstedt, and Schmidt (OBS) [65], and by Tkatchenko and Scheffler (TS) [66] using ultrasoft pseudopotentials. For the Brillouin zone sampling, the 4 x 5 x 5, 5 x 6 x 5 and 5 x 6 x 5 Monkhorst-Pack [87] mesh has been used for $Mg(NH_2BH_3)_2$, $Ca(NH_2BH_3)_2$ and $Sr(NH_2BH_3)_2$, respectively, in which the forces on the atoms are converged to less than 0.0005 eV/$\mathring{A}$. The maximum ionic displacement is within 0.005$\mathring{A}$ and the total stress tensor is reduced to the order of 0.02 GPa.

7.3 Results and discussion

7.3.1 Structural properties

The optimized crystal structures of $Mg(NH_2BH_3)_2$, $Ca(NH_2BH_3)_2$ and $Sr(NH_2BH_3)_2$ are shown in figures 7.1, 7.2 and 7.3, respectively. In which each formula unit contains one alkaline-earth metal atom, two pair of B and N atoms, where B is connected to H1, H2 and H3, and N is connected to H3 and H4 similar to as in alkali metal amidoboranes. Two NH_2BH_3 ligands are connected through metal (Mg, Ca and Sr) atoms. The optimized structural parameters and fractional coordinates using LDA and GGA within OBS, G06 and TS, are given in tables 7.1, 7.2, 7.3 and 7.4 along with experimental data. The unit cell volume obtained by LDA is underestimated by 16% for $Mg(NH_2BH_3)_2$, 13 % for $Ca(NH_2BH_3)_2$ and 8% for $Sr(NH_2BH_3)_2$. The same is overestimated by 9.6% for $Mg(NH_2BH_3)_2$, 6% for $Ca(NH_2BH_3)_2$ and 20% for $Sr(NH_2BH_3)_2$ using GGA. As in the case of alkali meal amidoboranes, in order to study the role of vdW interactions in $Mg(NH_2BH_3)_2$, $Ca(NH_2BH_3)_2$ and $Sr(NH_2BH_3)_2$ we have also carried out the calculations including vdW forces. The unit cell volume calculated by the dispersion correction methods underestimated by OBS

is 30% for $Mg(NH_2BH_3)_2$, 26% for $Ca(NH_2BH_3)_2$ and 24% for $Sr(NH_2BH_3)_2$. With G06 it is 11% for $Mg(NH_2BH_3)_2$, 9% for $Ca(NH_2BH_3)_2$ and 8% for $Sr(NH_2BH_3)_2$. And by TS is 9.5% for $Mg(NH_2BH_3)_2$, 5.7% for $Ca(NH_2BH_3)_2$, 4% for $Sr(NH_2BH_3)_2$. Interestingly, $Sr(NH_2BH_3)_2$ shows a considerable vdW interaction corrections in reproducing the experimental cell volume. Whereas $Mg(NH_2BH_3)_2$ and $Ca(NH_2BH_3)_2$ the correction brought through vdW interactions on the structural properties is found to be too strong. From the present calculations we conclude that GGA better reproduces the experimental structural parameters for $Mg(NH_2BH_3)_2$ and $Ca(NH_2BH_3)_2$, while TS is better for $Sr(NH_2BH_3)_2$. Hence all further calculations of $Mg(NH_2BH_3)_2$ and $Ca(NH_2BH_3)_2$ are done within the GGA and for $Sr(NH_2BH_3)_2$ are within the TS functionals.

Table 7.1: The optimized structural parameters of $Mg(NH_2BH_3)_2$, $Ca(NH_2BH_3)_2$ and $Sr(NH_2BH_3)_2$ along with experimental data.

Property	LDA	OBS	GGA	G06	TS	Expt
			$Mg(NH_2BH_3)_2$			
a($\AA$)	8.439	8.336	8.449	8.481	8.614	8.5722[a]
b($\AA$)	5.561	5.487	5.927	5.629	5.675	5.6048[a]
c($\AA$)	4.835	4.109	5.923	5.017	5.014	5.6216[a]
β^0	85.18	82.89	84.43	84.73	83.80	85.84[a]
V($\AA^3$)	226.18	186.57	295.31	238.55	243.73	269.38[a]
			$Ca(NH_2BH_3)_2$			
a($\AA$)	8.813	8.520	9.263	8.922	9.058	9.100(2)[b]
b($\AA$)	4.047	3.689	4.424	4.140	4.235	4.371(1)[b]
c($\AA$)	6.173	5.960	6.628	6.293	6.301	6.441(2)[b]
β^0	91.61	89.88	93.13	91.26	94.21	93.19(2)[b]
V($\AA^3$)	220.08	87.37	271.20	232.38	241.05	255.80[b]
			$Sr(NH_2BH_3)_2$			
a($\AA$)	7.505	7.125	8.284	7.927	7.665	8.166[c]
b($\AA$)	4.756	4.514	5.120	4.848	4.903	5.096[c]
c($\AA$)	7.180	6.541	7.945	6.645	7.097	6.725[c]
β^0	92.83	89.80	92.51	87.26	89.78	94.39[c]
V($\AA^3$)	256.04	210.39	336.72	255.15	266.79	279.11[c]

[a] Ref.[223]; [b] Ref.[136]; [c] Ref.[218];

Table 7.2: The optimized atomic fractional coordinates of $Mg(NH_2BH_3)_2$ along with experimental values.

Atom		LDA	OBS	GGA	G06	TS	Expt[a]
	x	0.821	0.819	0.825	0.821	0.825	0.82339
B	y	0.058	0.063	0.048	0.059	0.054	0.05324
	z	0.811	0.820	0.830	0.808	0.810	0.81951
	x	0.646	0.649	0.646	0.645	0.650	0.64574
N	y	0.039	0.037	0.050	0.038	0.044	0.04540
	z	0.755	0.732	0.788	0.753	0.759	0.77936
	x	0.903	0.906	0.897	0.903	0.900	0.89542
H1	y	0.899	0.912	0.887	0.901	0.891	0.88442
	z	0.679	0.657	0.728	0.686	0.689	0.71438
	x	0.118	0.117	0.108	0.121	0.113	0.11683
H2	y	0.249	0.260	0.219	0.247	0.236	0.23641
	z	0.266	0.244	0.240	0.267	0.273	0.25764
	x	0.836	0.821	0.838	0.832	0.837	0.84195
H3	y	0.040	0.035	0.034	0.042	0.041	0.04189
	z	0.065	0.119	0.037	0.053	0.055	0.03678
	x	0.635	0.653	0.636	0.634	0.644	0.63216
H4	y	0.067	0.045	0.090	0.064	0.076	0.08505
	z	0.546	0.479	0.620	0.552	0.558	0.60438
	x	0.396	0.394	0.403	0.396	0.392	0.39762
H5	y	0.866	0.863	0.891	0.868	0.875	0.87576
	z	0.205	0.203	0.191	0.207	0.210	0.19833
	x	0.000	0.000	0.000	0.000	0.000	0.00000
Mg	y	0.769	0.776	0.772	0.767	0.772	0.76966
	z	0.000	0.000	0.000	0.000	0.000	0.00000

[a] Ref.[223];

7.3.2 Electronic structure

The electronic structure of $Mg(NH_2BH_3)_2$, $Ca(NH_2BH_3)_2$ and $Sr(NH_2BH_3)_2$ is studied through the calculated band structure and density of states (DOS). In figures 7.4a, 7.4b and 7.4c, the band structures of $Mg(NH_2BH_3)_2$, $Ca(NH_2BH_3)_2$ and $Sr(NH_2BH_3)_2$ are presented, respectively. From the band structure, it is found that $Mg(NH_2BH_3)_2$, $Ca(NH_2BH_3)_2$

Table 7.3: The optimized atomic fractional coordinates of $Ca(NH_2BH_3)_2$ along with experimental values.

Atom		LDA	OBS	GGA	G06	TS	Other[a]	Expt[a]
	x	0.830	0.833	0.830	0.830	0.832	0.832	0.835(2)
B	y	0.090	0.078	0.090	0.084	0.032	0.032	0.064(3)
	z	0.776	0.780	0.777	0.782	0.790	0.790	0.815(4)
	x	0.670	0.673	0.670	0.667	0.670	0.670	0.675(2)
N	y	0.990	1.011	0.990	1.000	0.957	0.957	0.024(1)
	z	0.710	0.735	0.710	0.717	0.723	0.723	0.725(3)
	x	0.932	0.857	0.932	0.923	0.924	0.924	0.926
H1	y	0.937	1.050	0.937	0.928	0.873	0.873	0.922
	z	0.692	0.983	0.692	0.694	0.705	0.705	0.715
	x	0.151	0.139	0.151	0.149	0.141	0.141	0.145
H2	y	0.375	0.340	0.375	0.362	0.299	0.299	0.344
	z	0.267	0.248	0.267	0.261	0.255	0.255	0.212
	x	0.849	0.856	0.850	0.857	0.855	0.855	0.861
H3	y	0.064	0.050	0.064	0.056	0.005	0.005	0.008
	z	0.974	0.983	0.975	0.978	0.982	0.982	0.003
	x	0.637	0.642	0.637	0.632	0.639	0.639	0.653
H4	y	0.101	0.122	0.102	0.113	0.066	0.066	0.162
	z	0.569	0.602	0.570	0.577	0.586	0.586	0.598
	x	0.339	0.345	0.340	0.346	0.343	0.343	0.345
H5	y	0.746	0.803	0.746	0.763	0.729	0.729	0.803
	z	0.318	0.320	0.319	0.315	0.309	0.309	0.320
	x	0.000	0.000	0.000	0.000	0.000	0.000	0.000
Ca	y	0.600	0.609	0.600	0.599	0.557	0.557	0.560(3)
	z	0.000	0.000	0.000	0.000	0.000	0.000	0.000

[a] Ref.[136];

and $Sr(NH_2BH_3)_2$ are wide band gap insulators with the band gaps of 4.783 eV, 3.878 eV with GGA and 3.884 eV with TS, respectively. The valence band maximum and the conduction band minimum of $Sr(NH_2BH_3)_2$ is found to be along Γ-Z direction indicating that this compound is an indirect band gap insulator. On the other hand $Mg(NH_2BH_3)_2$ and $Ca(NH_2BH_3)_2$ are found to be direct band gap insulators as its valence band maximum and the conduction band minimum are found along the same direction Γ. The band gap value

Table 7.4: The optimized atomic fractional coordinates of $Sr(NH_2BH_3)_2$ along with experimental values.

Atom		LDA	OBS	GGA	G06	TS	Expt[a]
	x	0.348	0.340	0.337	0.330	0.338	0.353(1)
B	y	-0.017	-0.021	-0.005	-0.015	-0.016	0.000
	z	0.214	0.242	0.183	0.219	0.222	0.209(2)
	x	0.369	0.350	0.381	0.335	0.359	0.382(1)
N	y	0.279	0.288	0.265	0.279	0.278	0.263(2)
	z	0.285	0.319	0.257	0.301	0.288	0.315(2)
	x	0.215	0.199	0.210	0.201	0.205	0.223
H1	y	0.856	0.841	0.900	0.849	0.869	0.894
	z	0.265	0.292	0.234	0.266	0.277	0.261
	x	0.837	0.843	0.822	0.840	0.833	0.843
H2	y	0.478	0.470	0.505	0.488	0.473	0.524
	z	0.036	0.048	0.024	0.029	0.043	0.022
	x	0.980	0.973	0.946	0.951	0.964	0.964
H3	y	0.340	0.326	0.338	0.353	0.344	0.346
	z	0.261	0.298	0.219	0.276	0.271	0.246
	x	0.741	0.757	0.715	0.778	0.750	0.707
H4	y	0.380	0.381	0.370	0.382	0.368	0.333
	z	0.668	0.596	0.702	0.696	0.656	0.594
	x	0.525	0.523	0.536	0.627	0.543	0.509
H5	y	0.309	0.341	0.254	0.289	0.301	0.265
	z	0.618	0.613	0.641	0.552	0.613	0.611
	x	0.000	0.000	0.000	0.000	0.000	0.000
Sr	y	0.001	-0.000	-0.003	0.003	0.014	0.000
	z	0.000	0.000	0.000	0.000	0.000	0.000

[a] Ref.[218];

of these compounds follows the trend: $Mg(NH_2BH_3)_2 > Ca(NH_2BH_3)_2 \approx Sr(NH_2BH_3)_2$.

Total and partial density of states:

The calculated total and partial density of states (PDOS) of $Mg(NH_2BH_3)_2$, $Ca(NH_2BH_3)_2$ and $Sr(NH_2BH_3)_2$ are presented in figures 7.5, 7.6 and 7.7, respectively. The detailed discussion for each compound is as follows:

$Mg(NH_2BH_3)_2$: The total DOS is made up of five regions in energy (see figure 7.5): first

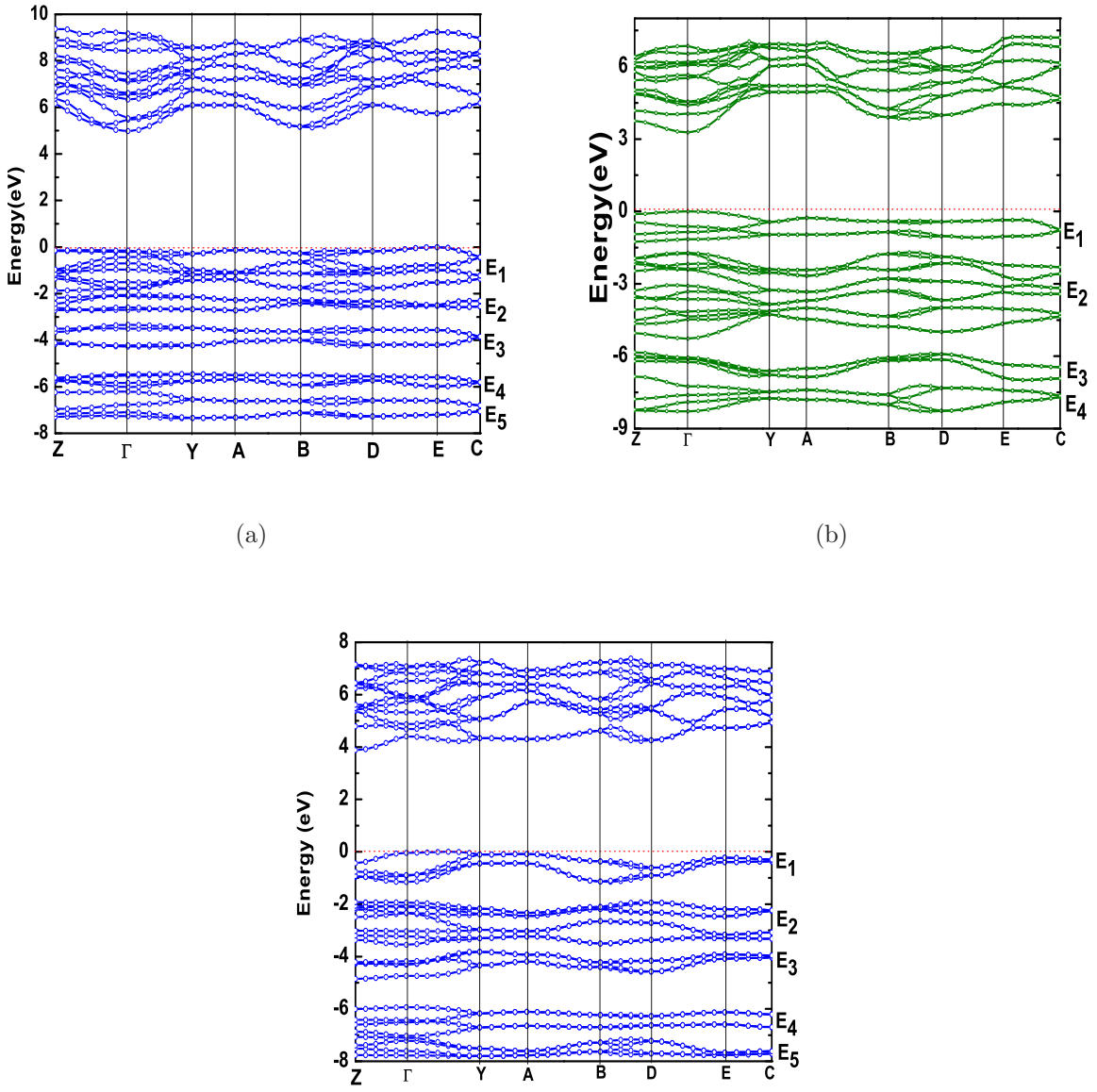

Figure 7.4: The band structure of alkaline-earth metal amidoboranes (a) $Mg(NH_2BH_3)_2$ (b) $Ca(NH_2BH_3)_2$ and (c) $Sr(NH_2BH_3)_2$. The zero represents the Fermi level.

region corresponds to states between -2 eV to 0 eV i.e., near to fermi level. It has B-p, N-p states, together with s states of H's connected to B. An important point is that a small contribution appears in the PDOS of Mg-s & p states at the same energy. The second region is from the states between -3 eV to -2 eV and it has B-p, N-p and s states of H's connected to B, together with Mg-s states. The third region corresponds to the peaks between -4.5 eV to -3.5 eV and is basically from B-p, N-p and H3-s states with admixture of Mg-s states. The states between -6 eV to -5.5 eV is the fourth region. It is made of states from N-p and s states of H's connected to N, together with a small contribution from B-s & p states. Finally, the fifth region is between -7.5 eV to -6 eV and it is dominating by B-s, N-p states along with s states of H's connected to B.

The conduction band has Mg-s & p, B-p and s states of H's connected to N. The p states from B, N and s states of H are hybridizing in all the energy regions, that implies a sp hybridization between B-H and N-H bonds. The study concludes that both B-H and N-H bonds are covalent in nature whereas Mg-N bonds are ionic in nature with a small covalency.

$Ca(NH_2BH_3)_2$: The total DOS is made of five regions in energy (see figure 7.6): first region corresponds to the peaks between -1.5 eV to 0 eV i.e., near to fermi level. It is made up of peaks coming from N-p and s states of H1 and H3, together with B-p and Ca-d states. The second region is for states between -4 eV to -1.5 eV and it is dominated by N-p, B-p, s states of H's connected to B along with an admixture of Ca-d states. The states between -5 eV to -4 eV is the third region, it has B-p, N-p states and s states of H1. Then, the fourth region is corresponds to the states between -7 eV to -6 eV. It is made of the peaks from N-p and s states of H's connected to N. The fifth region is from the states between -8 eV to -7 eV and it is dominating by B-s and s states of H's connected to B.

The conduction band has Ca-d states with a small contribution from s states of Ca and H's connected to N. The p states from B, N and s states of H hybridize in all the energy regions implying a sp hybridization between B-H and N-H bonds. The present study con-

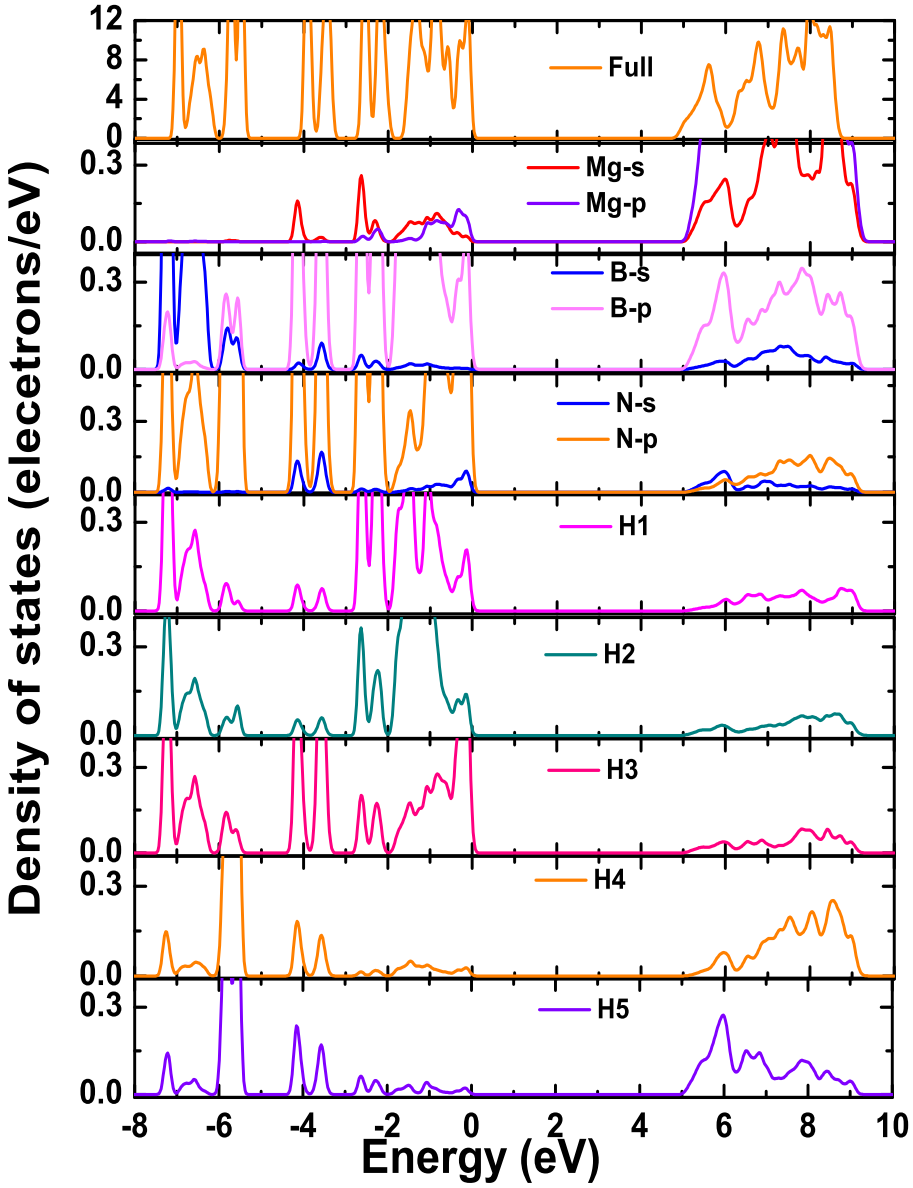

Figure 7.5: The total, partial and local density of states of $Mg(NH_2BH_3)_2$ calculated within GGA. The zero represents the Fermi level.

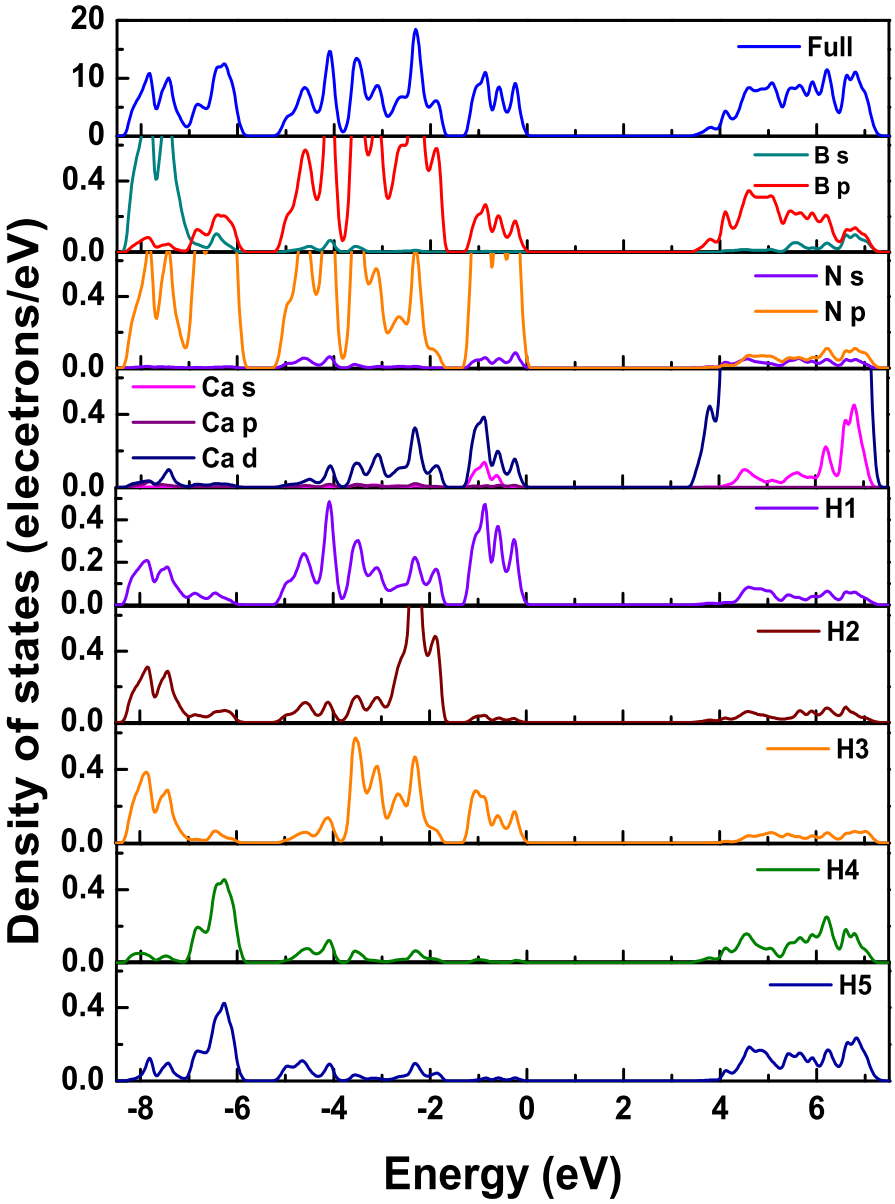

Figure 7.6: The total, partial and local density of states of $Ca(NH_2BH_3)_2$ calculated within GGA. The zero represents the Fermi level.

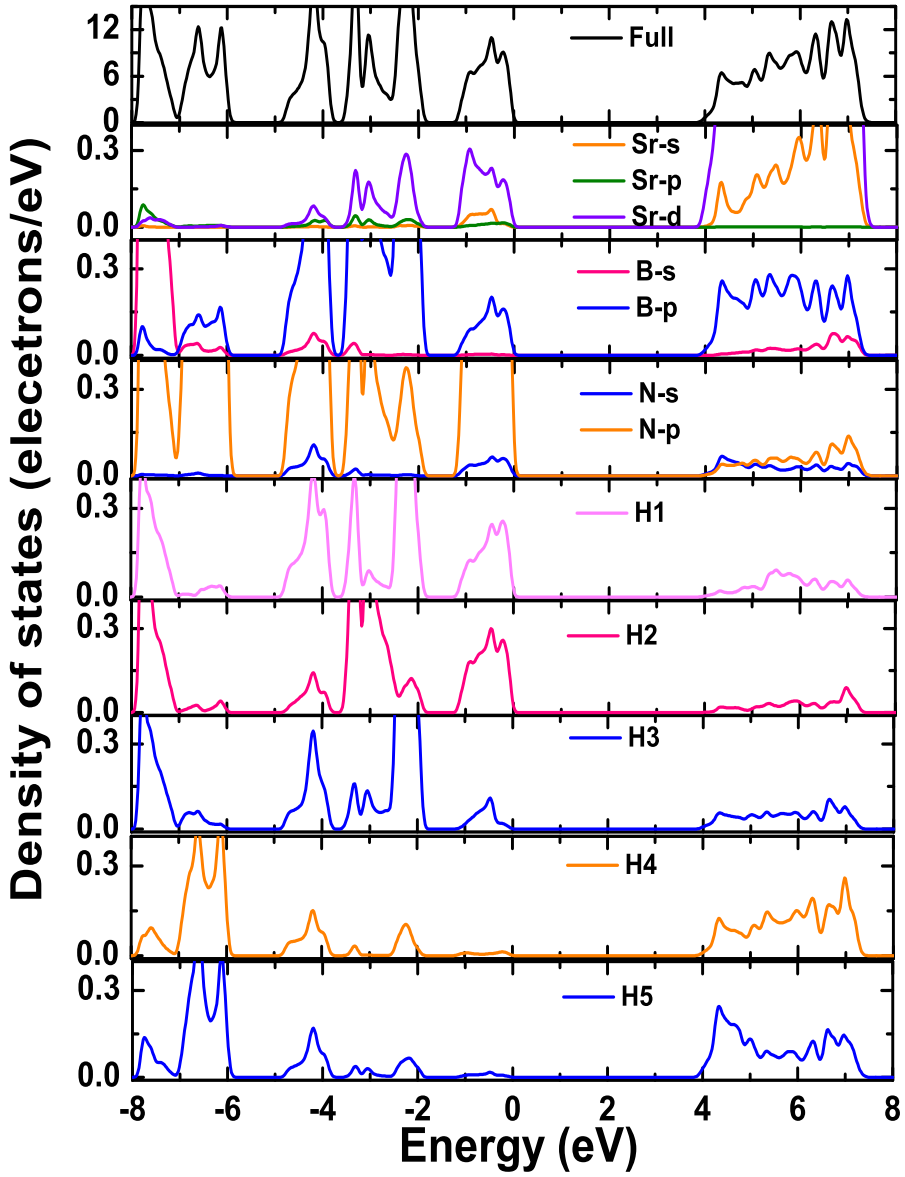

Figure 7.7: The total, partial and local density of states of $Sr(NH_2BH_3)_2$ calculated within TS. The zero represents the Fermi level.

cludes that both B-H and N-H bonds are covalent in nature whereas Ca-N bonds are ionic in nature with a small covalency.

$Sr(NH_2BH_3)_2$: The total DOS is made of five regions in energy (see figure 7.7): first region corresponds to states between -1 eV to 0 eV i.e., near to fermi level. It has B-p, N-p states, together with s states of H's connected to B. An important point is that a contribution appears in the PDOS of Sr-d states at the same energy, which indicates that the bonding is not totally ionic but contains also a small part of covalency. The second region is from the states between -3.5 eV to -2 eV and it has B-p, N-p and s states of H's connected to B, together with Sr-d states. The contribution from Sr-d states in above two regions is probably induced by a residual covalent bond with the neighboring atoms. The third region corresponds to the several peaks between -5 eV to -3.5 eV and is basically from B-p, N-p and all H-s states. The states between -7 eV to -6 eV is the fourth region. It is made of states from N-p and s states of H's connected to N, together with a small contribution from B-p states. Then, the fifth region is between -8 eV to -7 eV and it is dominating by B-s, N-p states along with all H-s states.

The conduction band has Sr-s & d, B-p and s states of H's connected to N. The p states from B, N and s states of H are hybridizing in all the energy regions implies a sp hybridization between B-H and N-H bonds. Overall the study concludes that both B-H, N-H bonds are covalent in nature, whereas there is a strong ionic bonding between Sr and N and mixed with a small covalency.

7.3.3 Bonding properties

Mulliken atomic and bond population analysis:

To quantify the charge distribution in $Mg(NH_2BH_3)_2$, $Ca(NH_2BH_3)_2$ and $Sr(NH_2BH_3)_2$, we have calculated Mulliken atomic charges and orbital contributions and these are presented in table 7.5. The Mulliken atomic charges for Mg, Ca and Sr are found to be positive while it

is negative for the B and N atoms. The hydrogens connected to B and N atoms are found to have negative and positive charges, respectively. This scenario clearly indicates the presence of protic and hydridic nature of B-H and N-H bonds in alkaline-earth metal amidoboranes. Then, to understand the bonding nature we have calculated the Mulliken bond populations for each bond and presented in table 7.6. The total overlap (bond) population for any pair of atoms in a molecule is in general made up of positive and negative contributions. If the total overlap population between two atoms is positive, they are bonded; if negative, they are antibonded [97]. A high positive bond population indicates a high degree of covalence. From the calculated bond populations it is found that all the bonds are covalent in nature except Mg-N bond which has negative population implying it is ionic in nature. The B-H bonds with high bond population, show their predominant covalent nature over N-H bonds in these compounds.

To know the percentage of the covalence, we have calculated the population ionicity of each bonds of these compounds as discussed earlier in the chapter 4. The lower limit i.e. $P_i = 0$ indicates a pure covalent bond while the upper limit (i.e) $P_i = 1$ indicates a purely ionic bond [97, 98, 156, 157]. As expected, B-H bonds show zero population ionicity and N-H bond show very low value (0.28) of population ionicity. The B-N bond with 0.4 population ionicity shows a dominating covalent character. So, B-N bond is no more a dative or coordinative bond in alkaline-earth metal amidoboranes, which results in the reduction of hydridic nature of H1, H2 and H3 atoms and the protic nature of H3 and H4 atoms. Moreover, the average ionicity value of all the bonds (B-N, N-H and B-H) in $Mg(NH_2BH_3)_2$, $Ca(NH_2BH_3)_2$ and $Sr(NH_2BH_3)_2$ are found to be 0.13, 0.19 and 0.20, respectively and these are relatively lower when compared to the average ionicity value of NH_3BH_3. From this discussions, we conclude that alkaline-earth metal amidoboranes exhibit relatively high covalency compared to NH_3BH_3.

The electron density iso surfaces and charge density distributions:

Another meaningful way to understand the electron distribution is to look at iso surface

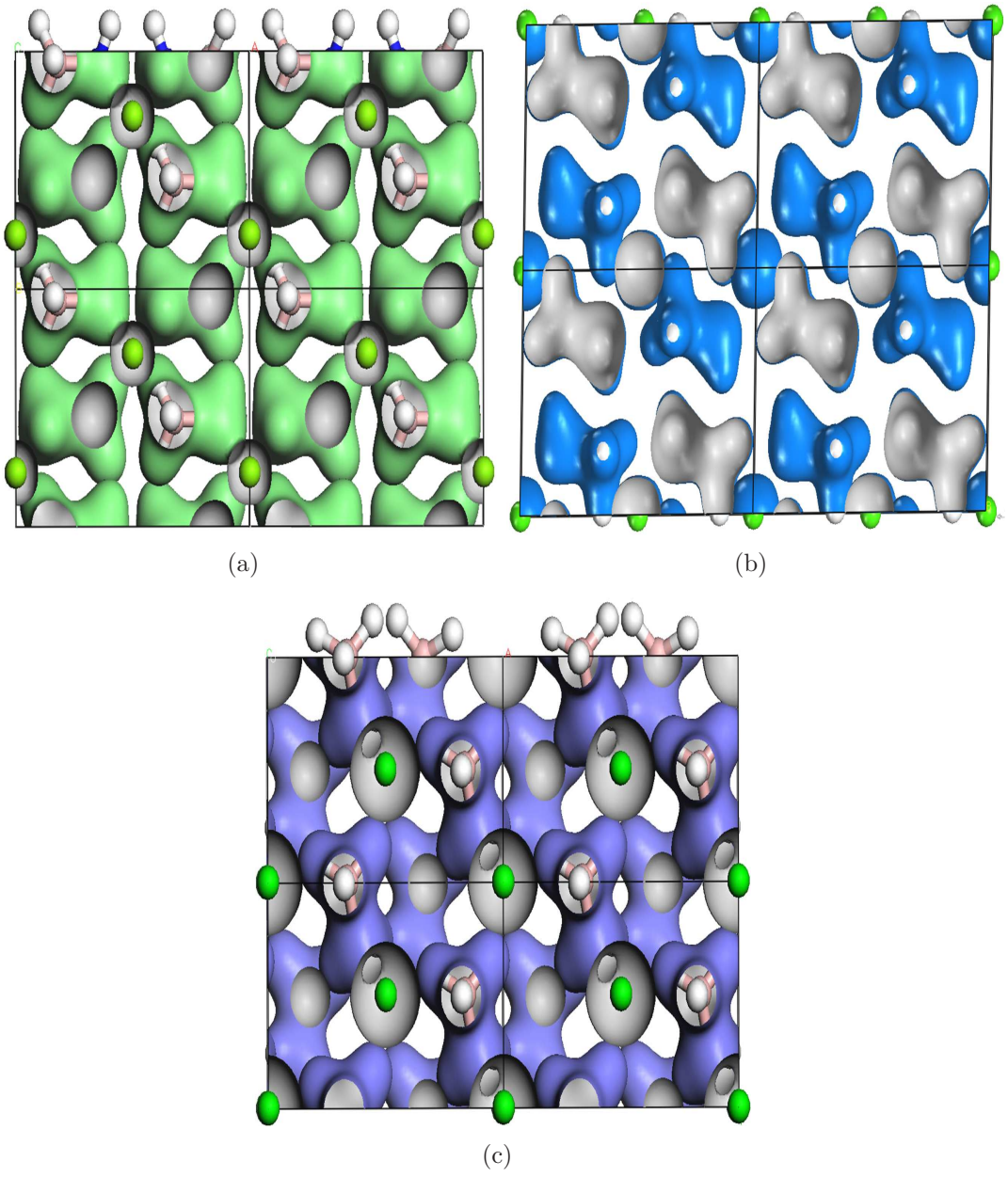

Figure 7.8: The total electron density iso-surfaces of alkaline-earth metal amidoboranes (a) $Mg(NH_2BH_3)_2$ (b) $Ca(NH_2BH_3)_2$ and (c) $Sr(NH_2BH_3)_2$ along b axis calculated within GGA. (Blue spheres represents Nitrogen atoms, pink spheres represents Boron atoms, green spheres represents metal (Magnesium, Calcium and Strontium) atoms and white spheres represents Hydrogen atoms).

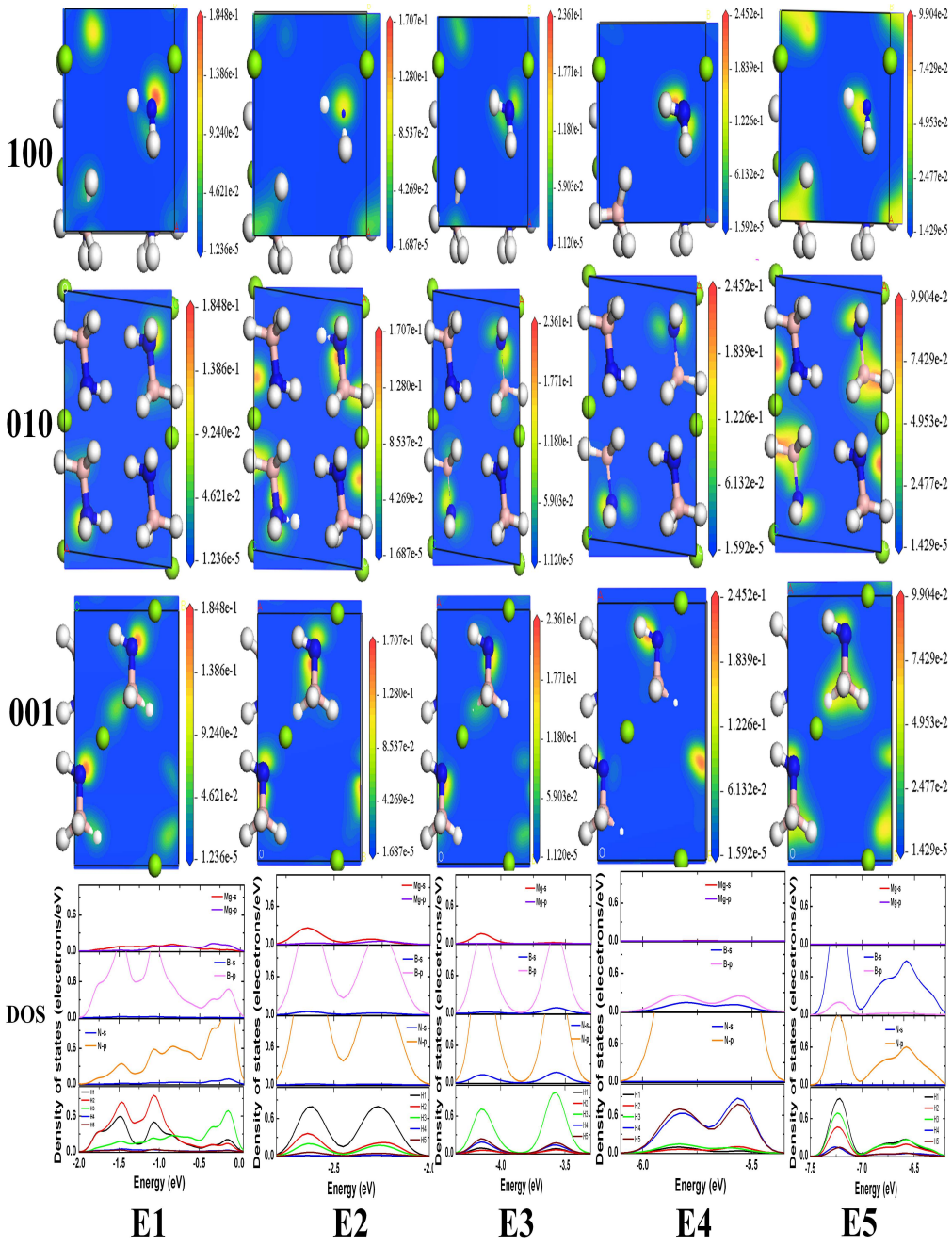

Figure 7.9: The charge density distributions of $Mg(NH_2BH_3)_2$ along (100), (010) and (001) planes, and the corresponding partial density of states (PDOS) are shown for different energy ranges in the valance band defined as E1=-2 to 0 eV (at Fermi level), E2=-3 to -2 eV, E3=-4.5 to -3.5 eV, E4=-6 to -5.5 eV and E5=-7.5 to -6 eV (Blue spheres represents Nitrogen atoms, pink spheres represents Boron atoms, green spheres represents Magnesium atoms and white spheres represents Hydrogen atoms).

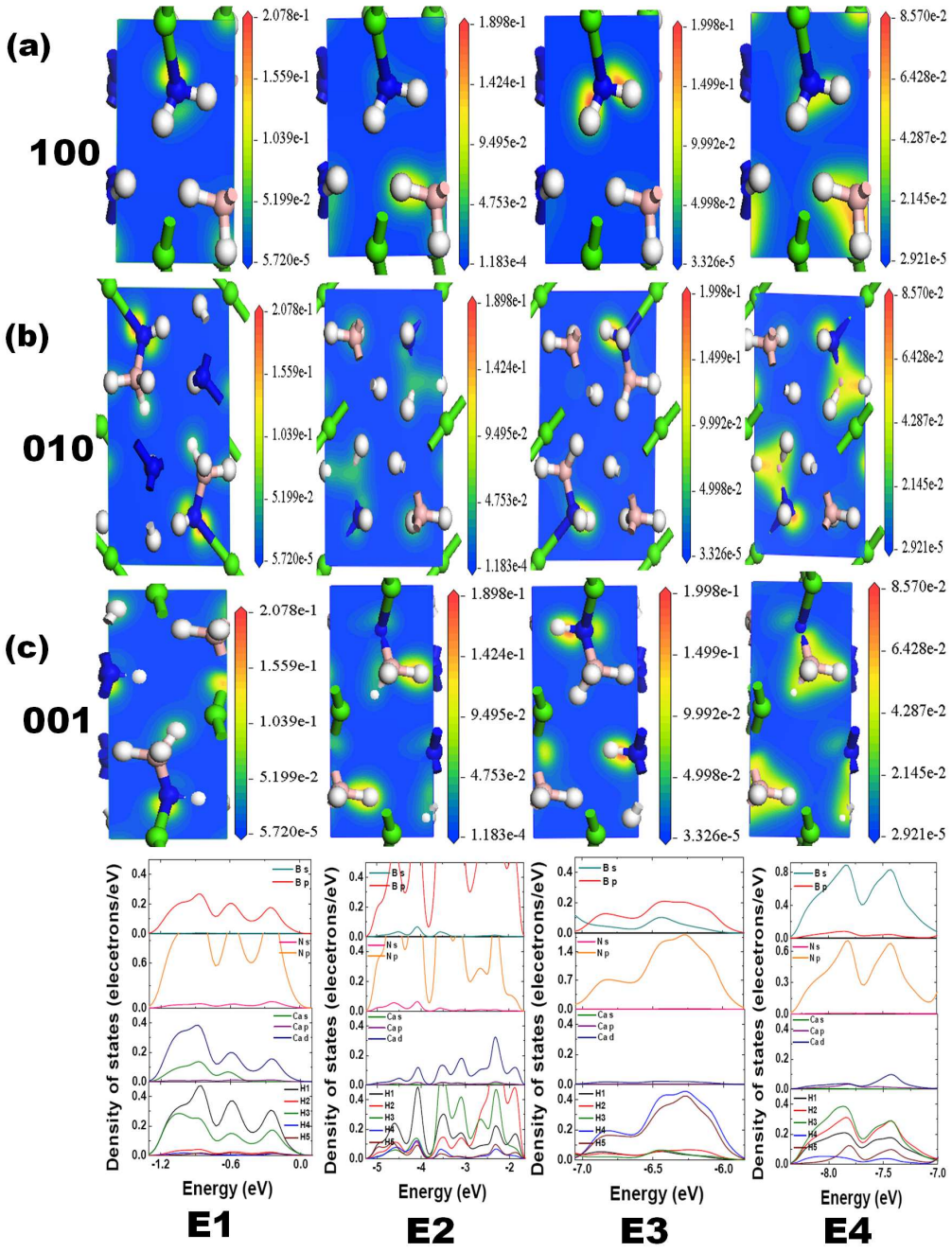

Figure 7.10: The charge density distribution plots of $Ca(NH_2BH_3)_2$ along (100), (010) and (001) planes, and the corresponding partial density of states (PDOS) are shown for different energy ranges in the valance band defined as E1=-1.5 to 0 eV (at Fermi level), E2=-5 to -1.5 eV, E3=-7 to -6 eV and E4=-8 to -7 eV (Blue spheres represents Nitrogen atoms, pink spheres represents Boron atoms, green spheres represents Calcium atoms and white spheres represents Hydrogen atoms).

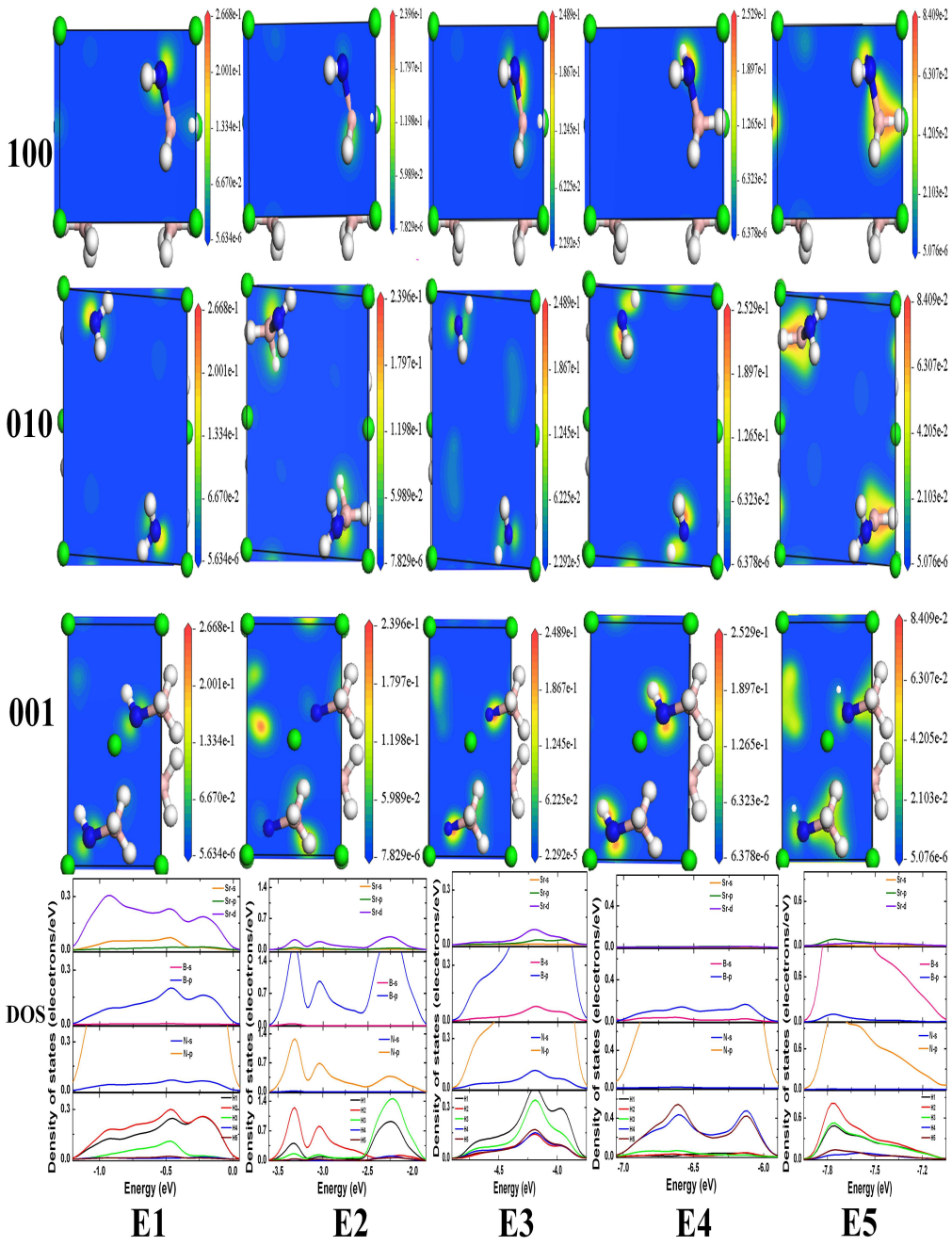

Figure 7.11: The charge density distributions of $Sr(NH_2BH_3)_2$ along (100), (010) and (001) planes, and the corresponding partial density of states (PDOS) are shown for different energy ranges in the valance band defined as E1=-1 to 0 eV (at Fermi level), E2=-3.5 to -2 eV, E3=-5 to -3.5 eV, E4=-7 to -6 eV and E5=-8 to -7 eV (Blue spheres represents Nitrogen atoms, pink spheres represents Boron atoms, green spheres represents Strontium atoms and white spheres represents Hydrogen atoms).

Table 7.5: The calculated Mulliken atomic charges and atomic populations of $Mg(NH_2BH_3)_2$, $Ca(NH_2BH_3)_2$ and $Sr(NH_2BH_3)_2$.

Atom	Compound	s	p	d	Total	Charge
	$Mg(NH_2BH_3)_2$	1.21	0.0	0.0	1.21	-0.21
H1	$Ca(NH_2BH_3)_2$	1.08	0.0	0.0	1.08	-0.08
	$Sr(NH_2BH_3)_2$	1.08	0.0	0.0	1.08	-0.08
	$Mg(NH_2BH_3)_2$	1.06	0.0	0.0	1.06	-0.06
H2	$Ca(NH_2BH_3)_2$	1.09	0.0	0.0	1.09	-0.09
	$Sr(NH_2BH_3)_2$	1.17	0.0	0.0	1.17	-0.17
	$Mg(NH_2BH_3)_2$	1.20	0.0	0.0	1.20	-0.20
H3	$Ca(NH_2BH_3)_2$	1.12	0.0	0.0	1.12	-0.12
	$Sr(NH_2BH_3)_2$	1.08	0.0	0.0	1.08	-0.08
	$Mg(NH_2BH_3)_2$	0.66	0.0	0.0	0.66	0.34
H4	$Ca(NH_2BH_3)_2$	0.62	0.0	0.0	0.62	0.38
	$Sr(NH_2BH_3)_2$	0.62	0.0	0.0	0.62	0.38
	$Mg(NH_2BH_3)_2$	0.66	0.0	0.0	0.66	0.34
H5	$Ca(NH_2BH_3)_2$	0.62	0.0	0.0	0.62	0.38
	$Sr(NH_2BH_3)_2$	0.67	0.0	0.0	0.67	0.33
	$Mg(NH_2BH_3)_2$	0.95	2.45	0.0	3.40	-0.40
B	$Ca(NH_2BH_3)_2$	0.87	2.43	0.0	3.30	-0.30
	$Sr(NH_2BH_3)_2$	0.90	2.40	0.0	3.30	-0.30
	$Mg(NH_2BH_3)_2$	1.67	4.39	0.0	6.06	-1.06
N	$Ca(NH_2BH_3)_2$	1.62	4.35	0.0	5.96	-0.96
	$Sr(NH_2BH_3)_2$	1.62	4.34	0.0	5.96	-0.96
Mg	$Mg(NH_2BH_3)_2$	0.16	5.34	1.70	5.50	2.50
Ca	$Ca(NH_2BH_3)_2$	1.85	6.00	0.58	8.43	1.57
Sr	$Sr(NH_2BH_3)_2$	1.80	6.00	0.44	8.23	1.77

of electron density and the electron density in (100), (010) and (001) planes. In figures 7.8a, 7.8b and 7.8c we present our calculated electron density iso surfaces of $Mg(NH_2BH_3)_2$, $Ca(NH_2BH_3)_2$ and $Sr(NH_2BH_3)_2$, respectively. The electron density around NH_2BH_3 ligand is distorted spherical in shape and it is spherical in shape around Mg, Ca and Sr atoms. The distorted spherical shape indicates the distribution/sharing of the charge in entire NH_2BH_3 ligand and spherical in shape indicates the localization of charge, which confirms the bonding

Table 7.6: The calculated bond populations (P), population ionicity(P_i) and bond lengths of $Mg(NH_2BH_3)_2$, $Ca(NH_2BH_3)_2$ and $Sr(NH_2BH_3)_2$.

Bond	Compound	P	P_i	Bond Length($\mathring{A}$)
	$Mg(NH_2BH_3)_2$	1.08	-0.07	1.25574
B-H1	$Ca(NH_2BH_3)_2$	0.91	0.09	1.24794
	$Sr(NH_2BH_3)_2$	0.95	0.05	1.22694
	$Mg(NH_2BH_3)_2$	1.03	-0.02	1.21505
B-H2	$Ca(NH_2BH_3)_2$	0.95	0.05	1.23039
	$Sr(NH_2BH_3)_2$	0.85	0.16	1.26984
	$Mg(NH_2BH_3)_2$	1.09	-0.08	1.24579
B-H3	$Ca(NH_2BH_3)_2$	0.90	0.10	1.25718
	$Sr(NH_2BH_3)_2$	0.98	0.02	1.22698
	$Mg(NH_2BH_3)_2$	0.75	0.28	1.03178
N-H4	$Ca(NH_2BH_3)_2$	0.76	0.27	1.03706
	$Sr(NH_2BH_3)_2$	0.75	0.28	1.02728
	$Mg(NH_2BH_3)_2$	0.77	0.25	1.03411
N-H5	$Ca(NH_2BH_3)_2$	0.75	0.28	1.03681
	$Sr(NH_2BH_3)_2$	0.77	0.25	1.02471
	$Mg(NH_2BH_3)_2$	0.62	0.45	1.55713
B-N	$Ca(NH_2BH_3)_2$	0.68	0.37	1.51234
	$Sr(NH_2BH_3)_2$	0.64	0.43	1.53220
N-Mg	$Mg(NH_2BH_3)_2$	-0.88	-	2.12724
N-Ca	$Ca(NH_2BH_3)_2$	0.14	0.99	2.42506
N-Sr	$Sr(NH_2BH_3)_2$	0.12	0.99	2.58303

in these compound is mainly covalent.

The calculated charge density distributions in (100), (010) and (001) planes and corresponding partial density of states (PDOS) at different energy ranges in the valence band as defined in the band structures of the $Mg(NH_2BH_3)_2$, $Ca(NH_2BH_3)_2$ and $Sr(NH_2BH_3)_2$ are presented in figures 7.9, 7.10 and 7.11, respectively. For $Mg(NH_2BH_3)_2$, the energy ranges are defined as E1=-2 to 0 eV (the Fermi level), E2=-3 to -2 eV, E3=-4.5 to -3.5 eV, E4=-6 to -5.5 eV and E5=-7.5 to -6 eV. From the plot (see figure 7.9), in the E1 energy region, the main states are from the hybridization between B 2p states and H1, H2 & H3 s states.

Table 7.7: The calculated shortest distances between inter and intra hydrogen atom of $Mg(NH_2BH_3)_2$, $Ca(NH_2BH_3)_2$ and $Sr(NH_2BH_3)_2$.

Bond	$Mg(NH_2BH_3)_2$	$Ca(NH_2BH_3)_2$	$Sr(NH_2BH_3)_2$
H1...H2	1.98130	1.98095	1.99328
H1...H3	2.04623	2.01284	1.98523
H1...H4	2.64214	2.16221	2.51776
H1...H5	2.54582	2.33750	2.08493
H2...H3	1.99285	1.99809	2.00447
H2...H4	2.49327	2.06456	2.87089
H2...H5	2.05254	2.27225	3.06669
H3...H4	3.14723	3.14620	2.53300
H3...H5	2.38942	2.21988	2.38659
H4...H5	1.63485	1.64905	1.64592

At the same time weak N 2p states are also found. In both E2 & E3 energy regions, equal contribution from 2p states of B & N atoms have been found. H1 and H3 s states are also contributing in E2 and E3 energy region, respectively. Strongly hybridized states between N 2p states and H3 & H4 s states are found in E4 energy region, while E5 energy region displays the hybridization between the B 2s and N 2p states.

For $Ca(NH_2BH_3)_2$, the energy ranges are defined as E1=-1.5 to 0 eV (the Fermi level), E2=-5 to -1.5 eV, E3=-7 to -6 eV and E4=-8 to -7 eV. From the plot (see figure 7.10), in the E1 energy region, the main states are the N 2p states. At the same time, a weak hybridization between B 2p states and H1 & H3 s states is also found in this energy region. In the E2 energy region, there is a strong hybridization between the 1s states of H1, H2, H3 atoms and 2p states of B, N respectively. The next region E3 displays a hybridization between N 2p and H4 & H5 s states, while E4 energy region displays the hybridization between the B 2s and N 2p states.

For $Sr(NH_2BH_3)_2$, the energy ranges are defined as E1=-1 to 0 eV (the Fermi level), E2=-3.5 to -2 eV, E3=-5 to -3.5 eV, E4=-7 to -6 eV and E5=-8 to -7 eV. From the plot (see figure 7.11), in the E1 energy region, strong N 2p states and Sr d states are found along with

weak B 2p states. The E2 energy region consists of hybridization between B 2p states and H1, H2 & H3 s states. At the same time a weak N 2p states also found. Equal contribution from 2p states of B & N atoms found in E3 energy region. A strong hybridization between N 2p states and H4 & H5 s states occurs in E4 region, while E5 energy region displays the hybridization between the B 2s and N 2p states.

The electron distribution between Mg or Ca or Sr atoms and the neighboring atoms is very low, which confirms that the bonding between Mg or Ca or Sr and NH_2BH_3 ligand is ionic. A high negative charge distribution around BH_3 group implies a dominating covalent bonding. From the charge density distribution plots once again we conclude that, a strong covalent bonding is observed between the B-H bonds which is less pronounced in the case of N-H bonds.

Dihydrogen bonding:

Dihydrogen bond is a kind of hydrogen bond, which indicates an interaction between a metal bond and an OH or NH group or any proton donor group. This dihydrogen bond can exist in one molecule or between two molecules and affects molecular structure, physical and chemical properties of solids. This also plays an important role in crystal assembly and in super molecular systems. So the investigation of dihydrogen bonds is of great importance [133, 158]. To understand the dihydrogen bonding in the alkaline-earth metal amidoboranes, we have calculated the inter and intra molecular H-H separations. The calculated shortest distances between inter and intra hydrogen atoms for $Mg(NH_2BH_3)_2$, $Ca(NH_2BH_3)_2$ and $Sr(NH_2BH_3)_2$ are listed in table 7.7. The intra hydrogens H4 & H5, which are connected to the N are having shortest distance is around 1.63 $\mathring{A}$ in all $Mg(NH_2BH_3)_2$, $Ca(NH_2BH_3)_2$ and $Sr(NH_2BH_3)_2$. We can conclude that, in alkaline-earth metal amidoboranes the long range interactions have a negligible effect as the electronic structure. The inter molecular H-H separations are beyond the typical dihydrogen bond separation implying the absence of the vdW interactions in alkaline-earth metal amidoboranes.

7.3.4 Mechanical properties

Alkaline-earth metal amidoboranes crystalize in the monoclinic structure unlike NH_3BH_3 and alkali metal amidoboranes. For monoclinic structure there are 13 independent elastic constants, namely C_{11}, C_{22}, C_{33}, C_{44}, C_{55}, C_{66}, C_{12}, C_{13}, C_{15}, C_{23}, C_{25}, C_{35}, and C_{46}. As we discussed earlier in chapter 4, since alkaline-earth metal amidoboranes are molecular crystals, LDA is the best choice in calculating the elastic constants [147]. From the calculated elastic constants, $Mg(NH_2BH_3)_2$, $Ca(NH_2BH_3)_2$ and $Sr(NH_2BH_3)_2$ satisfy the Born's stability criteria thereby revealing the mechanically stability of these compounds (see table 7.8). In general C_{11}, C_{22} and C_{33} denote the mechanical stiffness along the X, Y and Z directions. The trends of the mechanical stiffness along three directions in $Mg(NH_2BH_3)_2$, $Ca(NH_2BH_3)_2$ and $Sr(NH_2BH_3)_2$ are as follows: For $Mg(NH_2BH_3)_2$ we find $C_{11} > C_{22} > C_{33}$ and for $Ca(NH_2BH_3)_2$, $C_{11} \approx C_{33} > C_{22}$ whereas $C_{11} \approx C_{22} > C_{33}$ for $Sr(NH_2BH_3)_2$. From this analysis we came to a conclusion that $Mg(NH_2BH_3)_2$, $Ca(NH_2BH_3)_2$ and $Sr(NH_2BH_3)_2$ are mechanically stiffer along X direction. The magnitude of the elastic constants decrease in the order $Ca(NH_2BH_3)_2 > Mg(NH_2BH_3)_2 > Sr(NH_2BH_3)_2$, indicates that $Ca(NH_2BH_3)_2$ is mechanically the stiffest system among three alkaline-earth amidoboranes.

The shear elasticity applied to the two-dimensional rectangular lattice such as in the (100), (010) and (001) planes in $Mg(NH_2BH_3)_2$, $Ca(NH_2BH_3)_2$ and $Sr(NH_2BH_3)_2$ can be estimated from the C_{44}, C_{55} and C_{66} elastic constants. The trends in the shear elasticity is as follows: For $Mg(NH_2BH_3)_2$ we find $C_{66} > C_{44} \approx C_{55}$ and for $Ca(NH_2BH_3)_2$, $C_{66} > C_{44} > C_{55}$ whereas $C_{44} > C_{66} > C_{55}$ for $Sr(NH_2BH_3)_2$. From the above, strong shear elasticity is found along (001) plane for $Ca(NH_2BH_3)_2$ and $Mg(NH_2BH_3)_2$ whereas for $Sr(NH_2BH_3)_2$ it is along (010) plane. The shear elasticity follows the trend $Ca(NH_2BH_3)_2 > Mg(NH_2BH_3)_2 > Sr(NH_2BH_3)_2$ confirming the high shear elasticity of $Ca(NH_2BH_3)_2$.

Further, we also calculated the polycrystalline elastic moduli from single-crystal elastic constants. The calculated bulk (B), shear (G), Young's modulus (E), and Poisson's ratio (σ) using the Voigt-Reuss-Hill (VRH) approximation [142–145, 162] are given in table 7.9. The

Table 7.8: The elastic constants, in GPa, of $Mg(NH_2BH_3)_2$, $Ca(NH_2BH_3)_2$ and $Sr(NH_2BH_3)_2$.

Compound	C_{11}	C_{22}	C_{33}	C_{44}	C_{55}	C_{66}	C_{12}	C_{13}	C_{15}	C_{23}	C_{25}	C_{35}	C_{46}
$Mg(NH_2BH_3)_2$	56.32	31.93	17.24	5.14	5.60	21.48	21.45	10.93	5.40	15.97	0.95	2.99	3.53
$Ca(NH_2BH_3)_2$	52.17	45.45	52.09	6.95	5.10	22.43	18.11	19.36	2.04	17.90	1.19	0.40	1.89
$Sr(NH_2BH_3)_2$	39.73	40.90	17.87	5.36	3.89	4.38	2.72	1.93	-0.55	5.81	3.21	7.79	-2.68

Table 7.9: The bulk (B), shear (G), Young's moduli (E), in GPa, G/B ratio, Poisson's ratio (σ) and Cauchy's pressure (C_{12} - C_{44}), in GPa, of $Mg(NH_2BH_3)_2$, $Ca(NH_2BH_3)_2$ and $Sr(NH_2BH_3)_2$.

Method	B_V	G_V	B_R	G_R	B	G	G/B	E	σ	C_{12}-C_{44}
$Mg(NH_2BH_3)_2$	22.47	14.28	10.25	5.49	14.28	7.87	0.55	19.94	0.26	16.31
$Ca(NH_2BH_3)_2$	28.94	13.18	28.49	9.60	28.71	11.39	0.39	30.17	0.32	11.16
$Sr(NH_2BH_3)_2$	13.27	8.59	2.05	1.36	7.66	4.97	0.64	12.19	0.23	-2.64

bulk modulus (B) for the $Mg(NH_2BH_3)_2$, $Ca(NH_2BH_3)_2$ and $Sr(NH_2BH_3)_2$ are calculated to be 14.28 GPa, 28.71 GPa and 7.66 GPa, respectively (see table 7.9). The Young's modulus (E) of the $Mg(NH_2BH_3)_2$, $Ca(NH_2BH_3)_2$ and $Sr(NH_2BH_3)_2$ are calculated to be 19.94 GPa, 30.17 GPa and 12.19 GPa, respectively. The calculated bulk and Young's modulii values once again confirms that $Ca(NH_2BH_3)_2$ is the stiffest compound among the three alkaline-earth metal amidoboranes. The stability of these crystals against shear has been scaled by calculating the Poisson's ratio (σ) value. From the σ values we conclude that $Ca(NH_2BH_3)_2$ is soft towards shape change whereas $Mg(NH_2BH_3)_2$ and $Sr(NH_2BH_3)_2$ are soft towards the volume change.

The ductile and brittle nature of the materials can be known from the elastic constants in terms of Cauchy's pressure (C_{12} - C_{44}) and G/B ratio. If Cauchy's pressure is positive, it indicates the ductile nature other wise the material is brittle [168]. The critical value of G/B ratio that separates ductile or brittle nature of the materials is 0.57. If G/B > 0.57 indicates brittle nature and G/B < 0.57 indicates ductile nature [162, 169]. The positive values of the Cauchy's pressures of $Mg(NH_2BH_3)_2$ and $Ca(NH_2BH_3)_2$ indicates their ductility behavior

Table 7.10: The shear anisotropy factors for (100) plane (A_1), for (010) plane (A_2), for (001) plane (A_3), the percentage of the anisotropy in the compressibility (A_B) and shear modulii (A_G) of $Mg(NH_2BH_3)_2$, $Ca(NH_2BH_3)_2$ and $Sr(NH_2BH_3)_2$ calculated at the theoretical equilibrium volume.

Method	A_1	A_2	A_3	A_B	A_G
$Mg(NH_2BH_3)_2$	0.422	1.300	1.894	0.222	0.302
$Ca(NH_2BH_3)_2$	0.471	0.330	1.461	0.007	0.157
$Sr(NH_2BH_3)_2$	0.398	0.330	0.233	0.732	0.726

whereas $Sr(NH_2BH_3)_2$ is brittle in nature with negative Cauchy's pressure and this has been confirmed from the calculated G/B ratios. The value of Cauchy's pressure of $Ca(NH_2BH_3)_2$ found to be low compared to the $Mg(NH_2BH_3)_2$, which is an indication of the higher ductility of $Mg(NH_2BH_3)_2$.

The shear anisotropy is a measure of the degree of anisotropy in bonding between the atoms in different planes. Here, we have calculated the shear anisotropy of $Mg(NH_2BH_3)_2$, $Ca(NH_2BH_3)_2$ and $Sr(NH_2BH_3)_2$ along (100), (010) and (001) shear planes (see table 7.10). The values of A_1, A_2 and A_3 are found to be differ from unity, indicating the shear anisotropic behavior of alkaline-earth metal amidoboranes. The percentage of the anisotropy in compressibility (A_B) and shear (A_G) are calculated as discussed in chapter 4. The percentage bulk modulus anisotropy A_B is found to be higher than the percentage shear modulus anisotropy A_G of $Mg(NH_2BH_3)_2$ and $Ca(NH_2BH_3)_2$, implying that these compounds are more anisotropic in shear than in compressibility. The A_G and A_B found to be equal for $Sr(NH_2BH_3)_2$.

Table 7.11: The average wave velocity (v_m), longitudinal(v_l) and transverse (v_t)modes and the Debye temperature (Θ_D) of $Mg(NH_2BH_3)_2$, $Ca(NH_2BH_3)_2$ and $Sr(NH_2BH_3)_2$.

Compound	v_m(Km/s)	v_l(Km/s)	v_t (Km/s)	Θ_D (K)
$Mg(NH_2BH_3)_2$	3.065	4.890	2.756	439.19
$Ca(NH_2BH_3)_2$	2.856	5.401	2.754	429.54
$Sr(NH_2BH_3)_2$	1.864	2.854	1.683	263.87

The Debye temperature (Θ_D), a fundamental quantity which correlates many physical properties such as specific heat and melting point of the solids, is an important thermodynamic parameter that can be calculated from elastic constants. Θ_D determines the thermal characteristics of the material, and a high value of Θ_D implies a high thermal conductivity. In the present study we have calculated the Debye temperatures (Θ_D) of $Mg(NH_2BH_3)_2$, $Ca(NH_2BH_3)_2$ and $Sr(NH_2BH_3)_2$ from the average wave velocity (v_m) which is the average of velocities of all longitudinal (v_l) and transverse (v_t) waves as discussed in chapter 4, and are listed in the table 7.11. From the calculated Θ_D values, we found that $\Theta_D(Mg(NH_2BH_3)_2) \approx \Theta_D(Ca(NH_2BH_3)_2) > \Theta_D(Sr(NH_2BH_3)_2)$. Therefore, $Mg(NH_2BH_3)_2$ and $Ca(NH_2BH_3)_2$ possess higher thermal conductivity than that of $Sr(NH_2BH_3)_2$. This is the first qualitative prediction of mechanical properties of the alkaline-earth metal amidoboranes which awaits experimental confirmation

7.4 Conclusions

The crystal structures of alkaline-earth metal amidoboranes ($Mg(NH_2BH_3)_2$, $Ca(NH_2BH_3)_2$ and $Sr(NH_2BH_3)_2$) are fully optimized using LDA and GGA functional, and it is found that GGA functionals are best choice for $Mg(NH_2BH_3)_2$ and $Ca(NH_2BH_3)_2$ to reproduce the experimental volume. Whereas for $Sr(NH_2BH_3)_2$, GGA-TS is better. Interestingly $Sr(NH_2BH_3)_2$ alone exhibit considerable vdW interactions effect to bind the crystal. The optimized structural parameters are in good agreement with the experimental data. From the band structure and density of states calculations, it is found that alkaline-earth metal amidoboranes are wide band gap insulators. The band gap values for $Mg(NH_2BH_3)_2$, $Ca(NH_2BH_3)_2$ and $Sr(NH_2BH_3)_2$ are 4.783 eV, 3.878 eV and 3.884 eV, respectively. These band gaps are lower than those of alkali metal amidoboranes. From the charge density distribution and bond population analysis we conclude that there exists a strong covalent bond between B-H and N-H atoms. From the calculated elastic constants the alkaline-earth metal

amidoboranes are found to be mechanically stable and $Ca(NH_2BH_3)_2$ is found to be less plastic than $Mg(NH_2BH_3)_2$ and $Sr(NH_2BH_3)_2$.

Chapter 8

Conclusions and Future work

8.1 Summary

A detailed theoretical study on simple prototype metal hydride i.e., beryllium hydride and its oligomers to a complex hydride namely ammonia borane, along with its derivatives such as alkali, alkaline-earth metal amidoboranes and ploy aminoboranes have been studied using density functional theory calculations. Although they show significant differences in their crystal structures and chemical composition, they do possess some common features. The geometry of these compounds are optimized and we calculated band structure and density of states of the solids to under stand the bonding characteristics. As these are molecular solids, the van der Waals (vdW) corrections to the total energy has been considered to obtain the experimental volume at semi-empirical level. The mechanical stability of these compounds are assessed from comparison of the elastic constants. The bonding properties are explained from the Mulliken atomic and bond populations analysis and charge density distributions. These systems contain simultaneously H^{+1} and H^{-1} and thus lead to dihydrogen bonding; the role of dihydrogen bonding on structural stability has been explored. Further, the structure dependent properties are addressed by considering the molecular level calculations of $(BeH_2)_n$; n=1-10 and $H(NH_2BH_2)_nH$ (n = 1 - 4). The HOMO-LUMO gaps and reaction

descriptors have been explored.

Beryllium hydride and its oligomers:

Beryllium hydride and its oligomers electronic structure properties have been carried out at HF, B3LYP and B3P86 methods with 6-31+G** and 6-311++G** basis sets. The band gap $\triangle E_{(LUMO-HOMO)}$, ionization potential (IP), electron affinity (EA), chemical potential (μ), hardness (η), softness (S) and polarizabilities (α) of beryllium hydride oligomers have been calculated. From the band gap, chemical potential, hardness and softness of molecules, BeH_2, Be_3H_5, Be_5H_{10}, Be_7H_{14} and Be_9H_{18} molecules have been found to be more stable compared to Be_2H_4, Be_4H_8, Be_6H_{12}, Be_8H_{16} and $Be_{10}H_{20}$ molecules. The calculated IR spectra of BeH_2 and Be_2H_4 molecules were found to be in good agreement with the experimental values. The IR spectra of molecules have five fundamental bands (475 to 575, 840 to 890, 1410 to 1520, 1610 and 2150 cm^{-1}) that determine the molecular structure stability.

Ammonia borane:

The low temperature phase of complex hydride ammonia borane optimized using LDA and GGA functional, and it was found that both the functionals are not efficient to reproduce the experimental volume, where the vdW interactions play an important role in crystallizing NH_3BH_3. Hence, vdW forces were taken into account through semiempirical methods such as OBS, G06 and TS. We found that, the TS is the better choice in reproducing the experimental volume with 5% error. The optimized structural parameters are in good agreement with the experimental data. From the band structure and density of states calculations, it is found that NH_3BH_3 has an indirect band gap of 5.65eV (5.90eV) with LDA (GGA) along the Γ-Z direction indicating that the compound is an insulator. The effect of vdW interactions is found to be very less while calculating the electronic properties. From the charge density distribution and bond population analysis we conclude that there exists a strong covalent bond between B-H atoms. From the calculated elastic constants the material is found to be mechanically stable at ambient and external pressures up to 6 GPa. Upon increase of pressure, NH_3BH_3 becomes stiffer and hard to compress. Low temperature phase of NH_3BH_3

is found to be less plastic than the high temperature phase. The orthorhombic NH_3BH_3 has lower shear anisotropy along (100) shear plane and higher anisotropy along (001) shear plane. The structural, mechanical and vibrational properties of NH_3BH_3 under hydrostatic compression up to 10 GPa reveal that NH_3BH_3 is soft towards the compression and becomes hard upon pressures.

Polyaminoboranes:

The dehydrogenation by catalytic and thermal decomposition of NH_3BH_3 results polyaminoboranes $(NH_2BH_2)_n$, which again come under the BNH_x compounds and are promising materials for chemical hydrogen storage. The electronic structure calculations of aminoborane oligomers have been carried out at MP2, HF, B3LYP and B3P86 methods with 6-31+G** and 6-311++G** basis sets. The band gap $\triangle$E(LUMO-HOMO), ionization potential (IP), chemical potential (μ), hardness (η), softness (S) and electronegativity (χ) of aminoborane oligomers have been calculated. From the total and relative energies, the coil structure aminoborane oligomers are found to be more stable compared to other structured oligomers. For the dimer and the trimer, the ring structure oligomers are found to have high band gap whereas for tetramer coil structure has higher band gap. The band gap increase with the size in coil structure oligomers, whereas the band gap decrease with the size in ring, square wave and zigzag structures. The B-H orbitals participate in the HOMO levels, whereas for the LUMO levels, only the N-H orbitals are present. From MEP, it is clear that aminoborane oligomers have high electrostatic potential from the B-H bonds and N-H bonds have low electrostatic potential, i.e., B-H bonds behave like donors and N-H bonds behave like acceptors, which led to form considerable "dihydrogen bonding" and end-to-end or side-by-side interactions. The IR and Raman spectra of molecules have four fundamental bands (from 100 cm^{-1} to 1400 cm^{-1}, from 1500 cm^{-1} to 1800 cm^{-1}, from 2300 cm^{-1} to 2700 cm^{-1} and 3600 cm^{-1} to 3800 cm^{-1}). The modes from 2300 cm^{-1} to 2700 cm^{-1} and 3600 cm^{-1} to 3800 cm^{-1} are due to N-H and B-H bonds stretching modes respectively. The N-H and B-H bond dissociation energies reveal that, N-H bonds are easily dissociated compared to the

B-H bonds.

Alkali metal amidoboranes:

New families of metal amidoboranes have been developed by replacing one H in NH_3BH_3 by an alkali or alkaline earth metal. The role of the metal atom on the physical and chemical properties of NH_3BH_3 has been discussed in subsequent chapters. The crystal structures of alkali metal amidoboranes ($LiNH_2BH_3$, $LiNH_3BH_4$ and $NaNH_2BH_3$) are fully optimized using LDA and GGA functionals; GGA functionals are found to reproduce the experimental volume better. Interestingly, alkali metal amidoboranes not showing any effect of vdW interactions. The optimized structural parameters are in good agreement with the experimental data. From the band structure and density of states calculations, it is found that alkali metal amidoboranes are wide band gap insulators. The band gap values for $LiNH_2BH_3$, $LiNH_3BH_4$ and $NaNH_2BH_3$ are 4.081 eV, 5.618 eV and 3.963 eV, respectively with GGA which are lower than that of ammonia borane. From the charge density distribution and bond population analysis we conclude that there exists a strong covalent bond between B-H and N-H atoms. From the calculated elastic constants the alkali metal amidoboranes are found to be mechanically stable and $LiNH_2BH_3$ found to be less plastic than $LiNH_3BH_4$ and $NaNH_2BH_3$.

Alkaline-earth metal amidoboranes:

Finally, alkaline-earth metal amidoboranes ($Mg(NH_2BH_3)_2$, $Ca(NH_2BH_3)_2$ and $Sr(NH_2BH_3)_2$) crystal structures are fully optimized using LDA and GGA functional, and found that GGA functionals are the best choice for $Mg(NH_2BH_3)_2$ and $Ca(NH_2BH_3)_2$ to reproduce the experimental volume. Whereas for $Sr(NH_2BH_3)_2$ it is GGA-TS. Interestingly $Sr(NH_2BH_3)_2$ alone exhibit considerable vdW interactions effect to bind the crystal. The optimized structural parameters are in good agreement with the experimental data. From the band structure and density of states calculations, it is found that alkaline-earth metal amidoboranes are wide band gap insulators. The band gap values for $Mg(NH_2BH_3)_2$, $Ca(NH_2BH_3)_2$ and $Sr(NH_2BH_3)_2$ are 4.783 eV, 3.878 eV and 3.884 eV, respectively. These band gaps are

lower than those of alkali metal amidoboranes. From the charge density distribution and bond population analysis we conclude that there exists a strong covalent bond between B-H and N-H atoms. From the calculated elastic constants the alkaline-earth metal amidoboranes are found to be mechanically stable and $Ca(NH_2BH_3)_2$ found to be less plastic than $Mg(NH_2BH_3)_2$ and $Sr(NH_2BH_3)_2$.

In summary, we have studied the electronic structure and bonding properties of hydrogen storage materials ($(BeH_2)_n$; n=1-10, NH_3BH_3 $H(NH_2BH_2)_nH$; n = 1-4, $LiNH_2BH_3$, $LiNH_3BH_4$, $NaNH_2BH_3$, $Mg(NH_2BH_3)_2$, $Ca(NH_2BH_3)_2$ and $Sr(NH_2BH_3)_2$) using DFT. Ammonia borane exhibits considerable vdW interactions and these interactions have negligible effect on the properties of alkali and alkaline-earth metal amidoboranes. From the band gaps we found the following trend: Ammonia borane > Alkali metal amidoboranes > Alkaline-earth metal amidoboranes, which indicates the electronic stability of ammonia borane. The mechanical stiffness of these compounds shows the following trend: $Ca(NH_2BH_3)_2$ > $LiNH_2BH_3$ > $NaNH_2BH_3$ > $LiNH_3BH_4$ > $Mg(NH_2BH_3)_2$ > NH_3BH_3 > $Sr(NH_2BH_3)_2$, revealing the mechanical stiffness of $Ca(NH_2BH_3)_2$ over other compounds. From the bonding analysis, alkali metal amidoboranes shows the predominant covalency over ammonia borane and alkaline-earth metal amidoboranes. The alkali metal amidoboranes are predicted to possess high thermal conductivity than other compounds.

As more electrons are transferred from metal to $[NH_2BH_3]^-$ ions, the hydridic nature B-H bond of $[NH_2BH_3]^-$ ions increased, which enhances it activity compared to those in NH_3BH_3. The charged $[NH_2BH_3]^-$ ion creates more polar surroundings compared to the symmetric NH_3BH_3. Therefore, the barrier of the reaction between $[NH_2BH_3]^-$ ions would be lower than that between two neutral NH_3BH_3 molecules. From the electronic structure and bonding properties of these compounds we conclude that alkali and alkaline-earth metal amidoboranes possess improved dehydrogenation properties over ammonia borane.

8.2 Future work

Future work could focus on the vibrational properties and high pressure studies of alkali and alkaline-earth metal amidoboranes. The complete stability of these compounds has to be known through the phonon calculations. Finding the reaction path ways of hydrogen release and uptake is the great technical challenge. Another direction is to understand the stabilization of the amidoboranes with ammonite for promising hydrogen storage applications with desired dehydrogenation properties. Ammonia borane and amidoboranes are promising materials for hydrogen storage applications, but still yet to be addressed alot in terms of their reversibility for efficient fuel cell applications.

Bibliography

[1] L. Schlapbach, A. Zuttel, *Nature* 414 (2001) 353.

[2] *Chemical Hydrogen Storage* available at http://www1.eere.energy.gov/ hydrogenandfuelcells/storage/chem storage.html (2008).

[3] T. E. Lipman, M. A. DeLucchi, *Int. J. Vehicle Des* 17 (1996) 562

[4] J. O. M. Bockris, Energy: The Solar-Hydrogen Alternative. Architectural Press, London (1976)

[5] G. W. Crabtree, M. S. Dresselhaus, M. V. Buchanan, *Physics Today* 57 (2004) 39.

[6] A. Zuttel, A. Borgschulte, L. Schlapbach, *Hydrogen as a Future Energy Carrier.* Wiley VCH (2008)

[7] A. Leon, *Hydrogen Tecnology: Mobile and Portable Applications.* Springer (2008)

[8] *MRS Bulletin*, 27 (2002) 675.

[9] S. A. Sherif, N. Zeytinoglu, T. N. Veziroglu, *Int. J. Hydrogen Energy* 22 (1997) 683.

[10] Roman J. Press, K. S. V. Santhanam, Massoud J. Miri, Alla V. Bailey, G. A. Takacs, *Introduction to Hydrogen Technology*, John Wiley & Sons, Inc. (2009)

[11] J.N. Huiberts, R. Griessen, J.H. Rector, R.J. Wijngaarden, J.P. Dekker, D.G. de Groot, N.J. Koeman, *Nature* 380 (1996) 231-234.

[12] W. Grochala, P. P. Edwards, *Chem. Rev* 104 (2004) 1283.

[13] DJ. Westlake, *J. Less-Common Metals* 91 (1983) 1.

[14] G. Sandrock, *J. Alloys Compd.* 293-295 (1999) 877.

[15] P. Chen, Z. Xiong, J. Luo, J. Lin, K.L. Tan, *Nature* 420 (2002) 302.

[16] P. Chen, Z. Xiong, J. Luo, J. Lin, K.L. Tan, *J. Phys. Chem. B* 107 (2003) 10967.

[17] J. P. Jourdan, R. Roguenant, *Adv. Hydrogen Energy*, 1 (1979) 1401.

[18] R. Metkemeijer, P. Achard, *J. Power Sources*, 49 (1994) 271.

[19] A. Zuttel, *Materials Today (Oxford, United Kingdom)* 6 (2004) 24.

[20] A. Klerke, C. H. Christensen, J. K. Norskov, T. Vegge, *J. Mater. Chem.* 18 (2008) 1304.

[21] C. Zamfirescu, I. Dincer, *J. Power Sources.* 185 (2008) 459.

[22] C. H. Christensen, T. Johannessen, R. Z. Sorensen, R. Z. Soerensen, *Catal. Today* 111 (2006) 140.

[23] Y. H. Hu, E. Ruckenstein, *Ind. Eng. Chem. Res.* 45 (2006) 182.

[24] Y. H. Hu, E. Ruckenstein, *J. Phys. Chem. A* 107 (2003) 9737.

[25] T. Ichikawa, N. Hanada, S. Isobe, H. Y. Leng, H. Fujii, *J. Alloys Compd.* 404 to 406 (2005) 435.

[26] Z. Xiong, J. Hu, G. Wu and P. Chen, *J. Alloys Compd.* 395 (2005) 209.

[27] A. Sudik, J. Yang, D. Halliday and C. Wolverton, *J. Phys. Chem. C* 112 (2008) 4384.

[28] M. Gutowski, T. Autrey, *RSC Chemistry World,* Vol.3, No.3 (2006)

[29] R. V. Noorden, *RSC Chemistry World,* Vol.4, No.10 (2007)

[30] J. Crombie, *RSC Highlights in Chemical Science,* Iss. 4 (2009)

[31] V. Chapman, *RSC Highlights in Chemical Science,* Iss. 8 (2008)

[32] J. M. Crow, *RSC Highlights in Chemical Technology,* Iss. 1 (2008)

[33] P. O'Sullivan, *RSC Highlights in Chemical Technology,* Iss. 9 (2006)

[34] T. Umegaki, J. M. Yan, X. B. Zhang, H. Shioyama, N. Kuriyama, Q. Xu, *Int. J. Hydrogen Energy,* 34 (2009) 2303.

[35] L. Li, X. Yao, C. H. Sun, A. J. Du, L. N. Cheng, Z. H. Zhu, C. Z. Yu, J. Zou, S. C. Smith, P. Wang, H. M. Cheng, R. L. Frost, G. Q. M. Lu, *Advanced Functional Materials,* 19 (2009) 265.

[36] C. W. Hamilton, R. T. Baker, A. Staubitz, I. Manners, *Chem. Soc. Rev.* 38 (2009) 279.

[37] R. B. Biniwale, S. Rayalu, S. Devotta, M. Ichikawa, *Int. J. Hydrogen Energy,* 33 (2008) 360.

[38] H. Stephens Frances, V. Pons, R. Tom Baker, *Dalton Trans* 2613 (2007).

[39] R. J. Keaton, J. M. Blacquiere, R. T. Baker, *J. Am. Chem. Soc* 129 (2007) 1844.

[40] M. P. Vencislav, K. S. Gregory, J. H. Nancy, L. D. Luke, M. Hartl, C. S. Ashley, M. C. Donald, T. Autrey, *Dalton Trans.* 4514 (2008).

[41] B. Peng, J. Chen, *Energy Environ. Sci.* 1 (2008) 479.

[42] A. Karkamkar, C. Aardahl, T. Autrey , *Hydrogen Storage Materials*, Materials Matters, Sigma Aldrich, 2 (2007) 6.

[43] J. R. Weaver, S. G. Shore, R. W. Parry, *J. Chem. Phys.* 29 (1958) 1.

[44] J. Kohan off, *Electronic structure calculations for solids and molecules: Theory and Computational Methods* Cambridge University Press, Cambridge (2006)

[45] W. Koch, M.C. Holthausen, *A Chemist's Guide to Density Functional Theory*, Wiley Vch, New York (2002)

[46] R.G. Parr, W. Yang, *Density Functional Theory fo Atoms and Molecules*, Oxford University Press, Oxford (1989)

[47] M. Born, J. R. Oppenheimer, *Am. J. Phys* 84 (1927) 451.

[48] L. H. Thomas, *Proc. Cambridge Phil. Soc* 23 (1927) 542.

[49] E. Fermi, *Z. Phys* 48 (1928) 73.

[50] P. Hohenberg, W. Kohn, *Phys. Rev* 136 (1964) B864.

[51] W. Kohn, L. Sham, *Phys. Rev* 140 (1965) A1133.

[52] A. D. Becke, *J. Chem. Phys* 98 (1993) 1372.

[53] J. P. Perdew, M. Ernzerhof, K. Burke, *J. Chem. Phys* 105 (1999) 9982.

[54] K. Kim, K. D. Jordan, *J. Phys. Chem* 98 (1994) 10089.

[55] P. J. Stephens, F. J. Devlin, C. F. Chabalowski, M. J. Frisch, *J. Phys. Chem*, 98 (1994) 11623.

[56] F. Bloch, Z. Phys, 52 (1928) 555.

[57] M.L. Cohen, V. Heine, Solid State Physics, 24 (1970) 37.

[58] M.T. Yin, M.L. Cohen, *Phys. Rev. B* 25 (1982) 7403.

[59] D. Vanderbilt, *Phys. Rev. B* 41 (1990) 7892.

[60] M. C. Payne, M. P. Teter, D. C. Allan, T. A. Arias, J. D. Joannopoulos, *Rev. Mod. Phys* 64 (1992) 1045.

[61] G. Kerker, *J. Phys. C* 13 (1980) 189.

[62] L. Kleinman, D. M. Bylander, *Phys. Rev. Lett* 48 (1982) 1425.

[63] S. Grimme, *J. Comput. Chem* 27 (2006) 1787.

[64] P. Jurecka, J. Cerny, P. Hobza, D. R. Salahub, *J. Comput. Chem* 28 (2007) 555-569.

[65] F. Ortmann, F. Bechstedt, W. G. Schmidt, *Phys. Rev. B* 73 (2006) 205101.

[66] A. Tkatchenko, M. Scheffler, *Phys. Rev. Lett* 102 (2009) 073005.

[67] M. J. Frisch et al Gaussian 03, Revision B.04, Gaussian, Inc., Pittsburgh, PA (2003).

[68] B. Njegic, M. S. Gordon, *J. Chem. Phys* 125 (2006) 224102.

[69] K. R. S. Chandrakumar, S. K. Ghosh, *Nano. Lett* 8 (2008) 13.

[70] P. Chen, M. Zhu, *Mat. Today* 11 (2008) 36.

[71] J. L. C. Rowsell, O. M. Yaghi, *Angew. Chem. Int. Ed* 44 (2005) 4670.

[72] A. Karpfen, *Theort. Chim. Acta* 50 (1978) 49.

[73] G. S. Smith, Q. C. Johnson, D. K. Smith, D. E. Cox, R. L. Snyder, R. S. Zhou, A. Zalkin, *Solid. State. Commu* 67 (1988) 491.

[74] T. J. Tague, L. Andrews, *J. Am. Chem. Soc* 115 (1993) 12111.

[75] X. Wang, L. Andrews, *Inorg. Chem* 44 (2005) 610.

[76] A. Abdhurahman, A. Shukla, M. Dolg, *J. Chem. Phys* 112 (2000) 4801.

[77] A. Abdhurahman, *J. Phys. Chem. A* 107 (2003) 11547.

[78] D. R. Armstrong, J. Jamieson, P. G. Perkins, *Theort. Chim. Acta* 51 (1979) 163.

[79] Y. L. Chen, C. H. Huang and W. P. Hu, *J. Phys. Chem. A* 109 (2005) 9627.

[80] P. Geerlings, F. D. Proft, W. Langenaeker, *Chem. Rev* 103 (2003) 1793.

[81] S. Pal, K. R. S. chandrakumar, *J. Phys. Chem. A* 107 (2003) 11547.

[82] P. Politzer, F. Abu-Awwad, *Theort. Chim. Acta* 99 (1998) 83.

[83] J. Luo, Z. Q. Xue, W. M. Liu, J. L. Wu, Z. Q. Yang, *J. Phys. Chem. A* 110 (2006) 12005.

[84] T. A. Koopman, *Physica* 1 (1933) 104.

[85] M. P. Charles, E. Swenberg, *Electronic Processes in Organic Crystals and Polymers*, 2nd Ed., Oxford Science Publications, Oxford University Press, New York (1999).

[86] M. D. Segall, P. J. D. Lindan, M. J. Probert, C. J. Pickard, P. J. Hasnip, S. J. Clark, M. C. Payne, *J. Phys: Cond. Matt* 14 (2002) 2717.

[87] H. J. Monkhorst, J. D. Pack, *Phys. Rev. B* 13 (1976) 5188.

[88] P. Politzer, *J. Chem. Phys* 86 (1987) 1072.

[89] R. G. Parr, R. G. Pearson, *J. Am. Chem. Soc* 105 (1983) 7512.

[90] R. G. Pearson, *J. Chem. Educ* 64 (1987) 561.

[91] F. Fukui, T. Yonezawa, H. Shingu, *J. Chem. Phys* 20 (1952) 722.

[92] H.-M. Xiao, Y.-Y. Li, *Banding and electronic structures of metal azides: Sensitivity and conductivity*, Science in China, Ser. B. 38, 538 (1995).

[93] H.-M Xiao, Y.-Y. Li, *Banding and Electronic Structures of Metal Azides*, Sciences Press, Beijing (1996).

[94] Z. Zhou, R. G. Parr, *J. Am. Chem. Soc* 112 (1990) 5720.

[95] R. G. Pearson, *J. Org. Chem* 54 (1989) 1423.

[96] P. Shemella, Y. Zhang, M. Mailman, P. M. Ajayan, S. K. Nayak, *App. Phys. Lett* 91 (2007) 041201.

[97] R. S. Mulliken, *J. Chem. Phys* 23 (1955) 1833.

[98] M. D. Segall, R. Shah, C. J. Pickard, M. C. Payne, *Phys. Rev. B* 54 (1996) 16317.

[99] B. L. Davis, D. V. Dixon, E. B. Garner, J. C. Gordon, M. H. Matus, B. Scott, F. H. Stephens, *Angew. Chem. Int. Ed* 48 (2009) 6812.

[100] V. M. Parvanov, G. K. Schenter, N. J. Hess, L. L. Daemen, M. Hartl, A. C. Stowe, D. M. Camaioni, T. Autrey,*Dalton Trans* 4514 (2008).

[101] T. B. Marder, *Angew. Chem. Int. Ed* 46 (2007) 8116.

[102] R. von Helmolt, U. Eberle, *J. Power. Sources* 165 (2007) 833.

[103] M. A. Gutowska, L. Li, Y. Shin, C. M. Wang, X. S. Li, J. C. Linehan, R. S. Smith, B. D. Kay,B. Schmid, W. Shaw, M. Gutowski, T. Autrey,*Angew. Chem. Int. Ed* 44 (2005) 3578.

[104] A. Staubitz, A.P.M. Robertson, I. Manners, *Chem. Rev* 110 (2010) 4079.

[105] M. C. Denney, V. Pons, T. J. Hebden, D. M. Heinekey, K. I. Goldberg, *J. Am. Chem. Soc* 128 (2006) 12048.

[106] D. West, S. Limpijumnong, S. B. Zhang,*Phys. Rev. B* 80 (2009) 064109.

[107] M. Ramzan, F.Silvearv, A. Blomqvist, R. H. Scheicher, S. Lebegue, R. Ahuja, *Phys. Rev. B* 79 (2009) 132102;

[108] M. Ramzan, R. Ahuja, *J. Phys. Chem. Solids* 71 (2010) 1137.

[109] W. T. Klooster, T. F. Koetzle, P. E. M. Siegdahn, T. B. Richardson, R. H. Crabtree, *J. Am. Chem. Soc* 121 (1999) 6337.

[110] J. B. Yang, J. Lamsal, Q. Cai, W. J. James, W. B. Yelon, *App. Phys. Lett* 92 (2008) 091916.

[111] S. M. Lee, X Kang, P. Wang, H. Chung, Y. H. Lee, *Chem. Phys. Chem* 10 (2009) 1825.

[112] H. Cho, W. J. Shaw, V. Parvanov, G. K. Schenter, A. Karkamkar, N. J. Hess, C. Mundy, S. Kathmann, J. Sears, A. S. Lipton, P. D. Ellis, S. T. Autrey, *J. Phys. Chem. A* 112 (2008) 4277.

[113] S. G. Shore, R. W. Parry, *J. Am. Chem. Soc* 77 (1955) 6084.

[114] E. W. Hughes, *J. Am. Chem. Soc* 78 (1956) 502.

[115] E. L. Lippert, W. N. Lipscomb, *J. Am. Chem. Soc* 78 (1956) 503.

[116] S. G. Shore, R. W. Parry, *J. Am. Chem. Soc* 80 (1958) 8.

[117] C. F. Hoon, E. C. Reynhard, *J. Phys. C* 16 (1983) 6129.

[118] M. G. Hu, J. M. Van PAASSCHEN, R. A. GEANANGEL, *J. Inorg. Nucl. Chem* 39 (1977) 2174.

[119] M. E. Bowden, G. J. Gainsford, W. T. Robinson, *Aust. J. Chem* 60 (2007) 149.

[120] O. Gunaydin Sen, R. Schey, N. S. Dalal, A. Stowe, T. Autrey, *J. Phys. Chem. B* 111 (2007) 677.

[121] N. J. Hess, M. R. Hartman, C. M. Brown, E. Mamontov, A. Karkamar, D. J. Heldebrant, L. L. Daemen, T. Autrey, *Chem. Phys. Lett* 459 (2008) 85.

[122] N. J. Hess, M. E. Bowden, V. M. Parvanov, C. Mundy, S. M. Kathmann, G. K. Schenter, T. Autrey, *J. Chem. Phys* 128 (2008) 034508.

[123] A. Paolone, O. Palumbo, P. Rispoli, R. Cantelli, T. Aurtrey, *Mat. Sci. Eng. A* 521 (2009) 169.

[124] C. A. Morrison, M. M. Siddick, *Angew. Chem. Int. Ed* 43 (2004) 4780.

[125] S. Trudel, D. F. R. Gilson, *Inorg. Chem* 42 (2003) 2814.

[126] R. Custelcean, Z. A. Dreger, *J. Phys. Chem. B* 107 (2003) 9231.

[127] A. Liu, Y. Song, *J. Phys. Chem. B* 115 (2011) 7.

[128] A. Liu, S.T. Xie, S. Dabiran-Zohoory, Y. Song, *J. Phys. Chem. C* 114 (2010) 11635.

[129] C. Murli, Y. Song, *J. Phys. Chem. B* 113 (2009) 13509.

[130] Y. Song, C. Murli, Z.X. Liu, *J. Chem. Phys* 131 (2009) 174506.

[131] S.T. Xie, Y. Song, Z.X. Liu, *Can. J. Chem* 87 (2009) 1235.

[132] S. Trudel, D.F.R. Gilson, *Inorg. Chem* 42 (2003) 2814.

[133] R. H. Crabtree, P. E. M. Siegbahn, O. Eisenstein, A. L. Rheingold, T. F. Koetzle, *Acc. Chem.Rev* 29 (1996) 348.

[134] S.K. Ravhi, Ke. Xuezhi, J. Zhang, Z. Lin, C.V. Sven, M. Hartl, S. Sinogeikin, L. Daemen, L.C. Andrew, C. Chen, Y. Zhao, *Chem. Phys. Lett* 495 (2010) 203.

[135] Y. Lin, H. Ma, C.W. Matthews, B. Kolb, S. Sinogeikin, T. Thonhauser, W.L. Mao, *J. Phys. Chem. C* 116 (2012) 2172.

[136] H. Wu, W. Zhou, T. Yildirim, *J. Am. Chem. Soc* 130 (2008) 14834.

[137] C. R. Miranda, G. Ceder, *J. Chem. Phys* 126 (2007) 184703.

[138] D. M. Ceperley, B. J. Alder, *Phys. Rev. Lett* 45 (1980) 566.

[139] J. P. Perdew, A. Zunger, *Phys. Rev. B* 23 (1981) 5048.

[140] J. P. Perdew, K. Burke, M. Ernzerhof, *Phys. Rev. Lett* 77 (1996) 3865.

[141] J. P. Perdew, J. A. Chevary, S. H. Vosko, K. A. Jackson, M. R. Pederson, D. J. Singh, C. Fiolhais, *Phys. Rev. B* 46 (1992) 6671.

[142] P. Ravindran, L. Fast, P. A. Korzhavyi, B. Johansson, J. Wills, O. Eriksson, *J. Appl. Phys* 84 (1998) 4891.

[143] J. F. Nye, Physical Properties of Crystals, Oxford university Press, (1985).

[144] A. Reuss, Z. Angew, *Math Mech* 9 (1929) 49.

[145] R. Hill, *Phys. Soc. London* 65 (1979) 350.

[146] E. Francisco, M. A. Blanco, G. Sanjurjo, *Phys. Rev. B* 63 (2001) 094107.

[147] X. Chen, M. Alouani, *Phys. Rev. B* 82 (2010) 094443.

[148] K. Yamauchi, I. Hamada, H. Huang, T. Oguchi, *App. Phys. Lett* 99 (2011) 181904.

[149] T. Bučko, J. Hafner, S. Lebègue, J. G. Ángyán, *J. Phys. Chem. A* 114 (2010) 11814.

[150] P. Jurečka, J. Šponer, J. Černy, P. Hobza, *Phys. Chem. Chem. Phys* 8 (2006) 1985

[151] S. Lebègue, C. M. Araujo, O. Eriksson, B. Arnaud, M. Alouani, R. Ahuja, *J. Phys: Condens. Matter* 19 (2007) 036223.

[152] C. M. Araujo, S. Lebègue, O. Eriksson, B. Arnaud, M. Alouani, R. Ahuja, *J. App. Phys* 98 (2005) 096106.

[153] S. Lebègue, B. Arnaud, M. Alouani, P. E. Bloechl, *Phys. Rev. B* 67 (2003) 155208.

[154] Ch. Bheema Lingam, K. Ramesh Babu, S. P. Tewari, G. Vaitheeswaran, S. Lebègue, *physica status solidi: Rapid Research Letters* 5 (2010) 10.

[155] L. Wang, K. Bao, X. Meng, X. Wang, T. Jiang, T. Cui, B. Liu, G. Zou, *J. Chem. Phys* 134 (2011) 024517.

[156] J. He, E. Wu, H. Wang, R. Liu, Y. Tian, *Phys. Rev. Lett* 94 (2005) 015504.

[157] F. M. Hossain, G. E. Murch, I. V. Beova, B. D. Turner, *Solid. State. Commu* 149 (2009) 1201.

[158] R. Custelcean, J. E. Jackson, *Chem. Rev* 101 (2001) 1963.

[159] L. Pauling, *The Nature of The Chemical Bond*, 3rd Edition, Chapter 1 and 3, (1975).

[160] A. C. Switendick, *Z. Phys. Chem* 117 (1979) 89.

[161] B. K. Rao, P. Jena, *Phys. Rev. B* 31 (1985) 6726.

[162] V. Kanchana, *Eur. Phys. Lett* 87 (2009) 26006.

[163] Jr. L. G. Hector, J. F. Herbst, W. Wolf, P. Saxe, *Phys. Rev. B* 76 (2007) 014121.

[164] A. F. Chebanov, *Mat. Sci* 27 (1992) 184.

[165] S. Rajagopalan, *Il Nuovo cimento* 51B (1979) 222.

[166] J. N. Sherwood (Ed.), *The Plastically Crystalline State*, Wiley Interscience, Chichester (1979).

[167] Y. Filinchuk, A. H. Nevidomskyy, D. Chernyshov, V. Dmitriev,*Phys. Rev. B* 79 (2009) 214111.

[168] D. Pettifor, *Mater. Sci. Tech* 8 (1992) 345.

[169] S. F. Pugh, *Phil. Mag. B* 45 (1954) 823.

[170] V. Tvergaard, J. W. Hutchinson, *J. Am. Ceram. Soc* 71 (1983) 157.

[171] O. L. Anderson, *J. Phys. Chem. Solids* 24 (1963) 909.

[172] J. Joseph, E. Jemmis, *J. Am. Chem. Soc* 129 (2007) 4620.

[173] D. J. Heldebrant, A. Karkamkar, J. C. Linehan, T. Autrey, *Energy. Environ. Sci* 67 (1988) 491.

[174] G. Wolf, J. Baumann, F. Baitalow, F. P. Hoffmann, *Theormochim. Acta* 343 (2000) 19.

[175] D. A. Dixon, M. Gutowski, *J. Phys. Chem. A* 109 (2005) 5129.

[176] D. Jacquemin, E. A. Perpete, V. Wathelet, J. -M. Andre, *J. Phys. Chem. A* 108 (2004) 9616.

[177] J. S. Wang, R. A. Geanangel, *Inorganica Chimica Acta* 148 (1988) 185.

[178] P. M. Kuznesof, D. F. Shriver, F. E. Stafford, *J. Am. Chem. Soc* 90 (1968) 2557.

[179] S. Y. Pusatcioglu, H. A. McGee Jr., A. L. Fricke, J. C. Hassler, *J. Appl. Polym. Sci* 21 (1971) 1561.

[180] M. G. Hu, R. A. Geanangel, W. W. Wendlandt, *Theormochim. Acta* 23 (1978) 249.

[181] R. Komm, R. A. Geanangel, R. Liepins, *Inorg. Chem* 22 (1983) 1684.

[182] J. Li, S. M. Kathmann, G. K. Schenter, M. Gutowski, *J. Phys. Chem. C* 111 (2007) 3294.

[183] J. Li, S. M. Kathmann, H. Hu, G. K. Schenter, T. Aurtey, M. Gutowski, *Inorg. Chem* 49 (2010) 7710.

[184] A. Abdurahaman, M. Albrecht, A. Shukla, M. Dolg, *J. Chem. Phys* 110 (1999) 8819.

[185] S. M. Nakhmanson, M. B. Nardelli, J. Bernholc, *Phys. Rev. Lett* 92 (2004) 115504.

[186] Ch. Bheema Lingam, K. Ramesh Babu, S. P. Tewari, G. vaitheeswaran, *J. Comp. Chem* 32 (2011) 1734.

[187] Y. Mo, L. Song, W. Wu, Q. Zhang, *J. Am. Chem. Soc* 126 (2004) 3974.

[188] T. Kar, S. Scheiner, *J. Chem. Phys* 119 (2003) 1473.

[189] G. Merino, V. I. Bakhmutov, A. Vela, *J. Phys. Chem. A* 106 (2002) 8491.

[190] T. M. Gilbert, *J. Phys. Chem. A* 108 (2004) 2550.

[191] L. R. Thorne, R. D. Suenram, F. J. Lovas, *J. Chem. Phys* 78 (1983) 167.

[192] R. C. Weast, *CRC Handbook of Chemistry and Physics*, 65th edition, CRC Press, Boca Raton (1984).

[193] R. D. Suenram, L. R. Thorne, *Chem. Phys. Lett* 78 (1981) 157.

[194] W. L. Jolly, *Modern Inorganic Chemistry*, 2nd ed. McGraw-Hill, New York (1991)

[195] J. Mullay, *"Estimation of atomic and group electronegativities": Structure and Bonding*, Springer Berlin / Heidelberg (1987).

[196] J. S. Murray, P. Politzer, *WIREs Comput. Mol. Sci* 1 (2011) 153.

[197] T. B. Richardson, S. de Gala, R. H. Crabtree, *J. Am. Chem. Soc* 117 (1995) 12875.

[198] S. J. Grabowski, W. A. Sokalski, J. Leszczynski, *J. Phys. Chem. A* 108 (2004) 5823.

[199] S. J. Blanksby, G.B. Ellison, *Acc. Chem. Res* 36 (2003) 255.

[200] D. Y. Kim, H. M. Lee, J. Seo, S. K. Shin and K. S. Kim, *Phys. Chem. Chem. Phys* 12 (2010) 5446.

[201] Yong Shen Chua, Ping Chen, Guotao Wu, Zhitao Xiong, *Chem. Commun* 47 (2011) 5116.

[202] A.G. Myers, B.H.Yang, K.J. David, *Tetrahedron. Lett* 37 (1996) 3623.

[203] J. Schlesinger, A.B. Burg, *J. Am. Chem. Soc* 130 (2008) 14834.

[204] A.N. Torgersen, S.W. Jorgensen, US patent 2006/0097221 (2006)

[205] Y. Kawai, Y. Kojima, T. Haga, JP patent 2007/070203 (2007)

[206] Z.T. Xiong, C.K. Yong, G.T. Wu, P. Chen, W. Shaw, A. Karkamkar, T. Aurtey, M.O.Jones, S.R. Johnson, P.P. Edwards, W.I.F. David, *Nat. Mater* 7 (2008) 138.

[207] X.D. Kang, Z.Z. Fang, L.Y. Kong, H.M. Cheng, X.D. Yao, G.Q. Lu, P. Wang, *Ad. Mater* 20 (2008) 2756.

[208] Z.T. Xiong, Y.S. Chua, G.T. Wu, W.L. Xu, P. Chen, W. Shaw, A. Karkamkar, J. Linehan, T. Smurthwaite, T. Aurtey, *Chem. Commun* (2008) 5595.

[209] Z.T. Xiong, G.T. Wu, Y.S. Chua, J.J. Hu, T. He, W.L. Xu, P. Chen, *Energy. Environ. Sci* 1 (2008) 360.

[210] K.J. Fijakowski, W. Grochala, *J. Mater. Chem* 19 (2009) 2043.

[211] H.V.K. Diyabalanage, T. Nakagawa, R.P. Shrestha, T.A. Semelsberger, B.L. Davis, B.L. Scott, A.K. Burrell, W.I.F. David, K.R. Ryan, M.O. Jones, P.P. Edwards, *J. Am. Chem. Soc* 132 (2010) 11836.

[212] C. Wu. G. Wu, Z. Xiong, W.I.F. David, K.R. Ryan, M.O. Jones, P.P. Edwards, H. Chu, P. Chen, *Inorg. Chem* 49 (2010) 4319.

[213] K.R. Ryan, PhD-Thesis: A study of Ammonia Borane and Its Derivatives (2011).

[214] S.R. Johnson, W.I.F. David, D.M. Royse, M. Sommariva, C.Y. Tang, F.P.A. Fabbiani, M.O. Jones, P.P. Edwards, *Chem. Asian J* 4 (2009) 849.

[215] B. Zhong, X.X. Huang, G. Wen, X.D. Zhang, H.W. Bai, T. Zhang, H.M. Yu, *Solid. State. Commu*, 150 (2010) 1552.

[216] Y. Guo, G. Xia, Y. Zhu, L. Gao, X. Yu, *Chem. Commun* 46 (2010) 2599.

[217] Y. Li, F. Fang, Y. Song, Y. Li, Q. Zhang, L. Ouyang, M. Zhu, D. Sun, *Int. J. Hydrogen Energy* 37 (2012) 4274.

[218] Q.G. Zhong, C.X. Tang, C.H. Fang, F. Fang, D. Sin, L.Z. Ouyang, M. Zhu, *J. Phys. Chem. C* 114 (2010) 1709.

[219] Y.S. Chua, G.T. Wu, Z.T. Xiong, T. He, P. Chen, *Chem. Mater* 21 (2009) 4899.

[220] J. Spielmann, G. Jansen, H. Bandmann, S. Harder, *Angew. Chem* 120 (2008) 6386.

[221] W. Li, G. Wu, Y. Chua, Y.P. Feng, P. Chen, *Inorg. Chem* 51 (2012) 76.

[222] X.D. Kang, L.P. Ma, Z.Z. Fang, L.L. Gao, J.H. Luo, S.C. Wang, P. Wang, *Phys. Chem. Chem. Phys* 11 (2009) 2507.

[223] Y.S. Chua, G.T. Wu, Z.T. Xiong, A. Karkamkar, M.X. Jian, M.W. Wong, T. Autrey, P. Chen, *Chem. Commun* 46 (2010) 5752.

LIST OF PUBLICATIONS

(Portions of the results described in this thesis have been published, accepted and communicated)

1. **Ch. Bheema Lingam**, K. Ramesh Babu, Surya P. Tewari, G. Vaitheeswaran;
   Quantum chemical studies on beryllium hydride oligomers, *Computational and Theoretical Chemistry (2011) 963, 371-377.*

2. **Ch. Bheema Lingam**, K. Ramesh Babu, Surya P. Tewari, G. Vaitheeswaran;
   Structural, electronic, bonding and elastic properties of NH_3BH_3 : A density functional study, *Journal of Computational Chemsitry (2011) 32, 1734-1742.*

3. **Ch. Bheema Lingam**, K. Ramesh Babu, Surya P. Tewari, G. Vaitheeswaran;
   Density functional study of electronic, bonding and vibrational properties of $Ca(NH_2BH_3)_2$, *Journal of Computational Chemsitry (2012) 33, 987-997.*

4. **Ch. Bheema Lingam**, K. Ramesh Babu, Surya P. Tewari, G. Vaitheeswaran, S. Lebegue;
   Quasiparticle band structure and optical properties of NH_3BH_3, *Physica status solidi: Rapid Research Letters (2011) 5, 10-12.*

5. **Ch. Bheema Lingam**, K. Ramesh Babu, Surya P. Tewari, G. Vaitheeswaran, S. Lebegue;
   Electronic structure and Optical properties of $Ca(NH_2BH_3)_2$ studied from GW calculations, *Journal of Physical Chemistry C (2011) 115, 18795-18801.*

6. **Ch. Bheema Lingam**, K. Ramesh Babu, Surya P. Tewari, G. Vaitheeswaran;
   High pressure study on structural and vibrational properties of NH_3BH_3, *Journal of Physics.: Conference series (2012)* (in press).

7. **Ch. Bheema Lingam**, K. Ramesh Babu, Surya P. Tewari, G. Vaitheeswaran;
   Effect of van der Waals interaction in ammonia borane and its derivaties (To be submitted)

8. **Ch. Bheema Lingam**, K. Ramesh Babu, G. Vaitheeswaran, Surya P. Tewari, Puru Jena;
   Aminoborane oligomers: Structure, Reaction stabilities, Electrostatic Potential Surfaces and Bond Dissociation energies. (To be submitted)

9. **Ch. Bheema Lingam**, K. Ramesh Babu, Surya P. Tewari, G. Vaitheeswaran;
   Electronic structure, bonding and elastic properties of alkali metal amidoboranes (To be submitted)

10. **Ch. Bheema Lingam**, K. Ramesh Babu, Surya P. Tewari, G. Vaitheeswaran;
    Comparative study of Electronic structure of bonding and elastic properties of $Mg(NH_2BH_3)_2$, $Ca(NH_2BH_3)_2$ and $Sr(NH_2BH_3)_2$ from first principles. (To be submitted)

Other Publications: (Not included in the present Thesis)

1. K. Ramesh Babu, **Ch. Bheema Lingam**, S. Auluck, Surya P. Tewari, G. Vaitheeswaran;
   Structural, thermodynamic and optical properties of MgF_2 studied from first-principles theory, *Journal of Solid State Chemistry (2011) 184, 343-350.*

2. K. Ramesh Babu, **Ch. Bheema Lingam**, Surya P. Tewari, G. Vaitheeswaran;
   High-pressure study of Lithium Azide from density functional calculations, *Journal of Physical Chemistry A (2011) 115, 4521-4529.*

3. N. Yedukondalu, K. Ramesh Babu, **Ch. Bheema Lingam**, David J. Singh, G. Vaitheeswaran, V. Kanchana;
   Electronic structure, optical properties, and bonding in alkaline-earth halofluoride scintillators: BaClF, BaBrF, and BaIF,*Physical Review B (2011) 83, 165117.*

Conference proceedings:

1. **Ch. Bheema Lingam**, G. Vaitheeswaran, Surya P. Tewari;
   Ab initio Calculations of BeH_2 Crystal and BeH2 Polymer,*Proceedings of International Conference on "Hydrogen and Hydrogen Storage Methods and Materials, 2009.*

2. **Ch. Bheema Lingam**, Surya P. Tewari, G. Vaitheeswaran;
   Spectral Studies on One-Dimensional $(BeH_2)_n$ Polymers,*Proceedings of DAE-BRNS National symposium on Atomic, Molecular and Optical Physics, 2009.*

3. **Ch. Bheema Lingam**, K. Ramesh Babu, Surya P. Tewari, G. Vaitheeswaran;
   Electronic and optical properties of MgH_2,*Proceedings of 7th International High Energy Materials Conference & Exhibit, 2009.*

4. **Ch. Bheema Lingam**, K. Ramesh Babu, Surya P. Tewari, G. Vaitheeswaran;
   Ab initio study of electronic, structural, bonding and elastic properties of orthorhombic NH_3BH_3,*Proceedings of International workshop on Frontiers in Electronic Structure Calculations: Techniques and Applications, 2010.*

5. **Ch. Bheema Lingam**, K. Ramesh Babu, Surya P. Tewari, G. Vaitheeswaran;*Electronic structure properties of $H(NH_2BH_2)_nH$ oligomers,*
   Proceedings of International Conference on recent trends in Materials Science and Technology, 2010.

6. **Ch. Bheema Lingam**, K. Ramesh Babu, Surya P. Tewari, G. Vaitheeswaran;*Electronic structure of $Ca(NH_2BH_3)_2$,*
   Proceedings of Theoretical Chemistry Symposium, 2010.

7. **Ch. Bheema Lingam**, K. Ramesh Babu, Surya P. Tewari, G. Vaitheeswaran;
   Density Functional Study on High-Capacity Hydrogen Storage Ammonia Borane and Amidoboranes,*Proceedings of Symposium on Modern Trends in Inorganic Chemistry-XIV, 2011.*

8. K. Ramesh Babu, **Ch. Bheema Lingam**, G. Vaitheeswaran, Surya P. Tewari; Structural, electronic, elastic and thermodynamic properties of MgF_2,*Proceedings of 7th International High Energy Materials Conference & Exhibit, 2009.*

9. K. Ramesh Babu, **Ch. Bheema Lingam**, G. Vaitheeswaran , Surya P. Tewari; Ab initio study of electronic structure and bonding properties of $LiAlH_4$,*Proceedings of International workshop on Frontiers in Electronic Structure Calculations: Techniques and Applications 2010.*

10. K. Ramesh Babu, **Ch. Bheema Lingam**, Surya P. Tewari, G. Vaitheeswaran; Electronic structure, vibrational and thermodynamic properties of alkali metal azides, *Proceedings of International Conference on recent trends in Materials Science and Technology, 2010.*

11. K. Ramesh Babu, **Ch. Bheema Lingam**, Surya P. Tewari, G. Vaitheeswaran; Pressure induced phase transitions in $RbBH_4$,*Proceedings of 23rd AIRAPT International conference on High Pressure Science and Technology, 2011.*

12. K. Ramesh Babu, **Ch. Bheema Lingam**, G. Vaitheeswaran, Surya P. Tewari; Computational study of structural, elastic constants and related mechanical properties and their relevance to decomposition of alkali metal azides, *Proceedings of 8th International High Energy Materials Conference & Exhibit, 2011.*